

学位論文（要約）

**Variability of Kuroshio strength and its relation with ENSO/PDO
during the last 100 years based on coral skeletal radiocarbon**

（サンゴ骨格中の放射性炭素分析による
過去 100 年間の黒潮変動復元に関する研究）

平成 29 年 12 月 博士(理学)申請
東京大学大学院理学系研究科
地球惑星科学専攻

平林 頌子

**Variability of Kuroshio strength and its relation with ENSO/PDO
during the last 100 years based on coral skeletal radiocarbon**

Shoko Hirabayashi

Department of Earth and Planetary Science, and
Atmosphere and Ocean Research Institute,
The University of Tokyo

Submitted to The University of Tokyo
in partial fulfillment of the requirements for Degree of Doctor of Philosophy

December 2017

Acknowledgements

My deepest appreciation goes to my supervisor, Prof. Yusuke Yokoyama. He gave me great opportunities for promoting my research and encouraged me as an international researcher at the frontier of science. Without his guidance and persistent help, this dissertation would not have been possible. I also appreciate Dr. Yosuke Miyairi, Dr. Takahiro Aze and Dr. Masako Yamane for their generous support of high-resolution radiocarbon dating. They gave me plenty of advice for method development of small-mass radiocarbon dating and they were involved in the development of the new single stage accelerator mass spectrometer (AMS) at Atmosphere and Ocean Research Institute (AORI). Dr. Hiroyuki Matsuzaki also gave me machine time for radiocarbon dating with AMS at the Micro Analysis Laboratory, Tandem accelerator, University of Tokyo. Dr. Suzuki Atsushi provided helpful advice, especially when concerning the paleoceanography reconstruction based on corals. Dr. Takashi Okai provided a lot of time for me to measure trace elements in my corals with ICP-AES at National Institute of Advanced Industrial Science and Technology (AIST). I thank Ms. Yumiko Yoshinaga and Ms. Kana Takamori for laboratory assistance at AIST. Dr. Satoshi Nojima, Dr. Seiji Arakaki, Dr. Akira Iguchi and Mr. Hikaru Tomikawa helped me sample living *Porites* corals in Ushibuka, Kumamoto. Dr. Yasuo Maeda and Dr. Fernando Siringan conducted fieldwork in Philippines and gave me constructive comments about my study. Dr. Yukio Masumoto and Eitaro Oka gave me constructive comments about physical oceanography, which improved my study. I would also like to send my appreciation to Prof. Stephen Eggins for warm support at the Australian National University (ANU). I received generous support from Dr. Tezer Esat, Mr. Leslie Kinsley and Dr. Chantal Albert for U-series dating of corals at ANU, and for my time in Canberra, Australia. Prof. Allan Chivas reviewed my manuscript and gave me plenty of advice. Dr. Adam Sproson and Ms. Tomoko Bell checked my manuscript. I had support and encouragement of my research from the members of Prof. Yokoyama's laboratory and the Department of Ocean Floor Geoscience in AORI. I would like to express my gratitude to JSPS Fellows DC1 (JP14J09489) for their financial support. Finally, I would like to show my greatest appreciation to my parents for providing lots of support and encouraging my research life during my ph.D. course.

Acknowledgements

Abstract

The North Equatorial Current (NEC) bifurcates into the Kuroshio Current (KC) and the Mindanao Current (MC), which are both western boundary currents in the Pacific Ocean to the east of the Philippine coast. The NEC-KC-MC current system plays an important role in global climate change because it connects tropical and subtropical areas and transports heat poleward. The bifurcation latitude of the NEC migrates on annual and decadal scales due to effects from the El Niño-Southern Oscillation (ENSO) and the Pacific Decadal Oscillation (PDO) and their influence on the velocity and transport behavior of the KC and MC. Oceanographic observations have been conducted since the twentieth century to understand the relationship between western Pacific variability and climate changes and to predict future climates in response to continuing global warming. However, there is insufficient data to fully understand the mechanisms of oceanographic variability in seasonal, decadal and multi-decadal cycles of climate change with respect to ENSO, PDO and climate regime shift. Therefore, long, continuous and high-resolution datasets of oceanography and climate are urgently required.

Radiocarbon (^{14}C) in corals is a useful proxy to reconstruct water mass mixing in the ocean in the past. Radiocarbon is naturally produced in the upper atmosphere when cosmic radiation interacts with nitrogen atoms. It was also artificially produced by the atmospheric nuclear bomb testing in the 1950s and early 1960s. Once produced, radiocarbon is oxidized to $^{14}\text{CO}_2$ and mixes rapidly in atmosphere, entering the ocean through CO_2 exchange between the atmosphere and surface ocean. Corals incorporate ^{14}C from dissolved inorganic carbon in the surface ocean in their calcium carbonate skeletons. Therefore, a high-resolution coral skeletal radiocarbon record provides a continuous past oceanographic archive, and the comparison of corals from different basins or different current areas can help reconstruct spatio-temporal oceanographic variability in the past. However, high-resolution radiocarbon measurements in corals in the temperate region such as the Kuroshio Current area has not previously been possible because of their smaller skeletal growth rates.

The main aim of this thesis is to reconstruct Kuroshio variability and its relation to ENSO/PDO over the past 100 years using coral skeletal radiocarbon. To achieve this objective, I developed a new method of high-resolution age model

determination using Sr/Ca and refined a radiocarbon measurement technique for small-mass carbonates. Using these new methods, I report seasonal-scale radiocarbon data from Ishigaki in the Kuroshio Current and Currimao in the Kuroshio Loop Current regions. In this thesis, I demonstrate that corals can reconstruct physical oceanographic changes and mesoscale eddy variability in both areas of the Kuroshio and the Kuroshio Loop Current related to changes in climate modes such as ENSO and the PDO for the past 100 years in this thesis.

The results revealed that high-resolution coral skeletal radiocarbon in Ishigaki recorded the existence of three early radiocarbon spikes of nuclear bomb tests in the 1950s in the North Pacific western boundary current area. This new finding will be important in the field of nuclear physics and will contribute to understanding the mechanism of close-in fallout because no previous record farther northwest of Guam was available. These three early radiocarbon spikes revealed that the transport speed of radioactive materials from Guam and Kuroshio varied in the early 1950s and 1960s associated with the ENSO condition. Coral skeletal radiocarbon data can reconstruct physical oceanographic changes and mesoscale eddies in the western Pacific and South China Sea related to migration of the latitude of NEC bifurcation. Compared with other coral records previously reported for Guam, Palau, Langkai, Con Dao, and Hon Tre Island, the regime shift of the PDO in 1976 affects the western Pacific oceanographic features such as the strength of the Mindanao Dome, the Kuroshio Loop Current and mesoscale eddies in Kuroshio regions on decadal timescales.

The high-resolution radiocarbon dataset for the pre-1950 period, which is the period with few oceanic observations, also suggested that upwelling changes in the eastern tropical Pacific related to climate regime shift in 1900 and 1950 affected the ^{14}C contents over the western Pacific. It is also suggested that a climate regime shift might have influenced upwelling driven by the Mindanao Dome and mesoscale eddies in the Kuroshio region in the period from 1900 to 1950.

Further investigation is required to reveal the detailed mechanism of the relationship between climate modes and western Pacific variability, but I have helped initiate this by demonstrating the potential to reconstruct oceanography based on high-resolution radiocarbon tracing using the western Pacific corals.

Contents

Chapter 1	Introduction and Literature Review	1
1.1	Oceanography in the northwestern Pacific	3
1.1.1	The western boundary current of the North Pacific Subtropical Gyre	3
1.1.2	Observation of Western Boundary Currents	7
1.1.3	Migration of the North Equatorial Current bifurcation latitude	10
1.1.4	Kuroshio variability related to the migration of the NEC bifurcation latitude and climate change	15
1.2	Principle of radiocarbon dating and tracing	20
1.2.1	Natural Radiocarbon	20
1.2.2	Radiocarbon produced by atmospheric nuclear bomb testing	21
1.2.3	Reservoir effect	23
1.3	Radiocarbon as a tracer	24
1.4	Radiocarbon in corals	25
1.4.1	Previous studies	25
1.4.2	Relationships between climate change and radiocarbon variability in corals	27
1.5	Research aim and thesis structure	36
Chapter 2	The method for high-resolution age model determination for coral skeletons.....	39
2.1	Introduction.....	41
2.1.1	Purpose of this chapter.....	41
2.1.2	Problems of conventional methods.....	41
2.1.2.1	Age model	41
2.1.2.2	Radiocarbon dating as an oceanographic tracer.....	44
2.2	Age model development	45
2.2.1	Methods for measurement of Sr/Ca and oxygen isotopes in temperate corals	45
2.2.2	Results and discussion for Sr/Ca and oxygen isotopes in the temperate coral	47

2.3	Method development for high-resolution radiocarbon measurement	54
2.3.1	Method for Radiocarbon dating	54
2.3.2	Results and discussions.....	57
2.3.2.1	Improvements for the preparation of small-mass radiocarbon measurements.....	57
2.3.2.2	Method development using single-stage Accelerator Mass Spectrometry	65
2.4	Summary	67
Chapter 3 Multidecadal oceanographic changes in the western Pacific detected through high-resolution bomb-derived radiocarbon measurements in corals		69
3.1	Introduction.....	71
3.2	Materials and Methods	73
3.2.1	Ishigaki modern coral IY02-02	73
3.2.2	Currima0 modern coral PCURIN03	74
3.3	Results	77
3.3.1	Bomb-curve	77
3.3.2	Early ¹⁴ C spikes in the 1950s and 1960s	85
3.3.3	Post-bomb period	90
3.4	Discussion	96
3.4.1	Early bomb-testing-related $\Delta^{14}\text{C}$ Spikes.....	96
3.4.1.1	Reason for the $\Delta^{14}\text{C}$ spikes in the 1950s and 1960s	96
3.4.1.2	Comparison with corals in the western Pacific.....	97
3.4.1.3	The mechanism of close-in fallout	99
3.4.2	Post bomb test period (after 1970).....	100
3.4.2.1	$\Delta^{14}\text{C}$ Difference between Palau and Guam (Mindanao current)....	104
3.4.2.2	$\Delta^{14}\text{C}$ Difference between Ishigaki and Guam (Kuroshio current). 105	
3.4.2.3	Kuroshio intrusion variability in the South China Sea for the post-bomb-test period (Kuroshio Loop Current)	108
3.5	Summary	115

Chapter 4	Short-term fluctuations in natural radiocarbon recorded in coral skeletons from Kuroshio region (pre-1950)	117
4.1	Introduction	119
4.2	Materials and Methods	121
4.2.1	Modern corals from Ryukyu Islands	121
4.2.2	Modern corals from Luzon Island	122
4.2.3	Calculation of marine reservoir age (R) and local marine reservoir age (ΔR)	123
4.3	Results	124
4.4	Discussion	129
4.4.1	Seasonal fluctuations in regional radiocarbon reservoir age in 1940s	129
4.4.2	Decadal fluctuations in the regional radiocarbon reservoir age in the 1900s and 1940s	130
4.5	Summary	137
Chapter 5	Conclusion and Future work	139
5.1	General conclusions	141
5.2	Future perspectives	142
5.2.1	Improvement of the Ocean current transport modeling	142
5.2.2	Kuroshio variability reconstruction before 1950	145
5.2.3	Oceanographic reconstruction using deep-sea corals	148
References		149
Appendix of Chapter 3		171
Appendix of Chapter 4		187

Contents

Chapter 1 Introduction and Literature Review

1.1 Oceanography in the northwestern Pacific

1.1.1 The western boundary current of the North Pacific Subtropical Gyre

The North Pacific subtropical gyre, which is the clockwise circulation in the North Pacific Ocean, contains the North Equatorial Current (NEC), Kuroshio, the North Pacific Current, and the California Current in the mid-latitude of the Pacific (Figure 1.1). Kuroshio is the western boundary current (WBC) of this subtropical gyre (Figures 1.3, 1.4). The Kuroshio is the only current which transports warm heat flux from the tropics poleward in the North Pacific (Figure 1.2). The Kuroshio current has an impact on the weather and climate over East Asia, including Japan. There has been increasing interest in the variability of western boundary currents to predict their response to future global warming (Sakamoto et al., 2005; Sato et al., 2006). Yang et al. (2016) found observational and model support for an intensification and poleward movement of WBCs in response to anthropogenic climate change. Variability of the latitude-direction heat flux driven by ocean currents affects climate change (Hanawa, 2005). Heat flux by Kuroshio has decadal variability, which causes the amount of heat emission at the mid-latitude of the North Pacific and affects the strength of the Aleutian Low and subtropical gyre (Latif and Barnett, 1994; 1996). Latif and Barnett (1994; 1996) proposed the feedback model that Kuroshio variability changes the heat transport from ocean to atmosphere in the mid-latitude of the north Pacific, which influences on the strength of Aleutian low, and then Aleutian low has an impact on the North Pacific subtropical gyre. However, this feedback have not supported by the observational data yet.

The interaction between ocean heat transport variability and global climate change is also proposed by model simulation (Latif and Barnett, 1994; 1996). However, the response of Pacific WBCs under greenhouse warming is still uncertain because the natural variations of WBCs might conceal the long-term effect of global warming in the available observational data sets, especially in the Northern Hemisphere (Yang et al., 2016). Therefore, longer-term observations or proxy data are necessary to evaluate the dynamics of WBCs.

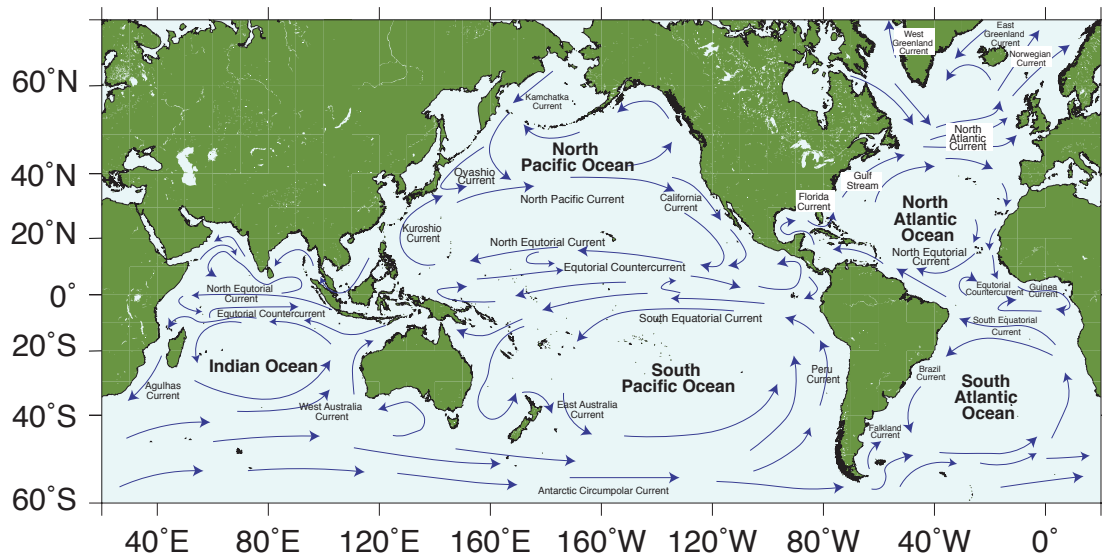


Figure 1.1 World surface ocean currents. The long-term wind-driven average oceanographic pattern is shown in this map. The North Equatorial Current, Kuroshio Current, North Pacific Current and California Current form the North Pacific subtropical gyre.

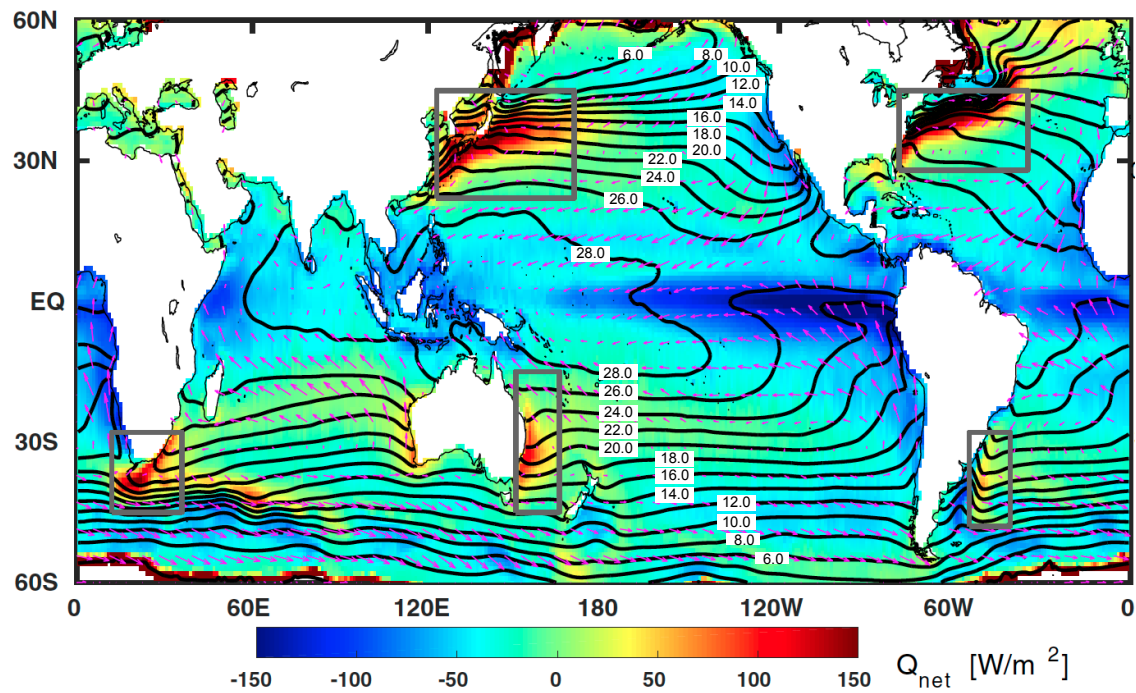


Figure 1.2 Distribution map of the net surface heat flux (Q_{net} ; colors, positive upward), annual sea surface temperature (black contours with 2°C intervals), and surface ocean wind (pink arrows) for the period 1984-2009 in the Pacific. The Western Boundary Currents, including Kuroshio in the North Pacific, can be clearly captured by the upward ocean surface heat flux. Modified from Yang et al. (2016).

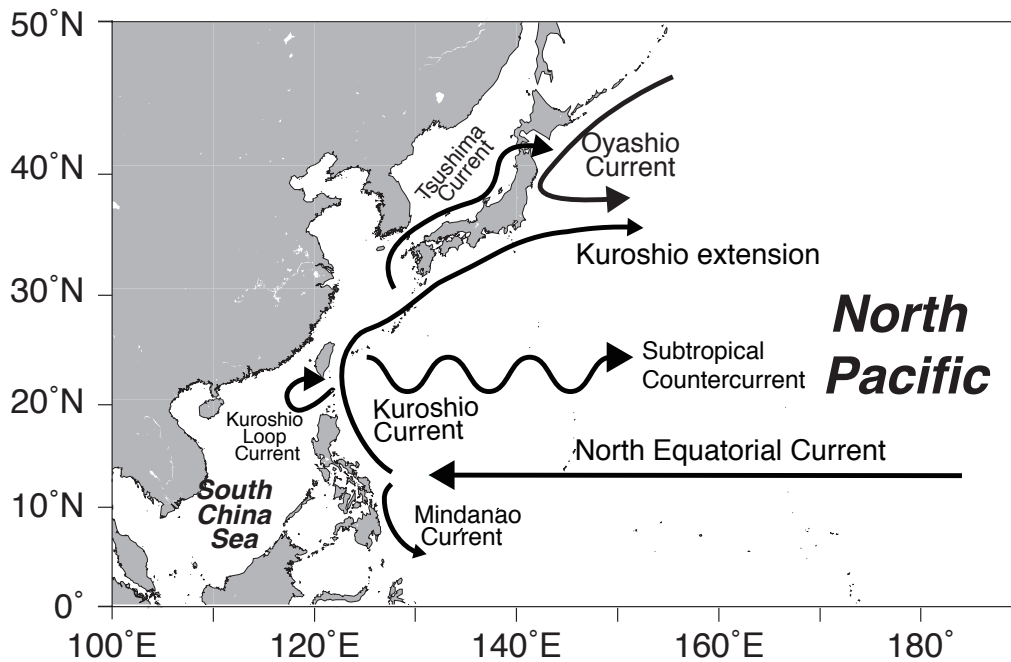


Figure 1.3 Schematic diagram of surface currents in the northwest Pacific

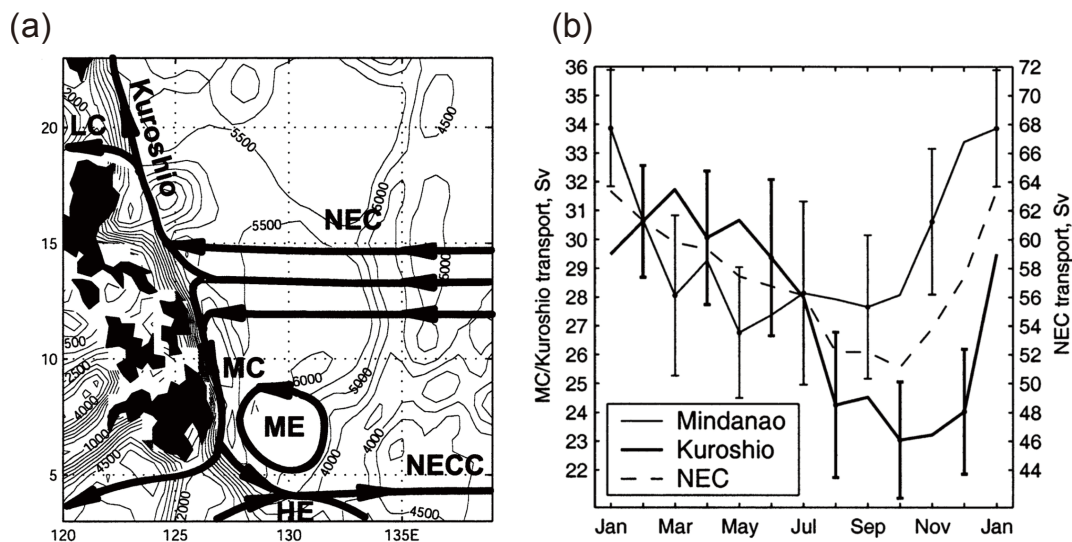


Figure 1.4 (a) Schematic currents (Kuroshio, the Luzon Current (LC), the Mindanao Current (MC), the North Equatorial Current (NEC), the North Equatorial Countercurrent (NECC) and the Halmahera (HE) and Mindanao (ME) eddies/domes) offshore the Philippines. (b) Seasonal transport of Kuroshio at 18.5°N, MC transport at 11°N (left y axis) and NEC transport (right y axis) in Sverdrup (1 Sverdrup = 1 Sv = 10⁶ m³ s⁻¹). Modified from Yaremchuk and Qu (2004).

1.1.2 Observation of Western Boundary Currents

The physical properties of ocean currents are typically investigated using shipboard, Argo float, and satellite observations. Observation of Kuroshio was started during World War II by the Japanese navy, but this observation was not continuous and lacks some intervals (Sugiyama et al., 2004). The first systematic oceanic investigation of the KC and adjacent regions along the 135°E meridian (CSK: Cooperative Study of the Kuroshio and Adjacent Regions) was conducted in 1965 (Masuzawa, 1967). The first NOAA (US National Oceanic and Atmospheric Administration) geo-stationary operational environmental satellite (GOES) was launched in 1975 and started observation of sea surface temperature (SST) in the 1980s by Advanced Very High Resolution Radiometer (AVHRR). Observations in the western Pacific including Asian and Oceania regions by JAXA (Japan Aerospace Exploration Agency) was started in 1987. The Argo float project was started in 2000 to provide information about oceanic properties on timescales from months to decades, including heat and freshwater storage and the magnitude of water transport. We have datasets for up to 50 years, with high-resolution data for only ~20 years. It is still difficult to understand the whole Pacific Western Boundary currents system because this requires not only the dataset for Kuroshio variability but also those for the NEC and Mindanao Current.

Based on research and observation over the past 15 years, variability of the Pacific Western Boundary currents has been reported (Gordon et al., 2014; Hu et al., 2015). The NEC mean westward transport is 40-50 Sv (1 Sverdrup = 1 Sv = $10^6 \text{ m}^3 \text{ s}^{-1}$) in the western tropical Pacific Ocean (Qiu and Joyce, 1992; Qu et al., 1998; Qiu and Chen, 2012). The NEC bifurcates into two currents east of the Philippines, the poleward Kuroshio Current (KC) and the equator ward Mindanao Current (MC) (Nitani 1972, Toole et al., 1990; Qiu and Lukas 1996) (Figure 1.3, 1,4a). The NEC bifurcation latitude is approximately 12-13°N at the surface. The KC of the Philippine coast has mean transport of 25 Sv, ranging from ~19 Sv in fall to ~30 Sv in spring (Qiu, 2001). In winter, the Kuroshio intrusion into the Luzon Strait has been observed to form the Kuroshio Loop Current in the northern South China Sea (SCS) (Sheremet, 2001; Qu et al., 2004; Caruso et al., 2006; Hsin et al., 2012; Nan et al., 2015).

Horizontal heat advection from the Pacific into the SCS by the Kuroshio Loop Current, and it is a key factor influencing the upper-layer heat content in the SCS. The heat content in SCS affects the monsoonal precipitation over the terrestrial climate of Asia because the water vapor of the monsoon originates in the SCS (Yokoyama et al., 2011). Furthermore, it is suggested that the interannual heat content variation of the upper-layer in the SCS is corresponds with ENSO (e.g., Zhang et al. 1996; Tomita and Yasunari 1996; Ose et al. 1997). Therefore, the understanding of the Kuroshio Loop Current variability is important in understanding of both East Asian monsoon and ENSO. However, the estimation of Kuroshio Loop Current is poorly understood because most existing observations are in particular locations and seasons (Potemra and Qu, 2009). For example, Wyrski (1961) estimated the mean Luzon transport as 0.5 Sv, whereas model estimates based on long-term hydrographic data, wind stress, geostrophic velocity, and other data range between 0.6 and 10.2 Sv westward (e.g., Chu and Li 2000; Qu et al. 2000; Lan et al. 2004; Hsin et al. 2012). Estimates based on short-term cruises from 1992 to 2007 also have large uncertainties (e.g., Tian et al. 2006; Liao et al. 2008; Yang et al. 2010; Hsin et al. 2012). Satellite altimeter data show that Kuroshio intrusion takes different pathways through the Luzon Strait as a result of eddies of various timescales (e.g., Yuan et al. 2006; Caruso et al. 2006). Therefore, the quantitative evaluation of the mutual relationship between oceanographic variability in the SCS and the global climatic change, such as ENSO, is unclear at this stage.

The Mindanao Current (MC) region is in the area of Indo Pacific Warm Pool, which plays an important role in the genesis of an El Niño event. The cold eddy called Mindanao Dome or Mindanao Eddy is also located in this area (Figure 1.4a), which is associated with the NEC and MC. There are many modeling studies to explain the mechanism of interannual variations in the Mindanao Dome and the relationship between the evolution of Mindanao Dome and ENSO (e.g. Tozuka et al., 2002). However, the observational data is still limited, and more is needed to validate the results reported by modeling studies. Kashino et al. (2011) reported that the relationship between Mindanao Dome and ENSO with interannual time scale using TRITON buoy data combined with Argo float data and surface wind data. They reported that the heat content in the upper-layer (above 300-m depth) in the Mindanao Dome decreased during the El Niño period of 2002-2003 and 2006-2007. Understanding the relationship between the Mindanao Dome and ENSO requires the observational data of MC

transport. However, the MC transport has large uncertainty, and various values are reported, i.e. from 13 to 39 Sv (Wijffels et al., 1995; Kashino et al., 2009; Hu et al., 2015).

In the Kuroshio region and Subtropical Countercurrent region in 20-23°N, mesoscale eddies, whose diameter ranges from 100 km to 300 km, are observed (Yuwaki et al., 1971; Shikakuma, 2002; Wang et al., 2010; Wu, 2013; Soeyanto et al., 2014). Mesoscale eddies transport the heat, carbon dioxide and nutrients, which affects global climate change. It is suggested that the activity of the mesoscale eddies in these area are closely related to the PDO more than ENSO (Hwang and Kao, 2002; Wu, 2013) on the interannual timescales.

The oceanographic variability in the whole western Pacific is strongly related to the global climatic change as I mentioned above. However, the relationship between the NEC-KC-MC system and climatic events such as ENSO and PDO remains difficult to study due to a lack of long duration and continuous observational records (Hu and Hu, 2014). The shipboard observation for all of the NEC, KC and MC is still limited such as in 1987-1988 by the United States-People's Republic of China Cooperative Studies of Air-Sea Interaction in the Tropical Western Pacific (US-PRC) (Toole et al., 1990) and in 2006 and 2008 by the R/V Mirai (Kashino et al., 2009). The oceanic data by satellite observation is limited only to the sea surface, so that the ocean internal structure can not be captured by satellite observations.

The NEC-KC-MC system is thought to have variability on intraseasonal (Qiu, 2001), interannual, decadal and longer timescales (Qiu and Chen, 2010; Wu, 2013), which makes it difficult to understand their mechanism. Therefore, further observation data in the western Pacific with longer, more continuous and higher resolution is required.

1.1.3 Migration of the North Equatorial Current bifurcation latitude

The NEC bifurcation latitude is believed to be an important index characterizing the surface ocean dynamics in the western boundary currents of KC and MC (Qiu and Lukas 1996; Qiu and Chen 2010). The NEC bifurcation latitude affects the dynamics of the KC at east of Luzon Island (Gordon et al., 2014), MC and Mindanao Dome (Zhao et al., 2013) and Kuroshio loop current into the South China Sea (Nan et al., 2013).

The NEC bifurcation latitude has been observed by the satellite since 1993. According to the sea surface height observed by satellite, the NEC bifurcation latitude has migrated from 8°N to 18°N over the last 22 years (Qiu et al., 2015) (Figure 1.5). It is thought that the migration of the NEC bifurcation latitude is triggered by wind fluctuations in the low-latitude North Pacific Ocean, particularly the surface wind forcing over the western tropical North Pacific along 12°N to 14°N (Qiu and Chen, 2010, 2012; Zhao et al., 2013; Qiu et al., 2015; Wu et al., 2016). This migration varies with seasonal cycles such as the East Asian Monsoon (Qiu and Lukas, 1996; Yaremchuk and Qu, 2004) and interannual-to-decadal timescale variation associated with ENSO and/or Pacific Decadal Oscillation (PDO) (Qiu and Chen, 2010; Wu, 2013; Gordon et al., 2014).

The NEC bifurcation latitude can change interannually from 11°N to 14.5°N (Qiu and Lukas, 1996). This bifurcation tends to migrate depending on ENSO, to the north during El Niño years and to the south during La Niña years (Qiu, 2001; Gordon et al., 2014; Hu et al., 2015) (Figures 1.5). The NEC bifurcation latitude tends to migrate northward when the Niño-3.4 index is positive (Qiu and Chen, 2010; Hu et al., 2015), but not fully representable by the ENSO variability. The Niño-3.4 index can explain only 25 % of the NEC bifurcation latitude (Qiu and Chen, 2010; Zhao et al., 2013). This is because the wind stress curl forcing west of 140°E is mostly uncorrelated to the ENSO variability, while the wind forcing west of 140°E can account for 15% of the migration of the NEC bifurcation latitude (Qiu and Chen, 2010).

On a longer timescale, the NEC bifurcation latitude has migrated southward from 1993 to 2015 (Qiu et al., 2015; Wu et al., 2016) (Figure 1.5). Such a long-term trend is not seen in the time series of the Niño-3.4 index, while long-term trend of PDO index was shown to be similar with the NEC bifurcation latitude (Qiu et al., 2015)

(Figure 1.5). PDO-related wind stress curl is imprinted to the tropical western Pacific along the 10°N to 15°N. The boundary between the tropical and subtropical gyre was shifted the southward forced by the anonymously negative wind stress curl between 10°N and 15°N, as the PDO phase switched gradually from positive to negative in the period from 1993 to 2013 (Qiu et al., 2015) (Figure 1.5).

Although the long-term change of the NEC bifurcation is not completely understood due to the shortage of direct observations (Chen and Wu, 2012), some previous studies tried to reproduce the variation of the NEC bifurcation latitude (Chen and Wu, 2012; Zhao et al., 2013) (Figure 1.6, 1.7). Zhao et al. (2013) reported the historical bifurcation latitude from 1965 to 2010 by reanalyzing Sea Surface Height (SSH) from AVISO (the Archiving, Validation, and Interpretation of Satellite Oceanographic) Data Project from 1992 to 2010 and wind stress data of the European Centre for Medium-Range Weather (ECMWF) Ocean Analysis System from 1959 to 2009. A 0.12° per year southward trend of the NEC bifurcation latitude occurred in the last two decades (Zhao et al., 2013) (Figure 1.6). Chen and Wu (2012) also reported a southward shift of the NEC bifurcation latitude in the past 60 years based on the Simple Ocean Data Assimilation (SODA). Over the past 60 years, the mean position of the NEC bifurcation latitude has shifted southward from 15.5°N to 13.9°N, at a rate of -0.028° per year, although it displayed a slight northward migration from 1970 to 1992 (Figure 1.7).

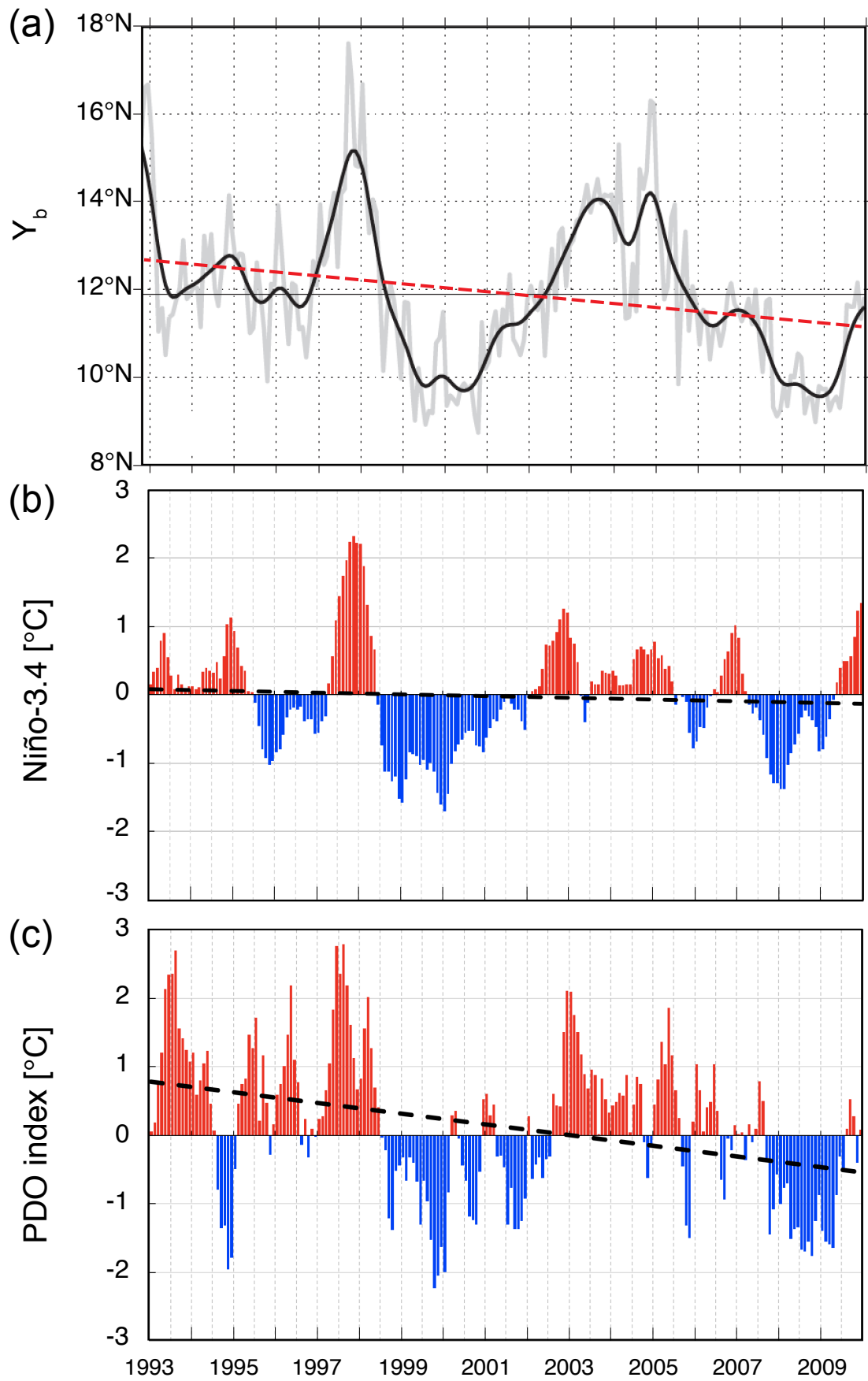


Figure 1.5 (a) The monthly NEC bifurcation latitude (Y_b) based on the satellite observation of sea surface data (gray line) and low-pass-filtered time series of NEC bifurcation latitude (solid black line). Modified from Qiu et al. (2010). The dashed red line shows the long-term southward shift of the NEC bifurcation latitude. (b) The time series of Niño-3.4 index and (c) PDO index. The dashed black line in (b) and (c) is the linear trend of each index. The long-term variation of the NEC bifurcation latitude has migrated progressively southward (red dashed line in Figure 1.5a), while the Niño-3.4 index does not shown such a long-term trend (black dashed line in Figure 1.5b). The PDO index has a multidecadal southward trend (Figure 1.5c), which is similar to long-term variation in the NEC bifurcation latitude (Figure 1.5a).

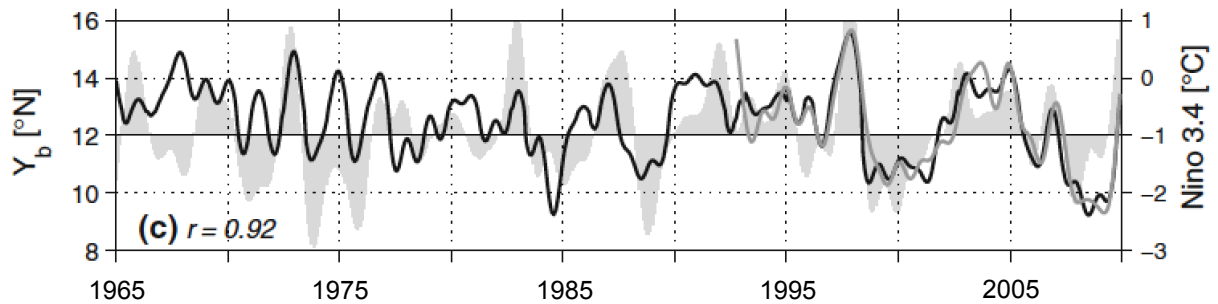


Figure 1.6 Observed (gray) and modeled (black) monthly NEC bifurcation latitude (Y_b). The modeled bifurcation latitude is based on the Archiving, Validation, and Interpretation of Satellite Oceanographic (AVISO) sea surface data from October 1992 to December 2010. The observed and modeled Y_b is in good agreement with a correlation $r = 0.92$ from 1993 to 2010. Gray bars indicate the Niño-3.4 index as the indicator of ENSO events. The correlation of Y_b and the Niño-3.4 index is $r = 0.53$, which means the NEC bifurcation latitude is not affected by only ENSO variability. Modified from Zhao et al. (2013).

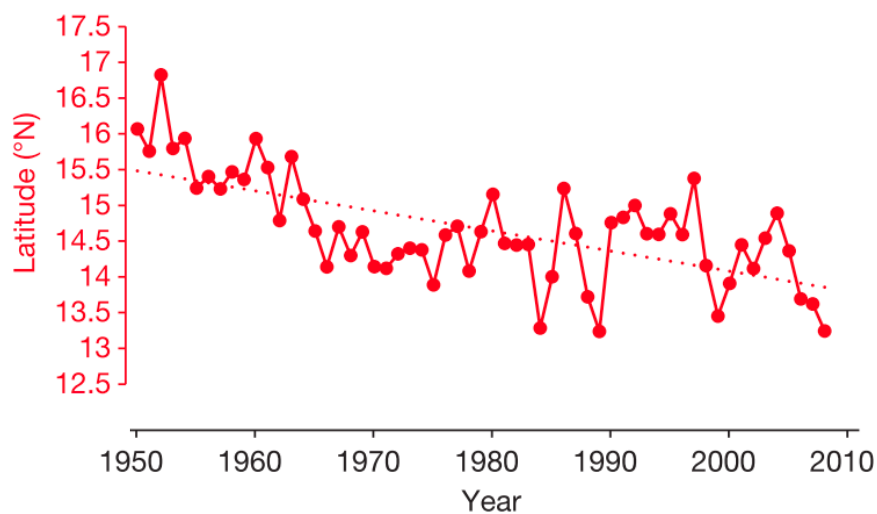


Figure 1.7 Time series of annual mean NEC bifurcation latitude from 1950 to 2010 based on the Simple Ocean Data Assimilation (SODA) version 2.2.4 (Carton et al., 2000). The NEC bifurcation latitude has a long-term southward shift over 60 years. For the decadal scale, the NEC bifurcation latitude migrated slightly northward from 1970 to 1992 and southward from 2000 to 2010, which is associated with the warm and cold PDO phases, respectively. Modified from Hu et al. (2015).

1.1.4 Kuroshio variability related to the migration of the NEC bifurcation latitude and climate change

The NEC-KC-MC current system varies with seasonal-to-decadal time-scales (Figures 1.4b, 1.5, 1.6, 1.7). The NEC is part of the North Subtropical Gyre, which is wind driven circulation. The NEC bifurcation latitude is thought to migrate meridional by the wind fluctuation along the Tropical North Pacific (Qiu and Chen, 2010; 2012). The wind stress curl in the area of 12-14°N dominates to the migration of the NEC bifurcation latitude, which is induced by fluctuation of the trade winds intensity related to ENSO and PDO for the interannual and decadal timescale, respectively. The variation in wind stress curl in the Philippine Sea is also controlled by the intensify of local trade winds related to the East Asia monsoon on seasonal scales (Kessler, 1990; Qiu and Joyce, 1992; Qiu and Lukas, 1996; Qu et al., 2008).

For the seasonal scale, the East Asian monsoon plays an important role for the migration of seasonal NEC bifurcation latitude because it causes the directly wind-driven Ekman transport and the anomalous circulation forced by local Ekman pumping in the Philippine Sea. Those two process tends to make the NEC bifurcation latitude northward shift in winter and southward in summer (Qiu and Lukas, 1996; Qu and Lukas, 2003; Wang and Hu, 2006; Gordon et al., 2014; Hu et al., 2015), accompanied by a change in the partition of the NEC transport between the KC and MC.

Basically, the trade winds fluctuation along the tropical Pacific related to ENSO and PDO causes the wind stress of 12-14°N in the western Pacific, which affects the migration of NEC bifurcation latitude. When the trade winds are intensified, negative wind stress curl is induced in the tropical North pacific and creates a southward migration of both the North Subtropical Gyre and NEC bifurcation latitude (Wu et al., 2016) on the interannual and decadal timescales. The wind patterns in the Pacific are associated with weakened westerlies when the trade winds are intensified, and the positive wind stress curl appears in the Philippine Sea, which induces the southward shift of NEC bifurcation latitude during the negative PDO phase (Wu et al., 2016) and La Niña years (Gordon et al., 2014). However, appeared wind stress pattern in the Philippine Sea is slightly different between PDO and ENSO, which causes a larger difference of the multi-decadal trend between NEC bifurcation latitude and Niño-

3.4 index (Figure 1.5a, 1.5b) than that between NEC bifurcation latitude and PDO index (Figure 1.5a, 1.5c) (Qiu et al., 2010; 2015).

For the interannual scale, the bifurcation latitude of the NEC moves northward during El Niño years, resulting in a minimum transport of the KC east of Luzon (e.g., Kim et al., 2004; Qu and Lukas, 2003) (Figure 1.8, 1.9). The situation reverses during La Niña years. The NEC bifurcation latitude migrates depending on the wind stress curl of the Pacific along the 12-14°N. This wind stress affects the northward shift of Kuroshio recirculation gyre, which coincide with the NEC bifurcation latitude migration during La Niña years (Gordon et al., 2014). The transport of KC at the east side of Luzon Island increased during the southward shift of NEC bifurcation latitude because the Kuroshio recirculation converged with the KC transported by NEC at the east side of Luzon Island (Gordon et al., 2014) (Figure 1.8). The increased KC transport at the east side of Luzon Island produced greater inertia, which caused the KC to flow a relatively straight path from east of Luzon to east of Taiwan (Wu et al., 2016). Because of this, the transport of Kuroshio Loop Current became smaller when the NEC bifurcation latitude migrated southward.

For the decadal scale, interactions between the Pacific WBCs and PDO occur on decadal timescales in a manner somewhat different to the interannual timescales for ENSO (Hu et al., 2015). The negative PDO phase after 1990s is linked to a southward shift of the NEC bifurcation latitude, and a strengthened NEC, because of intensified easterlies over the Western Pacific. Both the KC and the MC also strengthened during the negative PDO phase, which is inconsistent with the transport variability in case of ENSO (Hu et al., 2015). However, ENSO and PDO are linked, and are therefore not independent climate indices (Newman et al., 2003). Schneider and Cornuelle (2005) suggested that PDO is not driven by a single physical process that defines a climate mode, akin to ENSO. PDO arises from at least three different processes, namely, sea level pressure of the Aleutian low, ocean circulation within the Kuroshio-Oyashio extension, and ENSO (Gordon et al., 2014).

Although the KC transport is related to the meridional shift of the NEC bifurcation latitude, there is the opposite tendency of the KC transport in the northeast and southeast of Taiwan on interannual and longer timescales because of the mesoscale eddies originated from the Subtropical Countercurrent (Wu, 2013). In the Subtropical Countercurrent, which is located at 20-23°N, the westward-propagating mesoscale

eddies approach the western coast of Taiwan and collide with the KC. Northward shift of NEC increases mesoscale eddy activities in the Subtropical Countercurrent area and strikes the KC off east Taiwan. Therefore, the KC transport off the northwest Taiwan (downstream of the KC) becomes larger in positive PDO periods (Wu, 2013), while KC transport off southeast Taiwan weakens. This interannual change is due to the positive wind stress curl anomaly over the North Pacific tropical gyre prior to the El Niño years (Qiu and Lukas, 1996; Zhang et al., 2012). Gordon et al. (2014) used data from two cruises in spring 2011 and 2012 and detected that a southward shift of the NEC bifurcation latitude caused an increase of KC transport during La Niña and the negative phase of the PDO and vice-versa (Figure 1.8).

The evidence of long-term variation of KC and MC transport near the NEC bifurcation latitude has not been demonstrated based on long and continuous observational data (Nakamura, 2017). Kashino et al. (2005) reported that NEC and MC intensified, whereas KC offshore Philippines weakened during El Niño years, based on comparison of the El Niño year of 2006/07 and the La Niña year of 2007/08. Kim et al. (2004) reported that not only NEC and MC but also KC intensified during El Niño years based on a numerical model, which is inconsistent with Kashino et al. (2005). Therefore, long-term, high-vertical-resolution observations are needed to improve our understanding of the NEC-KC-MC current system.

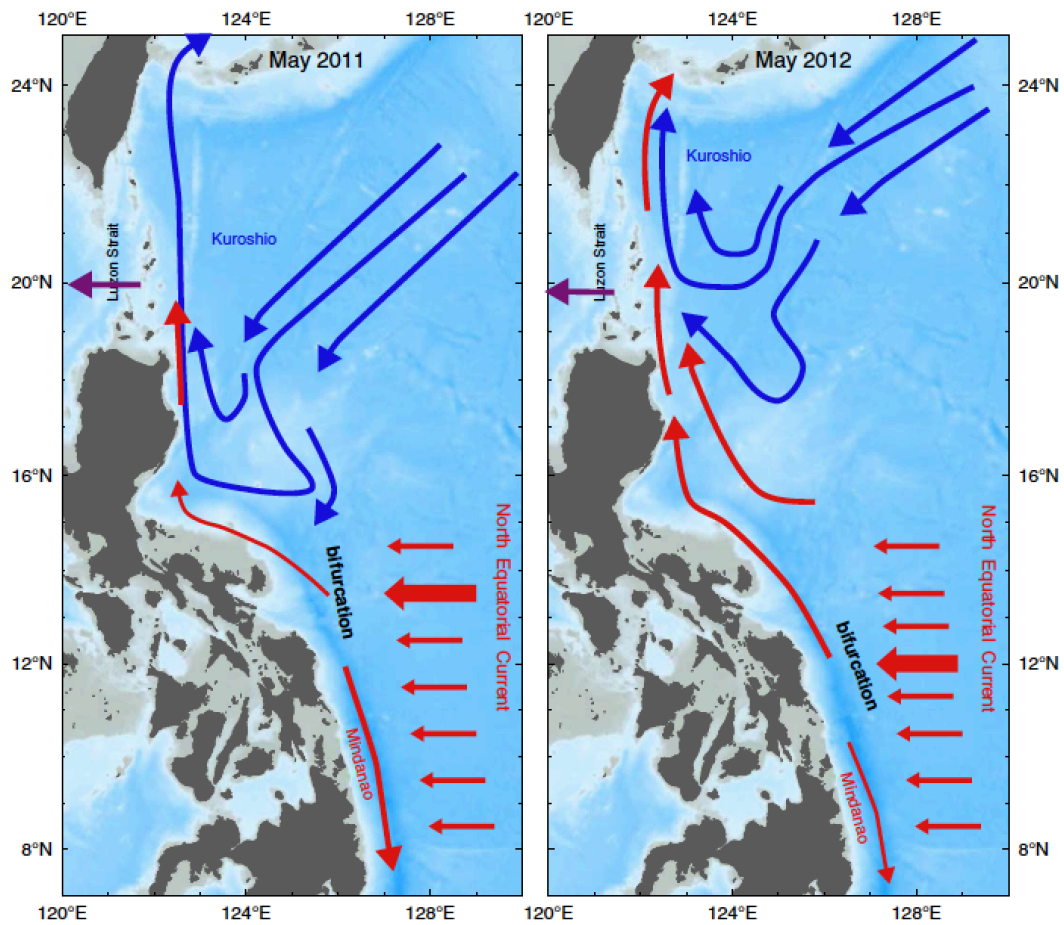


Figure 1.8 Schematic relationship between the NEC bifurcation latitude during El Niño (left)/La Niña (right) events and Kuroshio transport. The NEC bifurcation latitude migrates northward during El Niño years and southward during La Niña years. When the NEC bifurcation latitude migrates southward, Kuroshio transport east of Luzon Island is increased and vice-versa, which was observed during two research cruises of May/June 2011 and April/May 2012 in Lamongan Bay, on the east side of Luzon Island. Red arrows indicate the tropical waters of the NEC and blue arrows indicate the subtropical thermocline waters originated from the Kuroshio recirculation gyre. From Gordon et al. (2014).

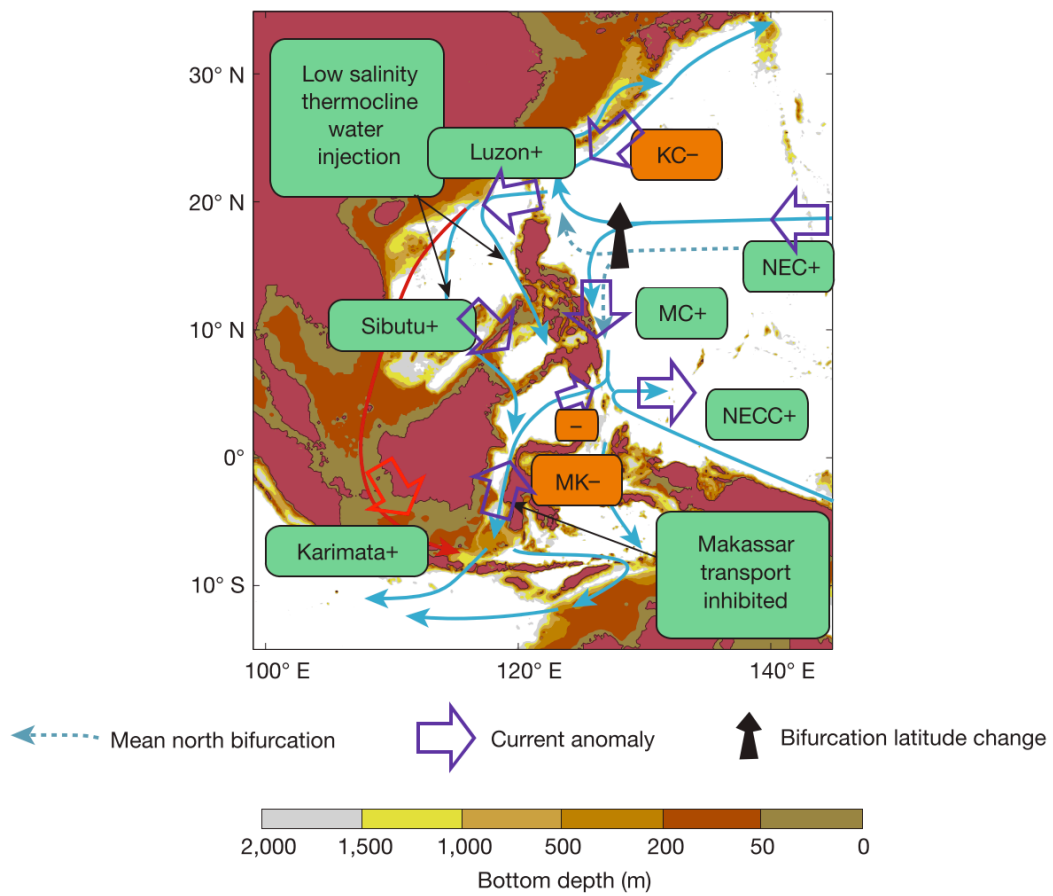


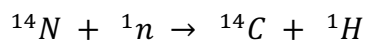
Figure 1.9 The schematic relationship between the NEC bifurcation latitude and transport variability in the western Pacific during El Niño years. The NEC bifurcation latitude migrates northward during El Niño years, the Kuroshio current (KC) transport is decreased and the Mindanao Current (MC) and Kuroshio Loop Current (Luzon) are increased. Modified from Hu et al. (2015)

1.2 Principle of radiocarbon dating and tracing

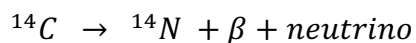
1.2.1 Natural Radiocarbon

Carbon exists in the form of three isotopes; ^{12}C , ^{13}C and ^{14}C . ^{12}C and ^{13}C are stable isotopes and ^{14}C is a radioisotope. It is estimated that the natural abundance ratio of carbon isotopes is $1:1 \times 10^{-2}:1 \times 10^{-12}$. Radiocarbon (^{14}C) is one of the most powerful tools for cosmogenic dating. The half-life of ^{14}C is 5730 ± 30 years (Stuiver and Polach, 1977). Therefore, radiocarbon dating is widely used in paleoclimatology and archeology for samples which are younger than 50,000 years.

^{14}C is naturally produced in the upper atmosphere by neutron bombardment with atmospheric nitrogen atoms. The actual reaction that produces ^{14}C is:



^{14}C is quickly oxidized and becomes $^{14}\text{CO}_2$, and then diffuses into the carbon exchange reservoir (atmosphere, biosphere and the oceans) via the carbon cycle (Mangerud, 1972) (Figure 1.10). An equilibrium is archived between the rate of newly produced ^{14}C in the upper atmosphere and ^{14}C lost by radioactive decay when irradiation by cosmic rays is almost constant. The ^{14}C level in the upper atmosphere is approximately equal to the amount of ^{14}C lost by the radioactive decay of ^{14}C to nitrogen as follows;



Because of this, the total amount of global ^{14}C was small variability before 1950. This principal of this steady ^{14}C concentration before 1950 is fundamental to the method of radiocarbon dating.

1.2.2 Radiocarbon produced by atmospheric nuclear bomb testing

Since the 1950s, atmospheric nuclear bomb tests have been conducted and artificial ^{14}C (bomb- ^{14}C) was added to the atmosphere until 1963 (Figure 1.11). The huge thermal neutron flux produced by nuclear bomb testing reacted with nitrogen atoms, producing a large amount of bomb- ^{14}C . Atmospheric ^{14}C content rapidly increased from 1955 due to atmospheric nuclear bomb testing and the ^{14}C level almost doubled in the mid-1960s (Hua et al., 2013) (Figure 1.11). Bomb- ^{14}C is also quickly oxidized and becomes $^{14}\text{CO}_2$, and then diffuses into the carbon exchange reservoir (atmosphere, biosphere and the oceans) via the carbon cycle. Bomb- ^{14}C diffuses into the surface ocean through air-sea CO_2 exchange, while the deep ocean is isolated from direct CO_2 exchange with the atmosphere.

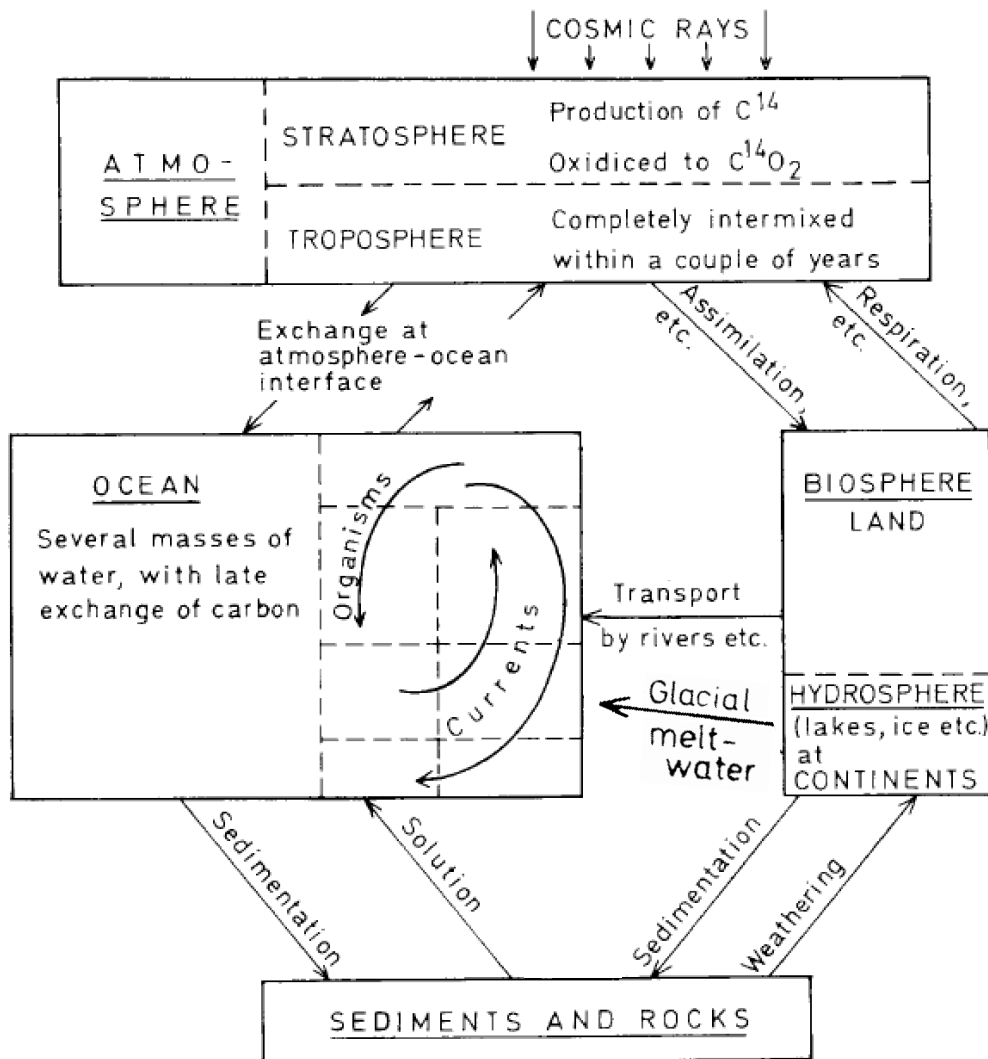


Figure 1.10 Schematic diagram of the carbon cycle. Modified from Mangerud (1972).

1.2.3 Marine Reservoir effect

Carbon dioxide diffusion into the ocean from the atmosphere via atmosphere-ocean CO₂ exchange takes ~10 years. The surface ocean is not in isotopic equilibrium with the atmosphere because of this time lag and ocean circulation such as upwelling, which brings ¹⁴C-depleted water to the surface. This difference is called the marine reservoir effect (R) and the averaged marine reservoir age of the surface ocean is ~400 years (e.g. Cordero et al., 2003). However, this marine reservoir effect is region-specific. For example, the marine reservoir age in the North Atlantic area is much younger than that of other high-latitude regions because strong convection (formation of North Atlantic Deep Water) limits upwelling of ¹⁴C-depleted water. This region-specific ¹⁴C age difference is called the local marine reservoir effect (ΔR).

The ¹⁴C content of the mixed layer of the ocean is an indicator for the air-sea gas exchange rates, and the intensity of upwelling from deeper layers (Toggweiler et al., 1991), which is related to climate mode changes such as El Niño-Southern Oscillation (ENSO).

1.3 Radiocarbon as a tracer

When we discuss the use of radiocarbon concentration in the ocean as a tracer, we have to calibrate the kinetic effects of carbon isotopes using the following equation defined by Stuiver and Polach (1977).

$$\Delta^{14}\text{C} (\text{‰}) = \delta^{14}\text{C} - 2(\delta^{13}\text{C}_{\text{PDB}} + 25) \times \left(1 + \frac{\delta^{14}\text{C}}{1000}\right)$$

$$\delta^{14}\text{C} = \left[\left\{ \frac{{}^{14}\text{C}/{}^{12}\text{C}}{\left(({}^{14}\text{C}/{}^{12}\text{C})_{\text{NIST}} \right)} \right\} - 1 \right] \times 1000 \text{‰}$$

$$\delta^{13}\text{C} = \left[\left\{ \frac{{}^{13}\text{C}/{}^{12}\text{C}}{\left(({}^{13}\text{C}/{}^{12}\text{C})_{\text{PDB}} \right)} \right\} - 1 \right] \times 1000 \text{‰}$$

Here, $\delta^{13}\text{C}$ is the carbon stable isotopic ratio of a material relative to the Pee Dee Belemnite (PDB) standard measured by the accelerator mass spectrometer (AMS) at the same time as the radiocarbon measurements. $\delta^{14}\text{C}$ is the ^{14}C isotopic ratio of a material relative to the modern standard (NIST Oxalic Acid (OxII) standard, National Institute of Standards and Technology in United States), without any correction for fractionation. $\Delta^{14}\text{C}$ is the ^{14}C isotopic ratio of a material relative to the modern standard after correction for fractionation to $\delta^{13}\text{C} = -25\text{‰}$.

Radiocarbon can be used not only as a dating method but also as a tracer of world ocean dynamics. International seawater sampling programs such as Geochemical Ocean Sections Study (GEOSECS) in 1970s and the World Ocean Circulation Experiment (WOCE) in the 1990s produced a map of the global distribution of ^{14}C of the dissolved inorganic carbon (DIC) in the ocean, which is transported from the North Atlantic to the Pacific through thermohaline circulation (Östlund and Stuiver, 1980; Stuiver et al., 1981; Kumamoto et al., 2013). For example, according to $\Delta^{14}\text{C}$ measurements of surface seawater from WOCE Section P09 collected in 1994 (Key 1996; McNichol et al., 2000; Ge et al., 2016) (<http://cdiac.ornl.gov/ftp/oceans/p09woce/>), $\Delta^{14}\text{C}$ values along the 137°E meridian were 87.5‰ at 7°N at the surface, whereas values at 10°N were 89.5‰ at a depth of 1.2 m

and 94‰ at 12.6°N at the surface. For the depth profile of $\Delta^{14}\text{C}$ values, $\Delta^{14}\text{C}$ at the WOCE Station P09-70 (7°N, 137°E) in 1994 were 87.5‰ at the surface, whereas values of 101.7‰ and 65.6‰ were reported at depths of 51.5 m and 102.3 m, respectively. The horizontal and vertical $\Delta^{14}\text{C}$ difference can be used for the discussion of water mass mixing as an oceanographic tracer. However, these datasets captured only snapshots from the time of data collection, thus they cannot be used to study long-term variations over several decades.

1.4 Radiocarbon in corals

1.4.1 Previous studies

Changes in oceanic mixed layer $\Delta^{14}\text{C}$ are related to the degree of exchange between the atmosphere and the surface ocean, and the intensity of upwelling from deeper layers. The calcium carbonate (aragonite) skeletons of reef-building corals contain annual density bands that record the $\Delta^{14}\text{C}$ values of surface water when the corals skeletons take up dissolved inorganic carbon (DIC) from ambient seawater (Druffel and Linick, 1978; Druffel, 1982, 1989). Therefore, $\Delta^{14}\text{C}$ variability in corals reflect changes in oceanic circulation such as upwelling or advection of ^{14}C depleted/enriched waters from other regions (e.g. Druffel, 2002; Fallon and Guilderson, 2008) (Figure 1.13).

The $\Delta^{14}\text{C}$ analysis of corals have been made by Moore and Krishnaswami (1974) in the Indian Ocean, Nozaki et al. (1978) in the Atlantic Ocean and Konishi et al. (1981) and Druffel (1981) in the Pacific Ocean. The time resolution of their studies were to two-year growth intervals, because of the large sample-size required for gas proportional or liquid scintillation counting. Radiocarbon dating using Accelerator Mass Spectrometry (AMS) was developed in the late 1970s. However, because of the initially low measurement accuracy and high cost, measurements by the AMS method were limited to only a few research institutes or universities. $\Delta^{14}\text{C}$ analysis of corals with AMS began in the 1990s (Brown et al., 1993) and used 8-25 mg coral samples. Thus,

only tropical corals, which have high skeletal growth rates, and therefore sufficient mass per year, have been able to be measured until recently (Figure 1.14).

Bomb- ^{14}C is absorbed into the surface ocean from the atmosphere with a time delay of ~ 10 years via the ocean cycle between atmosphere and ocean (Broecker and Peng 1982; Druffel and Suess 1983; Druffel 1987). Corals, in turn, incorporate in their calcium carbonate, bomb- ^{14}C from oceanic DIC. Previous studies revealed that the shape of the “bomb-curve”, which is the bomb- ^{14}C contents in corals from 1950 to the present day, is different from that of the atmosphere (Figure 1.11). The bomb- ^{14}C level rapidly increased in the 1950s and reached a maximum value in 1963, when the international “Treaty Banning Nuclear Weapons Testing in the Atmosphere, in outer Space and under Water” was signed. Thereafter, the $\Delta^{14}\text{C}$ level was attenuated in the atmosphere until reaching low levels today (Hua et al., 2013) (Figure 1.11). In the ocean, bomb- ^{14}C gradually increased from the early 1960s and reached a maximum value after the 1970s, whose timing was different in each location because of the atmosphere-ocean gas change rate or local oceanographic conditions (Figure 1.13). Previous studies focus on the slope and maximum values of the bomb curves and discuss gas exchange as a comparison in each ocean basin (e.g. Druffel, 2002) (Figure 1.13).

For example, there are 4 broad geographic areas in the Pacific based on the bomb curve reported from their corals (Figure 1.13) (Druffel, 2002). The first group, which has the highest $\Delta^{14}\text{C}$ values, is the area in the North Pacific equatorial gyre (Oahu and French Frigate Shoals); these records reached values of 188-189‰ in French Frigate Shoals (Druffel 1987) and 155-162‰ in Oahu by the early-1970s (Toggweiler, 1983). The second group, with the second highest $\Delta^{14}\text{C}$ values, is from the south Pacific equatorial gyre (Fiji, Tahiti) and the western tropical Pacific (Ponape); these have $\Delta^{14}\text{C}$ values of 120-135‰ by the mid-1970s and maintain that high value until 1980 (Druffel, 1987; Toggweiler et al., 1991; Konishi et al., 1981). The third group is from the tropical Pacific (Fanning and Tarawa) where $\Delta^{14}\text{C}$ results are 55-85‰ by the early 1970s and increased in 1980 (Druffel 1987; Toggweiler, 1983). The last group, with the lowest $\Delta^{14}\text{C}$ values in the Pacific, is from the eastern tropical Pacific (Galapagos), which is the center of intense upwelling in the equatorial east Pacific. These values are only 20-40‰ in the early 1970s, and were still rising in 1980s at the Galapagos (Druffel, 1981, 1987). This grouping mainly reflected the air-sea flux of CO_2 in Pacific (Figure 1.12, 1.13).

High-resolution ^{14}C measurements on coral skeletons can be used to reconstruct continuous and seasonal/interannual variability in ocean conditions (Guilderson et al., 2000; Druffel et al., 2014; Andrews et al., 2016) because coral skeletons incorporate DIC from ambient seawater. Nearly all previous studies using ^{14}C record in corals discussed the relationship between climate change and ocean variability based on data from the eastern and central Pacific (e.g., Druffel, 2002; Grottoli and Eakin, 2007) (Figure 1.14). Grumet et al. (2002) reported the first empirical evidence of surface flow across the equator at the western boundary using the bimonthly $\Delta^{14}\text{C}$ data from Kenya in the Indian Ocean for the period from 1947 to 1987. Low-resolution $\Delta^{14}\text{C}$ data from Okinawa reported by Konishi et al. (1981) constitute the only record of western Pacific Ocean boundary currents for the period from 1900 to 1980. High-resolution ^{14}C measurements (more than two points per year) of corals reported the bomb- ^{14}C curve (for the period from 1950 to 1980) is limited in the Tropics, especially in the Central Pacific along the 150°E line (Figure 1.14). Since these are the only data in this thesis reporting the whole bomb- ^{14}C curve in the KC area, the results for this region are important to compare with high-resolution $\Delta^{14}\text{C}$ data from other regions and to discuss the relationship between climates and the whole North Pacific Subtropical Gyre.

1.4.2 Relationships between climate change and radiocarbon variability in corals

Ocean conditions are variable on interannual or decadal timescales with respect to climate events such as ENSO and PDO. ENSO, which is one of the major global climate change events, is the interaction between the atmosphere and ocean in the tropical Pacific. During the neutral ENSO conditions, surface trade winds blow east across the tropical Pacific and the thermocline is deeper in the west relative to the east. During the El Niño conditions, the trade winds weaken and the thermocline gradient between east and west side of the Pacific becomes small, which means less upwelling along the Peru-Chile coast. During the La Niña conditions, the trade winds strengthen, and the west-east thermocline gradient become bigger, which makes the upwelling along the Peru-Chile coast intensified (Neelin and Latif, 1998). Therefore, the wind stress over the Tropical Pacific is varied and the intensity of the upwelling in the east Tropical Pacific is related to ENSO. The other main global climate in the Pacific, the

PDO, is defined as the SST difference in the central and north Pacific (Mantua et al., 1997), but the atmospheric and oceanographic pattern in the Tropical Pacific of the PDO is similar to those of the ENSO (Gershunov and Barnett, 1998; Newman et al., 2016). Because of this similar pattern of ENSO and PDO, some researcher called PDO as the decadal-ENSO (e.g. Zhang et al., 1997). Those ENSO and PDO changes the Peruvian upwelling strength, which causes the $\Delta^{14}\text{C}$ variability in the sea surface. For example, El Niño caused higher $\Delta^{14}\text{C}$ values relative to normal condition in corals from Galapagos, Fanning and Tarawa due to the weakened Peruvian offshore upwelling. Guilderson and Schrag (1998) showed an abrupt increase in the $\Delta^{14}\text{C}$ in the Galapagos coral in 1976. Grottoli et al. (2003) reported that the dramatic positive shift in the Fanning $\Delta^{14}\text{C}$ record beginning in 1947 coincides with the negative shift in the mid-1940s of the PDO.

Not only the East tropical Pacific, but also the western Pacific is affected by the climate mode of ENSO and PDO. The NEC is the part of North Subtropical Gyre, which is one of the circulation patterns driven by the wind stress, which is influenced by ENSO and PDO. The NEC bifurcates into KC and MC offshore of the Philippines, and migrates via the wind stress curl of the Pacific along the 12-14°N (Qiu and Chen, 2010). ENSO and PDO change the wind force along the tropical Pacific, and also affects the wind stress in the NEC area. Therefore, the NEC bifurcation latitude migrates related to the ENSO and PDO from interannual to decadal time scale.

This NEC bifurcation latitude changes the transport volume of KC, MC and Kuroshio Loop Current which intrudes into the Luzon Strait (Figure 1.8, 1.9). Furthermore, the NEC bifurcation latitude has influences on the mesoscale eddy activity in the KC region and the intensity of the Mindanao Dome in the MC region. Therefore, ENSO and PDO change wind stress along the tropical Pacific, and the NEC bifurcation latitude migrates, which affects the oceanographic dynamics and water mass mixing such as current strength of the western boundary currents and the intensity of local vertical upwelling in the northwest Pacific region (Figure 1. 15). The local vertical upwelling by the Mindanao Dome and mesoscale eddies change the ^{14}C contents in the surface northwest Pacific surface waters. Using this mechanism, the water mass mixing of the northwest Pacific related to the NEC migration, and its relations climate change such as ENSO/PDO based on the radiocarbon contents difference in the KC and MC region, namely the local marine reservoir age (ΔR), can be discussed.

The corals record the continuous the ^{14}C contents variability in the surface ocean with the various timescales from seasonal to decadal. Using multiple corals taken from northwest Pacific and analyzing high-resolution radiocarbon in the corals makes it possible for continuous reconstruction of water mass mixing in the northwest Pacific and therefore discussion of the relationships between oceanography and climate change. Both ENSO and PDO influence on the North subtropical Pacific such as water mass changes, especially in the western Pacific, is not well known. This water mass mixing varies with the time-scales of interannual and decadal in the upper ocean, but it is still not known which, because there are too few observations. Because of the lack of long and continuous observations, longer timescale variability in climate modes such as the PDO and associated climate shifts are documented for only the past 50 years. Therefore, the long, continuous and high-resolution observation data is required to understand the relationship between global climate change and northwestern Pacific variability. High-resolution radiocarbon datasets based on multiple corals taken from the western Pacific and South China Sea can provide the information of water mass mixing related to the climate changes for more than hundreds of years, which contributes to the field of paleoclimatology and physical oceanography.

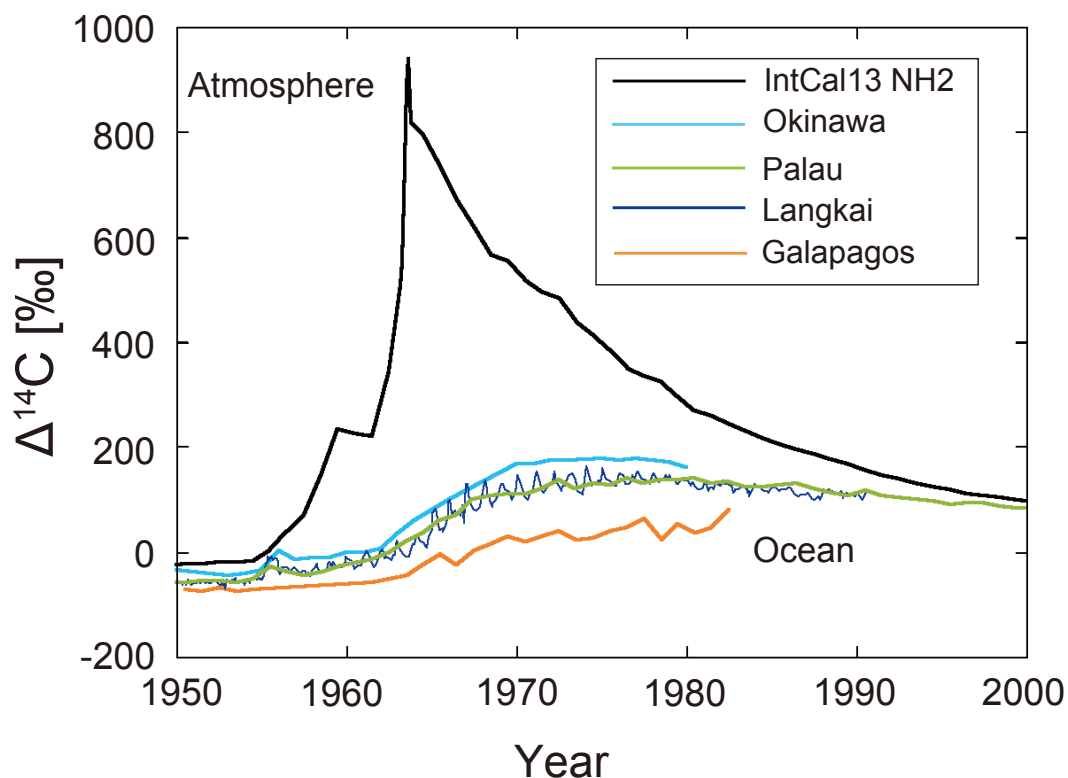


Figure 1.11 $\Delta^{14}\text{C}$ in the atmosphere and ocean (corals) in the period from 1950 to 2000. Data are from IntCal13 (Reimer et al., 2013) and corals from Okinawa (Konishi et al., 1981), Palau (Glynn et al., 2013), Langkai (Fallon and Guilderson, 2008) and Galapagos (Druffel, 1981, 1987). $\Delta^{14}\text{C}$ in the atmosphere increased until the international “Treaty Banning Nuclear Weapons Testing in the Atmosphere, in outer Space and under Water” was signed in 1963. After 1963, $\Delta^{14}\text{C}$ in the atmosphere have been decreased because radiocarbon takes into the surface ocean via the Atmosphere and Ocean CO_2 gas exchange. $\Delta^{14}\text{C}$ in the surface ocean increased from 1960s and becomes the maximum $\Delta^{14}\text{C}$ values after 1970s. This difference of the bomb-curve shape between the atmosphere and surface ocean is due to the Atmosphere and Ocean CO_2 gas exchange.

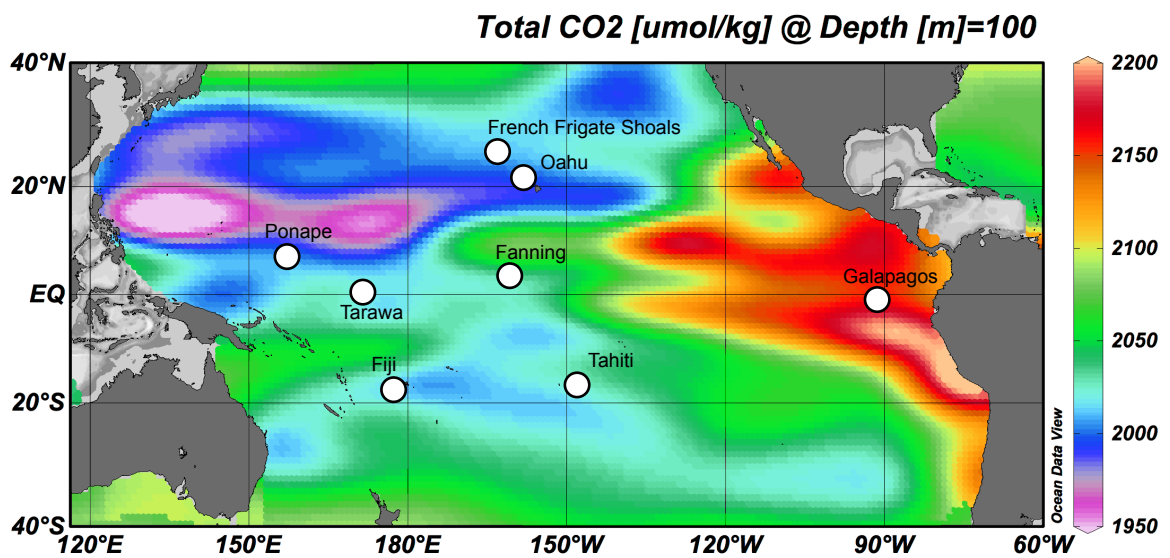


Figure 1.12 Total CO₂ in the Pacific Ocean at a depth of 100 m. Data source is “GLODAP Gridded Data” (Key et al., 2004) and plotted using Ocean Data View software version 4.6.2 (Schlitzer, 2014). White circles indicate the locations of the previous studies that reported bomb curves in the corals shown in Figure 1.13.

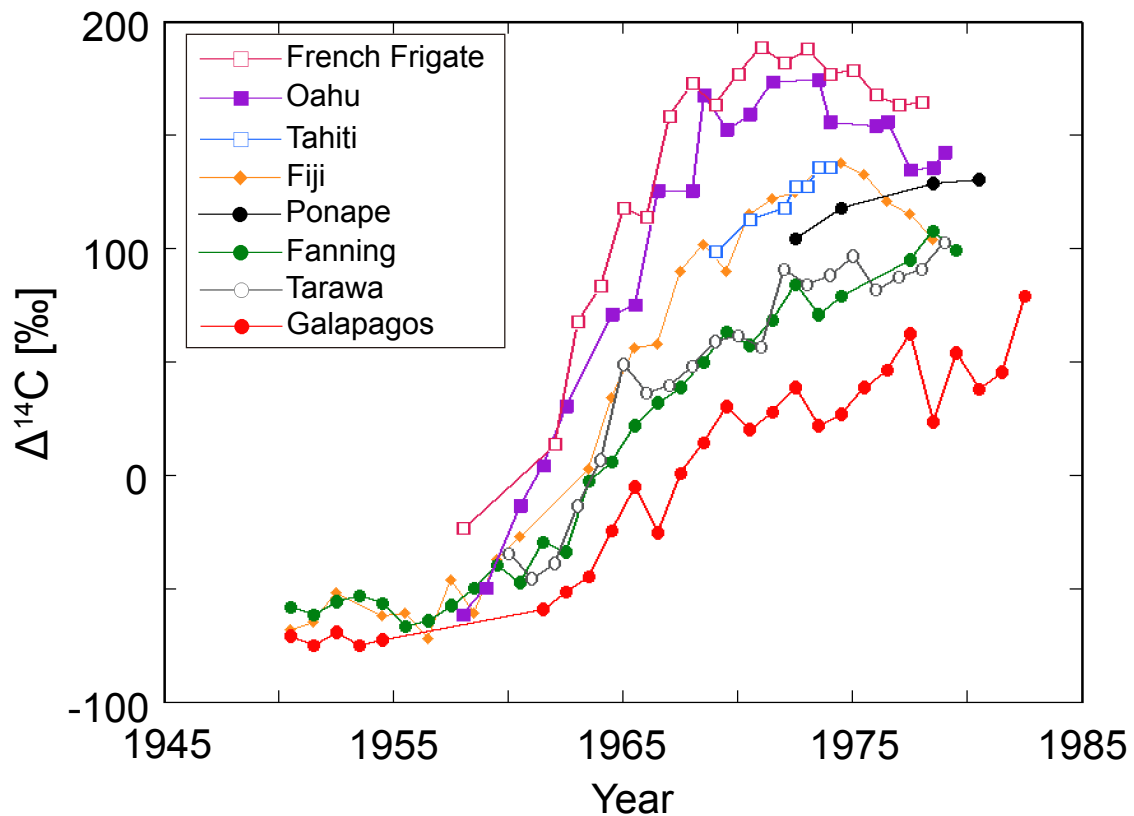


Figure 1.13 $\Delta^{14}\text{C}$ in Pacific corals from French Frigate Shoals (24°N; Druffel 1987), Oahu (21°N; Toggweiler, 1983), Tahiti (17°S; Druffel, 1987), Fiji (18°N; Toggweiler et al., 1991), Ponape (7°N; Konishi et al., 1981), Fanning (4°N; Druffel 1987), Tarawa (1°N; Toggweiler, 1983) and Galapagos (1°S; Druffel, 1981, 1987). There are 4 broad geographic areas in the Pacific based on the bomb curve, which is mainly reflected by the air-sea flux of CO_2 in Pacific as follows; 1) the area in the North Pacific equatorial gyre (Oahu and French Frigate Shoals) with the highest $\Delta^{14}\text{C}$ values, 2) the south Pacific equatorial gyre (Fiji, Tahiti) and the western tropical Pacific (Ponape) which is, the second highest $\Delta^{14}\text{C}$ values, 3) the tropical Pacific (Fanning and Tarawa) and 4) the eastern tropical Pacific (Galapagos), which is the center of intense upwelling in the equatorial east Pacific with the lowest $\Delta^{14}\text{C}$ values.

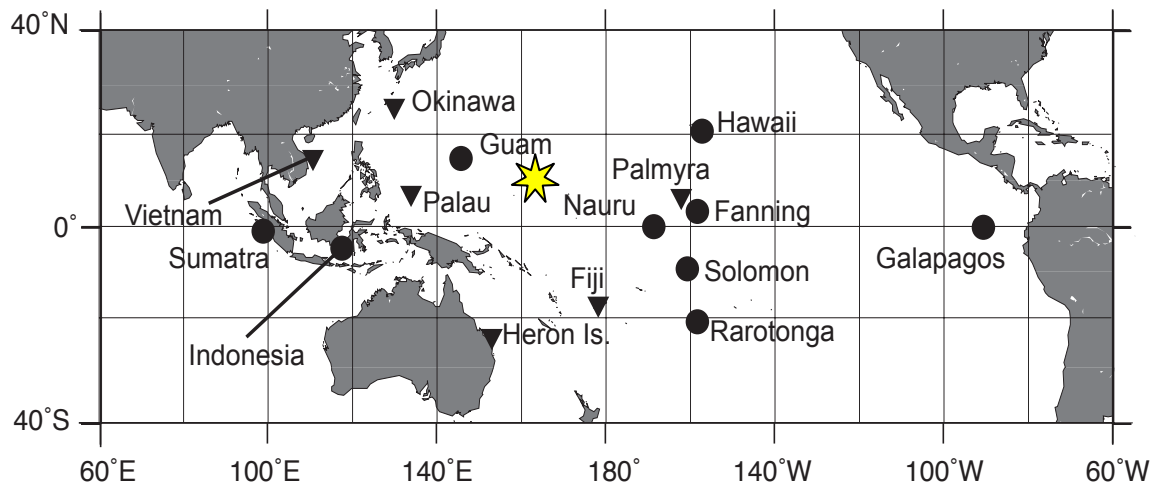
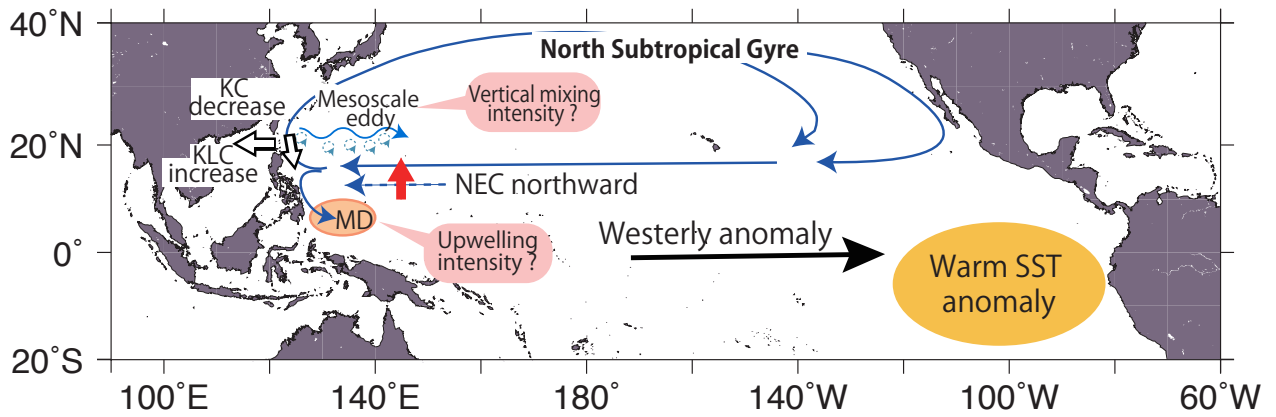


Figure 1.14 The map of coral skeletal radiocarbon reported previously in the Pacific. Triangle and circle symbols indicate the area of annual and seasonal data reported by previous studies, respectively. The yellow star is the location of the Pacific Proving Grounds. Seasonal data are limited in the central tropics, especially along the 150°E meridian and there are no seasonal data in the Kuroshio region.

(a) El Niño/Positive PDO phase



(b) La Niña/Negative PDO phase

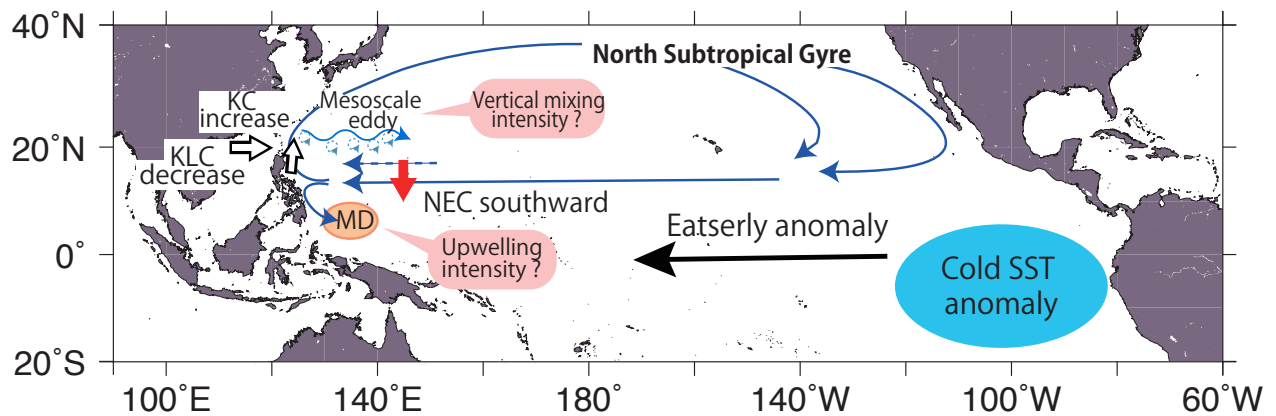


Figure 1.15 Schematic diagram of the relationship among the PDO/ENSO, North Equatorial Current (NEC) bifurcation latitude, Kuroshio (KC) and Kuroshio Loop Current (KLC). (a) When the El Niño/positive PDO phase, the intensified westerlies induces the northward shift of NEC bifurcation latitude, which causes of increased Kuroshio transport at the east off the Philippines and decreased KLC transport into the South China Sea. The warm SST anomaly along the Peru-Chile was occurred induced by the intensified westerlies, which indicates the weakened Peruvian upwelling. (b) When the La Niña/negative PDO phase, the weakened westerlies induces the southward shift of NEC bifurcation latitude, which causes of decreased Kuroshio transport at the east off the Philippines and increased KLC transport into the South China Sea. The cold SST anomaly along the Peru-Chile was occurred, which indicates the intensified Peruvian upwelling. The NEC bifurcation latitude would have influences on the mesoscale eddy activity in the KC region and intensity of the Mindanao Dome (MD) in the Mindanao Current region, but their detailed mechanism is not unclear because of the limited observation data.

1.5 Research aim and thesis structure

KC and MC have an important role in meridional distribution of the oceanic heat transport and affects the global climate change such as ENSO and PDO (Hanawa, 2005; Nakamura, 2016). Latif and Barnett (1994; 1996) proposed the feedback model that KC variability changes the heat transport from ocean to atmosphere in the mid-latitude of the north Pacific, which influences on the strength of Aleutian low, and then Aleutian low has an impact on the North Pacific subtropical gyre. However, this feedback have not supported by the observational data yet. The interaction between ocean heat transport variability and climate change such as PDO is also proposed by model simulation (Latif and Barnett, 1994; 1996). However, this is still under debate (Tani, 2010).

To reveal the detailed mechanism of KC variability, not only the KC itself but also the whole current dynamic of the northwest Pacific such as the NEC, MC, Kuroshio Loop Current, is needed to deepen our understanding. Additionally, many mesoscale eddies are generated in the KC area of the northwest Pacific. The activity of mesoscale eddies in the KC region and upwelling by Mindanao Dome in the MC region, affects the transport of heat content, salinity and nutrients, and varies the KC/MC transport and oceanic internal structure. Thus, we need to understand complex oceanic dynamics of the NEC-KC-MC current system and upwelling/vertical mixing in the northwest Pacific. However, the shipboard observations for the NEC, KC and MC is still limited, such as studies conducted in 1987-1988 by the United States-People's Republic of China Cooperative Studies of Air-Sea Interaction in the Tropical Western Pacific (US-PRC) (Toole et al., 1990) and in 2006 and 2008 by the R/V Mirai (Kashino et al., 2009). The oceanic data by satellite observation is limited to the sea surface, so that the ocean internal structure cannot be captured by satellite observation. Therefore, the northwest Pacific variability mechanism is still unclear due to the lack of long, continuous and high-resolution observation data.

Radiocarbon variability in the surface ocean reflects the water-mass mixing such as advection and upwelling. It is difficult to separate the different water masses by using satellite observation data. For example, the separation of the water mass of NEC and the Kuroshio recirculation, which joins the upstream of KC, is difficult based on the satellite observation data, and this is one of the reasons for poor understanding of KC

variability. Radiocarbon is a useful tracer for discussing such water mass mixing. The hermatypic coral takes the radiocarbon of the surface ocean into their skeleton. Therefore, radiocarbon in corals provides a continuous and reliable archive of oceanography, which can detect water mass changes such as advection and upwelling over a variety of timescales from seasonal to decadal. Analyzing high-resolution radiocarbon in multiple corals taken from the northwest Pacific makes it possible to reconstruct a continuous record of water mass mixing in the northwest Pacific, and discuss the relationships between oceanography and climate change. If this record can be compiled for the western Pacific, it will be possible to contribute to an understanding of the NEC-KC-MC system variability. However, because of the slow growth rates of corals in temperate regions such as those near the Japanese Islands, high-resolution radiocarbon dating has not previously been possible using corals in the Kuroshio region.

My objective in this thesis is to understand Kuroshio variability related to climate modes such as ENSO and PDO during the last 100 years based on high-resolution radiocarbon coral measurements. Reconstructed high-resolution coral skeletal radiocarbon records can contribute to the understanding of physical oceanographic changes and mesoscale eddy variability in the western Pacific related to the changing climate modes. I used multiple corals along the Kuroshio and Kuroshio Loop Current, and compared them with previously recorded data derived from corals located in the South China Sea, NEC and MC. Due to the lack of high-resolution radiocarbon data from the western boundary current, my new seasonal data from the Kuroshio and Kuroshio Loop Current will contribute to understanding the mechanism of the western Pacific variability compared with previously reported data from central tropical Pacific.

To achieve this research objective, I developed a new method for high-resolution age model determination and radiocarbon measurement with small-mass carbonates (Chapter 2). Using these new methods, I reported the seasonal scale of radiocarbon data from Ishigaki in the Kuroshio current and Currimaou in the Kuroshio Loop Current for the period after 1950 (Chapter 3) and pre-1950 (Chapter 4). I focused on the material transportation velocity by NEC and KC as an indicator of the North Pacific Subtropical gyre variability based on the bomb- ^{14}C advection recorded in corals taken from western Pacific (Chapter 3). I also discussed the water mass mixing among NEC, KC, MC, Kuroshio Loop Current, and vertical mixing by mesoscale eddies in the KC region and Mindanao Dome in the MC region based on the $\Delta^{14}\text{C}$ (Chapter 3) and

ΔR (Chapter 4) difference among the northwest Pacific and their relation to the NEC bifurcation latitude, which is believed to be an important index characterizing the surface ocean dynamics in the western boundary currents (Qiu and Lukas 1996; Qiu and Chen 2010) such as the velocity and transport behavior of the KC and MC (Hu et al., 2015). Finally, I provide the conclusions of this thesis and future work (Chapter 5).

**Chapter 2 The method for high-resolution age
model determination for coral skeletons**

2.1 Introduction

2.1.1 Purpose of this chapter

Growth-banded reef corals are widely distributed from tropical to subtropical seas. Corals incorporate a variety of isotopic and elemental tracers into their calcium carbonate (CaCO_3) skeletons with annual bands. Their records can span several centuries with high skeletal growth rates (usually ranging from 5 to 25 mm/year) (e.g. Grottooli and Eakin, 2007). Therefore, corals are rich archives of climatic changes with a high-resolution record of seasonal change such as sea-surface temperature (SST), in tropical and sub-tropical seas during the recent and distant past.

My aim in this chapter is to develop and demonstrate techniques to reconstruct Western Pacific oceanic variability. The biggest advantage for past climate reconstruction using coral skeletons is the reconstruction of paleoclimatic and paleoceanographic conditions on intra-annual to centennial timescales, which is usually difficult with other archives such as marine sediment cores and speleothems. To utilize this advantage, it is crucial to determine accurately a high-resolution age-model and to make accurate measurements for proxies with same time-resolution as the high-resolution age-model.

2.1.2 Problems of conventional methods

2.1.2.1 Age model

One of the ways to determine ages for corals is by counting annual bands in their skeletons using X-ray radiography. This is useful for tropical corals, which have constant growth rates. However, it is the possible cause of an incorrect age-model for subtropical corals because of slow growth rates and unclear annual bands in their skeletons. Thus, it is required to use some seasonal- or annual-cycle proxies in coral skeletons such as SST, which does not depend on coral vital effects, to determine accurate age-models. Proxy-based past sea surface temperature (SST) reconstructions commonly use trace elements or oxygen isotopes ($\delta^{18}\text{O}$) of annually-banded coral skeletons. However, previous studies reported that significant kinetic effects in skeletal

$\delta^{18}\text{O}$ due to slow-growth rates ($< 5 \text{ mm/yr}$) may confound environmental signals thereby hindering the use of temperate corals as reliable paleoceanographic recorders (e.g., McConnaughey, 1989; Allison et al., 1996; Felis et al., 2003; Fallon et al., 2003; Suzuki et al., 2005; Inoue et al., 2007) (Figure 2.1). Alternatively, environmental reconstructions may be accomplished using Sr/Ca ratios, which are, in theory, a “clean” temperature tracer because of stable seawater Sr/Ca proportions through time (de Villiers et al., 1995). A recent culturing study indicates that Sr/Ca ratios are a more reliable paleotemperature proxy, potentially producing accurate reconstructions from *Porites* corals, due to the insensitivity to temporal and inter-colonial variations in skeletal growth rate (Inoue et al., 2007; Hayashi et al., 2013) (Figures 2.2, 2.3). Testing these results requires environmental reconstruction from corals located along the periphery of their habitable range.

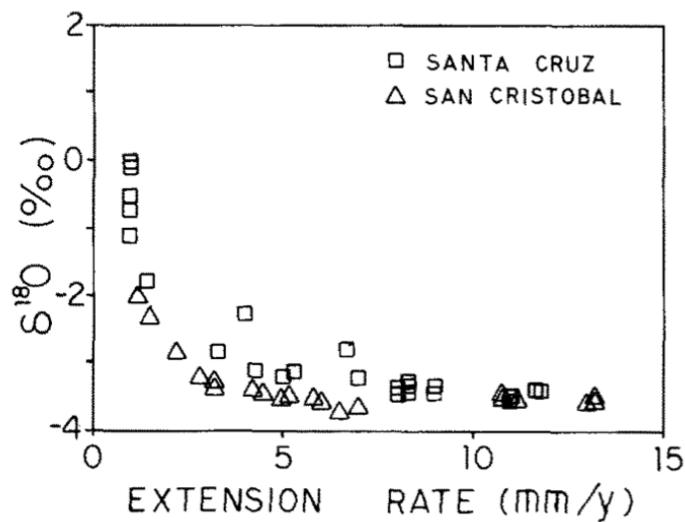


Figure 2.1 Relationship between the oxygen-isotope signal ($\delta^{18}\text{O}$) in corals and coral skeletal extension rate. From McConnaughey (1989).

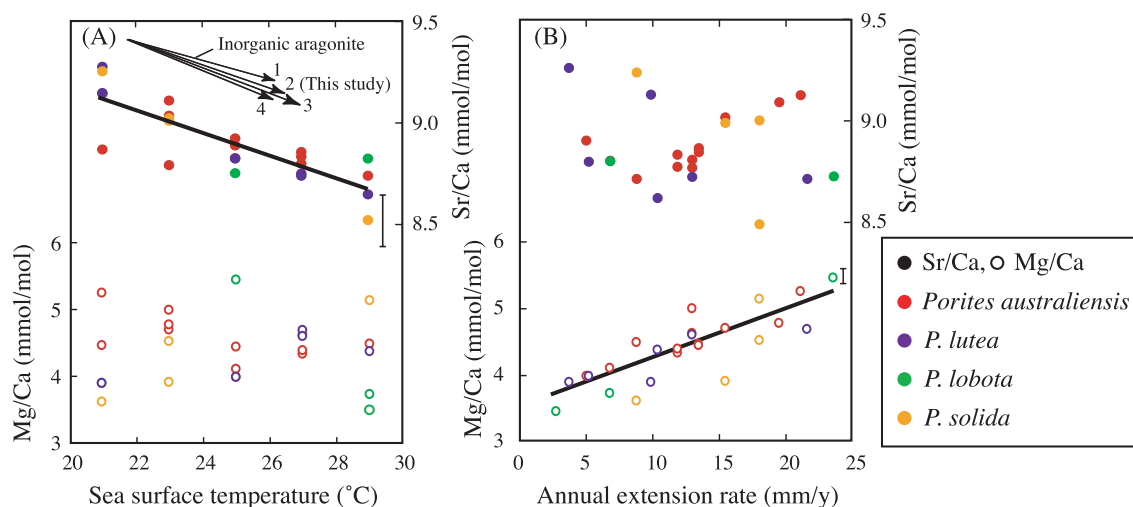


Figure 2.2 The relationship between cultured coral skeletal Sr/Ca and Mg/Ca ratio and (A) water temperature, (B) annual extension rate of their skeletons. The arrows shown in the upper part of figure (A) indicates the temperature dependency for inorganic aragonite precipitation and for the corals collected from the field. The positive correlation between annual extension rate and Mg/Ca is shown, while negligible correlation is shown for Sr/Ca. From Inoue et al. (2007).

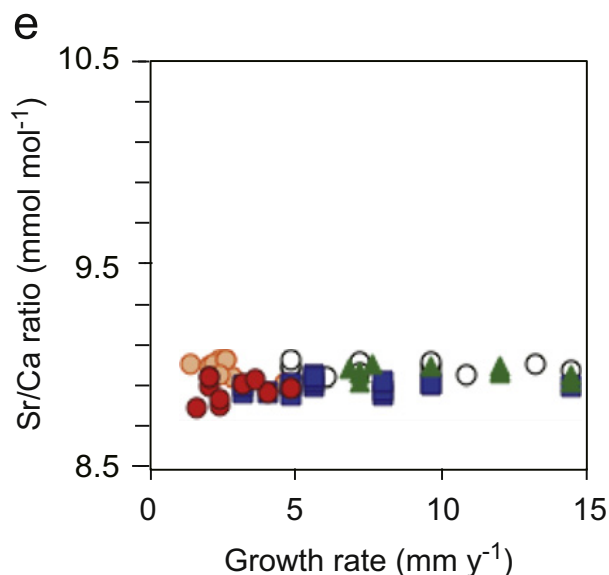


Figure 2.3 Coral growth-rate dependency of skeletal Sr/Ca ratio observed in laboratory culture experiments using five colonies of *Porites* spp. collected from Okinawa. From Hayashi et al. (2013).

2.1.2.2 Radiocarbon dating as an oceanographic tracer

The radiocarbon (^{14}C) composition of seawater is a reliable tracer of water mass advection and vertical mixing (Östlund and Stuiver, 1980; SCOR Working Group, 2007; Matsumoto and Yokoyama 2013). ^{14}C is naturally produced in the stratosphere when cosmic radiation interacts with nitrogen atoms. ^{14}C is also produced as a result of thermonuclear weapon explosions in the atmosphere in the late 1950s and early 1960s, which is so-called “bomb- ^{14}C ”. Because of the atmospheric nuclear bomb testing in the 1950s, atmospheric ^{14}C rapidly increased after 1955 and nearly doubled in the mid-1960s (Hua et al., 2013). ^{14}C in the atmosphere quickly oxidizes to become $^{14}\text{CO}_2$, which diffuses into the surface ocean through air–sea CO_2 exchange; the deep ocean is isolated from direct CO_2 exchange with the atmosphere. Therefore, bomb- ^{14}C in the coral skeletons is a sensitive proxy for water mass mixing if we can measure high-resolution radiocarbon contents in corals at a seasonal scale.

Coral skeletons, which are composed of CaCO_3 (aragonite), record the $\Delta^{14}\text{C}$ content in the surface ocean when they incorporate dissolved inorganic carbon from ambient seawater. After the atmospheric nuclear bomb testing in the 1950s, the $\Delta^{14}\text{C}$ in coral skeletons also increased because excess ^{14}C was absorbed from the atmosphere into the ocean surface through air–sea gas exchange. Because of the bomb- ^{14}C in the corals, their $\Delta^{14}\text{C}$ records can be used as a sensitive water-mass tracer and contribute to our understanding of ocean circulation, thereby improving ocean circulation models, especially in the post-bomb period. However, the sample-size for conventional radiocarbon dating of coral is more than 10 mg, while other proxies, for example SST proxies such as Sr/Ca ratio and $\delta^{18}\text{O}$, need only 100 μg . 10 mg of coral skeleton may equate to few years of growth, while 100 μg of corals represents a few weeks. This large amount of sample needed for radiocarbon measurement provides only the low-resolution reconstruction of ocean mixing (e.g. Konishi et al., 1981) even for the period after 1950. Reducing the sample-size required for high-resolution radiocarbon dating is a key priority.

2.2 Age model development

2.2.1 Methods for measurement of Sr/Ca and oxygen isotopes in temperate corals

Well-developed *Porites* colonies persist near the northerly limit of hermatypic corals at Ushibuka, Japan, in the Amakusanada, east of the East China Sea (32°N, 130°E) (Figure 2.4), where they experience large seasonal SST variations (the average amplitude is 11.7°C) and a winter minimum of approximately 14°C (Omata et al., 2006) (Figure 2.5). This results in very low growth rates at this location (Fallon et al., 1999), as compared to corals from similar latitudes in Bermuda (32°N) and Western Australia (29°S), the sites of the paleoceanographic mid-latitude hermatypic coral reconstructions reported to date, where winter temperatures remain above 18°C (Kuhnert et al., 1999, 2005). Here, I compare new, high-resolution Sr/Ca data, measured along the growth axes of *Porites* from Ushibuka, to previously published $\delta^{18}\text{O}$ data from the same specimens (Omata et al., 2006).

Specimens were collected on 16 September 1993 from a *Porites* colony at a depth of about 15 m in Ushibuka (32°1.8'N, 130°16'E) located slightly south of the northern limit of the coral reef at Iki Island, Japan (33°48'N; Yamano et al., 2001) and at a similar latitude as Shirigai Bay, Japan (32°N; Fallon et al., 1999). The nearest instrumental SST record is from Ushibuka Bay (32°12'N, 130°02'E), 4–5 km southeast of the sampling site, where average SST from 1964 to 1993 was 20.1°C and ranged from 12.2 to 28.4 °C. Winter SST at Ushibuka remains below the previously reported potential thermal limit of hermatypic corals (Omata et al., 2006).

Omata et al. (2006) performed microsampling of this coral for $\delta^{18}\text{O}$ analyses at 0.2 mm intervals along the growth axis of the recovered specimens. The internal precision of the mass spectrometer was 0.04‰ for $\delta^{18}\text{O}$, based on replicate measurements of the NBS-19 calcite standard (Omata et al., 2006). For Sr/Ca analyses by ICP-AES, I dissolved ~100 μg aliquots of the same powdered sample in 5 ml of 2% HNO_3 (Suzuki et al., 2003) and standard solutions prepared from JCp-1 (Okai et al., 2004) were measured after every third sample measurement. The relative standard deviation (RSD) based on replicate measurements of JCp-1 was 0.4% (see also Mishima et al., 2009). The reproducibility by measuring JCp-1 every 12 sample measurements

was 8.72 ± 0.066 mmol/mol (2 SD, $n = 46$), which agreed well with the reference value of 8.72 reported in Okai et al. (2004).

Following Omata et al. (2006), our age model is based on linear interpolation between peak seasonal environmental proxy values, in this case Sr/Ca. Annual averages and seasonal amplitude (differences from previous winter/summer to next summer/winter) were calculated for Sr/Ca and $\delta^{18}\text{O}$.

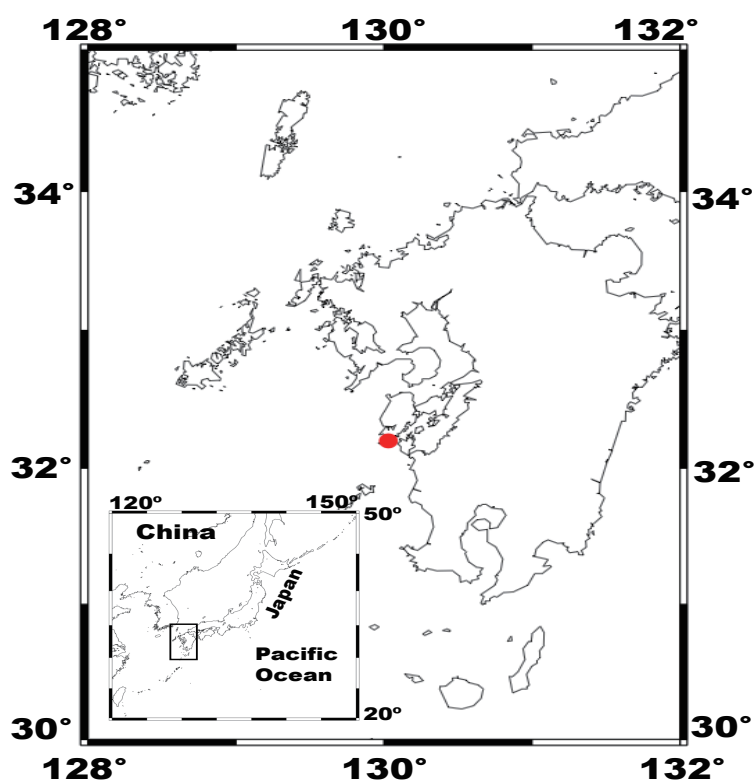


Figure 2.4 The location of Ushibuka, Kumamoto. Map modified from Hirabayashi et al. (2013).

2.2.2 Results and discussion for Sr/Ca and oxygen isotopes in the temperate coral

Based on our age model, this record spans the period from 1964 to 1993. Coral skeletal Sr/Ca exhibits distinct seasonality, with minimum (summer) and maximum (winter) values ranging from 8.71 mmol/mol to 9.86 mmol/mol, and a mean of 9.28 mmol/mol (Figure 2.5D). Growth rates averaged between seasonal layers range between 0.2 to 5.4 mm/6 months, with a mean value of 2.8 mm/6 months and a period of exceptionally small growth from February 1968 to August 1970 (Figure 2.5B). Annually averaged Sr/Ca and $\delta^{18}\text{O}$, as well as seasonal amplitude of Sr/Ca, exhibit no correlation to growth rate (Figure 2.6). The seasonal amplitude of $\delta^{18}\text{O}$ is significantly correlated with growth rate for values <5 mm/yr ($R^2 = 0.48$, $p \ll 0.01$) (Figure 2.6A).

My field results indicating insensitivity of Sr/Ca to changes in growth rate confirm conclusions of previous culture experiments (Inoue et al., 2007). My reanalysis of previously published $\delta^{18}\text{O}$ data (Omata et al., 2006) is also consistent with previous work suggesting a strong dependence on growth rate when extension is below 5 mm/yr (McConnaughey, 1989; Felis et al., 2003; Suzuki et al., 2005) (Figure 2.6A). There is no relationship between annually-average Sr/Ca ratios and annual growth rate (Figure 2.6B), suggesting that Sr/Ca can be utilized as a SST proxy as it is not influenced by growth rate changes. While there is a similar relationship for $\delta^{18}\text{O}$ (Figure 2.6C), the amplitude of $\delta^{18}\text{O}$ variations are positively correlated with growth rate, indicating that it is not entirely independent, whereas the amplitude of Sr/Ca variations exhibit no relationship to growth rate (Figure 2.6A). Thus I can conclude that the Sr/Ca thermometer is more robust for SST than $\delta^{18}\text{O}$, as was also reported previously (Hayashi et al., 2013).

This dependence on growth rate is especially apparent between 1968 and 1969, during which skeletal extension was exceptionally small (Figure 2.5 B, 2.5D). Over this period, the instrumental summer SSTs were in excess of 27 °C, with typical seasonal amplitude, but winter SSTs were below average (Figure 2.5C). While persistent seasonality that tracks SST is recognized in Sr/Ca, none is observed in $\delta^{18}\text{O}$, which instead highly reflects the low growth rates. I interpret this to indicate that $\delta^{18}\text{O}$ is affected by the low growth rate resulting from anomalously cold winter SST. Though

the Sr/Ca summer value for 1969 is relatively depressed, seasonality is still readily identified, suggesting Sr/Ca is impacted minimally by growth rate variations.

This growth rate dependency of $\delta^{18}\text{O}$ is related to the growth rate-related kinetic isotope disequilibrium effects proposed by McConnaughey (1989) (Figure 2.1). The kinetic fractionation of $\delta^{18}\text{O}$ happens during coral skeletal calcification in the calcifying fluid. Rapid skeletal growth rates induce strong kinetic effects in the calcifying fluid, but when the growth rate is more than ~ 5 mm/year, $\delta^{18}\text{O}$ becomes constant, independent of the growth rate (Figure 2.1). Therefore, we should use corals whose skeletal growth rate is more than 5 mm/year when we reconstruct SST based on coral skeletal $\delta^{18}\text{O}$. When the coral growth rate is less than 5 mm/year, $\delta^{18}\text{O}$ in the coral skeleton fluctuates because of both kinetic isotope disequilibrium effects and the $\delta^{18}\text{O}$ of ambient seawater. For the mechanism of Sr/Ca ratio, Sr^{2+} and Ca^{2+} in ambient sea water are incorporated into the coral skeletal fluid by the pump enzyme (Ca^{2+} -ATPase) at the same time. According to the coral mineralization by Wang and Xu (2001) and Inoue et al. (2007), the metal partition coefficients (K_d) of Sr^{2+} is very close to that of the host cation, Ca^{2+} . Because of similar K_d , the Sr/Ca ratio is less affected by the growth-rate-related kinetic effects (Inoue et al., 2007). Additionally, the $\delta^{18}\text{O}$ of the coral skeleton might be heavily dependent on the coral's health, while the Sr/Ca ratio is less affected (Hayashi et al., 2013). Therefore, the $\delta^{18}\text{O}$ of this Ushibuka coral could not record a clear seasonal cycle of SST during the low growth rate period from February 1968 to August 1970, while the Sr/Ca ratio could show a clear seasonality, although the amplitude of Sr/Ca variability was attenuated (Figure 2.5).

There are two intervals that do not exhibit these relationships. According to the instrumental record, the SST during the winter of 1976 was particularly cold yet $\delta^{18}\text{O}$ exhibits typical seasonal variability. This is likely because the 1976 to 1977 annual growth rate remained well above >5 mm/yr. Neither $\delta^{18}\text{O}$ nor Sr/Ca appear to capture the SST minima, which may be due to the cessation of growth that winter (Fallon et al., 1999). Omata et al. (2006) noted that the annual growth rate was below average from 1984 to 1987, during which the average annual minimum SST was not exceptionally cold. Thus, the anomalously low growth rate of 1985 appears to be in response to factors other than SST, such as local environmental stress perhaps making the coral more susceptible to bioerosion. In spite of the slow growth rate during this period,

seasonal variability in $\delta^{18}\text{O}$ is clearly observed that the combination of cold winter SST and slow growth rate (<5 mm/yr) together may result in depressed $\delta^{18}\text{O}$ amplitude.

The Sr/Ca-sea surface temperature sensitivity determined using the Ushibuka coral (Figure 2.7b; Table 2.1) is within the range compiled from published tropical coral SST reconstructions (Corrège, 2006), indicating that Sr/Ca based SST reconstructions provide a reliable record from low-growth rate corals from temperate regions. I calculated the $\delta^{18}\text{O}$ -SST sensitivity in two ways, using all $\delta^{18}\text{O}$ data and only high-growth (> 5mm/yr) coral data. Both sensitivities are within the range of values reported by Gagan et al. (2012) (Figure 2.7a; Table 2.1). However, $\delta^{18}\text{O}$ from high-growth intervals is more highly correlated with SST than that of low-growth intervals, indicating growth-rate dependent sensitivity in $\delta^{18}\text{O}$. Conversely, Sr/Ca sensitivity is independent of growth rate making it a more robust environmental indicator in low-growth corals.

Sr/Ca sensitivity is independent of growth rate making it a more robust environmental indicator in low-growth corals. Sr/Ca ratios have a clear seasonality and independence of vital effects such as slow growth rates of their coral skeletons. For sampled living corals, we know the date of corals' outer surface at the time of field collection. Thus, we measure the Sr/Ca ratio of coral skeletons and counting summer and winter peaks from the top of coral skeletons, we can precisely create an age model with seasonal resolution even for the slow growth rate affected by low SST events in the past. Therefore, the Sr/Ca ratio is a suitable proxy for the age model, and comparison with annual bands from X-ray radiographs makes a high-resolution and accurate age-model possible.

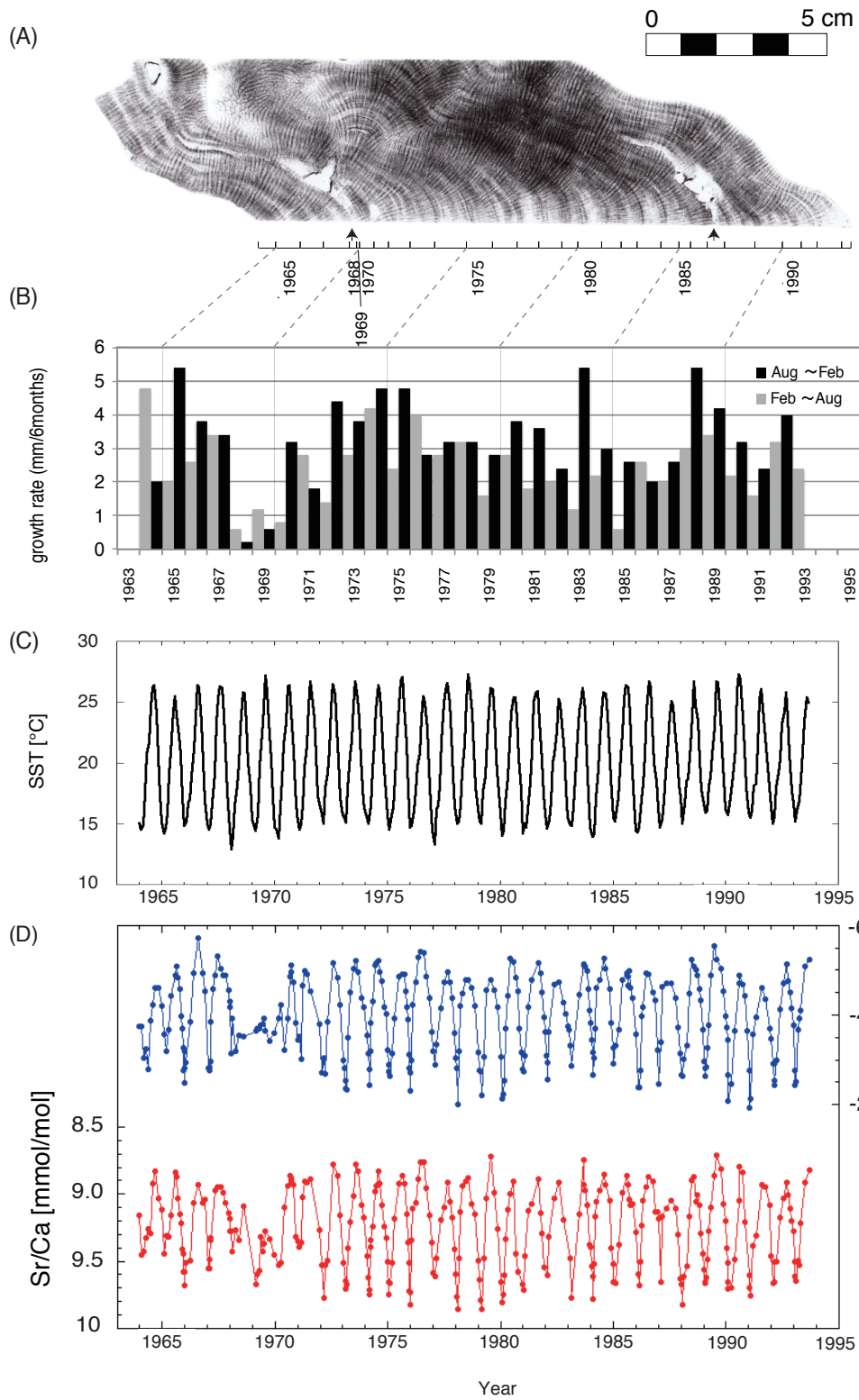


Figure 2.5 (A) X-ray radiograph of the coral specimen from Ushibuka (Omata et al., 2006). (B) Linear growth rate of *Porites* coral examined in this study. Linear growth rates were calculated based on the distance between maximum and minimum in Sr/Ca. (C) Ten-day average SST at Ushibuka (32°12'N, 130°02'E) based on the monthly reports of the Japan Meteorological Agency. (D) $\delta^{18}\text{O}$ (blue, Omata et al., 2006) and Sr/Ca (red) of *Porites* versus time over the period from 1964 to 1993. From Hirabayashi et al. (2013).

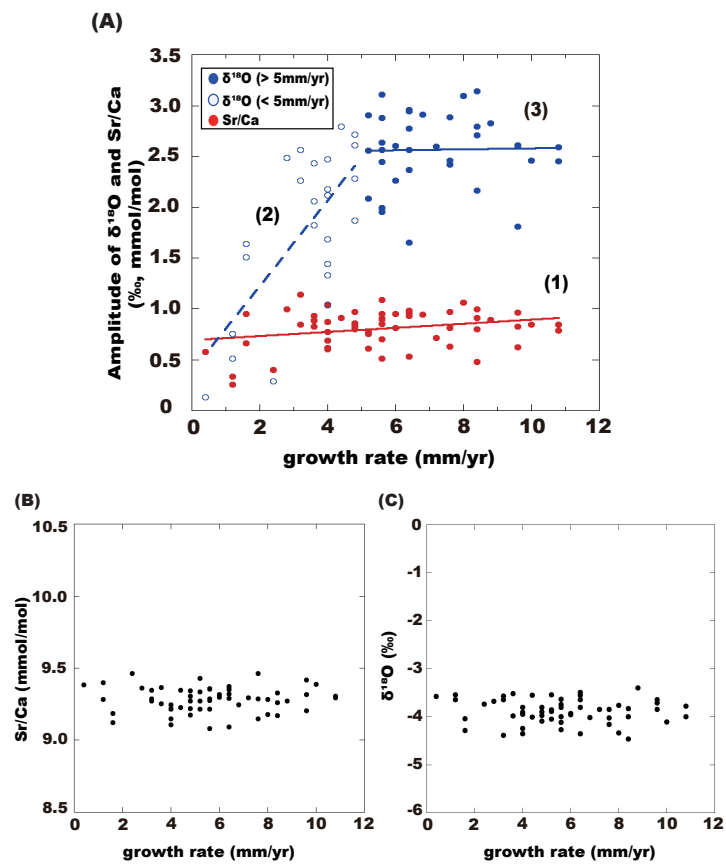


Figure 2.6 (A) The relationship of growth rate and $\delta^{18}\text{O}$ amplitude (blue filled circles (>5 mm/yr) and blue open circles (<5 mm/yr) (Omata et al., 2006)) and Sr/Ca (red). In this figure, the formula obtained for the Sr/Ca-growth rate relationship was (1) $\text{Sr/Ca} = 0.691 + 0.0407 \times \text{growth rate}$ ($R^2 = 0.07$, $p = 0.03$). For $\delta^{18}\text{O}$, the relationships were (2) $\delta^{18}\text{O}$ (<5 mm/yr) = $0.389 + 0.841 \times \text{growth rate}$ ($R^2 = 0.48$, $p \ll 0.01$) and (3) $\delta^{18}\text{O}$ (>5 mm/yr) = $2.53 + 0.0102 \times \text{growth rate}$ ($R^2 = 0.0005$, $p = 0.92$). (B) The relationship of growth rate and annual average of Sr/Ca. (C) The relationship of growth rate and annual average $\delta^{18}\text{O}$ (Omata et al., 2006). From Hirabayashi et al. (2013).

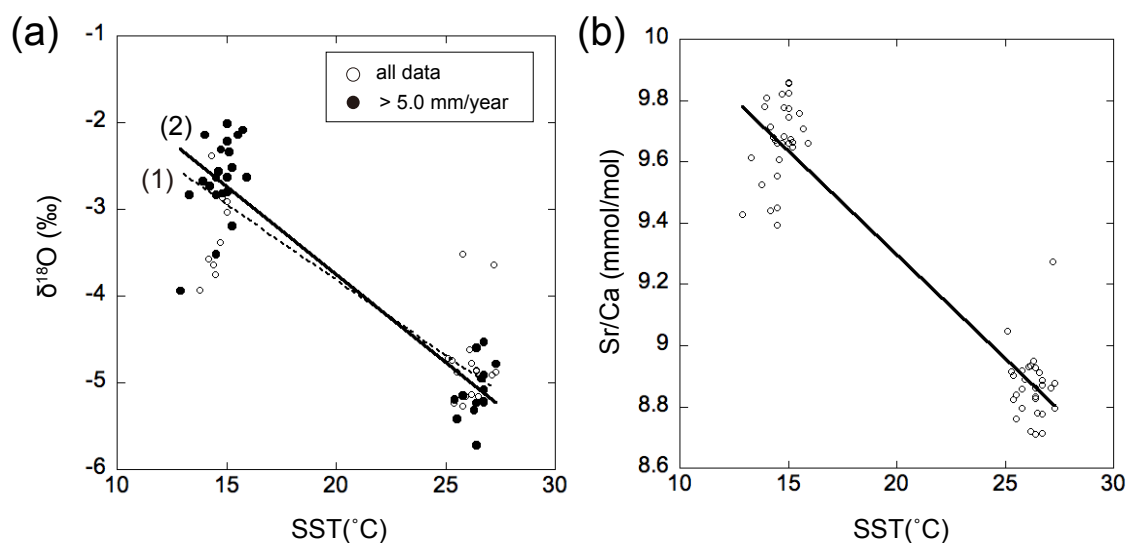


Figure 2.7 The $\delta^{18}\text{O}$ -SST sensitivity (a) and Sr/Ca-SST sensitivity (b) determined using the Ushibuka coral (USB93). I calculated the $\delta^{18}\text{O}$ -SST sensitivity in two ways, using all data (open circles and dashed regression line (1)) and only high-growth (>5 mm/yr) coral data (filled circles and solid regression line (2)). The detailed values of both sensitivities are shown in the Table 2.1.

Table 2.1 Summary of the Sr/Ca and $\delta^{18}\text{O}$ vs. SST calibrations

	Reference	a	b	R^2
Sr/Ca-temperature sensitivity	Corrège et al. (2006)	10.553	-0.0607	
	Our Study	10.641	-0.0668	0.90
$\delta^{18}\text{O}$ -temperature sensitivity	Gagan et al. (2012)		-0.167 ± 0.028	
	Our study (all data)	-0.305	-0.1746	0.78
	Our study (> 5mm/yr)	0.306	-0.2027	0.85

Note: Calibrations are of the type: $\text{Sr/Ca (mmol/mol)} = a + b \times \text{SST (}^\circ\text{C)}$ and $\delta^{18}\text{O (}\text{‰}) = a + b \times \text{SST (}^\circ\text{C)}$. R^2 is the correlation coefficient. All corrections of my study is significant with $p < 0.05$.

2.3 Method development for high-resolution radiocarbon measurement

2.3.1 Method for Radiocarbon dating

Our graphitization procedure consisted of 4 steps: (1) sample CO₂ gas production by dissolution with phosphoric acid (H₃PO₄); (2) purification of the gas in vacuum lines via a series of cryogenic traps; (3) reduction to solid graphite; and (4) Accelerator Mass Spectrometry (AMS) analysis (Yokoyama et al., 2007). The standard sample IAEA-C1 (Marble, ¹⁴C activity (pMC) = 0 ± 0.02 %) (Rozanski, 1991) was used for evaluating the secondary contamination during preparation of the carbonate samples for the radiocarbon dating. Firstly, I checked the contamination level with the conventional method for radiocarbon dating with the sample amount for 1000, 750, 500, 250 and 100 µg. Exact procedures varied according to the requirements of the sample and are detailed as follows.

(1) Sample CO₂ gas production by dissolution with phosphoric acid (H₃PO₄)

Carbonate samples were dissolved with 85% phosphoric acid (H₃PO₄) to produce CO₂ in a vacuum test tube. In our conventional method, we use blood-collecting vessels as a vacuum test tube. Samples were placed in the tube and evacuated using a needle attached to the vacuum line system. The tube is then placed in the heat block (80 °C) with phosphoric acid introduced through an air-tight cylinder. The tube is removed from the heat block when the sample dissolution is complete. The product CO₂ is passed through the vacuum line via a needle attached to the vacuum line system.

For the new method for small mass carbonate samples, I newly designed one end of a two-pronged tube as a vacuum test tube instead of a blood-collecting vessel (Figure 2.8). I tested the length, position and volume of the pronged tube many times to check which shape of one end of a two-pronged tube would be suitable for preparation of small-mass carbonate sample. Before using this new tube, it is cleaned with HCl acid or acetone and baked in the oven to remove potential contaminants. Samples were weighed into inert silver capsules and inserted into one end of a two-pronged tube with 1 cm³ of phosphoric acid in the other prong. The tubes were then evacuated by insertion

into a vacuum line before the acid was allowed to mix with the sample powder. Tubes were immersed in a water bath at 80 °C for approximately 20 minutes in order to complete sample dissolution, then loaded into the graphitization line.

(2) Purification of the gas in vacuum lines via a series of cryogenic traps

The product CO₂ is passed through the vacuum line via a needle attached to the vacuum line system in the conventional method and via Swagelok Ultra-Torr type vacuum fitting for the new method. Cryogenic purification of gaseous samples involved the removal of water vapor and any non-condensable gases with a trap comprising a mixture of ethanol and liquid nitrogen at -100 °C, and collection of solid CO₂ with a trap of pure liquid nitrogen at -196 °C.

(3) Reduction to solid graphite

The gas is reduced in the graphitization reactor with Fe catalyst under a hydrogen atmosphere. Fe catalyst affects the efficiency of graphitization, and the pre-heating process of the Fe catalyst before sample processing can be reduced the contamination level (Santos et al., 2007). In the conventional method, we used Fe catalyst (Merck, 250 mesh grain size) which was reduced at 450 °C for 1 hour before sample processing. For the new method, Fe catalyst (Aldrich, 325 mesh grain size) was used instead of Merck Fe powder and which was reduced at 650 °C for 3 hours before sample processing (pre-heating). Pressure in each graphitization cell was inspected to ensure that the reaction went to completion.

(4) Accelerator Mass Spectrometry (AMS) analysis

Finally, the graphite is pressed into target holders and analyzed using a Single-stage Accelerator Mass Spectrometer (AMS). Before 2013, the target was analyzed at Department of Nuclear Engineering and Management, University of Tokyo using AMS (MALT; Micro Analysis Laboratory, Tandem accelerator, The University of Tokyo). The MALT accelerator is a 5UD Pelletron™ tandem van de Graaf (produced by National Electrostatics Corporation, USA) and maximum 5 MV voltage is available (Matsuzaki et al., 2007).

A single stage AMS (YSAMS) from the National Electrostatics Corporation was installed at the Atmosphere and Ocean Research Institute at the University of

Tokyo in 2013. The stripper, analyzing magnet, 90° electrostatic analyzer (ESA) and detector are all mounted on a 250 kV high-voltage platform in air. In the ion source, we can put the 40 samples in the graphite target holder called disk, and measure them at the same time rotating the disk every 6 minutes per 1 sample. I also developed the method for high-resolution radiocarbon measurements using small-mass carbonate samples with this new machine.

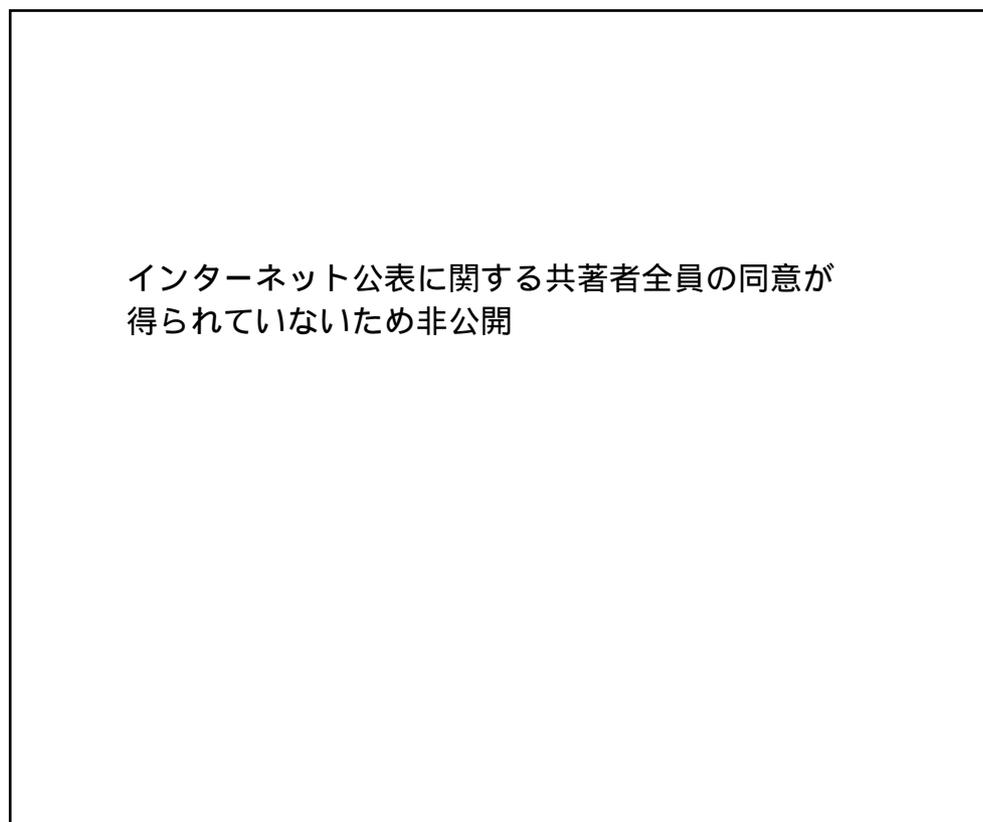


Figure 2.8 The two types of vacuum test tubes, blood-collecting vessel and one end of a two-pronged tube.

2.3.2 Results and discussions

2.3.2.1 Improvements for the preparation of small-mass radiocarbon measurements

2.3.2.1.1 Possibility of sample CO₂ gas production by dissolution with phosphoric acid (H₃PO₄) with conventional and new methods as of August 2012

I compared the conventional method using blood-collecting vessels with the new method using one end of a two-pronged tube to check the possibility for preparation of small-mass carbonate ¹⁴C measurements. My results showed that samples less than 500 µg with blood-collecting vessels did not become graphite and it was impossible to measure them, while the samples less than 500 µg prepared with one end of a two-pronged tube became graphite and could be measured with AMS. This result suggest that it is suitable to use one end of a two-pronged tube for preparation of a small-mass carbonate ¹⁴C measurement because of higher CO₂ recovery rates than that from the blood-collecting vessels (Figure 2.9). This is because the conductance of one end of a two-pronged tube between the graphitization line and vacuum test tube is better than that of a blood-collecting vessel. However, the contamination of modern carbon was still high even when I used one end of a two-pronged tube for preparation as of August 2012 (Figure 2.10). The relationship between ¹³C current value and contamination level also showed that the higher ¹³C current made the lower contamination level and vice versa (Figure 2.11). One reason for the high contamination level was that PCTFE (polychlorotrifluoroethylene) rings of the graphitization cell became loose and outer air intruded into the graphitization cells during the heating from the graphitization reaction. The PCTFE is weak to high temperature so that some of PCTFE rings had thermal deformation after finishing the heating. Therefore, I changed those parts to PEEK (Poly Ether Ether Ketone) rings, which have heat-resisting properties. Also, I spread ultra-high vacuum grease (Apiezon, L grease) on the O-rings of the inside valve of the vacuum line every time to avoid air contamination, and keep the high vacuum pressure in the graphitization cells. Another possible reason for the high contamination level was the cleaning protocol of the tubes before preparation.

Thus, I also checked the contamination level for several different ways of cleaning the tubes (see below 2.3.2.1.3). Additionally, I also reconsidered which Fe catalyst would provide a high efficiency of graphitization and the method of pre-heating of Fe catalyst to reduce contamination (see below 2.3.2.1.2).

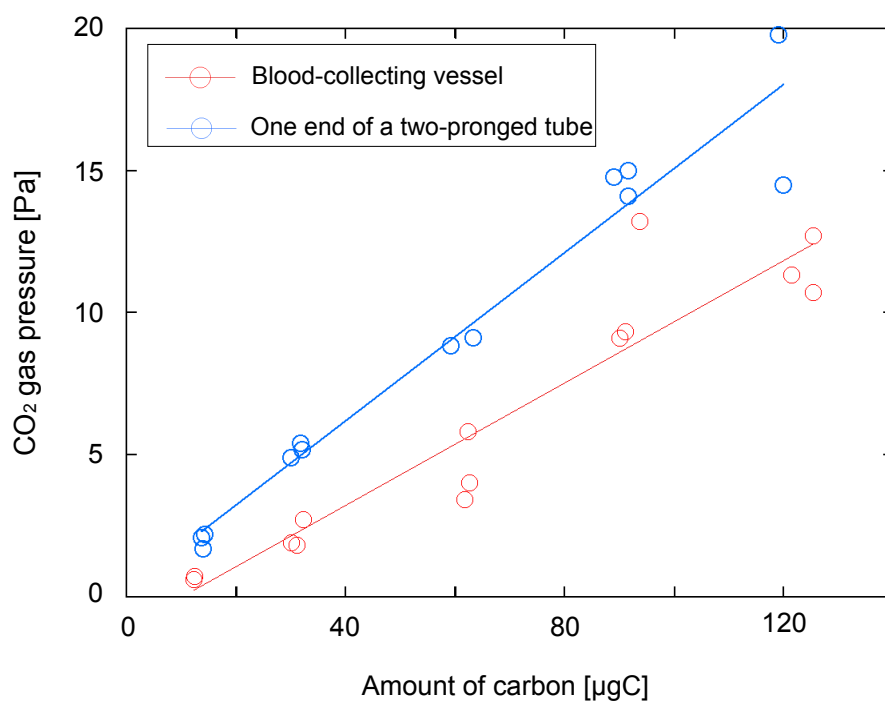


Figure 2.9 CO₂ gas pressure introduced to the vacuum line from the blood-collecting vessels (red) and one end of a two-pronged tubes (blue).

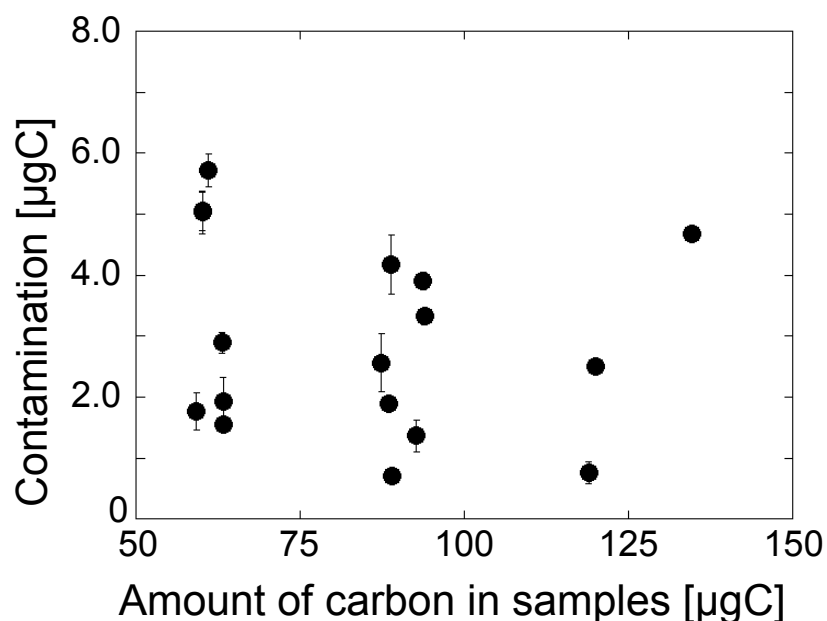


Figure 2.10 The contamination level with the conventional method of preparation using small-mass carbonate samples (IAEA-C1) in 2012.

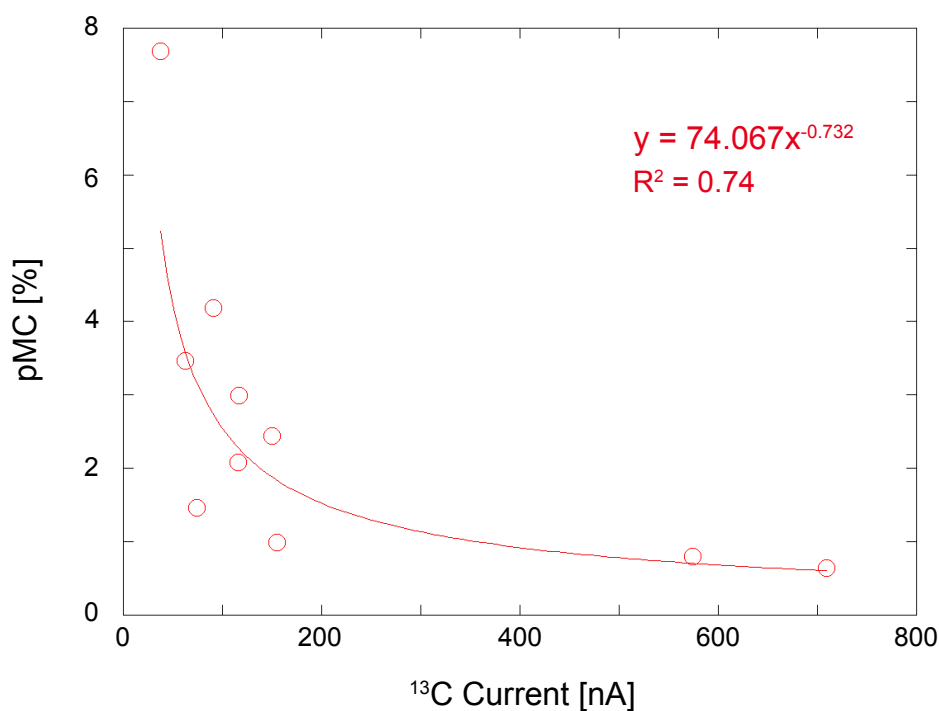


Figure 2.11 The relationship between ¹³C current intensity and contamination level. In this measurement, the standard material of IAEA-C1 (¹⁴C activity (pMC) = 0 %) was used. Uncontaminated values should be pMC = 0, but because of the contamination during the preparation for graphitization, higher values were obtained in 2012.

2.3.2.1.2 Further evaluation of Fe catalyst for purification of the gas in vacuum lines

When I performed the experiment of 2.3.2.1.1, I used Fe powder from Merck (particle size = 10 μm , 99.5%) as Fe catalyst, which is the conventional method in our lab. According to Santos et al. (2007), C beam currents with a catalyst of Sigma-Aldrich Fe powder yields a high current and makes the pressing procedure easier, without substantially affecting the C beam current intensity and background levels (Santos et al., 2007). The surface of the Fe powder is different between Merck and Aldrich powder products (Santos et al. 2007), and those characteristic affects the homogeneity of the mixture of Fe catalyst and carbon, and minimal contamination. I followed Santos et al. (2007) and checked the efficiency of Sigma-Aldrich-325 mesh as a Fe catalyst and compared with Merck Fe powder using one end of a two-pronged tube. The results showed that the success rate of graphitization using Merck was lower than that of Sigma-Aldrich (Figure 2.12). The averaged current using Merck was 133.0 ± 23 nA, which was lower than that of Sigma-Aldrich, 186.4 ± 104.2 nA, with 500 μg sample amount. This result suggested that Sigma-Aldrich product provides enough current intensity for ^{14}C measurement due to the optimal surface condition such as the homogeneity and less sintering of the mixture of carbon and Fe catalyst (Santos et al., 2007). Thus, the Sigma-Aldrich Fe catalyst is suitable for small-mass ^{14}C measurement and was therefore utilized as a catalyst for ^{14}C analysis with corals in Chapter 3 and Chapter 4. However, the stability of the current and the contamination level was still not sufficient in November 2012.

Additionally, I evaluated the pre-heating method for reduction of Fe catalyst (Aldrich) before sample processing to reduce carbon contamination. I compared the conventional reduction method as 450 $^{\circ}\text{C}$ for 1 hour with the new method as 650 $^{\circ}\text{C}$ for 3 hours before sample processing using IAEA-C1. The results showed that the pre-heating at 650 $^{\circ}\text{C}$ for 3 hours (averaged amount of contamination = 0.52 ± 0.21 μgC) was better method for remove contamination than that at 450 $^{\circ}\text{C}$ for 1 hour (averaged amount of contamination = 0.76 ± 0.15 μgC) (Figure 2.13). However, the contamination level with the new pre-heating method was not stable and sufficient for the measurement of small-mass radiocarbon measurement due to other problems for cleaning method such as procedure of the one end of a two-pronged tube. In this

evaluation, I cleaned the one end of a two-pronged tube using acetone. Therefore, farther improvement for reduction of contamination level was needed (see 2.3.2.1.3).

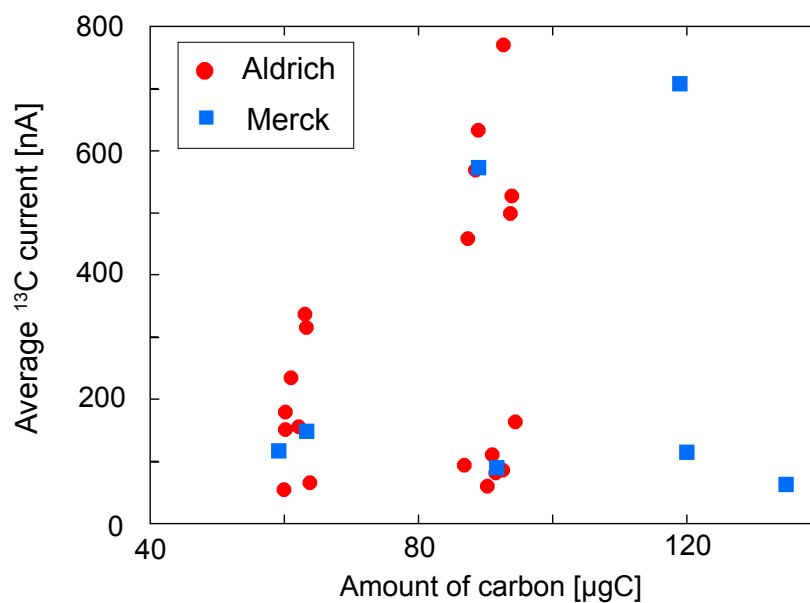


Figure 2.12 Average ¹³C current beam intensity during AMS measurement using samples graphitized with Fe catalyst from Aldrich (red) and Merck (blue) iron powder in November 2012. Samples with the Aldrich Fe catalyst had larger ¹³C current intensities than those utilizing the Merck product, although the stability of ¹³C current beam was to be improved.

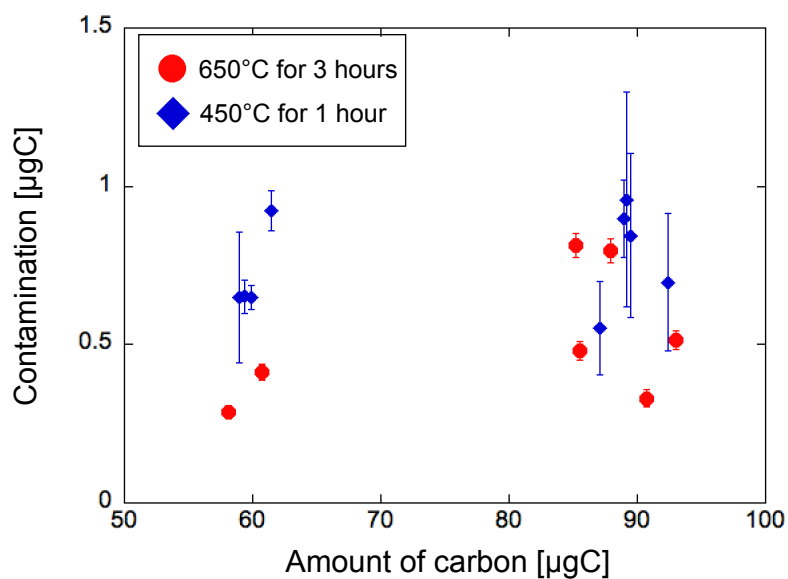


Figure 2.13 The contamination level with the conventional method of pre-heating (450 °C for 1 hour) and the new method (650 °C for 3 hour) using small-mass carbonate samples (IAEA-C1). It shows that higher contamination with the method of pre-heating at 450 °C for 1 hour than that with the new method (650 °C for 3 hour), although further improved for the lower contamination was required.

2.3.2.1.3 Cleaning procedure of the one end of a two-pronged tube

One end of a two-pronged tube is made of glass and reusable for preparation. I checked several ways of cleaning this as follows; 1) cleaning tubes with acetone in the ultra-sonic bath and baking them in a oven at 450 °C for 1 hour, 2) soaking them in HCl overnight and rinsing them with ultrapure water in the ultra sonic bath and 3) baking them in oven after procedure 2. The temperature and length of baking after cleaning with HCl was a) 450 °C for 1 hour, b) 450 °C for 5 hours, and c) 300 °C for 5 hours. The results showed that the contamination level was lowest when cleaned them with HCl and baked at 450 °C for 5 hours (Table 2.2; Figure 2.14). The backing temperature at 450 °C is almost the upper limit of the melting point for one end of a two-pronged tube. Hydrochloric acid eliminates inorganic matter and the backing process eliminates organic carbon. The combined cleaning procedure of soaking HCl and baking in an oven with the high temperature can eliminate both organic and inorganic matters sufficiently so that the contamination level was reduced.

Therefore, ^{14}C measurement with small-mass carbonate samples (less than 500 μg) can be done using one end of a two-pronged tube cleaned with HCl and baked for 5 hours, and graphitized with Sigma-Aldrich Fe powder pre-heated at 650 °C for 3 hours as the Fe catalyst, and which is almost the same sample amount as needed for a Sr/Ca ratio measurement. Combination of these improvements allows the small-mass carbonate of 500 μg to be measured with the precision of a 0.07%.

Table 2.2 The amount of contamination for cleaning procedures of cleaning of one end of a two-pronged tubes

	Contamination (μgC)	\pm
Washed with acetone and baked for 1 hour at 450°C	0.54	0.14
Washed with HCl	0.36	0.06
Washed with HCl and baked for 1 hour at 450°C	0.32	0.02
Washed with HCl and baked for 5 hour at 300°C	0.30	0.03
Washed with HCl and baked for 5 hour at 450°C	0.29	0.02

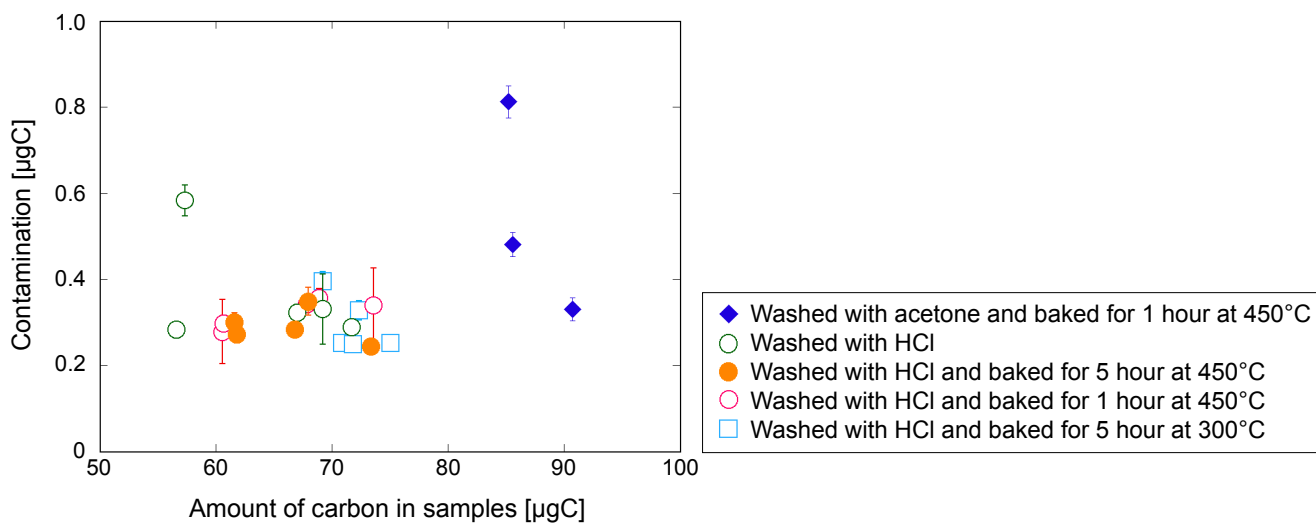


Figure 2.14 Contamination level variability with several cleaning procedures of one end of a two-pronged tube using acetone and HCl. The contamination levels are shown in Table 2.1.

2.3.2.2 Method development using single-stage Accelerator Mass Spectrometry

I was involved in the development of the new single stage AMS (YSAMS) installed in 2013, which is the only single stage AMS in Japan. The single stage AMS is only for ^{14}C measurement, and stable measurements are possible with a single stage AMS because of the lower voltage for the accelerator and the small machine size. This development took more than 3 years. The measurement precision of YSMAS with the normal-mass samples is $\sim 0.1\%$, which is evaluated by reproducibility based on replicate measurements of IAEA-C6. After 3 years, I achieved the measurement precision of $\sim 0.3\%$ for small-mass samples, which is also based on replicate measurements of IAEA-C6 with small-mass carbon contents. Results were evaluated with value known standard of IAEA-C6, 150.73 ± 0.15 pMC as measured value, whose reference value is 150.61 ± 0.11 pMC reported by Rozanski (1991) (Figure 2.15). It takes more than 3 days for one ^{14}C measurement with normal-mass carbonates (~ 1 mgC), and more than 2 days with small-mass carbonates (~ 50 μgC), to get better accuracy and precision. Especially for the measurement with small-mass carbonates, I revealed that the position of graphite target critically affects the $\delta^{13}\text{C}$ values for $\delta^{13}\text{C}$ correction in the equation of $\Delta^{14}\text{C}$ (see 1.3 in Chapter 1) based on small-mass carbonate measurement experience. We can put 40 samples in the disk at the same time, and rotate the disk during measurement. However, the slight difference of the sample position during rotating the disk makes accuracy become worse. To avoid this, I put 4 tuning samples diagonally in the disk, and found the parameter of ion source and magnets which made best accuracy and canceled the effect of disk position dependency before every small-mass ^{14}C measurement.

Across the world AMS community, the measurement precision of 0.3% for small-mass samples is in the top level among all AMS facilities. For example, values of 0.5% in MALT (Micro Analysis Laboratory, Tandem accelerator, The University of Tokyo) (Matsuzaki et al., 2007) and NIES-TERRA (The tandem accelerator for Environmental Research and Radiocarbon Analysis at the National Institute for Environmental Studies) (Yoneda et al., 2004) were reported with the normal sample amounts using the Tandem accelerator. Values of 0.3% at the Australian National University (Fallon et al., 2010) and University of Glasgow (Freeman et al., 2008), and

0.4 % in Lund University, Sweden (Skog et al., 2010), were reported for normal sample amounts using the same single-stage AMS. Accordingly, high-resolution radiocarbon measurements with small-mass samples became possible in AORI.

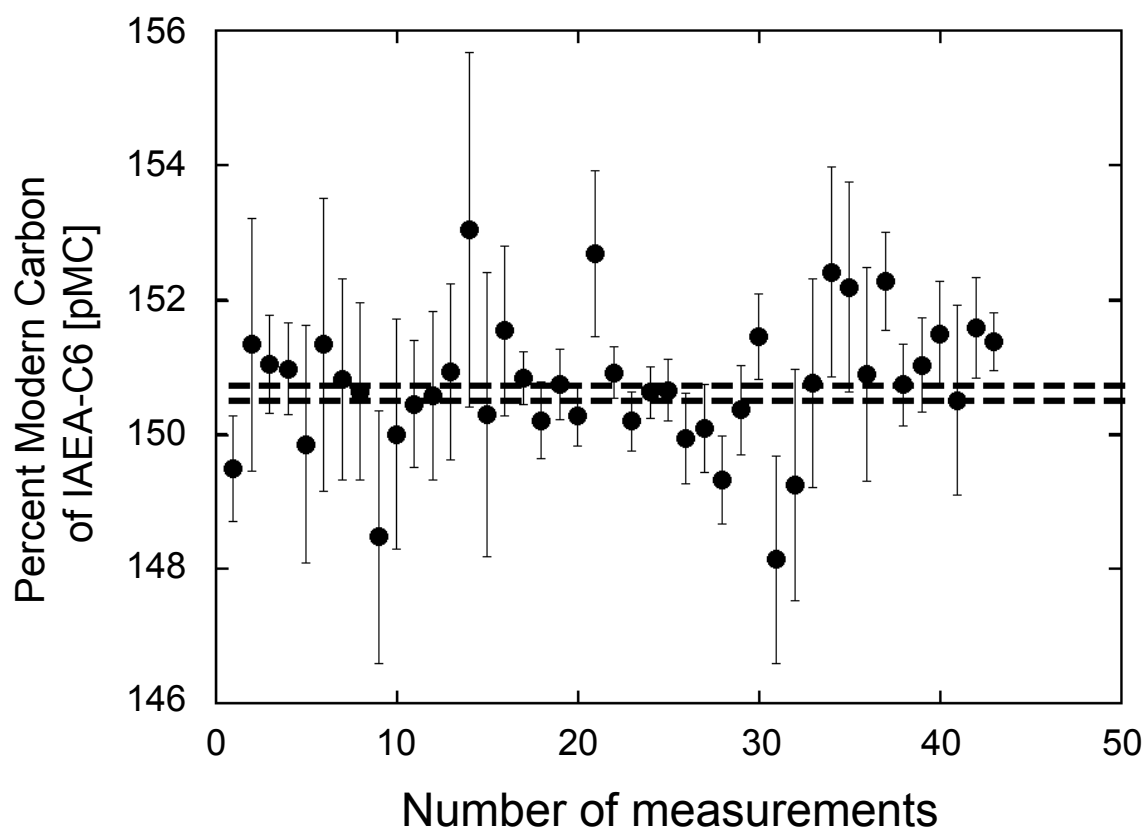


Figure 2.15 Results from radiocarbon standard of IAEA-C6 using single-stage AMS in AORI for small-mass samples, 150.73 ± 0.15 pMC as measured value. Dashed black lines indicate reference value of IAEA-C6 = 150.61 ± 0.11 pMC reported by Rozanski (1991).

2.4 Summary

In this chapter, I developed the necessary methods for the reconstruction of paleoceanography with high-resolution radiocarbon measurements using coral skeletons. Firstly I evaluated the proxies of SST in temperate corals, which have slow growth rates, for a high-resolution age-model. The Sr/Ca ratio in *Porites* coral clearly records seasonal SST variability even for periods of slow-growth rate, demonstrating that Sr/Ca is a suitable proxy to produce age models with seasonal resolution. After that, I reconsidered the conventional preparation methodology for radiocarbon measurement with small-mass carbonate samples. I found the optimum preparation conditions for both low contamination and current stability for analysis with reconsideration of preparation tubes, Fe catalyst and cleaning methods. A combination of these two aspects in this chapter provides the means to attempt high-resolution paleoceanographic reconstruction using coral skeletons that follows in Chapters 3 and 4.

Chapter 3 Multidecadal oceanographic changes in the western Pacific detected through high-resolution bomb-derived radiocarbon measurements in corals

3.1 Introduction

The North Equatorial Current (NEC) bifurcates into the Kuroshio Current (KC) and the Mindanao Current (MC), which are both western boundary currents in the Pacific Ocean to the east of the Philippine coast (e.g., Nitani 1972; Toole et al. 1990; Qiu and Lukas 1996; Lukas et al. 1996). The NEC-KC-MC current system (Figures 1.3 and 1.4) plays an important role in climate change because it connects tropical and subtropical areas and transports heat poleward (Qiu and Lukas, 1996; Gordon et al., 2014). The bifurcation latitude of the NEC migrates on annual and decadal scales due to effects from the El Niño-Southern Oscillation (ENSO) and the Pacific Decadal Oscillation (PDO) and their influence on the velocity and transport behavior of the KC and MC (Hu et al., 2015).

The migration of the NEC bifurcation latitude also affects the path and transport of the KC through the Luzon Strait. The surface ocean circulation in the South China Sea (SCS), which is mainly driven by the East Asian monsoon, is cyclonic in winter and anticyclonic in summer. To the north, the SCS connects with the Pacific Ocean through the Luzon Strait, where the Kuroshio intrudes into the SCS through the Luzon Strait. According to observations, transport through the Luzon Strait is generally higher in summer and lower in winter (e.g., Qu et al., 2000; Chu and Li 2000; Qu et al. 2004; Potemra and Qu 2009). The mechanism of KC intrusion into the SCS is still controversial but is thought to be primarily related to the East Asian monsoon and ENSO (Yuan et al. 2014). However, an accurate, observation-based estimate of the variation in Luzon Strait transport is not available (Qu et al. 2009). Furthermore, the frequency and characteristics of KC intrusions and their effects on circulation patterns in the northeast SCS are not well understood (Qu et al. 2009).

A complete understanding of the entire Kuroshio current system including the Kuroshio intrusion into the SCS (Kuroshio Loop Current) is difficult to obtain because most existing observations are focused on flows in particular locations and in particular seasons (Potemra and Qu, 2009). Long-term, high-vertical-resolution observations are needed to improve these models and our understanding of the Kuroshio and Kuroshio loop current system.

The radiocarbon (^{14}C) composition of seawater is a reliable tracer of mass advection and mixing in water bodies (e.g., Broecker et al., 1985; Druffel, 1981).

Atmospheric ^{14}C rapidly increased after 1955 due to atmospheric nuclear bomb testing, with the ^{14}C level nearly doubling in the mid-1960s (Hua et al., 2013). ^{14}C quickly oxidizes and reacts to form $^{14}\text{CO}_2$, which then diffuses into the surface layers of the ocean through air-sea CO_2 exchange, while the deep ocean is isolated from direct CO_2 , exchange with the atmosphere. The presence of bomb-derived $\Delta^{14}\text{C}$ allows excess ^{14}C in surface waters to be used as a very sensitive indicator of vertical and horizontal advection of water masses (Guilderson and Schrag, 1998). International seawater sampling programs such as the Geochemical Ocean Sections Study (GEOSECS) in the 1970s and the World Ocean Circulation Experiment (WOCE) in the 1990s produced maps of ^{14}C distributions in the world's oceans (Stuiver et al., 1981; Kumamoto et al., 2013). However, these data sets captured only snapshots from the time of data collection, thus, they cannot be used to study long-term variations over several decades.

The calcium carbonate (aragonite) skeletons of reef-building corals contain annual density bands that record the $\Delta^{14}\text{C}$ values of surface water when the corals skeletons take up dissolved inorganic carbon (DIC) from the ambient seawater (Druffel and Linick, 1978; Druffel, 1982, 1989). After atmospheric nuclear bomb testing in the 1950s, the $\Delta^{14}\text{C}$ in coral skeletons also included bomb-derived ^{14}C that was absorbed from the atmosphere into the ocean surface through air-sea gas exchange, with ~ 10 year-delay for isotopic equilibrium (Broecker and Peng, 1982; Druffel and Suess, 1983; Druffel, 1987). Therefore, the $\Delta^{14}\text{C}$ content of corals began to increase after the 1960s (e.g., Nozaki et al., 1978; Grottoli and Eakin, 2007), whereas atmospheric $\Delta^{14}\text{C}$ started to increase in the 1950s (Hua et al., 2013). This feature is known as the “bomb peak” or “bomb curve” (Grottoli and Eakin, 2007; Hua, 2009). This ^{14}C bomb peak varies in timing and magnitude among corals from different locations because of local differences in the air-sea CO_2 exchange rate and physical oceanic processes (Druffel, 2002; Grottoli and Eakin, 2007).

High-resolution ^{14}C measurements of coral skeletons can be used to reconstruct continuous and seasonal/interannual variability in ocean conditions (Guilderson et al., 2000; Druffel et al., 2014; Andrews et al., 2016) because coral skeletons incorporate dissolved inorganic carbon (DIC) from ambient seawater. Nearly all previous studies using ^{14}C record in corals discuss the relationship between climate change and ocean variability based on data from the eastern Pacific (e.g., Druffel, 2002; Grottoli and Eakin, 2007). Low-resolution $\Delta^{14}\text{C}$ data from Okinawa reported by Konishi et al. (1981)

constitute the only records of western Pacific Ocean boundary currents for the period from 1900 to 1980. Using the new analytical method described in Chapter 2, it is possible to measure the seasonal-scale radiocarbon concentration in the coral skeletons with slow growth rates. Since these are the only data reported for the whole bomb- ^{14}C curve in the KC area, the results for this region cannot be easily compared with high-resolution $\Delta^{14}\text{C}$ data from other regions.

In this chapter, I report high-resolution $\Delta^{14}\text{C}$ data for modern corals from Ishigaki Island to the southwest of Japan and Currimao, a municipality on the northwest coast of Luzon Island, Philippines. I compared coral data reported from Guam (Andrews et al., 2016) and Palau (Glynn et al., 2013) in order to understand the relationship between the NEC-KC-MC current system and climate change. I also compare these data with the coral data reported from Guam (Andrews et al. 2016), Con Dao (Mitsuguchi et al. 2007), and Hon Tre Island (Bolton et al. 2016) to understand the relationship between North Pacific western boundary currents and SCS circulation around the Luzon Strait.

3.2 Materials and Methods

3.2.1 Ishigaki modern coral IY02-02

A vertical coral core, IY02-02, was extracted with an air drill from a living *Porites* sp. colony at a water depth of about 5 m off of Yasurazaki on the northeastern coast of Ishigaki Island (Okinawa; 24°N, 124°E; Figure 3.1b) in 2002 (Hirabayashi et al., 2017a). This coral sampling site is an open ocean setting and free from freshwater input from rivers (Tottori et al., 2004). IY02-02 was microsampled by the micromilling technique of Suzuki et al. (2003) at 1.0 mm intervals along the growth axis based on the X-ray radiograph of the coral specimen. The age model is based on linear interpolation between peak seasonal environmental Sr/Ca ratios (Figure 3.2, Figure A3.1), which is a proxy for sea surface temperature, measured by ICP-AES following Chapter 2. The averaged annual growth rate of this coral was 13.2 mm/yr, with a range from 9 to 21 mm/yr for the period from 1947 to 1998, hence, microsampling at 1.0 mm intervals corresponds to 1 month time resolution. Each sample (1–2 mg) from IY02-02 was prepared using a specially designed vacuum line for small samples (Yokoyama et al.,

2010). I measured 109 samples with ages ranging from 1947 to 1998. For the ^{14}C spikes in 1950s and early 1960s (see below 3.3.2), I measured samples before and after the ^{14}C spikes and confirmed the highest spike values and decided the timing of the appearance of those spikes. Graphite target samples were then analyzed with a single-stage accelerator mass spectrometer (YS-AMS) (Yamane et al., 2014; Yokoyama et al., 2016) at the Atmosphere and Ocean Research Institute, University of Tokyo. Radiocarbon data are reported as $\Delta^{14}\text{C}$, the per mil (‰) deviation from the activity of pre-industrial wood standard defined by Stuiver and Polach (1977), which is corrected for isotope fractionation to a $\delta^{13}\text{C}$ value of -25.0‰ relative to the Pee Dee Belemnite (PDB) and for decay since the time of formation. The error associated with $\Delta^{14}\text{C}$ measured by AMS was evaluated as the counting statistics of the measured total counts for each sample via the following equation:

$$\sigma = 1/\sqrt{N}$$

where N means the measured total counts of samples.

3.2.2 Currimao modern coral PCURIN03

A modern coral (*Porites lutea*) core, PCURIN03, was taken from the coast of Currimao ($17^{\circ}59.098'\text{N}$, $120^{\circ}28.809'\text{E}$), Luzon Island, at a water depth of 4.8 m in November 2004 (Figure 3.1c, Hirabayashi et al., 2017b). The averaged annual growth rate of the coral was 18.1 mm/yr, with a range from 9 to 28 mm/yr for the period from 1945 to 1994. According to the ERSST.v2 data of this area (18°N , 120°E), averaged SST was 27.6°C , with the range from 24.0 to 30.3°C for this period. PCURIN03 was micro-sampled at 0.8-mm intervals, and the Sr/Ca ratios were measured to determine sample age using the method of chapter 2. Each sample (2–5 mg) from PCURIN03 was prepared using a specially designed vacuum line for small samples (see also Chapter 2) (Yokoyama et al. 2010), and 6–10 mg of each sample from PCURIN03 was prepared following the method of Yokoyama et al. (2007). I measured 158 samples in ages ranging from 1945 to 1994. For the ^{14}C spikes in 1950s and early 1960s (see below 3.3.2), I measured both before and after samples of ^{14}C spikes and confirmed the highest spike values, and decided the timing at which those spikes appeared using the same method as the Ishigaki coral. For the ^{14}C spikes in 1950s and early in 1960s (see below 3.3.2), I measured oth before and after samples of ^{14}C spikes and confirmed the highest

spike values and deduced the timing of those spikes appeared as same method of the Ishigaki coral. Graphite target samples were then analyzed with the same way as the Ishigaki modern coral (see also 3.2.1; Hirabayashi et al., 2017a) and reported as $\Delta^{14}\text{C}$. The $\Delta^{14}\text{C}$ measurement error was evaluated as I mentioned above in case of the Ishigaki coral.

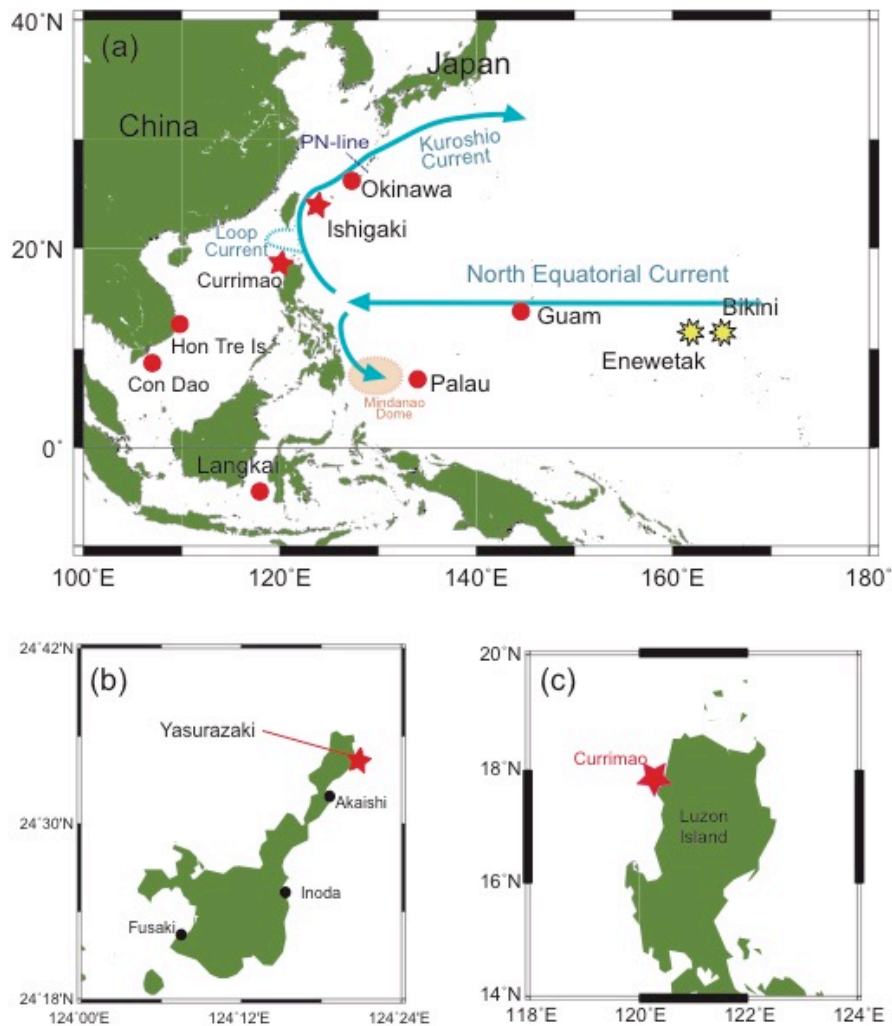


Figure 3.1 Map of the western Pacific including the South China Sea and coral sample sites reported in this thesis (Ishigaki and Currimao; red stars) and previous studies (Okinawa (Konishi et al., 1981), Guam (Andrews et al., 2016), Palau (Glynn et al., 2013), Langkai (Fallon and Guilderson, 2008), Con Dao (Mitsuguchi et al., 2007) and Hon Tre Island (Bolton et al., 2016)). The US Pacific Proving Grounds at Bikini and Enewerak atolls are shown as yellow stars. Modified figure from Hirabayashi et al. (2017a).

3.3 Results

3.3.1 Bomb-curve

The $\Delta^{14}\text{C}$ values in the Ishigaki coral increased from -38‰ to 163‰ and $\Delta^{14}\text{C}$ values in the Currimao coral increased from -28‰ to 178‰ during the 1960s due to nuclear tests in the Pacific (Figure 3.3). Although a portion of the Ishigaki coral in the 1970s has no data, the overall structure can be captured clearly. As similar bomb curve is also seen in other records from the western Pacific and SCS, such as Okinawa (Konishi et al., 1981), Guam (Andrews et al., 2016), Palau (Glynn et al., 2013), Langkai (Fallon and Guilderson, 2008), Hon Tre Island (Bolton et al., 2016) and Con Dao (Mitsuguchi et al., 2007) (Figure 3.3, 3.5). The $\Delta^{14}\text{C}$ values for Ishigaki maintained an average of 150‰ from 1970 to 1980, whereas the level gradually decreased after 1980 to a value of 98‰ in 1997. The average $\Delta^{14}\text{C}$ value of Currimao in the 1970s was 146.7‰ , which lies between the average $\Delta^{14}\text{C}$ values in Guam (Andrews et al. 2016) and Ishigaki and is lower than that in Con Dao (Mitsuguchi et al. 2007) (Figure 3.7).

A comparison of each of the bomb-curves from the 1960–1970s in the Ishigaki Currimao data and previously published data indicates that the slopes in SCS (Currimao, Hon Tre Island (Bolton et al., 2016), Con Dao (Mitsuguchi et al., 2007)) are higher than those of Ishigaki, Guam (Andrews et al., 2016), Langkai (Fallon and Guilderson, 2008) and Palau (Glynn et al., 2013) (Figure 3.3, 3.5, 3.6). The Palau samples (Glynn et al., 2013) have a gentler slope from 1963, and a lower maximum value than the other locations (Figure 3.5). In the Okinawa samples, both the $\Delta^{14}\text{C}$ value for 1950 and the maximum value were considerably higher than in other places because the seawater in this area has a long residence time at the surface and is well equilibrated by air-sea CO_2 exchange (Grottoli and Eakin, 2007). Konishi et al. (1981) performed low-resolution ^{14}C measurements of the Okinawa coral in which the year of onset for the bomb-related $\Delta^{14}\text{C}$ increase appears to occur 1 year earlier than at Ishigaki, however, the magnitude of the rise in $\Delta^{14}\text{C}$ is equivalent to that at Ishigaki (Table 3.1).

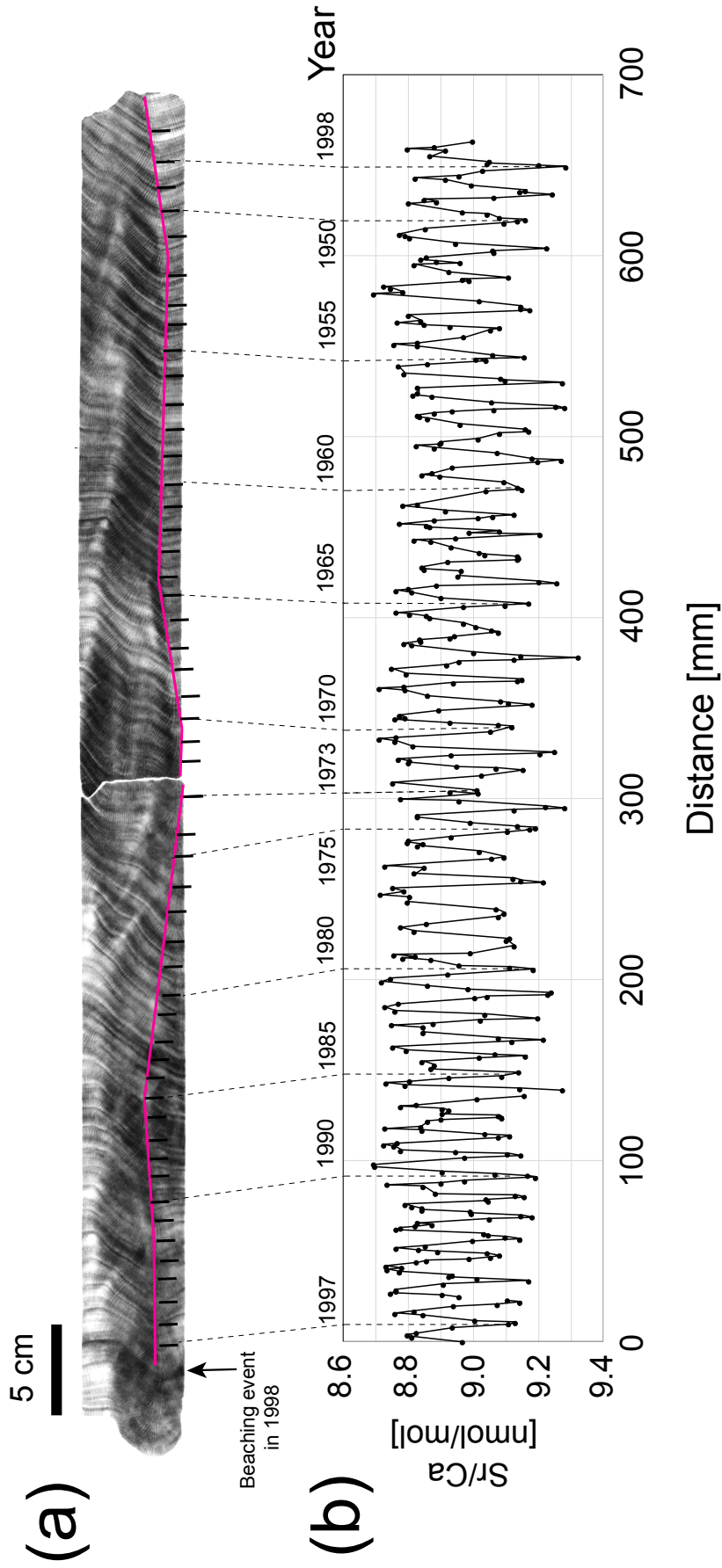


Figure 3.2 (a) X-ray radiograph and (b) Sr/Ca ratio of the Ishigaki coral specimen (IY0202). I constructed the age model using X-ray photograph and peak counting of Sr/Ca

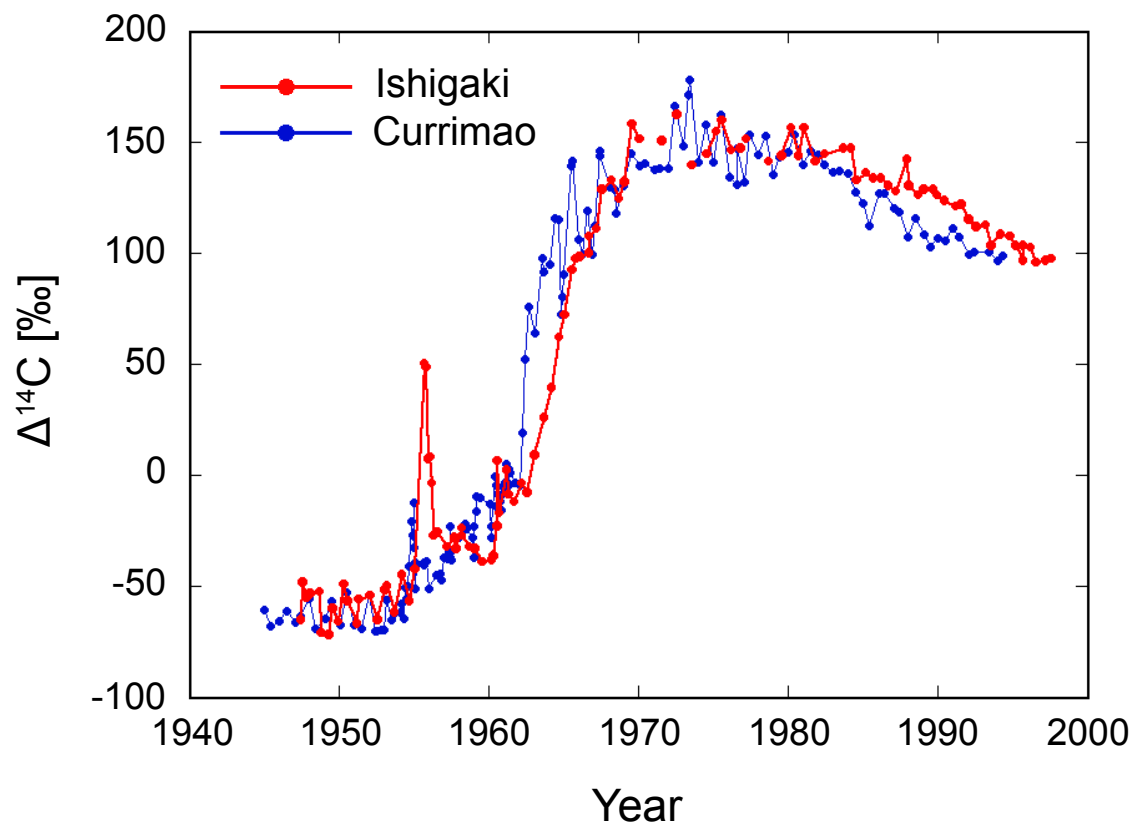


Figure 3.3 $\Delta^{14}\text{C}$ data for corals from Ishigaki (red) and Currimao (blue). Some $\Delta^{14}\text{C}$ data for the Ishigaki coral in the 1970s are not available.

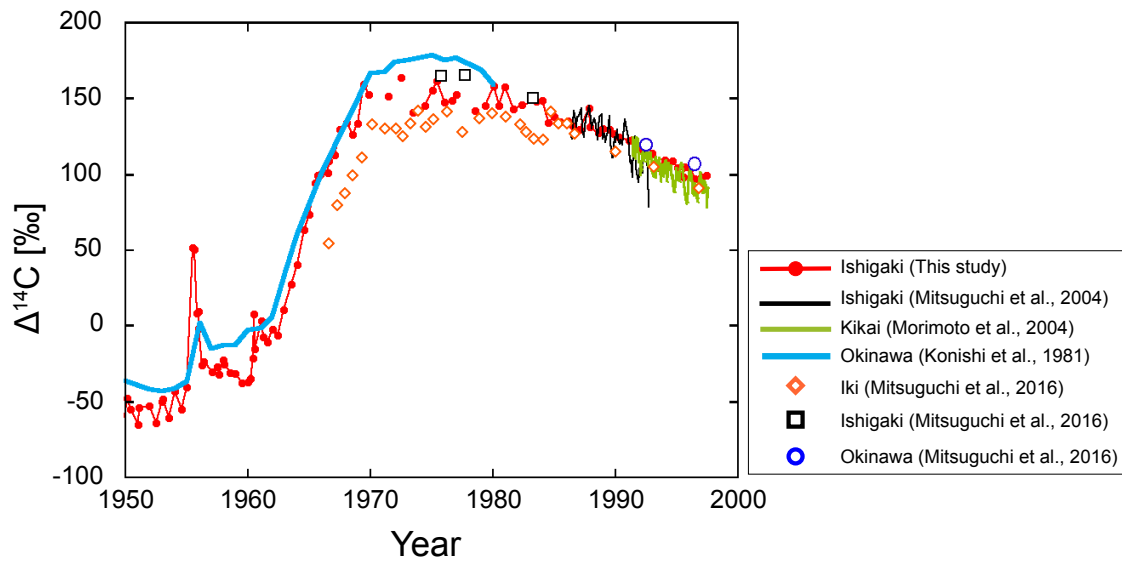


Figure 3.4 Comparison of $\Delta^{14}\text{C}$ data reported from Ishigaki (this study; Mitsuguchi et al., 2004; 2016), Okinawa (Konishi et al., 1981; Mitsuguchi et al., 2016), Kikai (Morimoto et al., 2004), and Iki (Mitsuguchi et al., 2016). Although the $\Delta^{14}\text{C}$ data from Ishigaki (Mitsuguchi et al., 2004) and Kikai (Morimoto et al., 2004) showed the seasonal variability, the averaged $\Delta^{14}\text{C}$ values in the period after the 1980s are almost the same as my $\Delta^{14}\text{C}$ data from Ishigaki.

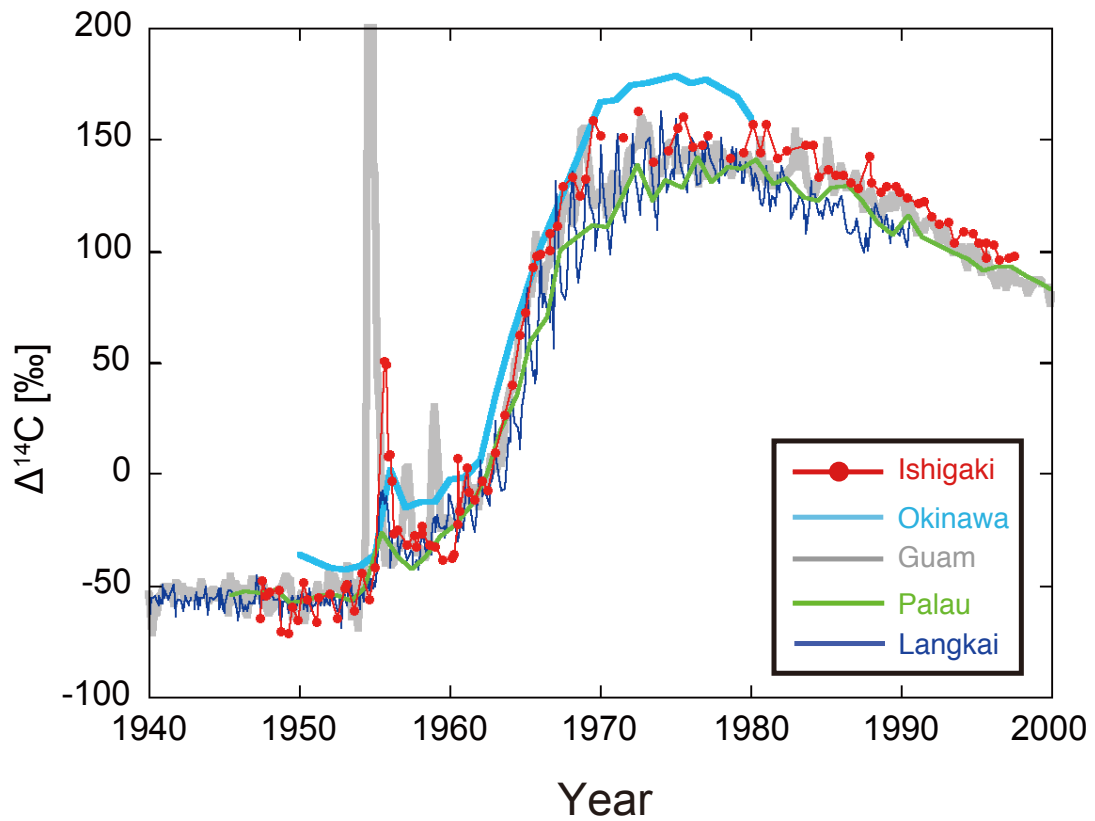


Figure 3.5 $\Delta^{14}\text{C}$ data for corals in the western Pacific from Ishigaki (red, this study), Okinawa (Konishi et al., 1981), Guam (Andrews et al., 2016), Palau (Glynn et al., 2013), and Langkai (Fallon and Guilderson, 2008). Some $\Delta^{14}\text{C}$ data for the Ishigaki coral in the 1970s are not available. From Hirabayashi et al. (2017a).

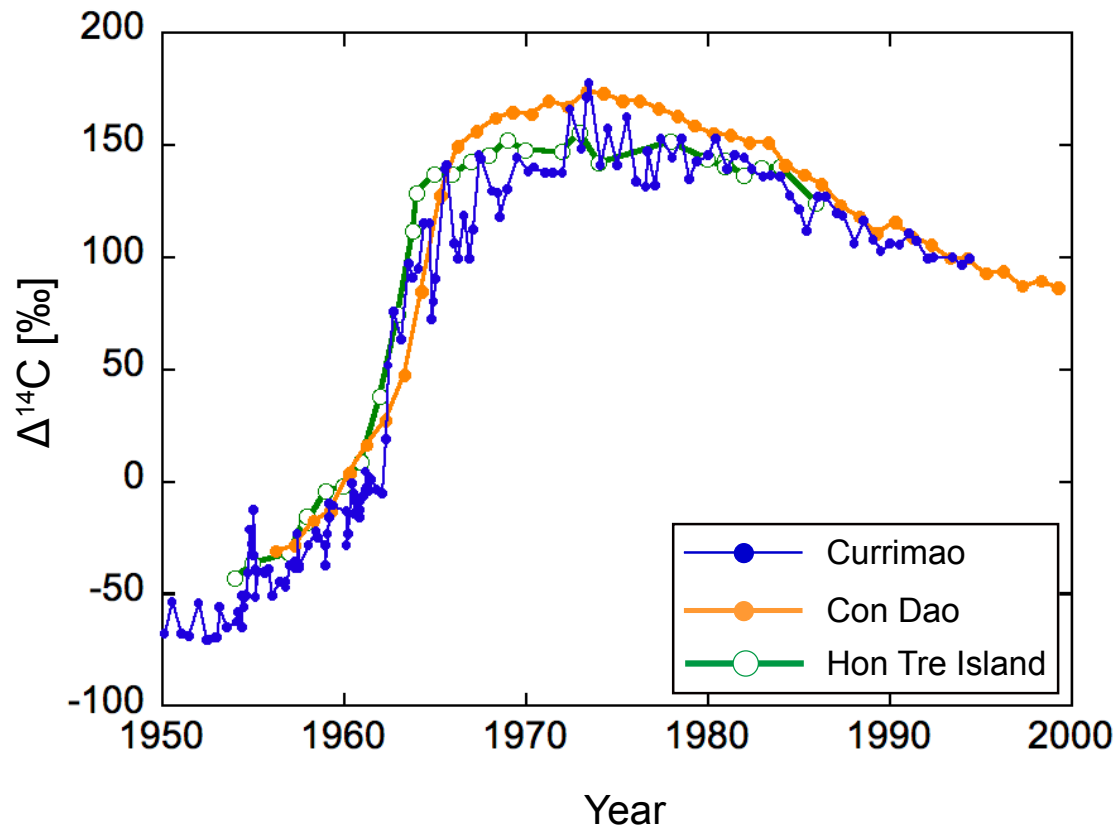


Figure 3.6 $\Delta^{14}\text{C}$ data for corals in the South China Sea from Currimao (blue, this study), Con Dao (Mitsuguchi et al., 2007) and Hon Tre Island (Bolton et al., 2016). $\Delta^{14}\text{C}$ data from Con Dao and Hon Tre Island are annual and those from Currimao are seasonal.

Table 3.1 Comparison of bomb-related $\Delta^{14}\text{C}$ increases from Ishigaki, Currimao (this study), Okinawa (Konishi et al., 1981), Guam (Andrews et al., 2016), Palau (Glynn et al., 2013), Langkai (Fallon and Guilderson, 2008), Con Dao (Mitsuguchi et al., 2007) and Hon Tre Island (Bolton et al., 2016).

Site	$\Delta^{14}\text{C}$ at 1950 (‰)	Maximum (‰)	Amount of bomb-derived increase (‰)
Ishigaki	-56	163	219
Currimao	-68	178	246
Okinawa	-36	179	215
Guam	-59	160	219
Palau	-57	142	199
Langkai	-54	163	217
Con Dao	-53	174	227
Hon Tre Is.	-56	157	213

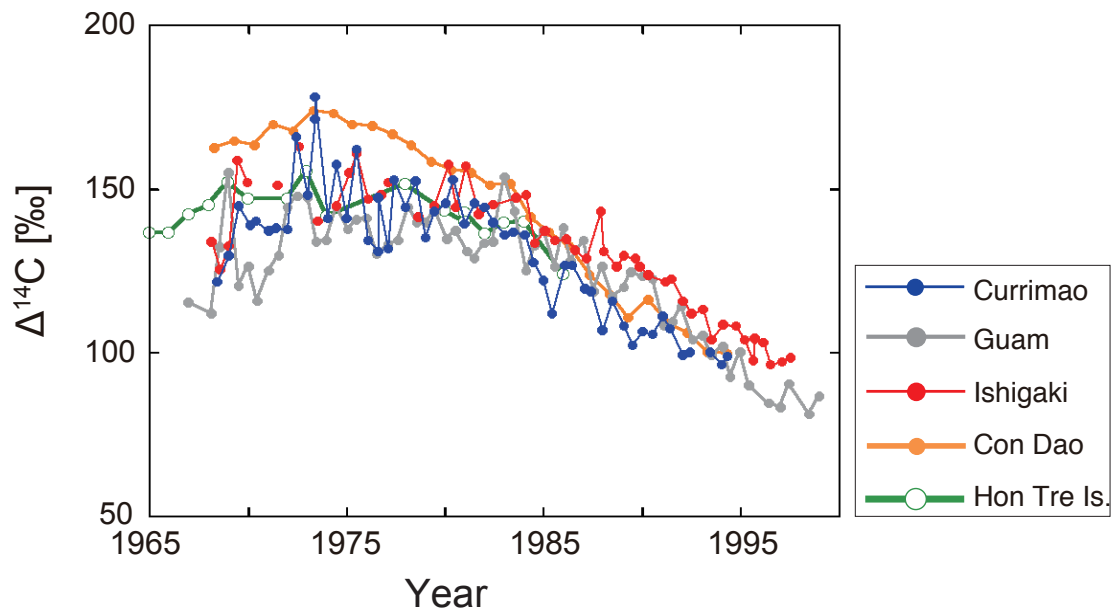


Figure 3.7 $\Delta^{14}\text{C}$ recorded in corals from Ishigaki, Currimao (this study), Guam (Andrews et al., 2016), Con Dao (Mitsuguchi et al., 2007) and Hon Tre Island (Bolton et al., 2016) for the period from 1965 to 2000. Modified figure from Hirabayashi et al. (2017b).

3.3.2 Early ^{14}C spikes in the 1950s and 1960s

Three unusually rapid $\Delta^{14}\text{C}$ increases (three early ^{14}C spikes) were observed in the 1950s and early 1960 in the Ishigaki coral (Figure 3.3, 3.8). Natural $\Delta^{14}\text{C}$ variability of the Ishigaki coral is ± 8.5 ‰, which is evaluated from the standard deviation of $\Delta^{14}\text{C}$ variability before 1950. Using this value as noise, I calculated the signal-noise ratio for three early ^{14}C spikes. The spikes' values were 50.8 ± 4.3 ‰, -23.4 ± 6.6 ‰ and 7.20 ± 5.7 ‰, respectively. The bomb curve was approached by approximate equation without three early ^{14}C spikes, and evaluated the amplitude of ^{14}C spikes. The amplitudes were 102, 20 and 42 ‰, respectively (Figure 3.8) and use these data as signals. The signal-noise ratios are 12.0, 2.4 and 5.0, respectively. Therefore, these three ^{14}C spikes are significant values compared to the natural ^{14}C variability. Three early ^{14}C spikes are observed in the Ishigaki coral for the periods from January 1955 to February 1957, September 1957 to August 1959, and March 1960 to September 1961, which confirms the recent findings for Guam corals (Andrews et al., 2016) (Figure 3.5, 3.10d). The timing of three early ^{14}C spikes in Ishigaki slightly lagged by 0.82, 0.81 and 1.53 years those from Guam, respectively (Figure 3.10d, Table 3.2).

A clear early ^{14}C spike in Currimao is observed only once, from July 1954 to January 1956 (Figure 3.3, 3.9, 3.10a). I calculated the signal-noise ratio as I mentioned above. The first signal-noise ratio for the ^{14}C spike in 1950s was 10.5, as the natural ^{14}C variability (noise) was ± 4.5 ‰, and the amplitude of first spike was 47 ‰ (Figure 3.9). The amplitude of ^{14}C variability and signal-noise ratio after first ^{14}C spike in late 1950s and early 1960s are almost constant at ~ 20 ‰ and 5, respectively (Figure 3.9), which suggested that ^{14}C variability after first ^{14}C spikes indicated usual seasonal variability such as seasonal local upwelling at Currimao. Because the seasonal $\Delta^{14}\text{C}$ difference in the late 1950s and early 1960s increased in Currimao, the second and third ^{14}C spike could not be recognized clearly, which is similar to the data from Langkai (Fallon and Guilderson, 2008).

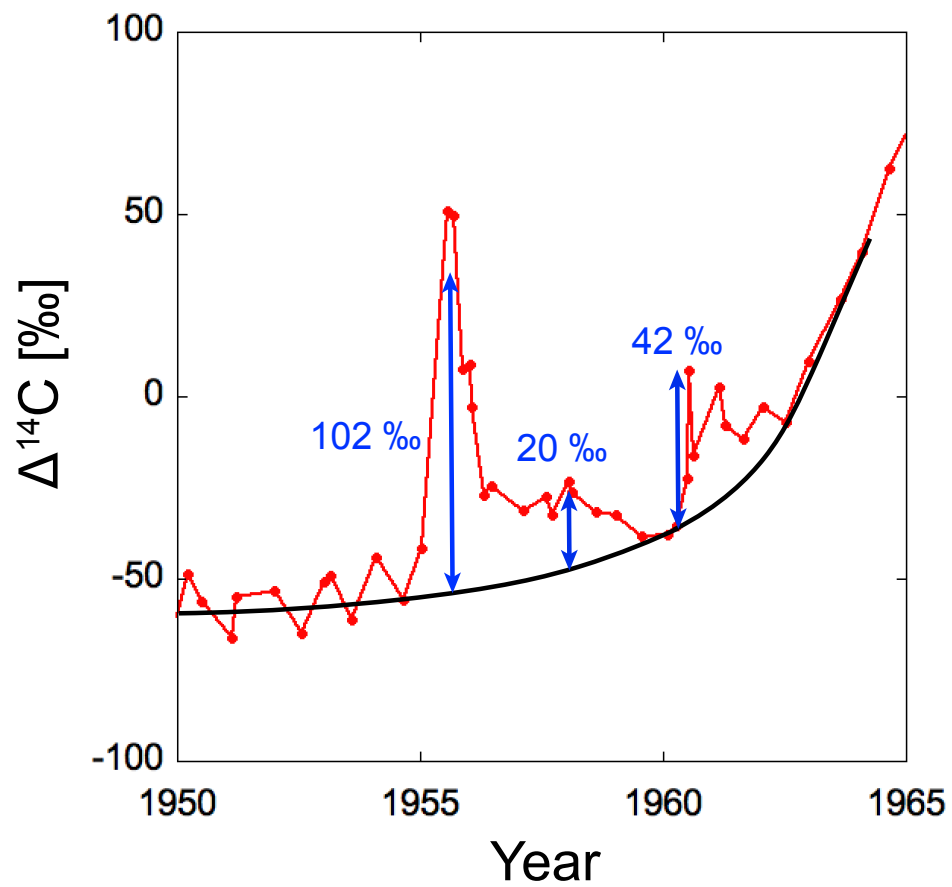


Figure 3.8 Three ^{14}C spikes in Ishigaki (red) and the approximate curve (black). The blue arrows and numbers shows three ^{14}C spikes and their respective amplitude compared with the approximate curve.

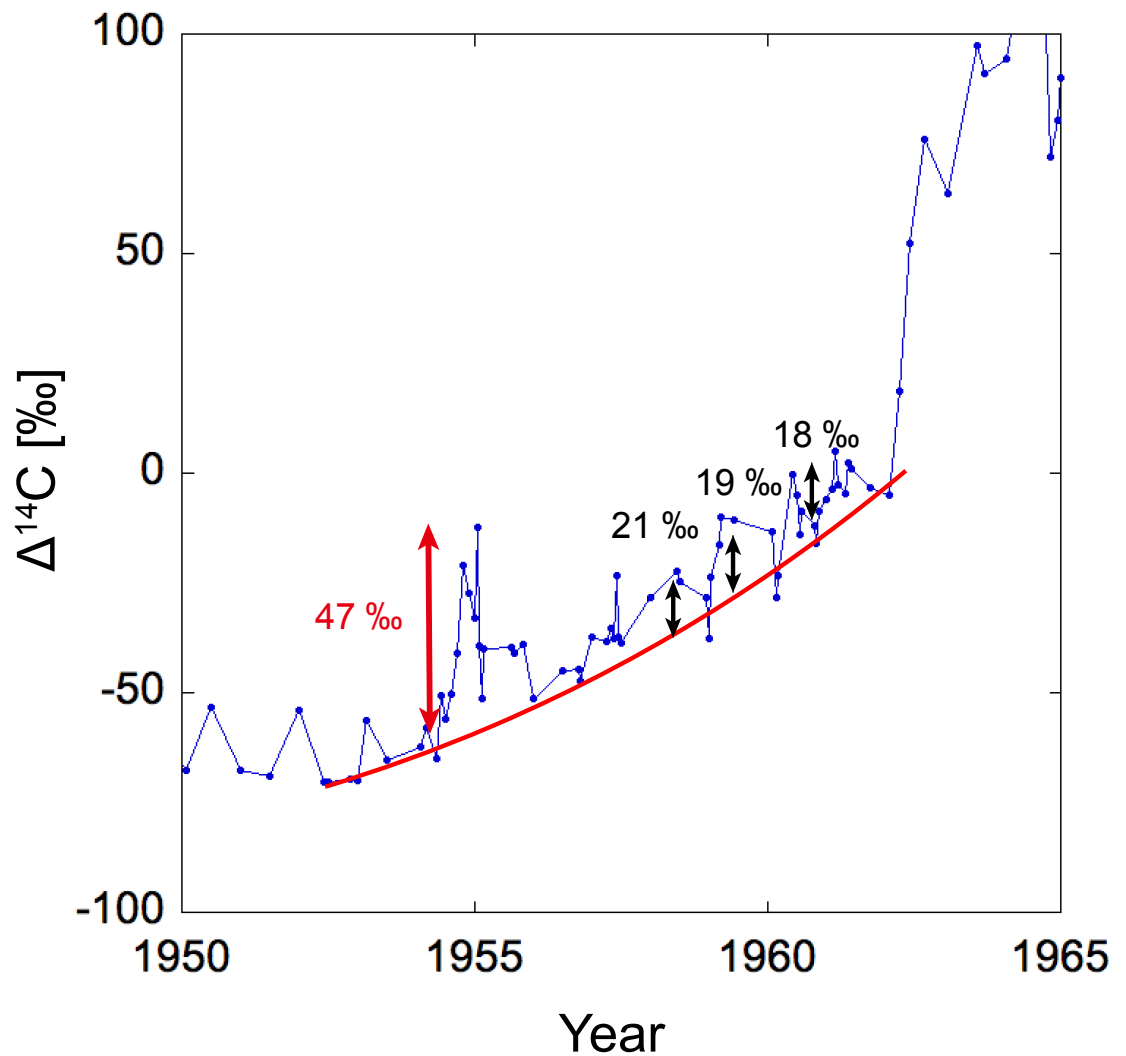
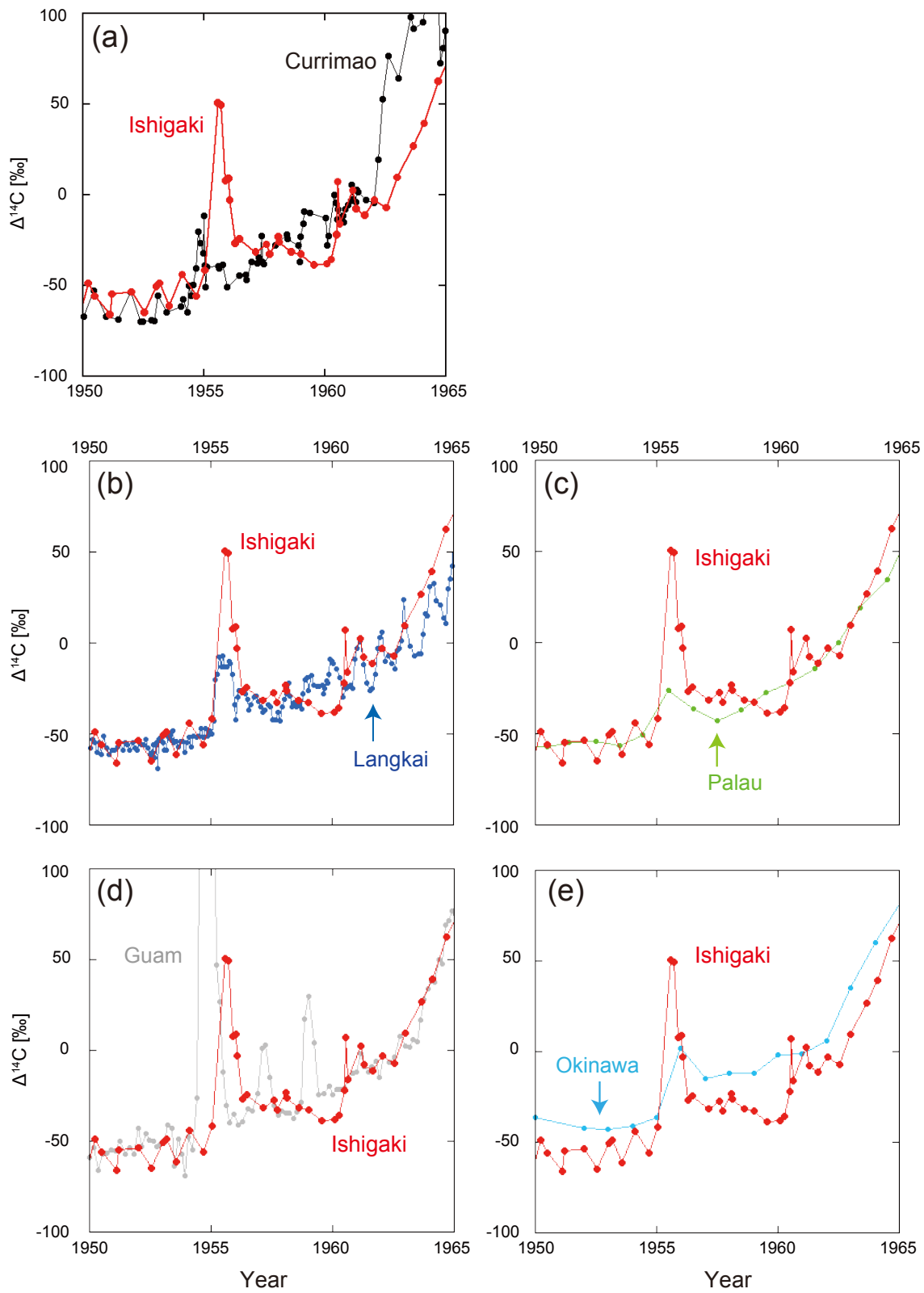


Figure 3.9 The ^{14}C variability in Currimao (blue) and approximate curve (red). The red arrow and numbers shows the first ^{14}C spike in from July 1954 to January 1956 and its amplitude compared with the approximate curve. The black arrows shows the seasonal ^{14}C variability driven by local upwelling at Currimao because those amplitude (black numbers) are almost constant.

Table 3.2 The Date of the nuclear bomb testing conducted in 1950s and the three early bomb- ^{14}C spikes recorded in the Guam (Andrews et al., 2016) and Ishigaki coral (Hirabayashi et al., 2017a).

Operation	Testing Date (year)	Date of early ^{14}C spikes appeared (year)		
		Guam	Ishigaki	$\pm 1 \sigma$
Castle	1954.16-1954.37	1954.75	1955.57	0.05
Redwing	1956.39-1956.55	1957.25	1958.06	0.04
Hardtack I	1958.36-1958.57	1959.00	1960.53	0.03

Figure 3.10 $\Delta^{14}\text{C}$ comparison from 1940 to 1965 between Ishigaki and (a) Currimao, (b) Langkai (Fallon and Guilderson, 2008), (c) Palau (Glynn et al., 2013), (d) Guam (Andrews et al., 2016), and (e) Okinawa (Konishi et al., 1981). Three early ^{14}C spikes are observed in Ishigaki and Guam. Modified figure from Hirabayashi et al. (2017a). Ishigaki and Guam corals recorded the three ^{14}C spikes.



3.3.3 Post-bomb period

The average $\Delta^{14}\text{C}$ value in Currimao in the 1970s was 146.7 ‰, which lies between the average $\Delta^{14}\text{C}$ values in Guam (Andrews et al. 2016) and Ishigaki and is lower than that in Con Dao (Mitsuguchi et al. 2007) (Figure 3.7). A limited number of $\Delta^{14}\text{C}$ data are available for the 1970s in coral obtained from Hon Tre Island, yet the averaged $\Delta^{14}\text{C}$ is slightly higher than that in Currimao. Although each data point from Hon Tre Island represents an annual average of respective years, comparisons are made for other locations in the SCS in Figures 3.7 and 3.13. To estimate seasonal changes in the magnitude of $\Delta^{14}\text{C}$ in SCS, I referred to the seasonal variation in 1969 in Hon Tre Island reported by Bolton et al. (2016). They showed that $\Delta^{14}\text{C}$ in spring/summer is lower than that in autumn/winter in the Hon Tre Island. Thus, although Bolton et al. (2016) reported annual $\Delta^{14}\text{C}$ value except 1969 in Hon Tre Island, it is likely that higher values were marked in summer and lower values in winter than the annual value in Hon Tre Island shown in Figure 3.13b and 3.13c. After 1986, $\Delta^{14}\text{C}$ in Currimao was lower than the values in Guam (Andrews et al. 2016), Ishigaki (this study; Hirabayashi et al., 2017a), and Con Dao (Mitsuguchi et al. 2007) (Figure 3.7). The seasonality in $\Delta^{14}\text{C}$ in Currimao also decreased from 1975 to 1995 (Figure 3.12).

From 1972 to 1975, when $\Delta^{14}\text{C}$ in Currimao exhibited significant seasonal variability (Figure 3.12), the $\Delta^{14}\text{C}$ level increased to the levels observed in Con Dao in the summers of 1972 and 1973 (Figure 3.13b). The winter $\Delta^{14}\text{C}$ in Currimao decreased to the level in Guam during this period (Figure 3.13c). It is difficult to compare the $\Delta^{14}\text{C}$ values of Ishigaki during this period with other regions because of the lack of data in the 1970s; however, the $\Delta^{14}\text{C}$ level of Ishigaki fluctuated between that of Guam and Currimao, whereas the $\Delta^{14}\text{C}$ values in Ishigaki in the 1980s and 1990s were higher than those in Currimao (Figure 3.7). The $\Delta^{14}\text{C}$ values of both Ishigaki and Guam did not show clear seasonal differences from 1972 to 1975.

Although the long-term trend in $\Delta^{14}\text{C}$ values of Ishigaki (Mitsuguchi et al., 2004) and Kikai (Morimoto et al., 2004) in the period after 1980s are similar to my $\Delta^{14}\text{C}$ data from Ishigaki (Hirabayashi et al., 2017a), the $\Delta^{14}\text{C}$ data from Ishigaki (Mitsuguchi et al., 2004) and Kikai (Morimoto et al., 2004) showed the seasonal variability (Figure 3.4). Mitsuguchi et al. (2004) suggested that $\Delta^{14}\text{C}$ in Ishigaki generally decreased in summer, except 1985, 1987 and 1992. They suggested that this might reflect local upwelling driven

by summer monsoon wind stress. The coral sampling site at Ishigaki does not experience seasonal local upwelling induced by the East Asian monsoon (Yamamoto, 1999; Sowa et al., 2014). Yamamoto (1999) reported that there is no vertical mixing or local upwelling in summer at my coral sampling site, Yasurazaki, based on the SST observation. Sowa et al. (2014) also reported that there is little evidence of winter upwelling based on seawater Ba measurements at Fusaki, Inoda, and Akaishi in Ishigaki (Figure 3.1b), which are close to our coral sampling site. Therefore, seasonal variability in Ishigaki reported by Mitsuguchi et al (2004) possibly did not reflect the seasonal upwelling. One possible reason for their Ishigaki $\Delta^{14}\text{C}$ data is the problem of $\delta^{13}\text{C}$ correction for fractionation in the equation mentioned in Chapter 1. Usual $\delta^{13}\text{C}$ of Ishigaki corals varies within the range of -5 ‰ to 0 ‰ (Suzuki et al., 2003). When unexpected $\delta^{13}\text{C}$ value was used for the fractionation correction, $\Delta^{14}\text{C}$ value easily varies more than 30 ‰. For example, when $\delta^{13}\text{C} = -58$ ‰ and $\delta^{13}\text{C} = 33$ ‰ were used for the samples covering the 1970s, $\Delta^{14}\text{C}$ become 180 ‰ and 61‰, respectively, while $\Delta^{14}\text{C}$ values should be ~150 ‰ (Figure 3.11). Because the Ishigaki coral in Mitsuguchi et al. (2004) was measured by AMS system at the National Institute for Environmental Studies, Tandem accelerator for Environmental Research and Radiocarbon Analysis (NIES-TERRA), the stable and accurate $\delta^{13}\text{C}$ measurement with NIES-TERRA maybe has a problem and Ishigaki $\Delta^{14}\text{C}$ values showed seasonal-like variability. Morimoto et al. (2004) measured Kikai $\Delta^{14}\text{C}$ values using NIES-TERRA as well. They did not mentioned clear reasons for seasonal $\Delta^{14}\text{C}$ variability in Kikai but their data might be affected by problems associated with $\delta^{13}\text{C}$ correction for fractionation.

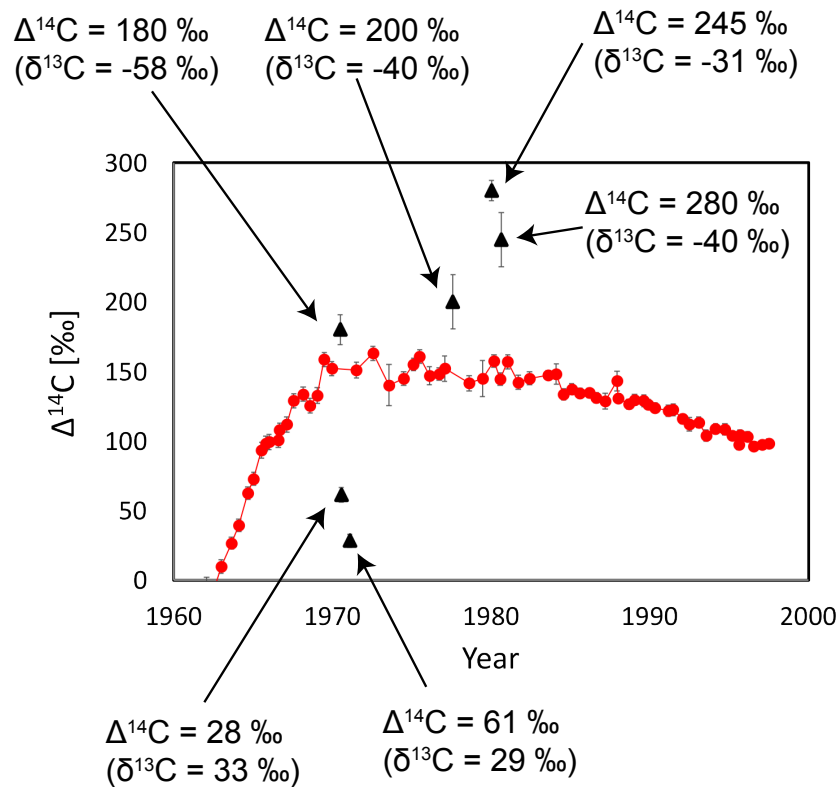


Figure 3.11 The example of the problem of $\delta^{13}\text{C}$ correction for fractionation. $\Delta^{14}\text{C}$ data of Ishigaki used in the discussions in this thesis (red) and unexpected $\Delta^{14}\text{C}$ values due to the problem of $\delta^{13}\text{C}$ correction (black). Usual $\delta^{13}\text{C}$ of Ishigaki corals varies within the range from -5 ‰ to 0 ‰ (Suzuki et al., 2003). When unexpected $\delta^{13}\text{C}$ value was used for the fractionation correction, $\Delta^{14}\text{C}$ value easily varies more than 30 ‰.

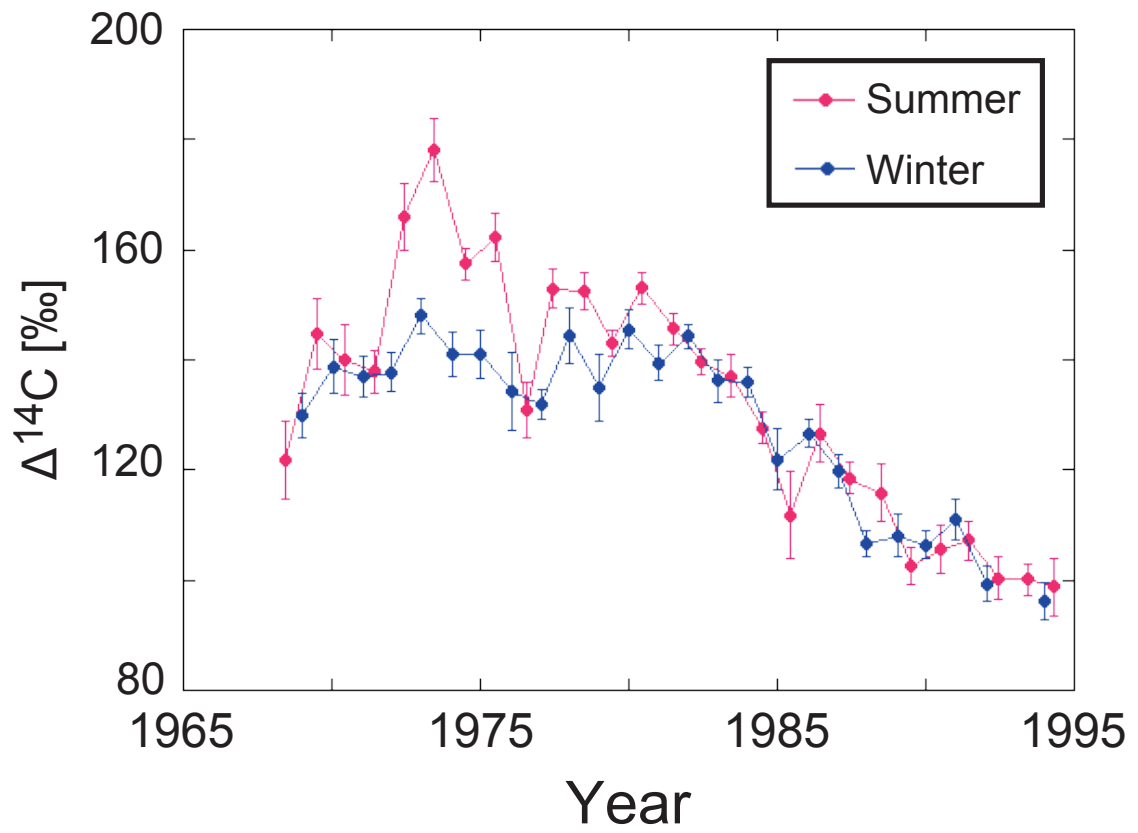


Figure 3.12 Seasonal $\Delta^{14}\text{C}$ of Currimao coral. From Hirabayashi et al. (2017b).

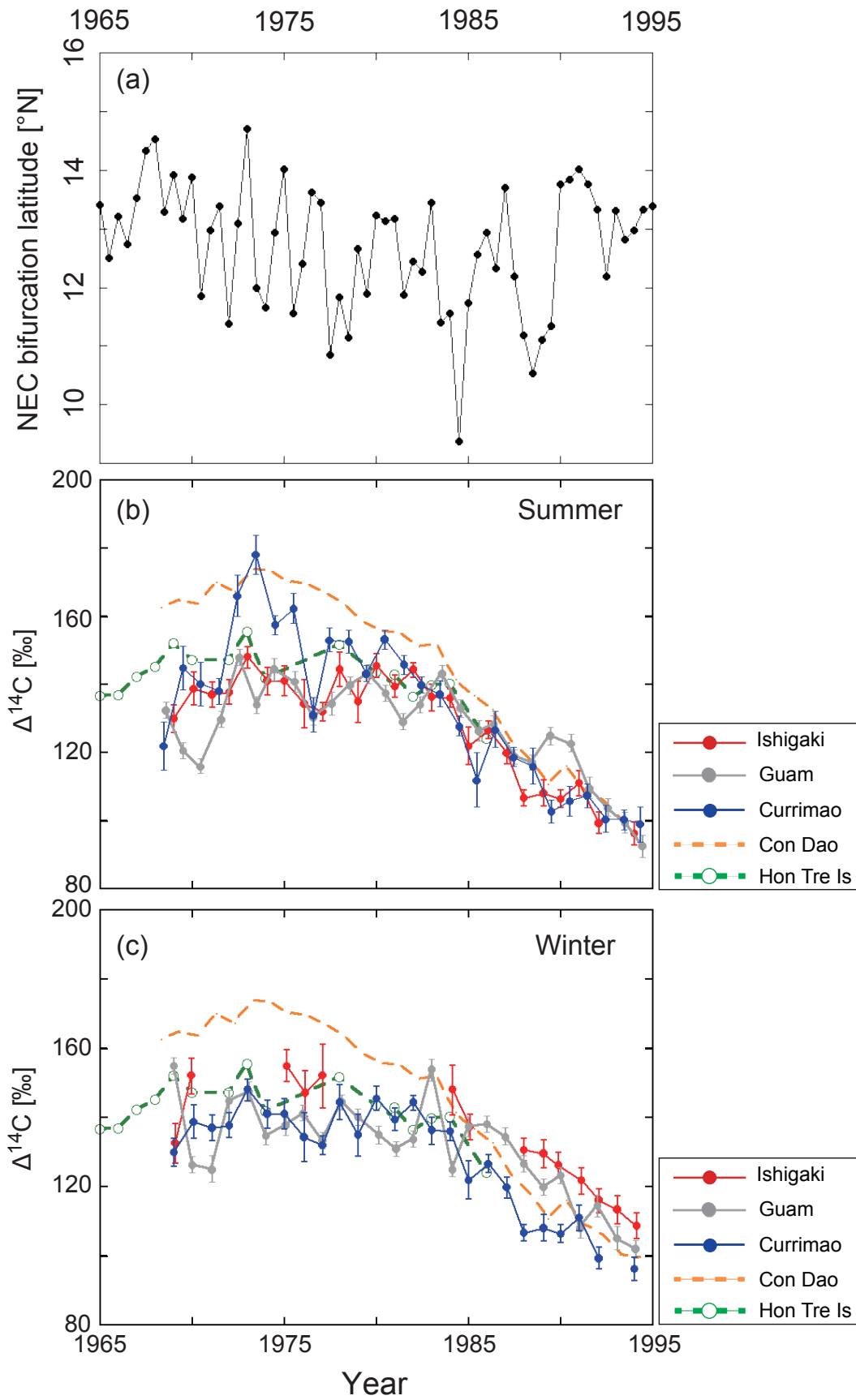


Figure 3.13 (a) Seasonal average NEC bifurcation latitudes from 1965 to 1995 based on Zhao et al. (2013). Summer averaged latitude refers to the average latitude value of June and July. Winter averaged latitude refers to the average value of January and February. $\Delta^{14}\text{C}$ in (b) summer and (c) winter recorded in the corals sampled from Currimaao (this study), Guam (Andrews et al. 2016), and Ishigaki (This study). The $\Delta^{14}\text{C}$ in Con Dao (Mitsuguchi et al. 2007) and Hon Tre Island are annual. Modified figure from Hirabayashi et al. (2017b).

3.4 Discussion

3.4.1 Early bomb-testing-related $\Delta^{14}\text{C}$ Spikes

3.4.1.1 Reason for the $\Delta^{14}\text{C}$ spikes in the 1950s and 1960s

Three early $\Delta^{14}\text{C}$ spikes were recorded in the Ishigaki coral for the periods from January 1955 to February 1957, September 1957 to August 1959, and March 1960 to September 1961 (Table 3.2). Those spikes had not been reported in the Kuroshio region. Andrews et al. (2016) mentioned that no records are available farther northwest of Guam because previous studies could not catch the evidence of early bomb- ^{14}C spikes in the west area of Guam.

There are three possible reasons of the three unusual $\Delta^{14}\text{C}$ spikes, (1) the modern carbon contamination during the preparation of graphitization, (2) the wrong age model and (3) ^{14}C enriched carbon taken into coral skeletons in those periods. The atmospheric ^{14}C was 13.8‰ in 2015, when I did the radiocarbon measurements with this coral (Graven et al., 2017). The first spike in Ishigaki corals was much higher than the atmospheric ^{14}C level in 2015. The second and third spikes were lower than the 2015 ^{14}C , but contamination with atmospheric ^{14}C of 50 – 90% would be needed to match the ^{14}C level of those spikes. CO_2 gas pressure in the vacuum line was monitored (Chapter 2) every time and such high contamination from the air was not observed. Additionally, I checked the age model using the X-ray photograph of this coral skeleton and peak counting of Sr/Ca and confirmed that there is no mistakes of the age model of this coral. Therefore, the reason of three $\Delta^{14}\text{C}$ spikes is (3) ^{14}C enriched carbon taken into coral skeletons in those periods. From 1950 to early 1960, the US Pacific Proving Grounds at Bikini and Enewetak atolls conducted tests in 1954 (Operation Castle), 1956 (Operation Redwing), and 1958 (Operation Hardtack I), whose total yield at the surface of land, lagoon and sea were 48.09 Mt, 15.95 Mt and 22.93 Mt, respectively (Andrews et al., 2016). This atmospheric nuclear bomb test was the source of ^{14}C enriched carbon in the Ishigaki coral.

3.4.1.2 Comparison with corals in the western Pacific

Three early $\Delta^{14}\text{C}$ spikes were recorded in the Ishigaki coral, which are closely linked to three independent nuclear bomb tests in the US Pacific Proving Grounds at Bikini and Enewetak atolls conducted in 1954, 1956, and 1958. These events were also detected in the coral records from Guam (Andrews et al., 2016) (Figure 3.10). Of the three bomb spikes, the peak value in 1954 was the largest and that in 1956 was the smallest. Conversely, a bomb-related radiocarbon peak is found only for 1955 at Currimao, Okinawa, Palau, and Langkai. The 1955 ^{14}C spike at Langkai appears nearly simultaneously in the Ishigaki record. These high ^{14}C contents are thought to have been transported directly from the US Pacific Proving Grounds through the NEC, the KC, and the MC as “close-in fallout” (Kellogg et al., 1957; Fallon and Guilderson, 2008; Glynn et al., 2013; Andrews et al., 2016) because the operations were performed within only a few years and the data cannot be explained by $^{14}\text{CO}_2$ absorption through air-sea CO_2 exchange. Bautista et al. (2016) and Chang et al. (2016) also reported iodine-129 in the corals collected from South China Sea and Guam originated from 1950s nuclear operations in the US Pacific Proving Grounds derived via the circulation of the North Pacific Gyre. Although their resolution is coarser than that from the present study, three independent results confirmed oceanographic transportation pathways of these nuclides. Andrews et al. (2016) noted that Guam is the only location where all three nuclear test operations can be detected. However, as this study demonstrates, it is possible to observe these signals in other locations along the NEC, KC, and MC with high-resolution ^{14}C measurements, except for those places with strong seasonality due to exchanges between different water masses, such as Currimao and Langkai (Fallon and Guilderson, 2008).

The timing of the three ^{14}C spikes in the Ishigaki corals each exhibited a lag of about 1 year behind the Guam corals because of the difference in distance from the US Pacific Proving Grounds sites. Andrews et al. (2016) estimated the NEC speed between the US Pacific Proving Grounds site and Guam as $\sim 0.1\text{--}0.2\text{ m s}^{-1}$. The KC speed is known to be much faster than that of the NEC, at approximately $0.5\text{--}1\text{ m s}^{-1}$, yet Sakaguchi et al. (2016) estimated an average speed 0.2 m s^{-1} for the KC using $^{236}\text{U}/^{238}\text{U}$ in coral collected from Iki Island, Japan. The speed was deduced from the distance between the US Pacific Proving Grounds sites and Iki Island considering also the time

differences between the date of the nuclear bomb tests and when the $^{236}\text{U}/^{238}\text{U}$ signal appeared in the Iki coral. Due to the large sample size required for ^{236}U measurements (e.g., 0.3–0.5 g of coral skeleton) (Sakaguchi et al., 2016), results from this type of calculation have lower resolutions than ^{14}C -based studies. The averaged velocity of the NEC along 137°E varies from 0.05 to 0.2 m s^{-1} in the area from 10°N to 13°N for the period from 1967 to 1988 above the depth of 250 m (Qiu and Joyce, 1992). This current speed also varies depending on the oceanographic influence of ENSO (Hu and Hu, 2014). They indicated that the westward NEC between 9.6°N and 11.4°N intensified to a greater extent under La Niña conditions than under El Niño conditions (Hu and Hu, 2014). Hence, it is expected that the stronger current of the NEC from the US Pacific Proving Grounds to the east coast of the Philippines can be observed under La Niña conditions since the sites from where the signals originated are located at Enewetak (11.5°N) and Bikini (11.6°N).

The Ishigaki coral (IY02-02) was microsampled at 1.0 mm intervals along the growth axis of the coral specimen. During the first ^{14}C spike in 1955, the coral growth rate was 0.83 mm/month , which means that one powered sample of the first ^{14}C spike has the record of 1.2 months. The samples during the period of the second and third ^{14}C spikes have the records of 0.9 months/sample and 0.7 months/sample evaluated from the coral growth rate of 1.12 mm/month and 1.50 mm/month for each period. For the calculation of KC velocity below, I considered this and evaluated the error for KC velocity. The KC velocity during 1956–1958 was determined to be $0.28 \pm 0.10 \text{ m s}^{-1}$ based on the arrival time difference between Guam and Ishigaki, assuming a speed of $\sim 0.1 \text{ m s}^{-1}$ for the NEC (cf., Qiu and Joyce, 1992; Andrews et al., 2016). Similar calculations were conducted for other periods, such as 1956–1958 and 1958–1961, for which speeds of $0.30 \pm 0.08 \text{ m s}^{-1}$ and $\sim 0.05 \text{ m s}^{-1}$ were determined, respectively. Considering the ENSO condition in 1954, 1956, and 1958, NEC may be strengthened in 1954 and 1956 due to La Niña conditions, which resulted in faster westward ^{14}C transport than the normal conditions in 1958. Accordingly, based on a NEC speed of $\sim 0.05 \text{ m s}^{-1}$ in 1958, which is a minimum estimation of averaged NEC velocity reported by Qiu and Joyce (1992), I determined a KC speed of $0.21 \pm 0.03 \text{ m s}^{-1}$, which is consistent with the uranium-based low-resolution estimate reported previously (Sakaguchi et al., 2016).

3.4.1.3 The mechanism of close-in fallout

The composition and structures of radioactive fallout have been studied since the 1950s. However, the mechanism of close-in fallout is still not clear. Close-in fallout is the radioactive material produced by atomic explosion, which reached and deposited in the range of 64 -129 km from the ground zero (Kellogg et al. 1957; Adams, 1957) and is complete within some 10 – 20 hours (Kellogg et al. 1957). Thermonuclear explosions produced an enormous burst of neutrons and vaporized surface materials such as coral skeletal carbonates (CaCO_3) at the Marshall Islands. It is suggested that the process of ^{14}C produced from coral reefs as follows: the high heat decomposition of coral skeletal carbonates produced calcium oxide (CaO) and some portion of CaO rehydrated to calcium hydroxide (Ca(OH)_2) and combined with CO_2 and became CaCO_3 and water (Adams, 1953; Miller, 1964). This reformed CaCO_3 would include $\text{Ca}^{14}\text{CO}_3$, and provided a direct infusion and dissolution at the sea surface as close-in fallout.

However, recently, some researchers suggested that this reaction proposed in the 1950s and 1960s is not enough to explain the amount of ^{14}C produced by nuclear bomb tests (Lachner et al., 2014). In fact, the ^{14}C spikes detected from the Guam coral greatly exceed the ^{14}C content that can be explained with the process of irradiation with pure CaCO_3 (Andres et al. 2016). Lachner et al. (2014) mentioned that ^{14}C produced in atmospheric N_2 might be incorporated in fallout CaCO_3 , which can be absorbed directly into coral grounds. Reactions in the pore water and in the surrounding water was also important to explain the measured amount of ^{14}C . The distance from the Pacific Proving Grounds and Ishigaki is too far for direct deposition of radioactive materials in Ishigaki. Therefore, the radioactive materials were necessarily absorbed into the surface ocean or were produced from the surrounding water by the nuclear bomb test. These newly discovered ^{14}C spikes in the Ishigaki coral will be important in the field of nuclear physics and will be contributed to an understanding of the mechanism of close-in fallout.

3.4.2 Post bomb test period (after 1970)

The $\Delta^{14}\text{C}$ values in all locations shown in Figures 3.2, 3.3 and 3.4 reached a maximum in the 1970s with high levels persisting until the 1980s. The time resolution of coral samples is an important factor in the detection of seasonal changes in the past. For example, low-resolution $\Delta^{14}\text{C}$ data from Okinawa reported by Konishi et al. (1981) are insufficient to detect such variations. On the contrary, seasonal $\Delta^{14}\text{C}$ measurements were conducted in corals from Langkai (Fallon and Guilderson, 2008) where distinct water mass introductions are happening due to the East Asian monsoon. Although high-resolution measurements were conducted for the corals from three other sites, namely Guam (Andrews et al., 2016), Ishigaki and Palau (the period from 1953 to 1957) (Glynn et al., 2013), no seasonal variability is evident. Thus, these sites are suitable to monitor the western NEC variation in the past since Palau and Ishigaki are located in the western boundary current. In the following sections, I discuss the variability of the KC and MC during the post-bomb-testing period based on calculated differences in the $\Delta^{14}\text{C}$ values between Palau and Guam and between Ishigaki and Guam, which are described as the Palau-Guam $\Delta^{14}\text{C}$ difference and the Ishigaki-Guam $\Delta^{14}\text{C}$ difference, respectively. The $\Delta^{14}\text{C}$ variability in the surface ocean reflects the upwelling intensity at each site. There are no seasonal cycles of $\Delta^{14}\text{C}$ variability related to the local upwelling at Ishigaki, Guam and Palau. Therefore, the Palau-Guam $\Delta^{14}\text{C}$ difference and the Ishigaki-Guam $\Delta^{14}\text{C}$ difference means the upwelling intensity by the Mindanao Dome in the MC region and mesoscale eddies in the KC region respectively. I took an average of the data of Guam and Ishigaki each year to convert from the seasonal data to annual data for calculating the differences between them, because only annual-scale $\Delta^{14}\text{C}$ records are available for Palau (Figure 3.14c). For determining the Ishigaki-Guam $\Delta^{14}\text{C}$ difference, I also calculated the seasonal difference between Ishigaki and Guam using data only obtained from the same timing because the Guam records have a higher temporal resolution than the Ishigaki data (Figure 3.14d). The NEC bifurcation latitude records reported by Zhao et al. (2013) and Hu et al. (2015) were also taken as an average to account for different temporal resolutions in $\Delta^{14}\text{C}$ in each area before comparing NEC variations and $\Delta^{14}\text{C}$ differences. I did not use the NEC bifurcation latitude records reported by Hu et al. (2015) for explaining seasonal Ishigaki-Guam $\Delta^{14}\text{C}$ differences due to the lower resolution of their data compared to the $\Delta^{14}\text{C}$ record in the Ishigaki

coral. The errors of the Ishigaki-Guam $\Delta^{14}\text{C}$ difference and the Palau-Guam $\Delta^{14}\text{C}$ difference were calculated by propagation of errors based on the counting error (see 3.2.1) from measurement of Ishigaki, Guam and Palau corals.

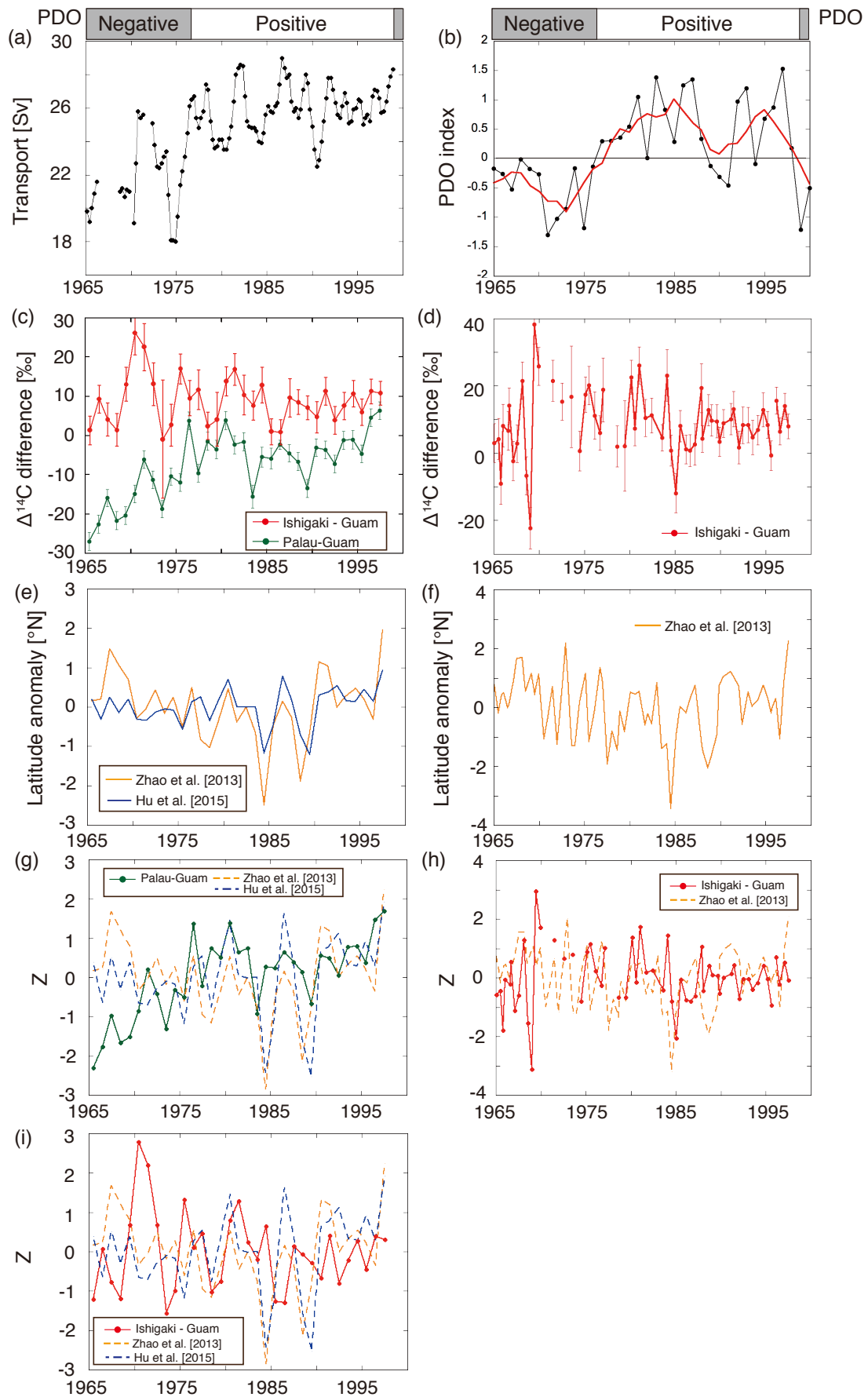


Figure 3.14 (a) Geostrophic volume transport of the Kuroshio Current (KC) across the PN-line (Qui, 2001) and 5-year running average of the PDO index reported by the Japan Meteorological Agency. PN-line is the observation line across the KC pathway in the East China Sea (27°N–29°N) shown in the Figure 3.1 (a). (b) Monthly (Black) and 5-year running average of PDO index reported by the Japan Meteorological Agency. (c) The annual Palau-Guam $\Delta^{14}\text{C}$ difference (green) and Ishigaki-Guam $\Delta^{14}\text{C}$ difference (red). (d) The seasonal Ishigaki-Guam $\Delta^{14}\text{C}$ difference (red). (e) Anomalies in the average annual North Equatorial Current (NEC) bifurcation latitude reported by Zhao et al. (2013) and Hu et al. (2015). (f) Anomalies in the seasonal NEC bifurcation latitude reported by Zhao et al. (2013). (g) Comparison with the annual Palau-Guam $\Delta^{14}\text{C}$ difference and anomalies in the averaged annual NEC bifurcation latitude shown in Figure 3.14(e). (h) Comparison with the seasonal Ishigaki-Guam $\Delta^{14}\text{C}$ difference and anomalies in the seasonal NEC bifurcation latitude shown in Figure 3.14(f). (i) Comparison with the annual Ishigaki-Guam $\Delta^{14}\text{C}$ difference and anomalies in the averaged annual NEC bifurcation latitude shown in Figure 3.14(e). When I compared the NEC bifurcation latitude with $\Delta^{14}\text{C}$ difference, both data were normalized as Z-score in Figure 3.14(g), (h), (i). Positive correlation between the Palau-Guam $\Delta^{14}\text{C}$ difference and NEC bifurcation latitude appeared after 1976 (Figure 3.14g), which suggests that the upwelling in the Mindanao Current region is intensified when the NEC bifurcation latitude migrates southward during positive PDO. Although there are no clear correlation between the Ishigaki-Guam $\Delta^{14}\text{C}$ difference and NEC bifurcation latitude (Figure 3.14h and 3.14i), the Ishigaki-Guam $\Delta^{14}\text{C}$ difference after 1976 become smaller than that before 1976 (Figure 3.14c, 3.14d). This is expected because the local vertical mixing induced by mesoscale eddies in the Kuroshio Current region was intensified after 1976. Modified figure from Hirabayashi et al. (2017a).

3.4.2.1 $\Delta^{14}\text{C}$ Difference between Palau and Guam (Mindanao current)

The Palau-Guam $\Delta^{14}\text{C}$ difference does not display clear annual variations between 1965 and 1997 (Figure 3.14c). However, the annual Palau-Guam $\Delta^{14}\text{C}$ difference exhibits a positive correlation after 1976 ($R = 0.51$, $p < 0.05$ for Zhao et al. (2013) and $R = 0.49$, $p < 0.05$ for Hu et al. (2015)), compared with the annual averaged NEC bifurcation latitude data (Zhao et al., 2013; Hu et al., 2015). The NEC bifurcation latitude is determined by wind forcing in the $12^\circ\text{N} - 14^\circ\text{N}$ band in the Pacific, which is related not only to ENSO but also to the PDO (Wu, 2013; Hu et al., 2015). Hence, the northward shifts in the NEC bifurcation latitude result from both PDO and ENSO activity (Wu, 2013; Gordon et al., 2014; Hu et al., 2015). The Mindanao Dome, whose location is geographically close to Palau and NEC bifurcation latitude, features prominent oceanic variability in the Mindanao Current region. Zhao et al. (2013) reported that the Mindanao Dome is affected by multidecadal southward migration of the bifurcation point because the sea surface height of the Mindanao Dome changes significantly when the bifurcation point stays at southerly latitudes. Both NEC bifurcation latitude and Mindanao Dome vary affected by the wind stress in the western Pacific and central Pacific induced by strength variability of tropical trade winds. The wind stress centered at 12°N in the western Pacific is responsible for the NEC bifurcation latitude and that centered at 6°N in the central Pacific is main cause the Mindanao Dome intensity. However, it is also suggested that the Mindanao Dome is also affected by migration of NEC bifurcation latitude, which is controlled by the different area of wind stress change of 6°N in the central Pacific (Zhao et al., 2013). The detailed mechanism of the interaction between NEC and Mindanao Dome is still unclear because the physical relationship between NEC and Mindanao Dome relations is much more complicated than mathematical expression in the previous model simulation studies. The variability of the Palau-Guam $\Delta^{14}\text{C}$ difference indicates the upwelling intensity changes in the Mindanao Dome, which is dominant site of upwelling in the Mindanao Current region. Therefore, I suggest that the increasing trend seen in the Palau-Guam $\Delta^{14}\text{C}$ difference, which increased from -18.7‰ in 1983 to 3.0‰ in 1987 and from -17.1‰ in 1989 to 0.6‰ in 1993, is due to enhanced vertical upwelling in the Mindanao Dome area and lower surface water $\Delta^{14}\text{C}$ values around Palau when NEC bifurcation latitude migrated southward in those period (Figure

3.14g). Although this time scale is shorter than that reported by Zhao et al. (2013), the $\Delta^{14}\text{C}$ data clearly indicate a shift in the NEC bifurcation point associated with a PDO phase change from negative to positive following a regime shift in 1976.

The strong correlation between the Palau-Guam $\Delta^{14}\text{C}$ difference and migration of the NEC bifurcation latitude found in this study suggests that the signals were resulted from not only the enhanced vertical mixing of Mindanao Dome are but also horizontal water mass advection reaching Palau (7°N , 134°E). However, judging from WOCE data, horizontal water mass exchanges would less significantly affect the Palau-Guam $\Delta^{14}\text{C}$ difference than vertical mixing. In previous studies, it was estimated that the NEC bifurcation latitude changed by a maximum of 3.2°N (Zhao et al., 2013; Hu et al., 2015) based on sea surface height observations, Rossby wave models (Zhao et al., 2013), and Simple Ocean Data Assimilation data. Considering $\Delta^{14}\text{C}$ in the western Pacific region, latitudinal difference within 3.2°N around Palau along 137°E , was only $\sim 2\text{‰}$ – 5‰ according to the measurements of surface seawater from WOCE Section P09 collected in 1994, whereas large differences in depth scale are seen as 87.5‰ at 7°N , 89.5‰ at 10°N , and 94‰ at 12.6°N at the surface. Therefore, I suggest that the Palau-Guam $\Delta^{14}\text{C}$ difference after 1976 was affected by changes in vertical mixing intensity, such as that observe in the Mindanao Dome area, accompanied by migration of the NEC bifurcation latitude.

3.4.2.2 $\Delta^{14}\text{C}$ Difference between Ishigaki and Guam (Kuroshio current)

Both the annual and seasonal Ishigaki-Guam $\Delta^{14}\text{C}$ differences gradually became smaller from 1970 to 1998 (Figures 3.14c and 3.14d). The KC transport volume increased from 1970 to 1990, with a larger average KC transport volume at the PN line in 1970 than that in 1990 (Figure 3.14a) (Qiu, 2001), which is the observation line across the KC pathway in the East China Sea (27°N – 29°N).

The Ishigaki-Guam $\Delta^{14}\text{C}$ difference does not exhibit a strong correlation with the averaged annual NEC bifurcation latitude data (Zhao et al., 2013; Hu et al., 2015) after 1976 ($R = -0.01$, $p = 0.97$ for Zhao et al. (2013) and $R = -0.01$, $p = 0.98$ for Hu et al. (2015)), in contrast to the Palau-Guam $\Delta^{14}\text{C}$ difference. The seasonal Ishigaki-Guam $\Delta^{14}\text{C}$ difference also lacks any correlation after 1976 ($R = 0.17$, $p = 0.30$ for Zhao et al.

(2013)). Therefore, I suggest that the Ishigaki-Guam $\Delta^{14}\text{C}$ difference is not significantly related to a shift in the NEC bifurcation point.

The coral sampling site at Ishigaki does not experience seasonal local upwelling induced by the East Asian monsoon (see Chapter 4; Hirabayashi et al., 2017c). Sowa et al. (2014) also reported that there is little evidence of winter upwelling based on seawater Ba measurements at Fusaki, Inoda, and Akaishi in Ishigaki (Figure 3.1b), which are close to our coral sampling site. There are two possible explanations for the seasonal Ishigaki-Guam $\Delta^{14}\text{C}$ difference, which was not correlated with NEC bifurcation latitude: first that the signal coming from upwelling off the Luzon Strait is produced by mesoscale eddies related to the Kuroshio Loop Current and second that the water is influenced by an unidentified local vertical mixing process induced by mesoscale eddies in some part of the KC area.

The consequences of eddy activity are still unclear (Nan et al., 2015), but several studies indicate that local vertical upwelling can be induced by mesoscale eddies according to nutrient and chlorophyll observations at the sea surface (Yuwaki et al., 1971; Shikakuma, 2002; Buranapratheprat et al., 2010; Wang et al., 2010). Vertical mixing by mesoscale eddies has been observed at the Luzon Strait, off Taiwan, and in the Ryukyu Islands area (Yuwaki et al., 1971; Wang et al., 2010; Shikakuma, 2002; Soeyanto et al., 2014), and water masses upwelling from deeper than 150 m has been observed at Okinawa Island (Shikakuma, 2002).

Previous studies have revealed that significant variability in the surface ocean currents around the southeast of Taiwan and to the east of the Ryukyu Islands results dominantly from mesoscale eddies (e.g., Takikawa et al., 2005; Thoppil et al., 2016). A cyclonic eddy in the upper 500 m was observed southeast of Miyako Island, located 133 km away from Ishigaki Island, which had an impact on the vertical structure of the Ryukyu Current in 2004 (Thoppil et al., 2016). Local vertical upwelling induced by mesoscale eddies has been also observed at the southern parts of Miyako Island and Okinawa Islands and in the east of Taiwan (Yuwaki et al., 1971; Shikakuma, 2002; Soeyanto et al., 2014), where water masses originate from depths of greater than 150 m (Shikakuma, 2002; Soeyanto et al., 2014). Ge et al. (2016) reported $\Delta^{14}\text{C}$ values for DIC in seawater near Okinawa Island (28°04.41'N, 127°07.80'E) of 43.5‰, 31.6‰, and 25.3‰ at water depths of 10, 150, and 200 m, respectively. There is no substantial regional difference in the $\Delta^{14}\text{C}$ of DIC between Okinawa and Ishigaki Island at the

surface (Mitsuguchi et al., 2016) (Figure 3.4). Based on the depth profile of $\Delta^{14}\text{C}$ values for DIC in seawater near Okinawa Island reported by Ge et al. (2016), $\Delta^{14}\text{C}$ values at the sea surface can be changed ~ 5 ‰ when the water mass at the surface mixes with 20 % of the water mass of 150m depth layer via local vertical mixing. It is possible to explain the variability in the Ishigaki-Guam $\Delta^{14}\text{C}$ difference by the local vertical upwelling induced by mesoscale eddies in the Kuroshio Current region. Thus, it is possible that $\Delta^{14}\text{C}$ in the Ishigaki corals was affected by induced mesoscale local vertical upwelling.

The Kuroshio intrusion into the South China Sea (SCS) through the Luzon Strait generates mesoscale eddies (Wu and Chiang, 2007) and induced cyclonic/anticyclone eddies at the northwestern end of the KC axis (Nan et al., 2015). Therefore, via the Luzon Strait, the KC has been affected by local vertical upwelling induced by mesoscale eddies around the Luzon Strait and the $\Delta^{14}\text{C}$ values at Ishigaki have been influenced by ^{14}C depleted water transported from greater water depths in the Luzon Strait.

Judging from the average volume of KC transport at the PN line, the KC off the northeast Taiwan has become enhanced since 1976 (Qiu, 2001). A positive PDO promotes a larger KC transport off northeast Taiwan (Wu, 2013). In the Subtropical Countercurrent region (20°N–23°N), the mesoscale eddies propagate westward and collide with the KC at the eastern coast of Taiwan (Hwang et al., 2004). This is the mechanism responsible for the increase in KC transport off northeast Taiwan (Wu, 2013). During the positive PDO period, as the NEC bifurcation latitude migrates northward, eddy activities were also increased (Chang and Oey, 2012). More abundant westward-propagating eddies meets the KC off east Taiwan in the Subtropical Countercurrent area, which increase the KC transport (Wu, 2013). Ishigaki Island is located off the east coast of Taiwan, hence, the ^{14}C in the sea surface water is probably affected by mesoscale eddies as is recorded in my coral. $\Delta^{14}\text{C}$ in the Ishigaki coral is generally higher than that of Guam because of well-equilibrated water existing in the region through air-sea CO_2 exchange in the area of Ryukyu Islands. After 1976, when the PDO shifted from negative to positive phases, the northward migration of NEC bifurcation latitude occurred with abundant westward-propagating mesoscale eddies off east Taiwan, which might have been seen as decrease in $\Delta^{14}\text{C}$ in the Ishigaki coral. This is expected because of the local vertical mixing induced by mesoscale eddies. It is also

observed as smaller decadal $\Delta^{14}\text{C}$ differences between Ishigaki Island and Guam after 1976 compared with the Ishigaki-Guam $\Delta^{14}\text{C}$ differences in the period of negative PDO conditions.

3.4.2.3 Kuroshio intrusion variability in the South China Sea for the post-bomb-test period (Kuroshio Loop Current)

I examined the mixing of water masses northwest of Luzon Island based on the $\Delta^{14}\text{C}$ values of Guam and Con Dao (representing water masses from the Pacific Ocean and the SCS, respectively; see Appendix of Chapter 3; Figure A3.3 ; Hirabayashi et al., 2017b) to evaluate strength variability of the Kuroshio Loop Current intrusion. Hon Tre Island is located on a coastal shelf surrounded by less than 100-m-deep waters (Bolton et al. 2016). Comparing with the Con Dao $\Delta^{14}\text{C}$ record reported by Mitsuguchi et al. (2007), $\Delta^{14}\text{C}$ in Con Dao is consistently higher than that in Hon Tre Island (Figure 3.7, Figure 3.13). This is attributed to the fact that Hon Tre Island coral site is affected by shallow coastal upwelling at $\sim 12^\circ\text{N}$ during the summer, whereas this upwelling-originated water mass does not reach Con Dao (Figure 3.15). The $\Delta^{14}\text{C}$ value of Ishigaki was affected by the mixing of water masses from the Pacific Ocean and Luzon Strait (Figure 3.15) because of the variation in the Kuroshio path. Because Kuroshio intrusion in the Pacific water mass takes different paths through the Luzon Strait because of eddies on various timescales (e.g., Li et al. 1998; Hu et al. 2000; Wu and Chiang 2007; Qu et al. 2009), and because surface circulation in the SCS exhibits seasonal variation, I discuss the changes in water masses reached to the Currimao separately for different seasons (summer and winter) and decades (1970s and 1980s) (Figure 3.15).

3.4.2.3.1 Decadal comparison

Because of the above-described reasons, the Con Dao coral records the $\Delta^{14}\text{C}$ signature of the SCS surface water. In contrast, the $\Delta^{14}\text{C}$ of Guam coral represents the value of Kuroshio water reaching the eastern coast of the Philippines. Thus, the degrees of changes in two water masses, both from Kuroshio and SCS, reaching the Currimao coast are responsible for fluctuations observed in $\Delta^{14}\text{C}$ of Currimao corals in the 1970s and early 1980s. It seems likely also that the area of mesoscale eddies changed between 1970s and 1980s. The coral record from Currimao indicates that the site was less influenced by vertical mixing driven by mesoscale eddies in the 1970s because $\Delta^{14}\text{C}$ in Currimao during this period was constantly higher than/or the same as that of Guam (Figure 3.7). After the mid-1980s, the $\Delta^{14}\text{C}$ in Currimao was the lowest among Guam, Con Dao, and Ishigaki although there are no data except for 1986 from the Hon Tre Island, because vertical mixing related to mesoscale eddies driven by Kuroshio intrusion likely diluted $\Delta^{14}\text{C}$ at the ocean surface.

3.4.2.3.2 Seasonal comparison

The intrusion of the Kuroshio Loop Current into the Luzon Strait is generally observed from November to March as a result of the northeast monsoon during the winter (e.g., Hsin et al. 2012; Nan et al. 2015). Observational data show that the anticyclonic intrusion of the Kuroshio can occur during any season, although winter is the most favorable time of the year (Yuan et al. 2006). This Kuroshio intrusion is affected by the bifurcation of the NEC on seasonal and interannual timescales. Kuroshio intrusion into the Luzon Strait tends to be stronger during El Niño years because bifurcation of the NEC migrates northward during El Niño years (Figure 1.8, 1.9); this results in a weaker Kuroshio current east of Luzon, which provides a favorable condition for the intrusion of Pacific waters through the Luzon Strait (Sheremet 2001; Yaremchuk and Qu 2004; Qu et al. 2004).

(1) Summers in the 1970s

Comparing $\Delta^{14}\text{C}$ among five sites depicted in Figure 3.13b, the highest and the lowest sites are Con Dao and Guam, respectively. Because of coarse resolution of the

coral record obtained from Hon Tre Island (i.e., annual instead of seasonal), I cannot compare directly with other coral $\Delta^{14}\text{C}$ results. However, Bolton et al. (2016) reported seasonal variability for 1969 and found that summer $\Delta^{14}\text{C}$ marked lowest in the year because of local upwelling. Assuming this upwelling had persisted during summers in the 1970s, $\Delta^{14}\text{C}$ in surface water around Hon Tre Island would possibly have been lower than that of Guam during the summer. The Currimao coral $\Delta^{14}\text{C}$ during summers in the 1970s, in particular between 1972 and 1975, records as high $\Delta^{14}\text{C}$ as Con Dao coral (Figure 3.13b). It seems unlikely that the water mass traveled via the area near the Hon Tre Island to Currimao. According to Zhao et al. (2013), the average NEC bifurcation latitude in summer is 12.5°N (Figure 3.13a), which is almost identical to the normal bifurcation point in summer (12.4°N from 1968 to 1994). Kuroshio intrusion into Luzon Strait tends to be stronger during strong El Niño years (Ho et al. 2004). However, the $\Delta^{14}\text{C}$ of Currimao from 1972 to 1973, which were strong El Niño years, was higher than that in Guam (Figure 3.13b). The NEC bifurcation latitudes in the summers of 1972 and 1973 were 13.1°N and 12.0°N , respectively (Figure 3.13a). The most northward migration of the NEC occurred in the winter of 1972/1973, when the NEC bifurcation latitude was 14.7°N (Figure 3.13a). The NEC bifurcation latitude in the summer of 1973 was not favorable for the intrusion of Pacific waters into the Luzon Strait. In the summer of 1972, Kuroshio intrusion into Luzon Strait was stronger than usual because of the higher NEC bifurcation latitude; however, the higher $\Delta^{14}\text{C}$ of Currimao compared with Guam indicates that the intrusion did not reach Currimao. Therefore, I suggest that the $\Delta^{14}\text{C}$ of Currimao was mainly affected by water mass advection from the central SCS via the East Asian summer monsoon rather than by Kuroshio intrusion or vertical mixing induced by mesoscale eddies (Figure 3.15b). The $\Delta^{14}\text{C}$ level in Ishigaki fluctuated between those of Currimao and Guam (Figure 3.13b). The $\Delta^{14}\text{C}$ value in Ishigaki reached that of Luzon Island in 1971, 1972, and 1975 and that of Guam in 1973, 1974, and 1978. No $\Delta^{14}\text{C}$ value was recorded in Ishigaki from 1976 to 1977. The sample site at Ishigaki is known for seasonal upwelling (Sowa et al. 2014; see also Chapter 4, Hirabayashi et al., 2017c). The higher $\Delta^{14}\text{C}$ value of Ishigaki likely resulted from the water mass that passed through the Luzon Strait via the Kuroshio Loop Current; the lower $\Delta^{14}\text{C}$ values likely resulted from the water mass that did not pass through the Luzon Strait and was transported directly to Ishigaki.

(2) Summers after the mid-1980s

Among the four locations except Hon Tre Island, the $\Delta^{14}\text{C}$ levels decreased in the following order: Ishigaki > Guam > Con Dao > Currimao (Figure 3.13b). This trend is different from that observed in the 1970s. Only 1986 data are available for Hon Tre Island but it is likely that the boreal summer value in $\Delta^{14}\text{C}$ was lower than that of Currimao because of upwelling reported by Bolton et al. (2016). It is difficult to ascertain the origin of the water mass that reached Currimao because the difference in $\Delta^{14}\text{C}$ between Guam and Con Dao became smaller after the mid-1980s compared with those in the 1970s, although the $\Delta^{14}\text{C}$ value in Con Dao was annual.

The average NEC bifurcation latitude from 1985 to 1994 was 12.5°N (Figure 3.13a), which migrated southward comparing to the average bifurcation latitude of 12.9°N from 1968 before the regime shift in 1976/1977. Southward shift of the NEC bifurcation corresponds to a stronger Kuroshio transport off the Philippines (Qu et al. 2004) (Figure 1.8). The previous studies reported based on the model simulation (Sheremet, 2001) and the laboratory study of this phenomenon (Sheremet and Kuehl, 2007), that the more Kuroshio transport increases, the greater the inertia produced, which makes less Kuroshio Loop Current intrusion into the Luzon Strait and the Kuroshio flow northward relatively straight path from off the east Philippine to east side of Taiwan (Wu et al., 2016). Considering Kuroshio transport off the Philippines in the 1970s and 1980s, Kuroshio intrusion into the Luzon Strait was probably weaker in the 1980s because stronger Kuroshio transport is not favorable for the penetration of Pacific waters into the SCS through the Luzon Strait (Qu et al., 2004; Wu et al., 2016). Therefore, I suggest that the water mass reaching northwest of Luzon in the 1980s originated from the SCS (Figure 3.15d).

I also suggest that different water masses reached northwest Luzon in 1985, 1989, and 1990. The $\Delta^{14}\text{C}$ in the Currimao coral decreased during these years; this trend was not observed in the other studied locations (Figure 3.13b). Abrupt northward migration of the NEC bifurcation latitude was also observed in 1985, 1989, and 1990 (Figure 3.13a). Hu et al. (2015) reported that Kuroshio intrusion into the Luzon Strait becomes stronger when the NEC bifurcation latitude migrates north. Thus, I suggest the following scenario during 1985, 1989, and 1990. Kuroshio intruded into the SCS but did not reach the region northwest of Luzon Island. Additionally, Kuroshio intrusion induced mesoscale eddies around Luzon Island (Nan et al., 2011, 2015) (The dashed

orange arrows in Figure 3.15d), causing the $\Delta^{14}\text{C}$ of Currimao to decrease as a result of vertical mixing.

(3) Winters in the 1970s

The fact that the $\Delta^{14}\text{C}$ values in Currimao were similar to those in Guam during the 1970s indicates that the water mass that reached this area may have originated from the Kuroshio Loop (Figure 3.15a). It is difficult to compare Currimao data with Con Dao and Hon Tre Island because of coarse resolution for the latter sites; however, I can conclude that SCS water masses did not reach Currimao given that $\Delta^{14}\text{C}$ in Hon Tre Island would have been higher than the values in Figure 3.13c.

Because of the lack of data for Ishigaki, it is difficult to deduce the mechanism of changes in the water mass around Ishigaki; however, the higher $\Delta^{14}\text{C}$ in Ishigaki, at least from 1975 to 1977 (Figure 3.13c), suggests that this region was not affected by mesoscale eddies around Taiwan or the Luzon Strait. The average NEC bifurcation latitude in the 1970s before the regime shift in 1976/1977 was 13.1°N , whereas the average latitude after 1985 was 12.7°N (Figure 3.13a). During the winter of 1972/1973, which fell during a strong El Niño year, the NEC bifurcation latitude was 14.7°N (Figure 3.13a), which is favorable for the intrusion of Pacific waters through the Luzon Strait (Sheremet 2001; Yaremchuk and Qu 2004; Qu et al. 2004). Because of this, $\Delta^{14}\text{C}$ in Currimao was similar to that in Guam, indicating that the Pacific water mass reached Currimao via a strong Kuroshio intrusion in the winter of 1972/1973 (Figure 3.15a). The Kuroshio Loop Current may have expanded southwestward to include the area northwest of Luzon Island because of the northward migration of the NEC bifurcation latitude (Figure 3.15a) (Hu et al. 2015).

(4) Winters after the mid-1980s

During winters after the mid-1980s, the $\Delta^{14}\text{C}$ values were lowest in Currimao among the studied locations, and the $\Delta^{14}\text{C}$ values in Guam and Ishigaki were similar (Figure 3.13c). In this period, $\Delta^{14}\text{C}$ data in 1986 are the only data reported from Hon Tre Island. Annual $\Delta^{14}\text{C}$ data in 1986 in Hon Tre Island are the same as those in Currimao, but considering the seasonal variation, winter $\Delta^{14}\text{C}$ in Hon Tre Island would be higher than Currimao. Therefore, during winters after the mid-1980s, the $\Delta^{14}\text{C}$ values

were lowest in Currimao among the studied locations. Although the Con Dao data are annual, the $\Delta^{14}\text{C}$ value in Con Dao was higher than that in Currimao during winter because of vertical mixing induced by mesoscale eddies northwest of Luzon Island. These mesoscale eddies are thought to be induced by Kuroshio intrusion into the Luzon Strait (Figure 3.15c). The average NEC bifurcation latitude after 1985 was 12.7°N , which is located south of the bifurcation point in the 1970s (Figure 3.13a). Therefore, Kuroshio intrusion into the Luzon Strait was weaker in the 1980s than in the 1970s, and the water mass of the Kuroshio did not reach northwest of Luzon Island (Figure 3.15c). However, Kuroshio intrusion induced mesoscale eddies in that area (The black dotted circle in Figure 3.15c), which caused the $\Delta^{14}\text{C}$ in Currimao to be the lowest among the five studied locations. According to Tseng et al. (2009), weakening of the monsoon decreases the extent of vertical mixing in the northern SCS. The East Asian winter monsoon velocity decreased from the 1970s to the 1980s (Song et al. 2012); thus, the area of mesoscale eddies decreased in size after 1976. However, I suggest that the mesoscale eddies lingered in the area northwest of Luzon Island.

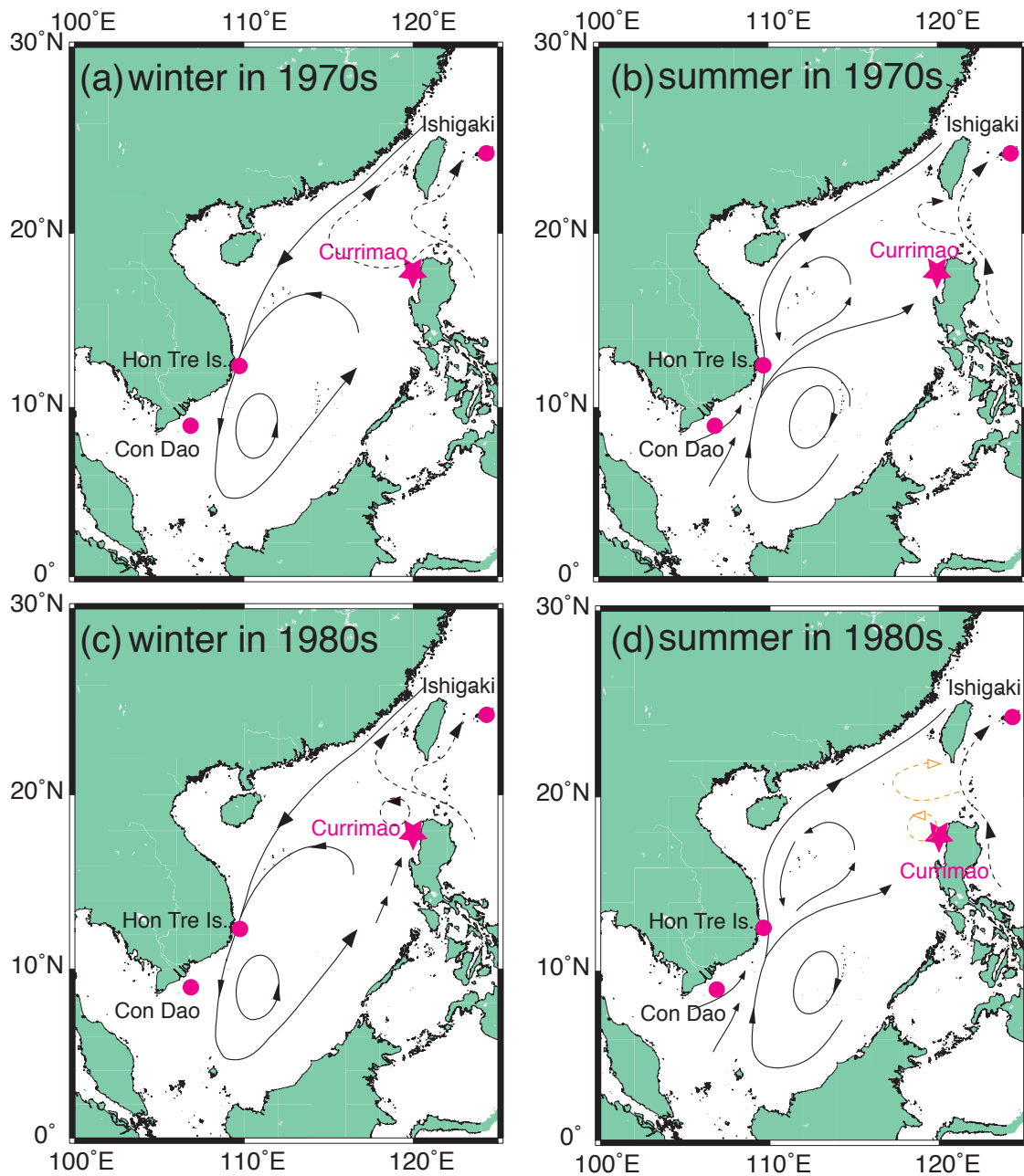


Figure 3.15 Schematic illustration of surface ocean circulation in the South China Sea. The main current (black solid lines) of the South China Sea is based on Wang and Li (2009). The path of the Kuroshio Loop Current (black dotted line) fluctuated in (a, b) the 1970s and (c, d) the 1980s. The orange arrows in (d) are for the periods 1985 and 1989-1990. From Hirabayashi et al. (2017b).

3.5 Summary

In this chapter, I measured high-resolution radiocarbon in corals taken from Ishigaki and Currimao, which located in Kuroshio and Kuroshio Loop Current, using the method developed in the Chapter 2. This is the first high-resolution radiocarbon data from the western boundary current area of North Pacific for the bomb- ^{14}C period and are compared with the previously reported radiocarbon data from Guam, Palau, Langkai, Con Dao and Hon Tre Island. I succeeded to detect the three early bomb spikes related to nuclear operations in the US Pacific Proving Grounds from Kuroshio region. I precisely evaluated the past speed of the KC using bomb-testing-related ^{14}C in corals from Ishigaki and Guam and suggested that the transport speed by the North Equatorial current and Kuroshio varied depending on the ENSO condition in the 1950s and 1960s. The Currimao coral's radiocarbon data only detected the first bomb- ^{14}C spike because the second and third bomb- ^{14}C spikes were hidden by the seasonal ^{14}C variability in the South China Sea, which is a similar trend to the radiocarbon data from Langkai.

Based on a comparison of my Ishigaki data with previously reported data from Guam and Palau, I suggest that $\Delta^{14}\text{C}$ in ocean surface layers is affected by upwelling related to southward migration of the NEC bifurcation latitude in the Mindanao Dome region and mesoscale eddies at the Luzon Strait and around the Ishigaki and Taiwan areas after 1976, when the PDO phase changed from negative to positive. On the decadal scale, a positive PDO engenders stronger Kuroshio transport, at the east side of Taiwan, which may have produced a smaller difference in $\Delta^{14}\text{C}$ between Ishigaki and Guam after 1976. The radiocarbon concentration in the Currimao coral also affected by the transport of a South China Sea water mass to the northwest of Luzon Island. This transport was triggered by the overall southward shift of the bifurcation latitude associated with the 1976 regime shift, which led to a decrease in the magnitude of Kuroshio intrusion into the Luzon Strait.

Further investigations with high spatial and temporal resolution are needed to clarify the detailed mechanism of the relationship between Kuroshio, Kuroshio Loop Current and climate change. However, the data presented herein contribute to our understanding of the physical oceanography of the North Pacific western boundary current.

**Chapter 4 Short-term fluctuations in natural
radiocarbon recorded in coral skeletons from
Kuroshio region (pre-1950)**

4.1 Introduction

In Chapter 3, I reconstructed oceanography along the Kuroshio current using bomb- ^{14}C in coral skeletons. However, this method is only useful after the 1950s, being the period after the nuclear bomb tests conducted at the Pacific Proving Grounds. Previous studies ignored the small ^{14}C variability. Therefore, the ^{14}C age difference of the atmosphere and ocean assumes almost constant and the small ^{14}C variability are treated as negligible variation. However, I revealed the seasonal-scale ^{14}C variability reflects water mass advection and vertical mixing in Chapter 3. The new high-resolution ^{14}C measurement in Chapter 2 makes the negligible ^{14}C variability possible for discussion with respect to oceanography. The ^{14}C age difference of atmosphere and ocean is defined as the marine reservoir age (R) and the local difference of R is defined as the local marine reservoir age (ΔR) (see 4.2.3). In this chapter, I use the local marine reservoir age (ΔR) as a proxy for water mass change for the period before 1950 in this chapter, to extend the time-scale of investigation will allow further discussion of the relationship between oceanography in the west Pacific and climate change. Radiocarbon is the unique radioactive material which can be used as an oceanographic tracer before 1950. However, Uranium-236 is limited after 1950 because of Uranium-236 produced in seawater by nuclear bomb-testing in the 1950s. Naturally produced Uranium-236 is difficult to be measured by present AMS techniques because the natural concentration of Uranium-236 in sea water is lower than the lower limit of Uranium-236 concentration analysis with AMS at this stage. Thus, ^{14}C is suitable proxy for seasonal oceanographic reconstruction even the period before 1950.

For the reconstruction of oceanography before the 1950s, the local marine reservoir age (ΔR) can be used as a tracer. Seawater is commonly depleted in ^{14}C relative to the ambient atmosphere, resulting in surface water ‘aged’ as much as 400 years on average in the low to mid-latitude global oceans. This is called the marine reservoir age (R) defined by Stuiver et al. (1986). Because inherited radiocarbon signatures differ by region, depending on the local environment, the marine reservoir effects are region-specific (Southon et al., 2002). For example, radiocarbon ages in polar regions appear to be ‘old’, whereas the marine reservoir effect is minimal in highly ventilated ocean regions (Matsumoto and Yokoyama, 2013; Yokoyama et al., 2016). These differences reflect local reservoir ages (ΔR), which can be calculated

following methods (Ulm 2006; Hua et al., 2015); 1) measuring the ^{14}C content before AD 1955 using historical age-known marine samples such as corals and shell specimens (Southon et al., 2002; Ulm, 2002; Hua et al., 2004; Petchey and Ulm, 2012), 2) Radiocarbon dating of paired shell fragments and charcoal in archaeology contexts (Ortlieb et al., 2011; Petchey and Ulm, 2012; Latorre et al., 2017) and 3) measuring the ^{14}C content of coral samples that are independently uranium-thorium dated (McGregor et al., 2008; Yu et al., 2010; Hua et al., 2015).

R and ΔR values for a given location/region are generally assumed to be almost constant over time when calibrating marine ^{14}C ages (Stuiver et al., 1986). However, recent studies suggest that ΔR varies not only spatially but also temporally because of the changes of ocean circulation associated with important climate changes such as the last glacial and deglaciation period (e.g. Sikes et al., 2000; Siani et al., 2001, 2013; Bondevik et al., 2006; Sarnthein et al., 2011; Skinner et al., 2015). For the last 10,000 years, the reservoir ages also varied more than hundreds years reported from the Pacific (see Appendix of Chapter 4). For example, Hua et al. (2015) reported that large ΔR variability in eastern Australia is evident for the period $\sim 5.4\text{-}8$ ka BP, which is consistent with ΔR variability in the southern Peru-northern Chile in southeastern Pacific (Fontugne et al., 2004; Ortlieb et al., 2011) affected by the intensity of the upwelling along the Peru-Chile coast related to the intensity of El Niño-Southern Oscillation (ENSO) and positions of the Intertropical Convergence Zone and the South Pacific Convergence Zone.

Here I report high-resolution ^{14}C dates from the modern corals collected from Ishigaki Island and the northwest part of Luzon Island. The Ryukyu Islands (Ishigaki and Kikai Island) are located in the Kuroshio current and the northwestern part of Luzon Island is located near the Kuroshio Loop Current. Therefore, these three locations are suitable for reconstruction of whole Kuroshio current. I also compare my data with previously reported data from the Pacific Ocean and consider possible causes of the spatio-temporal changes of ΔR in the period since the 1900s.

4.2 Materials and Methods

4.2.1 Modern corals from Ryukyu Islands

Vertical coral cores were extracted with an air drill from living *Porites* sp. colonies in the Ryukyu Islands, at Ishigaki Island (Okinawa; 24°N, 124°E) in 2002, and at Kikai Island (Kagoshima; 29°19'N, 130°E) in 2009. Core IY02-02 was obtained at a water depth of about 5m off Yasurazaki on the north-eastern coast of Ishigaki Island. Core KAR09 was obtained at a water depth of about 3.5m off the south-east coast of Kikai Island (Kawakubo et al., 2014). Both sites are in an open ocean setting (Tottori et al., 2004; Morimoto et al., 2007), free from freshwater input from rivers, and thus hard-water effects did not influence my analyses.

Coral powder was obtained from core KAR09 by the micromilling technique of Suzuki et al. (2003) at 3-year intervals between 1901 and 1948 on the basis of Sr/Ca ratios and X-ray positive radiographs from Kawakubo et al. (2014). Core IY0202 was micro-sampled at 1.0-mm intervals, and Sr/Ca ratios were determined by the method of Chapter 2 (Hirabayashi et al., 2013). Approximately 10mg of powdered samples for KAR09 were graphitized for radiocarbon dating using the method described by Yokoyama et al. (2007), whereas 1–3mg samples of core IY02-02 were prepared using a specially designed vacuum line for small samples (See Chapter 3; Hirabayashi et al., 2017a; Yokoyama et al., 2010). The graphite target samples were then analyzed with a single-stage accelerator mass spectrometer (YS-AMS; Yamane et al., 2014) at the Atmosphere and Ocean Research Institute, University of Tokyo.

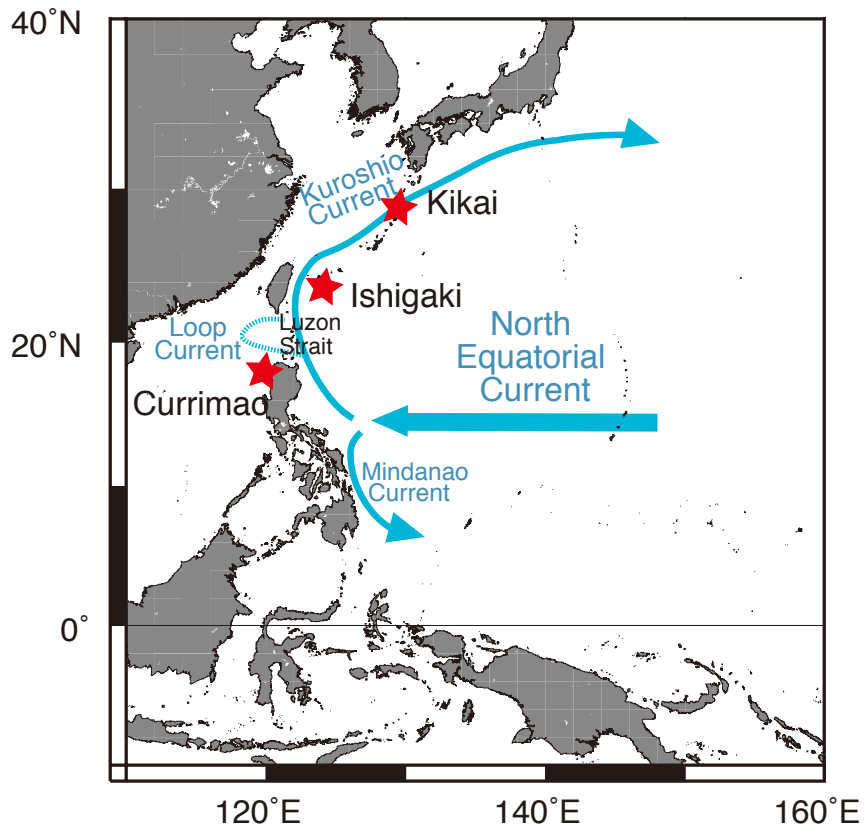


Figure 4.1 Regional map showing locations of Ishigaki and Kikai Islands in the Ryukyu Island chain and Currimao offshore Luzon Island (red stars).

4.2.2 Modern corals from Luzon Island

A modern coral (*Porites lutea*) core, PUCRIN03, was collected from the Currimao coast (17°59'N, 120°29'E) in Luzon along the Northern South China Sea coast of the Philippines at a water depth of 4.8 m in 2004. PCURIN03 was micro-sample at 0.8-mm intervals for Sr/Ca ratio measurements and radiocarbon dates (Chapter 2, Hirabayashi et al., 2013). I measured the Currimao coral with same method as Ishigaki coral I mentioned above, but 6-10 mg of each sample from PCURIN03 for radiocarbon dating was graphitized for radiocarbon dating (Chapter 3, Hirabayashi et al., 2017b).

4.2.3 Calculation of marine reservoir age (R) and local marine reservoir age (ΔR)

The marine reservoir age (R) is defined by Stuiver et al. (1986) as the difference between the ^{14}C age of the marine ($^{14}\text{C}_M$) and terrestrial samples ($^{14}\text{C}_T$) at a known time (t);

$$R(t) = {}^{14}\text{C}_M(t) - {}^{14}\text{C}_T(t)$$

Here, time (t) was determined by counting Sr/Ca peaks for modern corals. $^{14}\text{C}_T(t)$ is determined using the atmospheric calibration curve IntCal13 (Reimer et al., 2013) and $^{14}\text{C}_M(t)$ is measured ^{14}C values with AMS in AORI.

The local marine reservoir age (ΔR) can be calculated as the difference between $^{14}\text{C}_M$ measured using corals and marine ^{14}C ages estimated by marine global model ocean such as Marine13 (Reimer et al., 2013);

$$\Delta R(t) = {}^{14}\text{C}_M(t) - {}^{14}\text{C}_{MAR}(t).$$

I estimated errors for R (σ_R) and ΔR ($\sigma_{\Delta R}$) as follows:

$$\sigma_R = \sqrt{(\sigma_{IntCal13 \text{ model age}})^2 + (\sigma_{sample \text{ age}})^2}$$

$$\sigma_{\Delta R} = \sqrt{(\sigma_{Marine13 \text{ model age}})^2 + (\sigma_{sample \text{ age}})^2}$$

in which $\sigma_{IntCal13 \text{ model age}}$ and $\sigma_{Marine13 \text{ model age}}$ is the estimate of the IntCal13 and Marine13 calibration curve error, derived from an average of 1σ span of the age, respectively. $\sigma_{sample \text{ age}}$ is the measurement error of the radiocarbon age of the samples.

4.3 Results

The results are presented in Table 4.1 and Figures 4.2 and 4.3. Local reservoir ages that I determined for samples from Kikai Island varied from -73 ± 35 to 27 ± 62 years, with a mean value of -36.6 years for the period 1901–1948 (Figure 4.5; Table 4.1). The 3-year average of ΔR determined from Ishigaki Island for 1947–1950 was -36.0 years, which is consistent with the average ΔR value (-36.6 years) from Kikai Island for 1901–1948 (Figure 4.5). High resolution ΔR data (2–3 data points per year) from Ishigaki Island showed large fluctuations in the late 1940s, varying from -136 ± 42 to 62 ± 50 years (Figure 4.4; Table 4.1). This fluctuation in the late 1940s is also shown by the modern Currimao coral, where ΔR varied from -70 ± 35 to 46 ± 34 years with a mean value of -5.8 years (Figure 4.4; Table 4.1).

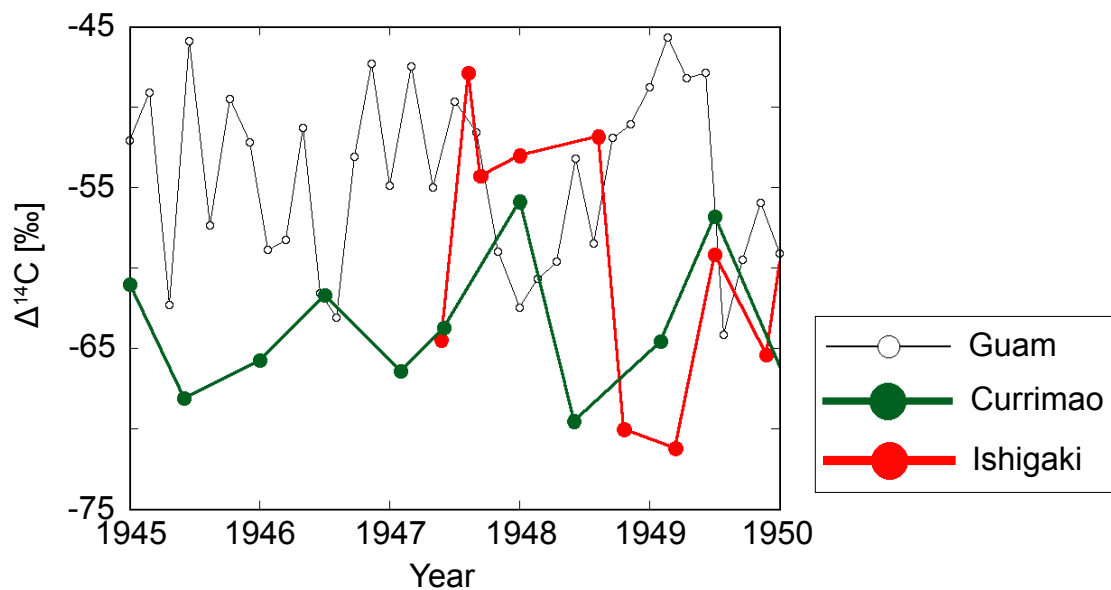


Figure 4.2 Comparison of $\Delta^{14}\text{C}$ values from Ishigaki Island (red), Currimao (green) and Guam (open circles) (Andrews et al., 2016).

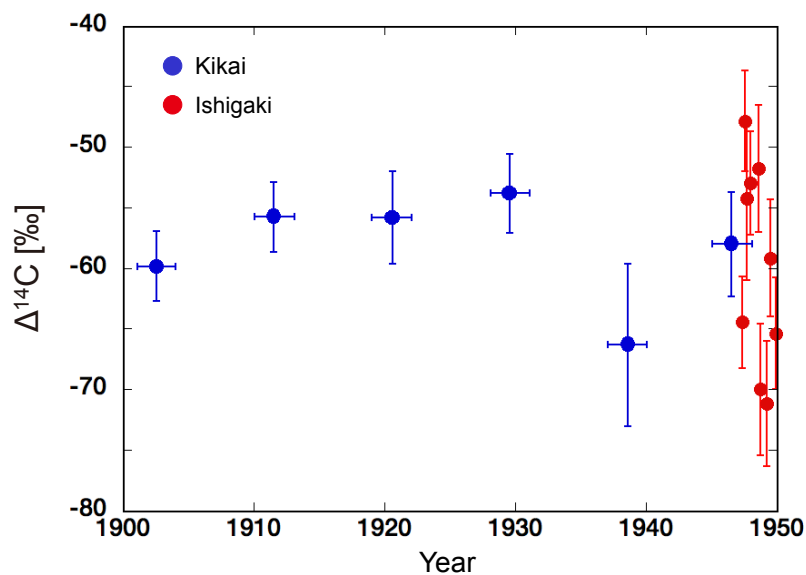


Figure 4.3 Comparison of $\Delta^{14}\text{C}$ values from Kikai (blue) and Ishigaki (red) Islands.

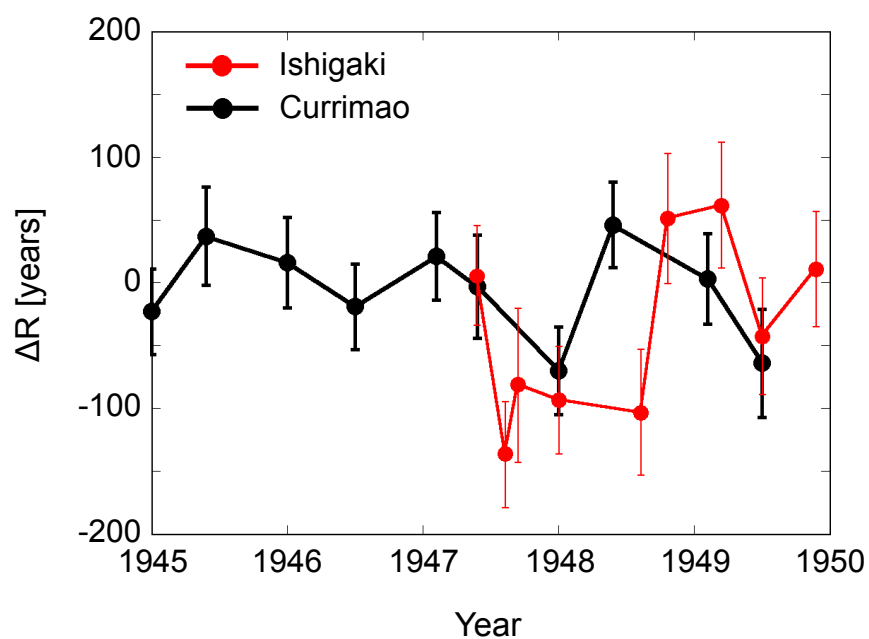


Figure 4.4 Short-term ΔR fluctuation from 1945 to 1950 recorded in corals from Ishigaki Island (red) and Currimao (black).

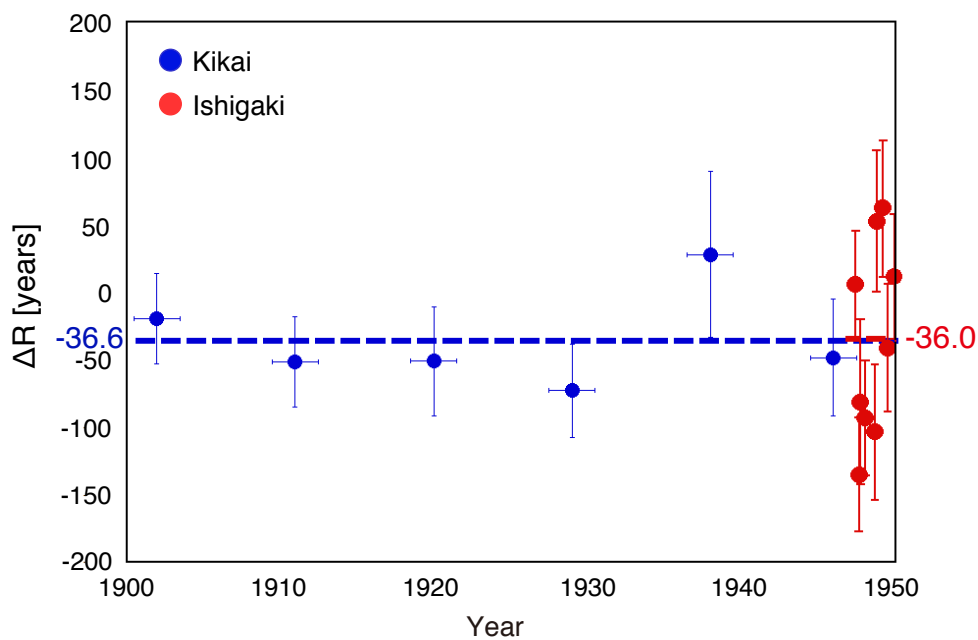


Figure 4.5 Comparison of ΔR values from Kikai (blue) and Ishigaki (red) Islands. The numbers indicate the averaged ΔR values of Kikai (blue) and Ishigaki (red) Islands. From Hirabayashi et al. (2017c).

Table 4.1
 ^{14}C ages of the corals from Kikai Island, Ishigaki Island (Hirabayashi et al., 2017c) and Currimao and their reservoir age R and ΔR .

Sample Name	Lab No.	Analyzed Period	^{14}C age (yr BP)	R (yr)	\pm	ΔR (yr)	\pm	
KAR09-C2-D3	YAUT-021307	1901-1903	431	24	352	25	-20	34
KAR09-C2-D1	YAUT-021321	1910-1912	396	24	296	25	-52	33
KAR09-C2-C4	YAUT-021619	1919-1921	396	33	269	34	-52	40
KAR09-C2-C3	YAUT-021313	1928-1930	379	26	231	27	-73	35
KAR09-C2-C1	YAUT-021303	1937-1939	486	57	321	58	27	62
KAR09_C2_B7b	YAUT-018734	1945-1947	416	37	226	38	-49	43
IY0202-G89	YAUT-019514	1947.4	472	33	279	34	6	40
IY0202-G85	YAUT-017422	1947.6	331	35	137	36	-136	42
IY0202-G81	YAUT-016939	1947.7	385	57	191	57	-81	61
IY0202-G75	YAUT-019525	1948	374	36	179	37	-93	43
IY0202-G69	YAUT-016938	1948.6	364	44	168	45	-103	50
IY0202-G65	YAUT-019516	1948.8	520	47	323	48	52	52
IY0202-G58	YAUT-019517	1949.2	530	45	333	45	62	50
IY0202-G55	YAUT-017424	1949.5	427	41	229	42	-42	47
IY0202-G50	YAUT-019515	1949.9	480	40	281	40	11	46

Continued

Sample Name	Lab No.	Analyzed ^{14}C age Period (yr BP)	\pm	R (yr)	\pm	ΔR (yr)	\pm	
PCURIN-F4-55	YAUT-032815	1949.5	404	36	207	37	-64	43
PCURIN-F4-71	YAUT-032807	1949.08	471	27	274	28	3	36
PCURIN-F4-85	YAUT-032813	1948.4	514	25	318	27	46	34
PCURIN-F4-97	YAUT-032812	1948	397	26	202	27	-70	35
PCURIN-F4-105	YAUT-032816	1947.4	463	34	270	35	-3	41
PCURIN-F4-129	YAUT-032819	1947.1	487	26	294	27	21	35
PCURIN-F4-139	YAUT-032804	1946.5	446	25	255	27	-19	34
PCURIN-F4-155	YAUT-032817	1946	481	28	291	29	16	36
PCURIN-F4-159	YAUT-032818	1945.4	501	32	312	33	37	39
PCURIN-F4-171	YAUT-032802	1945	441	25	253	27	-23	34

4.4 Discussion

4.4.1 Seasonal fluctuations in regional radiocarbon reservoir age in 1940s

The results for Ishigaki Island showed short-term, seasonal-scale fluctuations of ΔR from 1947 to 1950 (Figure 4.4), but not equivalent to the cycles that Mitsuguchi et al. (2004) reported. Mitsuguchi et al. (2004) reported seasonal cycles of $\Delta^{14}\text{C}$ from 1985 to 1999 in coral from the same sampling site of my Ishigaki coral, Yasurazaki in Ishigaki Island, which they attributed to local upwelling induced by the East Asian monsoon. The reason for this discrepancy is uncertain, but additional analyses of new coral samples from the same region over a time interval spanning both data sets will resolve this.

Short-term ΔR fluctuation was also shown in the Currimao coral. However, there is also no clear seasonal cycle detected in the Currimao corals. Although Currimao has local upwelling in winter shown in Chapter 3 (Hirabayashi et al., 2017b), there is no clear seasonality of ΔR changes in this area for this period. The $\Delta^{14}\text{C}$ difference between summer and winter is smaller than for post-bomb period (1968-1994) (see in Chapter 3, Hirabayashi et al., 2017b). According to reconstructed wind velocity data reported by Song et al. (2012), winter wind velocity in the 1940s was the smallest in the period from 1818 to 2000. Because of weak winter monsoon wind velocity in the South China Sea, the $\Delta^{14}\text{C}$ difference between winter and summer was unclear in this period. The other possibility to explain less seasonality is that the $\Delta^{14}\text{C}$ difference between the surface and deeper ocean layers for the period before the 1950s was smaller than that of the period after the 1950s because there were high concentrations of radiocarbon input into the surface layer derived nuclear bomb test after the 1950s, as mentioned in Chapter 3.

The negative shift of the PDO phase occurred in 1947/1948 (Mantua et al., 1997). Grotoli et al. (2003) reported that the ^{14}C record of Fanning Island ($3^{\circ}54'32''\text{N}$, $159^{\circ}18'88''\text{W}$), which showed a positive shift in $\Delta^{14}\text{C}$ between 1947 and 1956 that coincides with the negative shift of PDO in the mid-1940s. However, the $\Delta^{14}\text{C}$ records of Guam (Andrews et al. 2016), Currimao and Ishigaki corals did not show a positive shift related with the PDO (Figures 4.2 and 4.4). This is because the area near Fanning

Island is directly affected by the upwelling of the central Pacific (Grottoli et al., 2003), while the western Pacific is affected through the North Equatorial Current.

In this period, the NEC bifurcation latitude was not observed. Judging from the PDO condition of the mid-1940s, the NEC bifurcation latitude would have migrated southward in the mid-1940s and Kuroshio transport on the east side of Luzon Island increased, while the Kuroshio Loop Current's transport through the Luzon Strait would decrease. Smaller transport of Kuroshio Loop Current might cause a decrease in upwelling at Currimao driven by mesoscale eddies, which resulted in the smaller seasonality of ΔR in Currimao. Yamazaki et al. (2016) reconstructed the Kuroshio transport at Tatsukushi based on the nitrogen isotopes in the coral and they suggested that Kuroshio transport decreased from 1947 to 1950. The Kuroshio current area would be possibly affected by a less number of mesoscale eddies (Wu 2013), but it is difficult to discuss this with record of only 3 years in Ishigaki. Further data will be required to understand this issue for the period before 1950.

4.4.2 Decadal fluctuations in the regional radiocarbon reservoir age in the 1900s and 1940s

Most of the published ΔR values for the early 1900s from the Kuroshio region are positive, whereas those for the 1940s are negative (Table 4.2, Figure 4.6). Coral from Okinawa Island provides ΔR values for the 1940s that are considerably lower than those from Ishigaki and Kikai Islands (Konishi et al., 1981), which Yoneda et al. (2007) attributed to the semi-enclosed estuarine environment of Naha port, from which the coral samples were obtained. Except for Okinawa, all the reported average ΔR values for the Kuroshio region for the 1940s are negative, including those from Ishigaki and Kikai Islands. Thus, ΔR values in the Kuroshio region changed from positive values in the early 1900s to negative values in the 1940s.

The positive-to-negative shift in the ΔR is not restricted to the Kuroshio region; it is apparent throughout the western Pacific (Table 4.2, Figure 4.6). Yoneda et al. (2007) reported that in the region of the North Equatorial Current (NEC), which is the source region of the Kuroshio Current, ΔR was 78 years in the early 1900s on the basis of analyses of pre-bomb molluscan shells from Palau and Ponape. In contrast, ΔR

values obtained from $\Delta^{14}\text{C}$ data on corals from Guam, Palau, Hawaii and Fanning Island in the equatorial Pacific are negative for 1945–1950 (Druffel, 1987; Druffel et al., 2001; Grottoli et al., 2003; Glynn et al., 2013; Andrews et al., 2016). This may be biased because the ΔR values of the 1900s shown in Table 4.2 are from data for 23 years, from 1892 to 1915, whereas ΔR values in the 1940s are for 10 years, for the period from 1940 to 1950. However, the positive values are dominant if we only consider the period from 1900 to 1903, while negative values are apparent in all sites from 1940 to 1950. Although there are no ΔR data in Palau and Ponape during the period from 1900 to 1903, I suggest that the positive-to-negative shift of ΔR occurred at least along the NEC and Kuroshio in the area from Guam to Kikai Island. The consistency of the positive-to-negative shifts of ΔR over much of the western Pacific suggests that sea-surface ^{14}C contents there have fluctuated over a period of <50 years, which in turn suggests that higher temporal and spatial resolution ΔR reconstructions are needed to allow high-precision dating of past events.

The positive-to-negative shifts of ΔR in the western Pacific probably reflect the migration of areas of upwelling along the Peru and Chile coast that might be related to the El Niño–Southern Oscillation (ENSO) and the Pacific Decadal Oscillation (PDO). Newman et al. (2016) indicated that the area of cold SST tongue in the eastern tropical Pacific is expanded or reduced depending on the combination of ENSO and PDO, based on the reanalysis the ERSST dataset over the years from 1948 to 2008. Similar shifts have been reported from analyses of mid-Holocene corals from the South China Sea, where the change of ΔR has been attributed to upwelling in both the South China Sea and the Pacific, controlled by the East Asian Monsoon and ENSO, respectively (Yu et al., 2010) (See Appendix of Chapter 4). There were regime shifts of both ENSO and the PDO in 1900 and 1950 (Biondi et al., 2001). Coral-based $\Delta^{14}\text{C}$ data from Fanning Island co-varied with a PDO shift in the 1940s, which suggests that the PDO affected ocean circulation at that time (Grottoli et al., 2003). Vargas et al. (2007) identified $\Delta^{14}\text{C}$ variability since the late 19th century related to enhanced coastal upwelling due to inter-decadal ENSO-like climate change in a sediment core from off the coast of Peru and Chile.

Compared with ΔR values from the three sites of Guam, Palau and Ishigaki for the period of early-1900s and 1940s, the ΔR differences of both Palau-Guam and Ishigaki-Guam in the early-1990s are smaller than those in the 1940s (Figure 4.5).

Average ΔR difference of Ishigaki-Guam was 67 years in the 1900s, while that in 1940s was -23 years. There are no ΔR data from Palau in 1900, so I compared ΔR data of Palau in 1915 with that of Guam in 1903 (Table 4.2). The average ΔR difference of Palau-Guam was 96 years in the early-1900s, while that in the 1940s was -6 years. The ΔR difference in the area of both the Kuroshio and Mindanao currents suggested a decreasing trend of upwelling driven by mesoscale eddies in the Kuroshio region and by the Mindanao Dome in the Mindanao current region from 1900 to 1950. According to the SST around the Mindanao Dome (8°N , 134°E) from Extended Reconstructed Sea Surface Temperature (ERSST) version 2 (Smith and Reynolds, 2004), average SST in winters had the increasing trend from 1990 to 1950 and the highest SST period in winter was from 1943-1946 (Figure 4.7b). The Mindanao Dome is dominant in winter (Masumoto and Yamagata, 1991). Thus, the higher winter SST period might be because of the weakened trend of the Mindanao Dome. For the period from 1920 to 1940, the PDO condition was positive (Figure 4.7a) and the NEC bifurcation latitude would have migrated northward, which caused the weakened trend of the Mindanao Dome. The ΔR data for the past 100 years is limited and almost all the data in the 1900s shown in Table 4.2 was reported based on molluscan shells, which can provide ΔR for only few years. To elucidate the detailed mechanism of the relationship between either ENSO or the PDO shift and decadal ΔR changes in the western Pacific, long, continuous ΔR data from corals will be required. Understanding the mechanism and dynamics of oceanographic variability is also required to the precise radiocarbon dating of the marine samples with the high-resolution radiocarbon measurements. For example, there are 430-year-long corals in Kikai Islands, Ryukyu Islands (Kawakubo et al., 2014) and ~ 200 year-long corals in the Xisha Islands, South China Sea (Song et al., 2012) and fossil corals uplifted in Kikai Island and Luzon Island, South China Sea (see Appendix od Chapter 4). Using such long living corals or fossil corals of different periods can be revealed ΔR variability with various time scales, which will contribute to understand the relationship between oceanography variability and climate change.

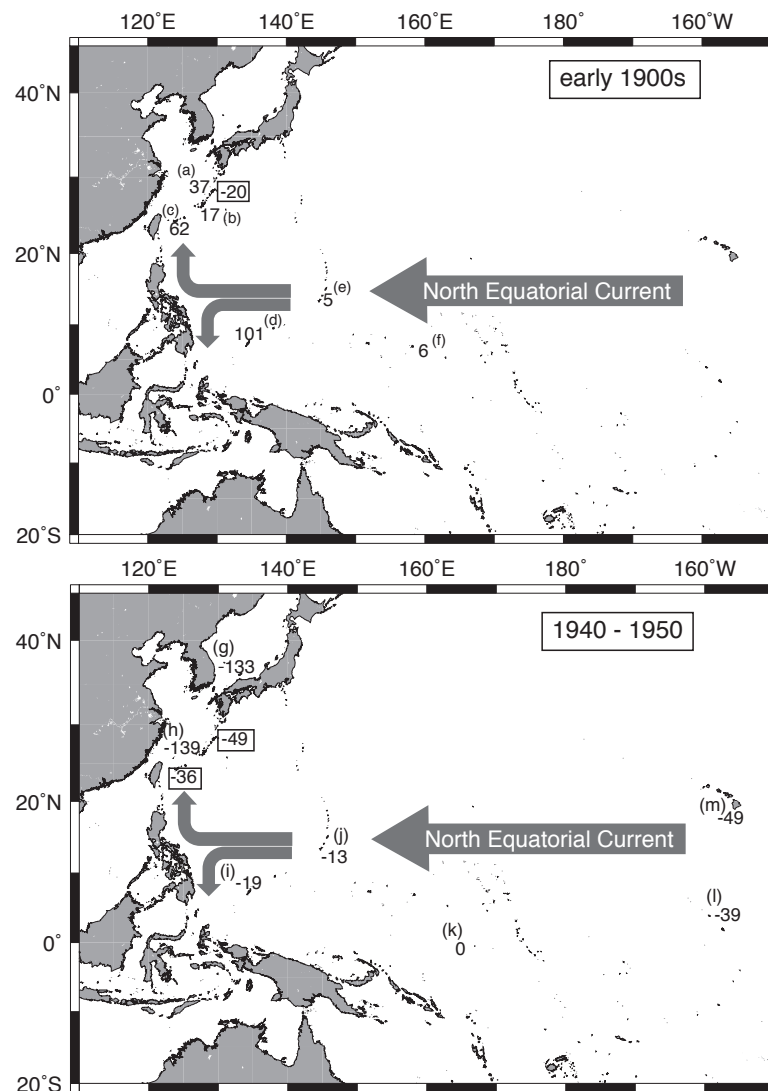


Figure 4.6 Maps showing ΔR data in the western Pacific for the early 1900s and 1940s. Values in boxes are those obtained in this study; others are from previous studies as follows: (a) Amami-Oshima, (b) Okinawa, (d) Palau, and (f) Ponape from Yoneda et al. (2007); (c) Ishigaki from Hideshima et al. (2001) and Yoneda et al. (2007); (e) Guam from Southon et al. (2002); (g) Korea from Kong and Lee (2005); (h) Okinawa from Konishi et al. (1981); (i) Palau from Glynn et al. (2013), (j) Guam from Andrews et al. (2016); (k) Nauru from Guilderson et al. (1998); (l) Fanning from Druffel (1987) and Grottoli et al. (2003); and (m) Hawaii from Druffel et al. (2001). From Hirabayashi et al. (2017c).

Table 4.2
 ΔR values for the 1900s and 1940s from this study and from previous studies of the Kuroshio and North Equatorial Current regions (Hirabayashi et al., 2017c)

Location	Analysis period	ΔR range (^{14}C yr)	ΔR average (^{14}C yr)	1σ	References
1900s	Amami-Oshima	-1 to 94	37	50	Yoneda <i>et al.</i> (2007)
	Kikai Is.	1901-1903	-20	33	This study
	Okinawa region	1900	-6 to 40	33	Yoneda <i>et al.</i> (2007)
1900s	Ishigaki	1892-1902	5 to 119	81	Yoneda <i>et al.</i> (2007) Hideshima <i>et al.</i> (2001)
	Guam	1903	5		Southon <i>et al.</i> (2002)
	Palau	1915	34 to 168	95	Yoneda <i>et al.</i> (2007)
North Equatorial Current	Ponape	1915	6	42	Yoneda <i>et al.</i> (2007)

Continued

Location	Analysis period	ΔR range (^{14}C yr)	ΔR average (^{14}C yr)	1σ	References
Kuroshio region	Kikai Is. 1945-1947		-49	44	This study
	Okinawa 1946-1950	-174 to -114	-139	25	Konishi <i>et al.</i> (1981)
	Ishigaki 1947-1950	-135 to 62	-36	78	This study
1940s	Guam 1945-1950	-61 to 134	-13	37	Andrews <i>et al.</i> (2016)
	Palau 1945-1949	-40 to 10	-19	20	Glynn <i>et al.</i> (2013)
	Nauru 1947-1950	-141 to 124	0	52	Guilderson <i>et al.</i> (1998)
	Fanning 1940-1950	-255 to 129	-39	89	Druffel (1987)
	Hawaii 1940-1950	-71 to -10	-49	19	Druffel <i>et al.</i> (2001)
North Equatorial Current					Grottoli <i>et al.</i> (2003)

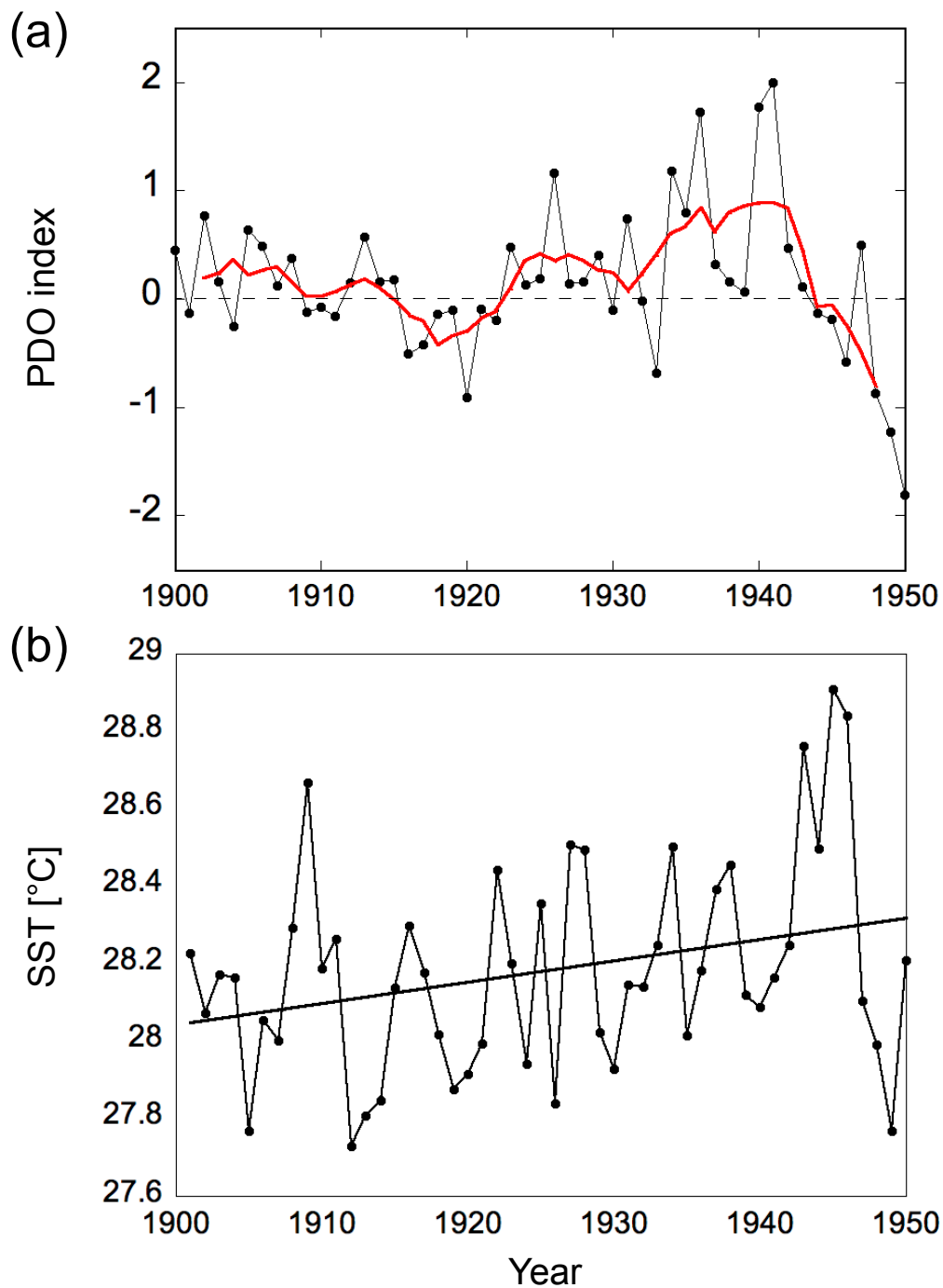


Figure 4.7 (a) Monthly (Black) and 5-year running average of PDO index reported by the Japan Meteorological Agency from 1900 to 1950. (b) Winter SSTs in the area of Mindanao Dome (8°N , 134°E). The data use the average of December, January and February as winter SSTs. From Extended Reconstructed Sea Surface Temperature (ERSST) version 2 (Smith and Reynolds, 2004).

4.5 Summary

I used the $\Delta^{14}\text{C}$ analyses of *Porites* corals from Ishigaki and Kikai Islands, which lie within the path of the Kuroshio Current off southern Japan, and Currimao located in the path of the Kuroshio Loop Current to discuss oceanographic changes in the western Pacific.

I found that the average ΔR from 1947 to 1950 for samples from Ishigaki Island was -36.0 years, which is consistent with the average ΔR value from 1901 to 1948 that I obtained for samples from Kikai Island. However, high-resolution ΔR data from Ishigaki Island for 1947–1950 fluctuated over a range of more than 150 years, from -136 ± 42 to 62 ± 50 years, and similar short-term fluctuations were shown in the Currimao coral.

My compilation of new ΔR data and previously published data from the western Pacific indicates a strong positive-to-negative shift in ΔR during the period from 1900 to 1950. This shift of the local marine reservoir effect will affect calibration of ^{14}C ages to provide calendar dates in the western Pacific for the radiocarbon measurement of marine samples.

Although the large-scale, short-term variation of ΔR that I identified provides some clues about the cause of previously identified temporal variations of ΔR in the Kuroshio region, further investigations at high spatial and temporal resolution are needed to better understand the cause of such changes and, in particular, to clarify the relationship of seasonal-to-decadal ΔR variability in the western Pacific with both ENSO and the PDO based on long, continuous ΔR data using corals. Understanding the mechanism and dynamics of oceanographic variability is also required to the precise radiocarbon dating of the marine samples with the high-resolution radiocarbon measurements.

Chapter 5 Conclusion and Future work

5.1 General conclusions

In this thesis, method development allowing high-resolution radiocarbon measurements for small-mass carbonate samples and seasonal age determination using a *Porites* coral with smaller skeletal growth rates in the temperate region (Ushibuka, Kumamoto) were successfully undertaken (Chapter 2, Hirabayashi et al., 2013). These new methods were applied to corals taken from the Kuroshio and Kuroshio Loop Current regions (Ishigaki and Currimao) to reconstruct oceanographic variability and its relation with climate changes such as ENSO and the PDO (Chapter 3 and 4) (Hirabayashi et al., 2017a, b, c). The key findings of this thesis are summarized as follows.

(1) The Sr/Ca ratio in corals is a good proxy for high-resolution age determination even for temperate corals. The Sr/Ca ratio and oxygen isotopes are proxies for sea surface temperature, but some previous studies suggested that those proxies have growth-rate dependence, particularly at low growth rates. To evaluate this, I measured Sr/Ca and oxygen isotopes using the coral taken from Ushibuka, which is near the northern limit of the coral reef of Japan. My results indicate that Sr/Ca is independent of coral growth rates, while oxygen isotopes vary, particularly at low growth rates affected by cold sea surface temperature events in 1968-1969. Therefore, we can precisely create an age model by counting seasonality of Sr/Ca peaks even for corals that experienced cold sea surface temperature events in the past and/or lived in areas colder than the tropics when we use the Sr/Ca ratio.

(2) Close-in radioactive fallout was detected for the first time in the Northwest Pacific with high-resolution radiocarbon measurements of the Ishigaki coral. Prior to this work, there were no records available farther northwest of Guam because previous studies could not identify evidence of early bomb-¹⁴C spikes. The mechanism of close-in fallout for radiocarbon is still unclear. This new finding will be important in the field of nuclear physics and will contribute to understanding the mechanism of close-in fallout such as the magnitude and horizontal and depth range of close-in fallout input.

(3) *Radiocarbon in corals is a good proxy for water mass mixing with seasonal to decadal time scales when high-resolution radiocarbon measurements are utilized for both pre-1950 and post-1950 periods.* My newly reported high-resolution radiocarbon data reveal that the transport speed from Guam and Kuroshio varied depending on the condition of El Niño-Southern Oscillations. The westward transportation by North Equatorial Current and Kuroshio was intensified in La Niña conditions compared with the normal oceanic condition for the period of 1954, 1956 and 1958. On the decadal timescale, the Pacific Decadal Oscillation affects western Pacific oceanographic features such as the strength of Mindanao Dome, the Kuroshio Loop Current and mesoscale eddies in Kuroshio regions. When the PDO index was positive after 1976, the upwelling by Mindanao Dome in Mindanao Current region and mesoscale eddies in Kuroshio region was intensified related to the migration of North Equatorial Current bifurcation latitude. The area and path that Kuroshio Loop Current intruded into South China Sea through the Luzon Strait was decreased as a result of changes in Kuroshio transport and the migration of the North Equatorial Current bifurcation latitude after a regime shift in 1976.

5.2 Future perspectives

5.2.1 Improvement of the Ocean current transport modeling

The new high-resolution bomb- ^{14}C data from the Kuroshio and Kuroshio Loop Current region (Chapter 3, Hirabayashi et al., 2017a, b) are useful to improve ocean current transport modeling. Because high-resolution radiocarbon measurement of corals were previously conducted only for the tropics, discussions of transport modeling did not include the dynamics of the Kuroshio and Kuroshio Loop Current.

Andrews et al. (2016) created an ocean current transport modeling using the data of close-in fallout from nuclear testing at Bikini and Enewetak atolls of the Marshall Islands (part of the Pacific Proving Grounds in the 1950s), and which was detected from previously reported coral records of Palau, Okinawa, Langkai and Lombok. In their modeling, to provide an estimate of fallout particle propagation,

Lagrangian transport simulations were conducted using ocean currents from a comprehensive ocean reanalysis called the Simple Ocean Data Assimilation version 2 (SODA2) (Carton et al., 2000).

However, because there were previously only low-resolution data of the Okinawa coral reported by Konishi et al. (1981) in Kuroshio and no data for the Kuroshio Loop Current region, their model cannot simulate transport by the Kuroshio current, while the Mindanao Current and Indonesian Throughflow can be simulated (Figure 5.1).

According to my new data of early bomb spikes in Currimao and Ishigaki, radioactive materials derived by the nuclear bomb test in 1954 arrived in Currimao slightly earlier than in Langkai and arrived in Ishigaki at almost the same time as in Langkai. In this model, it takes 6 months for the radioactive materials to travel from Bikini atoll to Langkai s, while it takes ~1 year to reach the Luzon Strait and Ryukyu Islands. This is thus new evidence that the Kuroshio Currents carried the radioactive materials with the same speed as the Mindanao Current and the Indonesian Throughflow.

Comparing with all the bomb spikes from Ishigaki and Guam revealed that the transport speed varies depending on ENSO (Chapter 3, Hirabayashi et al., 2017a). This work contributes to a high-resolution transport model which incorporates the climate conditions.

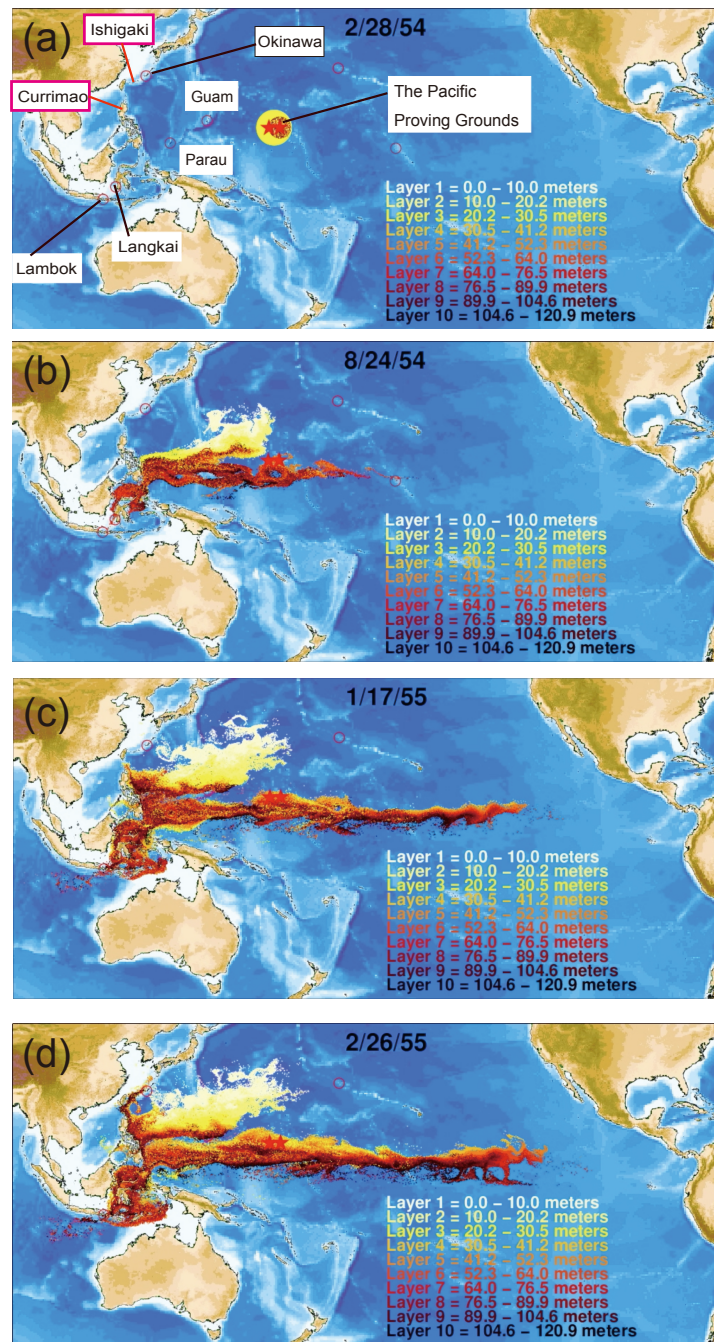


Fig 5.1 Snapshots of ocean current transport modeling reported by Andrews et al. (2016). The close-in fallout from Operation Castle was produced at the end of February 1954 (a). ^{14}C signal arrived at Langkai in August 1954 (b), while it reached Currimao (c) and the Ryukyu Islands (Ishigaki and Okinawa) (d) in January and February 1955, respectively. The transport by the Mindanao Current and the Indonesian Throughflow are shown in this model, while Kuroshio and Kuroshio Loop Current were not simulated.

5.2.2 Kuroshio variability reconstruction before 1950

In this thesis, I showed how to reconstruct oceanography based on coral skeletal radiocarbon for the period before 1950 in Chapter 4 (Hirabayashi et al. 2017c). The difference in radiocarbon concentration between the surface and deeper ocean is much smaller for the period before 1950 than that of after 1950. However, the local marine reservoir age (ΔR) can be a good proxy for the high-resolution oceanographic reconstruction even for temperate corals.

Corals are good archives for the reconstruction of paleoceanography because they can live for hundreds of years and produce seasonal skeletal bands. For example, there are 430-year-long corals in Kikai Islands, Ryukyu Islands (Kawakubo et al., 2014) and ~200 year-long corals in the Xisha Islands, South China Sea (Song et al., 2012). These corals will be able to provide the seasonal ΔR variability for more than 100 years, which reveals seasonal to decadal oceanographic changes in the past related to climate changes such as ENSO and the PDO. To confirm the relationship between either ENSO or PDO shift and short-term ΔR changes in the 1940s shown in the Ishigaki coral, higher time-resolution data are required to understand this short-term (seasonal) fluctuation of the local reservoir age. Short-term variation of ΔR that I identified in Chapter 4 provides some clues about the cause of previously identified temporal variations of ΔR in the Kuroshio region, further investigations at high spatial and temporal resolution are needed to better understand the cause of such changes and, in particular, to clarify the relationship of ΔR variability in the western Pacific with both ENSO and the PDO.

The variability in ΔR is important for not only as an oceanographic proxy but also for radiocarbon dating. We need to calibrate radiocarbon ages of marine samples to calendar ages. However, ΔR varies both temporally and spatially, although specific knowledge of that variability is limited, especially in the North Pacific. Therefore, many researchers calibrate radiocarbon ages with modern ΔR values from the nearest measured locality even when samples are much older or, in some cases, sometimes they calibrated marine samples with $\Delta R = 0$ (e.g. Kong et al., 2007). Previous studies have reported various ΔR values in the Kuroshio region off southwestern Japan (Table 5.1). For example, ΔR values reported from Taiwan, Ishigaki Island, and Okinawa are respectively 54 to 135 (Yoneda et al., 2007), 7 to 119 (Hideshima et al., 2001; Yoneda

et al., 2007), and –126 to 40 years (Konishi et al., 1981; Yoneda et al., 2007). These differences create large uncertainties in reconstruction of the timing of past geohazard events in the region (Kawana and Nakata, 1994; Suzuki et al., 2008; Araoka et al., 2013). Araoka et al. (2013) reported that Ishigaki Island has been regularly struck by tsunamis with a recurrence interval of 150–400 years, but the large ranges of ΔR values make it difficult to assign meaningful dates to these paleoseismic events (Komatsubara and Nishiyama, 2006). High-resolution ^{14}C dating of marine samples have become possible over the years, raising the need and importance for ΔR values to be produced in high-resolution for different time periods.

Table 5.1

Local marine reservoir ages previously reported from the Kurioshio region. There are differences among ΔR even in the same Kuroshio area. This uncertainty creates difficulties for precise calibration from ^{14}C ages to calendar ages for marine samples.

Locality	Longitude (°E)	Latitude (°N)	ΔR (year)	err	Materials	Reference
Keelung, Taiwan	121.1	24.9	54	41	Gastropoda	Yoneda et al., 2007
Keelung, Taiwan	121.1	24.9	101	53	Bivalvia	Yoneda et al., 2007
Keelung, Taiwan	121.1	24.9	135	42	Bivalvia	Yoneda et al., 2007
Danshui, Taiwan	121	25	113	37	Bivalvia	Yoneda et al., 2007
Keelung, Taiwan	121.1	24.9	71	35	Gastropoda	Yoneda et al., 2007
Keelung, Taiwan	121.1	24.9	90	39	Bivalvia	Yoneda et al., 2007
Ishigaki	124.33	24.55	7	40	Coral	Hideshima et al., 2001
Ishigaki	124	24	119	39	Gastropoda	Yoneda et al., 2007
Okinawa	127	27	40	31	Bivalvia	Yoneda et al., 2007
Okinawa	127	27	-6	30	Bivalvia	Yoneda et al., 2007
Okinawa	127.8	26.4	-126	7	Coral	Konishi et al., 1982

5.2.3 Oceanographic reconstruction using deep-sea corals

Generally, deep-sea coral populations tend to be found in waters with temperatures of 4 to 12 °C, allowing corals to occupy intermediate and deep temperate to tropical waters as well as high-latitude waters.

There are several kinds of deep-sea corals: (1) Aragonitic scleractinian corals, (2) proteinaceous corals, and (3) corals with internal calcite structures. Aragonitic scleractinian corals such as *Lopehlia pertusa* in the north-east Atlantic, have linear growth rates of 5-26 mm yr⁻¹ as estimated by aquarium observations (Mortensen et al., 1998). Proteinaceous corals such as *Antipathes dichotoma* have linear growth rates of 6.4 cm yr⁻¹ (Grigg, 1976). Corals with internal calcite structures such as *Corallium* spp. have estimated radial growth rates of much less than 1 mm yr⁻¹ (c.f. Druffel et al., 1990; Marschal et al., 2004; Roark et al., 2006). As I mentioned here, the growth rates of deep-sea corals are much lower than those of hermatypic corals except *Antipathes dichotoma*, but it is possible to measure radiocarbon in deep-sea corals using the high-resolution radiocarbon technique that I developed in Chapter 2 or if I farther improve the method of Chapter 2.

Because of the absence of observations of deep-sea scleractinian reefs in the Central and Northeast Pacific, and oceanographic conditions of both a shallow aragonite saturation horizon and high carbonate dissolution rates in those areas, the formation of deep-sea scleractinian reefs had been thought improbable. However, recently, deep-sea scleractinian coral reefs were found in the North Pacific by Baco et al. (2017). If deep-sea corals were to be discovered in additional North Pacific areas, their radiocarbon measurements combined with those from hermatypic corals will reveal three dimensional radiocarbon transport in the Pacific and will contribute to a major improvement in our understanding of the marine carbon cycle.

References

- Adams, C. E. (1957), The nature of individual radioactive particles, V. Fallout particles from Zuni and Tewa, Operation Redwing, *Res. Dev. Tech. Rep. USNRDL-TR-133*, 16 pp., U.S. Naval Radiological Defense Laboratory. San Francisco, California.
- Allison, N., A. W. Tudhope, and A. E. Fallick (1996) Factors influencing the stable carbon and oxygen isotopic composition of *Porites lutea* coral skeletons from Phuket, South Thailand, *Coral Reefs*, *15*, 43–57.
- Andrews, A. H., R. Asami, Y. Iryu, D. R. Kobayashi, and F. Camacho (2016), Bomb-produced radiocarbon in the western tropical Pacific Ocean: Guam coral reveals operation-specific signals from the Pacific Proving Grounds, *J. Geophys. Res. Ocean.*, *121*, 6351–6366.
- Araoka, D., Y. Yokoyama, A. Suzuki, K. Goto, K. Miyagi, K. Miyazawa, H. Matsuzaki, and H. Kawahata (2013), Tsunami recurrence revealed by *Porites* coral boulders in the southern Ryukyu Islands, Japan, *Geology*, *41*(8), 919–922, doi:10.1130/G34415.1.
- Baco, A. R., N. Morgan, E. B. Roark, M. Silva, K. E. F. Shamberger, and K. Miller (2017), Defying Dissolution: Discovery of Deep-Sea Scleractinian Coral Reefs in the North Pacific, *Sci. Rep.*, *7*(1), 1–11, doi:10.1038/s41598-017-05492-w.
- Bautista, A. T., H. Matsuzaki, and F. P. Siringan (2016), Historical record of nuclear activities from ¹²⁹I in corals from the northern hemisphere (Philippines), *J. Environ. Radioact.*, *164*, 174–181.
- Biondi, F., A. Gershunov, D. R. Cayan (2001), North Pacific Decadal Climate Variability since 1661, *J. Clim.*, *14*, 5–10.
- Bolton, A., N. F. Goodkin, E. R. M. Druffel, S. Griffin, and S. A. Murty (2016), Upwelling of Pacific Intermediate Water in the South China Sea Revealed by Coral Radiocarbon Record, *Radiocarbon*, *58*(1), 37–53, doi:10.1017/RDC.2015.4.
- Bondevik, S., J. Mangerud, H. H. Birks, S. Gulliksen, and P. Reimer (2006), Changes in North Atlantic radiocarbon reservoir ages during the Allerød and Younger Dryas. *Science*, *312*(5779), 1514–1517.

- Bradley, R. S. (2013), *Paleoclimatology: Reconstructing Climates of the Quaternary Academic Press*. Third edition.
- Broecker, W.S., and T.-H. Peng. (1982) *Tracers in the Sea. ELDIGIO Press*, New York, p690. Lamont-Doherty Earth Observatory, Palisades
- Broecker, W. S., T.-H. Peng, G. Östlund, and M. Stuiver (1985), The distribution of bomb radiocarbon in the ocean, *J. Geophys. Res.*, *90*, 6953–6970.
- Brown, T., G. Farwell, P. Grootes, F. Schmidt, and M. Stuiver (1993). Intra-Annual Variability of the Radiocarbon Content of Corals from the Galapagos Islands. *Radiocarbon*, *35*(2), 245-251. doi:10.1017/S0033822200013989
- Buranapratheprat, A., P. Laongmanee, N. Sukramongkol, R. Prommas, S. Promjinda, and T. Yanagi (2010), Upwelling induced by meso-scale cyclonic eddies in the Andaman Sea, *Coast. Mar. Sci.*, *34*(1), 68–73.
- Carton, J. A., G. Chepurin, X. Cao, and B. Giese (2000), A simple ocean data assimilation analysis of the global upper ocean 1950–95, Part I: *Methodology*, *J. Phys. Oceanogr.*, *30*, 294–309.
- Caruso, M. J., G. G. Gawarkiewicz, and R. C. Beardsley (2006), Interannual variability of the Kuroshio intrusion in the South China Sea, *J Oceanogr.*, *62*(4), 559–575, doi:10.1007/s10872-006-0076-0
- Chang, C. C., G.S. Burr, A. T. Jull, J. L. Russell, D. Biddulph, L. White, N. G. Prouty, Y-G Chen, C-C Shen, W. Zhou, D. D. Lam. (2016), Reconstructing surface ocean circulation with ¹²⁹I time series records from corals, *J. Environ. Radioact.*, *165*, 144-150.
- Chang, Y. L., and L. Y. Oey (2012), The philippines-taiwan oscillation: Monsoonlike interannual oscillation of the subtropical-tropical western north pacific wind system and its impact on the ocean, *J. Clim.*, *25*(5), 1597–1618, doi:10.1175/JCLI-D-11-00158.1.
- Chen, Z., and L. Wu (2012), Long-term change of the Pacific North Equatorial Current bifurcation in SODA, *J. Geophys. Res.*, *117*, C06016, doi:10.1029/2011JC007814
- Chu, P. C., and R. Li (2000), South China Sea isopycnal-surface circulation. *J Phys Oceanogr.*, *30*(9), 2419-2438.
- Cordero, R. R., H. Panarello, S. Lanzelotti, and C. M. F. Dubois (2003), Radiocarbon age offsets between living organisms from the marine and continental

- reservoir in coastal localities of Patagonia (Argentina), *Radiocarbon.*, 45, 9-15.
- Corrège, T. (2006), Sea surface temperature and salinity reconstruction from coral geochemical tracers, *Palaeogeogr.Palaeoclimatol. Palaeoecol.*, 232, 408–428.
- de Villiers, S., B. K. Nelson, and A. R. Chivas (1995), Biological Controls on Coral Sr/Ca and $\delta^{18}\text{O}$ Reconstructions of Sea Surface Temperatures., *Science*, 269(5228), 1247–9, doi:10.1126/science.269.5228.1247.
- Druffel, E. R. M. (1981), Radiocarbon in annual coral rings from the eastern tropical Pacific Ocean, *Geophys. Res. Lett.*, 8, 59-62
- Druffel, E. R. M. (1982), Banded corals: Changes in oceanic carbon-14 during the Little Ice Age, *Science*, 218(4567), 13–19.
- Druffel, E. R. M. (1987), Bomb radiocarbon in the Pacific: Annual and seasonal timescale variations, *J. Mar. Res.*, 45(3), 667–698.
- Druffel, E. R. M. (1989), Decade time scale variability of ventilation in the North Atlantic: High-precision measurements of bomb radiocarbon in banded corals, *J. Geophys. Res.*, 94, 3271–3285.
- Druffel, E. R. M. (2002), Radiocarbon in corals: Records of the carbon cycle, surface circulation and climate, *Oceanography*, 15(1), 122–127.
- Druffel, E. R. M., G. Shelia, D. S. Glynn, R. B. Dunbar, D. A. Mucciarone, and J. R. Toggweiler (2014), Seasonal radiocarbon and oxygen isotopes in a Galapagos coral: Calibration with climate indices, *Geophys. Res. Lett.*, 15, 5099–5105, doi:10.1002/2014GL060504.
- Druffel, E. R. M., L. L. King, R. A. Belastock, and K. O. Buesseler (1990), Growth rate of a deep-sea coral using ^{210}Pb and other isotopes, *Geochim. Cosmochim. Acta*, 54(5), 1493–1499, doi:10.1016/0016-7037(90)90174-J.
- Druffel, E. R. M., and T. W. Linick (1978), Radiocarbon in annual coral rings of Florida, *Geophys. Res. Lett.*, 5, 913–916.
- Druffel, E. R. M., G. Shelia, D. S. Glynn, R. B. Dunbar, D. A. Mucciarone, and J. R. Toggweiler (2014), Seasonal radiocarbon and oxygen isotopes in a Galapagos coral: Calibration with climate indices, *Geophys. Res. Lett.*, 41, 5099–5105, doi:10.1002/2014GL060504.

- Druffel, E. R. M., and H. E. Suess (1983), On the radiocarbon record in banded corals: Exchange parameters and net transport of $^{14}\text{CO}_2$ between atmosphere and surface ocean, *J. Geophys. Res.*, 88(C2), 1271, doi:10.1029/JC088iC02p01271.
- Druffel, E. R., S. Griffin, T. P. Guilderson, M. Kashgarian, J. Southon, and D. P. Schrag (2001), Changes of subtropical North Pacific radiocarbon and correlation with climate variability. *Radiocarbon*, 43(1), 15-25.
- Fallon, S. J., L. K. Fifield, and J. M. Chappell (2010), The next chapter in radiocarbon dating at the Australian National University: Status report on the single stage AMS, *Nucl. Instruments Methods Phys. Res. Sect. B Beam Interact. with Mater. Atoms*, 268(7–8), 898–901, doi:10.1016/j.nimb.2009.10.059.
- Fallon, S. J., and T. P. Guilderson (2008), Surface water processes in the Indonesian throughflow as documented by a high-resolution coral $\Delta^{14}\text{C}$ record, *J. Geophys. Res.*, 113, C09001, doi:10.1029/2008JC004722.
- Fallon, S. J., M. T. McCulloch, R. van Woesik, and D. J. Sinclair (1999), Corals at their latitudinal limits: Laser ablation trace element systematics in *Porites* from Shirigai Bay, Japan., *Earth Planet. Sci. Lett.*, 172, 221–238.
- Fallon, S. J., M. T. McCulloch, and C. Alibert (2003) Examining water temperature proxies in *Porites* corals from the Great Barrier Reef: A cross-shelf comparison, *Coral Reefs*, 22, 389–404.
- Felis, T., J. Pätzold, and Y. Loya (2003) Mean oxygen-isotope signatures in *Porites* spp. Corals: inter-colony variability and correction for extension-rate effects, *Coral Reefs*, 22, 328–336.
- Fontugne, M., M. Carré, I. Bentaleb, M. Julien, and D. Lavallée (2004), Radiocarbon reservoir age variations in the south Peruvian upwelling during the Holocene, *Radiocarbon*, 46(2), 531–537, doi:10.2458/azu_js_rc.46.4187
- Freeman, S. P. H. T., A. Dougans, L. McHargue, K. M. Wilcken, and S. Xu (2008), Performance of the new single stage accelerator mass spectrometer at the SUERC, *Nucl. Instruments Methods Phys. Res. Sect. B Beam Interact. with Mater. Atoms*, 266, 2225–2228, doi:10.1016/j.nimb.2008.02.085.
- Gagan, M. K., G. B. Dunbar, and A. Suzuki (2012), The effect of skeletal mass accumulation in *Porites* on coral Sr/Ca and $\delta^{18}\text{O}$ paleothermometry, *Paleoceanography*, 27, PA1203.

- Ge, T., X. Wang, J. Zhang, C. Luo, and Y. Xue (2016), Dissolved inorganic radiocarbon in the northwest Pacific continental margin, *Radiocarbon*, 58(03), 517–529.
- Gershunov, A., and T. P. Barnett (1998), Interdecadal modulation of ENSO teleconnections, *Bull. Amer. Meteor. Soc.*, 79, 2715–2725.
- Glynn, D., E. R. M. Druffel, S. Griffin, R. Dunbar, M. Osborne, and J. A. Sanchez-Cabeza (2013), Early bomb radiocarbon detected in Palau archipelago corals, *Radiocarbon*, 55(2), 1659–1664.
- Gordon, A. L., P. Flament, C. Villanoy, and L. Centurioni (2014), The nascent Kuroshio of Lamon Bay, *J. Geophys. Res. Oceans*, 119, 4251–4263, doi:10.1002/2014JC009882.
- Graven, H., C. E. Allison, D. M. Etheridge, S. Hammer, R. F. Keeling, I. Levin, H. A. J. Meijer, M. Rubino, P. P. Tans, C. M. Trudinger, B. H. Vaughn, and J. W. C. White (2017). Compiled records of carbon isotopes in atmospheric CO₂ for 5 historical simulations in CMIP6. *Geoscientific Model Development*, 10(12), 4405-4417.
- Grigg, R.W. (1976) Fishery management of precious and stony corals in Hawaii. Report No. UNIHI-SEAGRANT-TR-77- 03, University of Hawaii Sea Grant Program, Honolulu, HI
- Grottoli, A. G., and C. M. Eakin (2007), A review of modern coral $\delta^{18}\text{O}$ and $\Delta^{14}\text{C}$ proxy records, *Earth Sci. Rev.*, 81(1), 67–91, doi:10.1016/j.earscirev.2006.10.001.
- Grottoli, A. G., S. T. Gille, E. R. M. Druffel, and R. B. Dunbar (2003), Decadal timescale shift in the ^{14}C record of a central equatorial Pacific coral. *Radiocarbon*, 45, 91–99. DOI: 10.1017/S0033822200032422
- Grumet, N. S., T. P. Guilderson, and R. B. Dunbar (2002), Meridional transport in the Indian Ocean traced by coral radiocarbon, *J. Mar. Res.*, 60(5), 725–742.
- Guilderson, T., and D. Schrag (1998), Abrupt shift in subsurface temperatures in the tropical Pacific associated with changes in El Niño, *Science*, 281(5374), 240–243.
- Guilderson, T. P., D. P. Schrag, G. M. Wellington, E. Goddard, M. Kashgarian, G. M. Wellington, and B. K. Linsley (2000), Southwest subtropical Pacific surface water radiocarbon in a high-resolution coral record, *Radiocarbon*, 42(2), 249–256.

- Hanawa, K. (2005) Ocean General Circulation and Climate Change, *Journal of Geography*, 114 (3), 485-495
- Hayashi, E., A. Suzuki, T. Nakamura, A. Iwase, T. Ishimura, A. Iguchi, K. Sakai, T. Okai, M. Inoue, D. Araoka, S. Murayama, and H. Kawahata (2013), Growth-rate influences on coral climate proxies tested by a multiple colony culture experiment, *Earth Planet. Sci. Lett.*, 362, 198–206, doi:10.1016/j.epsl.2012.11.046.
- Hideshima, S., E. Matsumoto, O. Abe, and H. Kitagawa (2001), Northwest Pacific marine reservoir correction estimated from annually banded coral from Ishigaki island, southwest Japan, *Radiocarbon*, 43(2), 473–476.
- Hirabayashi, S., Y. Yokoyama, A. Suzuki, Y. Kawakubo, Y. Miyairi, T. Okai, and S. Nojima (2013), Coral growth-rate insensitive Sr / Ca as a robust temperature recorder at the extreme latitudinal limits of Porites, *Geochem. J.*, 47, e1–e5.
- Hirabayashi, S., Y. Yokoyama, A. Suzuki, Y. Miyairi, and T. Aze (2017a), Multidecadal oceanographic changes in the western Pacific detected through high-resolution bomb-derived radiocarbon measurements on corals, *Geochem. Geophys. Geosyst.*, 18, 1608–1617.
- Hirabayashi, S., Y. Yokoyama, A. Suzuki, Y. Miyairi, T. Aze, F. Siringan, and Y. Maeda (2017b), Radiocarbon variability recorded in coral skeletons from the northwest of Luzon Island, Philippines, *Geosci. Lett.*, 4(1), Article number 15, doi:10.1186/s40562-017-0081-8.
- Hirabayashi, S., Y. Yokoyama, A. Suzuki, Y. Miyairi, and T. Aze (2017c), Short-term fluctuations in regional radiocarbon reservoir age recorded in coral skeletons from the Ryukyu Islands in the north-western Pacific, *Journal Quat. Sci.*, 32(1), 1–6, doi:10.1002/jqs.2923.
- Ho, C.-R., Q. Zheng, N.-J. Kuo, C.-H. Tsai, and N. E. Huang (2004), Observation of the Kuroshio intrusion region in the South China Sea from AVHRR data, *Int. J. Remote Sens.*, 25(21), 4583–4591, doi:10.1080/0143116042000192376.
- Hsin, Y.-C., C.-R. Wu, and S.-Y. Chao (2012), An updated examination of the Luzon Strait transport, *J Geophys Res.*, 117, C03022
- Hu, D., S. Hu, L. Wu, L. Li, L. Zhang, X. Diao, Z. Chen, Y. Li, F. Wang, and D. Yuan (2013), Direct measurements of the Luzon undercurrent, *J. Phys. Oceanogr.*, 43(7), 1417–1425, doi:10.1175/JPO-D-12-0165.1.

- Hu, D., L. Wu, W. Cai, A. S. Gupta, A. Ganachaud, B. Qiu, A. L. Gordon, X. Lin, Z. Chen, S. Hu, G. Wang, Q. Wang, J. Sprintall, T. Qu, Y. Kashino, F. Wang, and W. S. Kessler (2015), Pacific western boundary currents and their roles in climate, *Nature*, 522(7556), 299–308, doi:10.1038/nature14504.
- Hu, J., H. Kawamura, H. Hong, and Y. Qi (2000). A review on the currents in the South China Sea: seasonal circulation, South China Sea warm current and Kuroshio intrusion. *Journal of Oceanography*, 56(6), 607-624.
- Hu, S., and D. Hu (2014), Variability of the Pacific North Equatorial Current from repeated shipboard acoustic Doppler current profiler measurements, *J. Oceanogr.*, 70, 559–571. DOI:10.1007/s10872-014-0253-5.
- Hua, Q. (2009), Quaternary Geochronology Radiocarbon : A chronological tool for the recent past, *Quat. Geochronol.*, 4(5), 378–390, doi:10.1016/j.quageo.2009.03.006.
- Hua, Q., M. Barbetti, and A. Z. Rakowski (2013), Atmospheric radiocarbon for the period 1950–2010, *Radiocarbon*, 55(4), 2059–2072.
- Hua, Q., G. E. Webb, J. Zhao, L. D. Nothdurft, M. Lybolt, G. J. Price, and B. N. Opdyke (2015), Large variations in the Holocene marine radiocarbon reservoir effect reflect ocean circulation and climatic changes, *Earth Planet. Sci. Lett.*, 422, 33–44, doi:10.1016/j.epsl.2015.03.049.
- Ulm, S. (2002), Marine and Estuarine Reservoir Effects in Central Queensland, Australia: Determination of ΔR Values, *Geoarchaeology - An Int. J.*, 17(4), 319–348, doi:10.1002/gea.10017.
- Hwang, C., and R. Kao (2002), TOPEX/POSEIDON-derived space–time variations of the Kuroshio current: applications of a gravimetric geoid and wavelet analysis, *Geophysical Journal International*, 151, 835–847.
- Hwang, C., C.-R. Wu, and R. Kao (2004), TOPEX/Poseidon observations of mesoscale eddies over the Subtropical Countercurrent: Kinematic characteristics of an anticyclonic eddy and a cyclonic eddy, *J. Geophys. Res. Oceans*, 109, C08013, doi:10.1029/2003JC002026.
- Inoue, M., A. Suzuki, M. Nohara, K. Hibino, and H. Kawahata (2007), Empirical assessment of coral Sr/Ca and Mg/Ca ratios as climate proxies using colonies grown at different temperatures, *Geophys. Res. Lett.*, 34(12), L12611, doi:10.1029/2007GL029628.

- Kashino, Y., N. España, F. Syamsudin, K. J. Richards, T. Jensen, P. Dutrieux, and A. Ishida (2009), Observations of the North Equatorial Current, Mindanao Current, and Kuroshio current system during the 2006/07 El Niño and 2007/08 La Niña, *J. Oceanogr.*, *65*(3), 325–333, doi:10.1007/s10872-009-0030-z.
- Kashino, Y., A. Ishida, and Y. Kuroda (2005), Variability of the Mindanao Current: Mooring observation results. *Geophys. Res. Lett.*, *32*, L18611. doi:10.1029/2005GL023880.
- Kashino, Y., A. Ishida, and S. Hosoda (2011), Observed ocean variability in the Mindanao Dome region, *J. Phys. Oceanogr.*, *41*, 287–302.
- Kawakubo, Y., Y. Yokoyama, A. Suzuki, T. Okai, C. Alibert, L. Kinsley, and S. Eggins (2014), Precise determination of Sr/Ca by laser ablation ICP-MS compared to ICP-AES and application to multi-century temperate corals, *Geochem. J.*, *48*(2), 145–152, doi:10.2343/geochemj.2.0295.
- Kawana, T., and T. Nakata (1994), Timing of Late Holocene Tsunamis Originated around the Southern Ryukyu Islands, Japan, Deduced from Coralline Tsunami Deposits, *J. Geog.*, *103*(3), 352–376, doi:10.1017/CBO9781107415324.004.
- Kellogg, W. W., R. R. Rapp, and S. M. Greenfield (1957), Close-in Fallout, *J. Meteorol.*, *14*(1), 1–14.
- Kessler, W.S. (1990) Observations of long Rossby waves in the northern tropical Pacific, *J. Geophys. Res.*, *95*(C4), 5183–5,17, <http://dx.doi.org/10.1029/JC095iC04p05183>.
- Key, R. (1996). WOCE Pacific Ocean Radiocarbon Program. *Radiocarbon*, *38*(3), 415-423. doi:10.1017/S003382220003006X
- Key, R. M., A. Kozyr, C. L. Sabine, K. Lee, R. Wanninkhof, J. L. Bullister, R. A. Feely, F. J. Millero, C. Mordy, and T.-H. Peng (2004), A global ocean carbon climatology: Results from Global Data Analysis Project (GLODAP), *Global Biogeochem. Cycles*, *18*(4), doi:10.1029/2004GB002247.
- Kim, Y. Y., T. D. Qu, T. Jensen, T. Miyama, H. Mitsudera, H. W. Kang, and A. Ishida (2004), Seasonal and interannual variations of the North Equatorial Current bifurcation in a high-resolution OGCM, *J. Geophys. Res.*, *109*(C3), 19, doi:10.1029/2003jc002013.

- Komatsubara, T., and A. Nishiyama (2006), Introduction to paleoseismology using historical records, *Earth Sci. (Chikyu Kagaku)*, 60, 253–261.
- Konishi, K., T. Tanaka, and M. Sakanoue (1981), Secular variation of radiocarbon concentrations in seawater: Sclerochronological approach, in *Proceedings of the Fourth International Coral Reef Symposium*, pp. 181–185, Marine Science Center, University of the Philippines, Manila.
- Kong, G. S., and C. W. Lee (2005), Marine Reservoir Corrections (ΔR) for Southern Coastal Waters of Korea, *J. Korean Soc. Oceanogr.*, 10(2), 124–128.
- Kuhnert, H., J. Pätzold, B. Hatcher, K.-H. Wyrwoll, A. Eisenhauer, L. B. Collins, Z. R. Zhu, and G. Wefer (1999), A 200-year coral stable isotope record from a highlatitude reef off Western Australia, *Coral Reefs*, 18, 1–12.
- Kuhnert, H., T. Crüger, and J. Pätzold (2005), NAO signature in a Bermuda coral Sr/Ca record, *Geochem. Geophys. Geosyst.*, 6, Q04004.
- Kumamoto, Y., A. Murata, T. Kawano, S. Watanabe, and M. Fukasawa (2013), Decadal changes in bomb-produced radiocarbon in the Pacific ocean from the 1990s to 2000s, *Radiocarbon*, 55(2), 1641–1650.
- Lachner, J., M. Christl, V. Alfimov, I. Hajdas, P. W. Kubik, T. Schultz-König, L. Wacker, and H.-A. Synal (2014), 41Ca, 14C and 10Be concentrations in coral sand from Bikini atoll, *J. Environ. Radioact.*, 129, 68–72.
- Lan J, X. Bao X, and G. Gao (2004), Optimal estimation of zonal velocity and transport through Luzon Strait using variational data assimilation technique. *Chin. J. Oceanol. Limnol.*, 22, 335–339. doi:10.1007/BF02843626.
- Latif, M., and T. P. Barnett (1994), Causes of Decadal Climate Variability over the North Pacific and North America., *Science*, 266(5185), 634–7, doi:10.1126/science.266.5185.634.
- Latif, M., and T. P. Barnett (1996), Decadal climate variability over the North Pacific and North America: Dynamics and predictability, *J. Clim.*, 9(10), 2407–2423, doi:10.1175/1520-0442(1996)009<2407:DCVOTN>2.0.CO;2.
- Latorre, C., R. De Pol-Holz, C. Carter, and C. M. Santoro (2017), Using archaeological shell middens as a proxy for past local coastal upwelling in northern Chile, *Quat. Int.*, 427, 128–136, doi:10.1016/j.quaint.2015.11.079.

- Li, L., W. D. Nowlin, and S. Jilan (1998), Anticyclonic rings from the Kuroshio in the South China Sea, *Deep. Res. Part I Oceanogr. Res.*, *45*(9), 1469–1482, doi:10.1016/S0967-0637(98)00026-0.
- Liao, G., Y. Yuan, and X. Xu (2008), Three dimensional diagnostic study of the circulation in the South China Sea during winter 1998, *J. Oceanogr.*, *64*(5), 803–814, doi:10.1007/s10872-008-0067-4.
- Lukas, R., T. Yamagata, and J. P. McCreary (1996), Pacific low-latitude western boundary currents and the Indonesian throughflow, *J. Geophys. Res. Ocean.*, *101*(C5), 12209–12216, doi:10.1029/96JC01204.
- Mangerud, J. (1972), Radiocarbon dating of marine shells, including a discussion of apparent age of recent shells from Norway, *Boreas*, *1*(2), 143-172.
- Mantua, N.J., S. R. Hare, Y. Zhang, J. M. Wallace, and R. C. Francis (1997), A Pacific interdecadal climate oscillation with impacts on salmon production. *Bull. Amer. Meteor. Soc.*, *78*, 1069-1079.
- Marschal, C., J. Garrabou, J. G. Harmelin, and M. Pichon (2004), A new method for measuring growth and age in the precious red coral *Corallium rubrum* (L.), *Coral Reefs*, *23*(3), 423–432, doi:10.1007/s00338-004-0398-6.
- Masumoto, Y., and T. Yamagata (1991), Response of the Western Tropical Pacific to the Asian Winter Monsoon: The Generation of the Mindanao Dome, *J. Phys. Oceanogr.*, *21*(9), 1386–1398, doi:10.1175/1520-0485(1991)021<1386:ROTWTP>2.0.CO;2.
- Masuzawa, J. (1967). Ryofu-Marui's survey for CSK, January to March 1967. *Oceanogr. Mag*, *19*, 1–5.
- Matsumoto, K., and Y. Yokoyama (2013), Atmospheric $\Delta^{14}\text{C}$ reduction in simulations of Atlantic overturning circulation shutdown, *Global Biogeochemical Cycles*, *27*, 296–304, DOI: 10.1002/gbc.20035.
- Matsuzaki, H., C. Nakano, Y. Tsuchiya, K. Kato, Y. Maejima, Y. Miyairi, S. Wakasa, and T. Aze (2007), Multi-nuclides AMS performances at MALT., *Nucl. Instrum. MethodsB*, *259*, 36–40.
- McConnaughey, T. (1989), ^{13}C and ^{18}O isotopic disequilibrium in biological carbonates : I . Patterns, *Geochimica Cosmochim. Acta*, *53*, 151–162.
- McGregor, H. V, M. K. Gagan, M. T. McCulloch, E. Hodge, and G. Mortimer (2008), Mid-Holocene variability in the marine ^{14}C reservoir age for northern coastal

- Papua New Guinea, *Quat. Geochronol.*, 3(3), 213–225,
<https://doi.org/10.1016/j.quageo.2007.11.002>.
- McNichol, A. P., R. J. Schneider, K. F. Von Reden, A.R. Gagnon, K. L. Elder, R. M. Key, and P. D. Quay (2000), Ten years after—The WOCE AMS radiocarbon program. *Nuclear Instruments and Methods in Physics Research Section B: Beam Interactions with Materials and Atoms*, 172(1), 479-484.
- Miller, C. F. (1964), *Biological and Radiological Effects of Fallout From Nuclear Explosions*, 82 pp., Stanford Res. Inst., Menlo Park, Calif.
- Mishima, M., H. Kawahata, A. Suzuki, M. Inoue, T. Okai, and A. Omura (2009), Reconstruction of the East China Sea palaeoenvironment at 16 ka by comparison of fossil and modern Faviidae corals from the Ryusyus, southwestern Japan, *J. Quat. Sci.*, 24, 928–936.
- Mitsuguchi, T., H. Kitagawa, E. Matsumoto, Y. Shibata, M. Yoneda, T. Kobayashi, T. Uchida, and N. Ahagon (2004), High-resolution ^{14}C analyses of annually-banded coral skeletons from Ishigaki Island, Japan: implications for oceanography, *Nuclear Instruments and Methods in Physics Research Section B: Beam Interactions with Materials and Atoms*, 223, 455-459.
- Mitsuguchi, T., P. X. Dang, H. Kitagawa, M. Yoneda, Y. Shibata (2007), Tropical South China Sea surface ^{14}C record in an annually-banded coral, *Radiocarbon*, 49(02), 905–914, doi:10.1017/S0033822200042776.
- Mitsuguchi, T., M. Hirota, A. Yamazaki, T. Watanabe, and H. Yamano (2016), Post-bomb coral $\Delta^{14}\text{C}$ record from Iki Island, Japan: possible evidence of oceanographic conditions on the northern East China Sea shelf, *Geo-Marine Letters*, 36(5), 371-377.
- Mortensen, P. B., H. T. Rapp, and U. Båmstedt (1998), Oxygen and carbon isotope ratios related to growth line patterns in skeletons of *Lophelia pertusa* (L) (Anthozoa, Scleractinia): Implications for determination of linear extension rate, *Sarsia*, 83(5), 433–446, doi:10.1080/00364827.1998.10413702.
- Moore, W.S. and Krishnaswami, S. (1974), Correlation of X-radiography revealed banding in corals with radiometric growth rates. *In: Proceedings, 2nd International Coral Reef Symposium, Brisbane, Australia*, pp.269–276.
- Morimoto, M., H. Kayanne, O. Abe, and M. T. McCulloch (2007), Intensified mid-Holocene Asian monsoon recorded in corals from Kikai Island, subtropical

- northwestern Pacific, *Quat. Res.*, 67(2), 204–214, doi:10.1016/j.yqres.2006.12.005.
- Morimoto, M., H. Kitagawa, Y. Shibata, and H. Kayanne (2004), Seasonal radiocarbon variation of surface seawater recorded in a coral from Kikai Island, subtropical northwestern Pacific, *Radiocarbon*, 46(2), 643-648.
- Nakamura, H. (2017), Kuroshio path and volume transport variations from Luzon Island to the eastern coast of Kyusyu, *Oceanography in Japan*, 26(4), 113-147.
- Nakamura, H., K. Nishii, B. Taguchi, and Y. Kosaka (2016), Impacts of Extratropical Coupled Ocean-Atmosphere Variability on Seasonal Predictability, *Annual Report of the Earth Simulator April 2015-March 2016*, 117-121.
- Nan, F., H. Xue, P. Xiu, F. Chai, M. Shi, and P. Guo (2011), Oceanic eddy formation and propagation southwest of Taiwan, *J. Geophys. Res. Oceans*, 116, C12045. doi:10.1029/2011JC007386
- Nan, F., H. Xue, F. Chai, D. Wang, F. Yu, M. Shi, P. Guo, and P. Xiu (2013), Weakening of the Kuroshio Intrusion into the South China Sea over the Past Two Decades, *J. Clim.*, 26(20), 8097–8110, doi:10.1175/JCLI-D-12-00315.1
- Nan F, H. Xue, and F. Yu (2015), Kuroshio intrusion into the South China Sea: A review., *Prog. Oceanogr.*, 137, 314-333.
- Neelin, J. D., and M. Latif (1998), El Nino dynamics, *Physics Today*, 51(12), 32-36.
- Newman, M., M. A. Alexander, T. R. Ault, K. M. Cobb, C. Deser, E. D. Lorenzo, N. J. Mantua, A. J. Miller, S. Minobe, H. Nakamura, N. Schneider, D. J. Vimont, A. S. Phillips, J. D. Scott, and C. A. Smith (2016), The Pacific decadal oscillation, revisited, *Journal of Climate*, 29(12), 4399-4427.
- Newman, M., G. P. Compo, and M. A. Alexander (2003), ENSO-forced variability of the Pacific decadal oscillation, *J. Clim.*, 16(23), 3853–3857.
- Nitani, H. (1972), Beginning of the Kuroshio. In: Stommel H, Yashida K (eds) *Kuroshio: Physical Aspects of the Japan Current*. University of Washington Press, pp 129-163.
- Nozaki, Y., D. M. Rye, K. K. Turekian, and R. E. Dodge (1978), A 200 year record of carbon-13 and carbon-14 variations in a Bermuda coral, *Geophys. Res. Lett.*, 5(10), 825–828.
- Okai, T., A. Suzuki, S. Terashima, M. Inoue, M. Nohara, H. Kawahata, and N. Imai (2004), Collaborative analysis of GSJ/AIST geochemical reference materials

- JCp-1 (coral) and Jct-1 (Giant Clam). *Chikyukagaku (Geochemistry)*, 38, 281–286.
- Omata, T., A. Suzuki, H. Kawahata, S. Nojima, K. Minoshima, and A. Hata (2006), Oxygen and carbon stable isotope systematics in Porites coral near its latitudinal limit: The coral response to low-thermal temperature stress, *Global Planet. Change*, 53, 137–146.
- Ortlieb, L., G. Vargas, and J. F. Saliège (2011), Marine radiocarbon reservoir effect along the northern Chile-southern Peru coast (14-24°S) throughout the Holocene, *Quat. Res.*, 75(1), 91–103, doi:10.1016/j.yqres.2010.07.018.
- Ose, T., Y. Song, and A. Kitoh (1997), Sea surface temperature in the South China Sea: An index for the Asian monsoon and ENSO system, *J. Meteor. Soc. Japan*, 75, 1091–1107.
- Östlund, H. G., and M. Stuiver (1980), GEOSECS Pacific Radiocarbon, *Radiocarbon*, 22(1), 25-53. doi:10.1017/S0033822200004707.
- Petchey, F., and S. Ulm (2012), Marine Reservoir Variation in the Bismarck Region: An Evaluation of Spatial and Temporal Change in ΔR and R Over the Last 3000 Years, *Radiocarbon*, 54, 45–58, doi: 10.2458/azu_js_rc.v54i1.13050.
- Potemra, J. T., and T. Qu (2009), Seas of Southeast Asia, *Encyclopedia of Ocean Sciences 2nd ed.*, Academic Press, pp 305-316. doi: <http://doi.org/10.1016/B978-012374473-9.00598-1>.
- Qiu, B. (2001), Kuroshio and Oyashio Currents, in *Encyclopedia of Ocean Science, 2nd ed.*, Academic Press, New York, pp 358-369.
- Qiu, B., D. L. Rudnick, I. Cerovecki, B. D. Cornuelle, S. Chen, M. C. Schönau, J. L. McClean, and G. Gopalakrishnan (2015), The Pacific North Equatorial Current: New insights from the origins of the Kuroshio and Mindanao Currents (OKMC) Project. *Oceanography*, 28(4), 24-33.
- Qiu, B., and R. Lukas (1996), Seasonal and interannual variability of the North Equatorial Current, the Mindanao Current, and the Kuroshio along the Pacific western boundary, *J. Geophys. Res.*, 101(C5), 12315–12330, doi:95JC03204.0148-0227/96/95JC-03204\$09.00.
- Qiu, B., and S. Chen (2010), Interannual-to-Decadal Variability in the Bifurcation of the North Equatorial Current off the Philippines, *J. Phys. Oceanogr.*, 40(11), 2525–2538, doi:10.1175/2010JPO4462.1.

- Qiu, B., and S. Chen (2012), Multidecadal Sea Level and Gyre Circulation Variability in the Northwestern Tropical Pacific Ocean, *J. Phys. Oceanogr.*, *42*(1), 193–206, doi:10.1175/JPO-D-11-061.1.
- Qiu, B., and T. M. Joyce (1992), Interannual variability in the mid- and low-latitude western North Pacific, *J. Phys. Oceanogr.*, *22*(9), 1062–1079.
- Qu, T., Y. Y. Kim, M. Yaremchuk, T. Tozuka, A. Ishida, T. Yamagata (2004), Can Luzon Strait transport play a role in conveying the impact of ENSO to the South China Sea?, *J. Clim.*, *17*(18), 3644–3657.
- Qu, T. D., J. P. Gan, A. Ishida, Y. Kashino, and T. Tozuka (2008), Semiannual variation in the western tropical Pacific Ocean, *Geophys. Res. Lett.*, *35*(16), L16602, <http://dx.doi.org/10.1029/2008GL035058>.
- Qu, T., H. Mitsudera, and T. Yamagata (1998), On the western boundary current in the Philippine Sea, *J. Geophys. Res.*, *103*(C4), 7537–7548.
- Qu T, H. Mitsudera H, and T. Yamagata (2000) Intrusion of the North Pacific waters into the South China Sea. *J. Geophys. Res.*, *105*, 6415-6424. doi:10.1029/1999JC900323.
- Qu, T., and R. Lukas (2003), The bifurcation of the North Equatorial Current in the Pacific. *Journal of Physical Oceanography*, *33*(1), 5-18.
- Qu, T., Y. T. Song, and T. Yamagata (2009), An introduction to the South China Sea throughflow: its dynamics, variability, and application for climate, *Dyn Atmos Oceans*, *47*, 3–14, doi:10.1016/j.dynatmoce.2008.05.001.
- Reimer, P., E. Bard, A. Bayliss, J. W. Beck, P. G. Blackwell, C. B. Ramsey, C. E. Buck, H. Cheng, R. L. Edwards, M. Friedrich, P. M. Grootes, T. P. Guilderson, H. Haflidason, I. Hajdas, C. Hatté, T. J. Heaton, D. L. Hoffmann, A. G. Hogg, K. A. Hughen, K. F. Kaiser, B. Kromer, S. W. Manning, M. Niu, R. W. Reimer, D. A. Richards, E. M. Scott, J. R. Southon, R. A. Staff, C. S. M. Turney, and J. van der Plicht (2013), IntCal13 and Marine13 Radiocarbon Age Calibration Curves 0–50,000 Years cal BP, *Radiocarbon*, *55*(4), 1869–1887, doi:10.2458/azu_js_rc.55.16947.
- Roark, E. B., T. P. Guilderson, R. B. Dunbar, and B. L. Ingram (2006), Radiocarbon Based Ages and Growth Rates : Hawaiian Deep Sea Corals, *Mar. Ecol. Prog. Ser.*, *327*, 1-14, Retrieved from <http://www.jstor.org/stable/24870713>.

- Rozanski, K. (1991), Consultants' group meeting on ^{14}C reference materials for radiocarbon laboratories. February 18–20, 1991, Vienna, Austria. Internal Report, IAEA, Vienna.
- Santos, G. M., M. Mazon, J. R. Southon, S. Rifai, and R. Moore (2007), Evaluation of iron and cobalt powders as catalysts for ^{14}C -AMS target preparation, *Nucl. Instruments Methods Phys. Res. Sect. B Beam Interact. with Mater. Atoms*, 259(1), 308–315, doi:<https://doi.org/10.1016/j.nimb.2007.01.220>.
- Sakaguchi, A., T. Nomura, P. Steier, R. Golser, K. Sasaki, T. Watanabe, T. Nakakuki, Y. Takahashi, and H. Yamano (2016), Temporal and vertical distributions of anthropogenic ^{236}U in the Japan Sea using a coral core and seawater samples, *J. Geophys. Res. Oceans*, 121, 4–13, doi:10.1002/2015JC011109.
- Sakamoto, T. T., H. Hasumi, M. Ishii, S. Emori, T. Suzuki, T. Nishimura, and A. Sumi (2005), Responses of the Kuroshio and the Kuroshio Extension to global warming in a high-resolution climate model, *Geophys. Res. Lett.*, 32, L14617.
- Sarnthein, M., P. M. Grootes, A. Holbourn, W. Kuhnt, and H. Kühn (2011), Tropical warming in the Timor Sea led deglacial Antarctic warming and atmospheric CO_2 rise by more than 500yr, *Earth Planet. Sci. Lett.*, 302(3), 337–348, doi:<https://doi.org/10.1016/j.epsl.2010.12.021>.
- Sato, Y., S. Yukimoto, H. Tsujino, H. Ishizaki, and A. Noda (2006), Response of North Pacific ocean circulation in a Kuroshio-resolving ocean model to an Arctic Oscillation (AO)-like change in Northern Hemisphere atmospheric circulation due to greenhouse-gas forcing, *J. Meteorol. Soc. Jpn.*, 84(2), 295–309.
- Schlitzer, R. (2014), Ocean Data View. [Available at <http://odv.awi.de>]
- Schneider, N., and B. D. Cornuelle (2005), The forcing of the Pacific decadal oscillation. *Journal of Climate*, 18(21), 4355–4373.
- SCOR Working Group (2007), GEOTRACES - An international study of the global marine biogeochemical cycles of trace elements and their isotopes, *Chemie der Erde - Geochemistry*, 67(2), 85–131, doi:10.1016/j.chemer.2007.02.001.
- Sheremet, V. A. (2001), Hysteresis of a western boundary current leaping across a gap, *J. Phys. Oceanogr.*, 31, 1247–1259. doi:10.1175/1520-0485(2001)031<1247:HOAWBC>2.0.CO;2

- Sheremet, V. A., and J. Kuehl (2007), Gap-leaping western boundary current in a circular tank model, *J.Phys.Oceanogr.*, *37*, 1488–1495.
- Shikakuma, S. (2002), Mesoscale eddy and upwelling at the south of Okinawa Island, Japan, in *Annual Report of Okinawa Prefectural Fisheries Experimental Station*, pp. 82–84, Okinawa Prefectural Fisheries Experimental Station, Okinawa, Japan. [Available at <http://www.pref.okinawa.jp/fish/jihou/jihouh12.html>.]
- Siani, G., M. Paterna, E. Michel, R. Sulpizio, A. Sbrana, M. Arnold, and G. Haddad (2001), Mediterranean Sea Surface Radiocarbon Reservoir Age Changes Since the Last Glacial Maximum, *Science*, *294*(5548), 1917–1920.
- Siani, G., E. Michel, R. De Pol-Holz, T. Devries, F. Lamy, M. Carel, G. Isguder, F. Dewilde, and A. Lourantou (2013), Carbon isotope records reveal precise timing of enhanced Southern Ocean upwelling during the last deglaciation, *Nat. Commun.*, *4*(2758), 1–9, doi:10.1038/ncomms3758.
- Sikes, E. L., C. R. Samson, T. P. Guilderson, and W. R. Howard (2000), Old radiocarbon ages in the southwest Pacific Ocean during the last glacial period and deglaciation, *Nature*, *405*, 555–559.
- Skinner, L., I. N. McCave, L. Carter, S. Fallon, A. E. Scrivner, and F. Primeau (2015), Reduced ventilation and enhanced magnitude of the deep Pacific carbon pool during the last glacial period, *Earth Planet. Sci. Lett.*, *411*, 45–52, doi:<https://doi.org/10.1016/j.epsl.2014.11.024>.
- Skog, G., M. Rundgren, and P. Sköld (2010), Status of the Single Stage AMS machine at Lund University after 4years of operation, *Nucl. Instruments Methods Phys. Res. Sect. B Beam Interact. with Mater. Atoms*, *268*(7–8), 895–897, doi:10.1016/j.nimb.2009.10.058.
- Smith, T.M., and R.W. Reynolds (2004), Improved Extended Reconstruction of SST (1854–1997), *J. Climate*, *17*, 2466–2477, [https://doi.org/10.1175/1520-0442\(2004\)017<2466:IEROS>2.0.CO;2](https://doi.org/10.1175/1520-0442(2004)017<2466:IEROS>2.0.CO;2)
- Soeyanto, E., X. Guo, J. Ono, and Y. Miyazawa (2014), Interannual variations of Kuroshio transport in the East China Sea and its relation to the Pacific Decadal Oscillation and mesoscale eddies, *J. Geophys. Res. Oceans*, *119*, 3595–3616, doi:10.1002/2013JC009529.

- Song, S., Z. Peng, W. Zhou, W. Liu, Y. Liu, and T. Chen (2012), Variation of the winter monsoon in South China Sea over the past 183years: Evidence from oxygen isotopes in coral, *Glob. Planet. Change*, 98–99, 131–138, doi:10.1016/j.gloplacha.2012.08.013.
- Southon, J. R., M. Kashgarian, M. Fontugne, B. Metivier, and W. W.-S. Yim (2002), Marine reservoir corrections for the Indian Ocean and Southeast Asia, *Radiocarbon*, 44, 167–180, DOI: 10.1017/S0033822200064778.
- Sowa, K., T. Watanabe, H. Kan, and H. Yamano (2014), Influence of land development on Holocene Porites coral calcification at Nagura Bay, Ishigaki Island, Japan, *PLoS ONE*, 9(2), e88790.
- Stuiver, M., G. W. Pearson, and T. Braziunas (1986), Radiocarbon age calibration of marine samples back to 9000 cal yr BP., *Radiocarbon*, 28, 980–1021, DOI: 10.1017/S0033822200060264.
- Stuiver, M., and H. A. Polach (1977), Discussion: Reporting of ^{14}C Data. *Radiocarbon* 19(3), 355–363.
- Stuiver, M., H. G. Östlund, and T. A. McConnaughey (1981), GEOSECS Atlantic and Pacific ^{14}C distribution, *Scope (Kalamazoo)*, 16, 201–21.
- Sugiyama Y., Tedokon I., and Toyoshima S. (2004), Status of Oceanographic research and ocean condition in the south of Japan during World War II, *Technical bulletin on hydrography and oceanography (Kaiyou Jouhoubu gihou)*, 22, 63–68.
- Suzuki, A., M. K. Gagan, K. Fabricius, P. J. Isdale, I. Yukino, and H. Kawahata (2003), Skeletal isotope microprofiles of growth perturbations in *Porites* corals during the 1997–1998 mass bleaching event, *Coral Reefs*, 22, 357–369.
- Suzuki, A., K. Hibino, A. Iwase, and H. Kawahata (2005) Intercolony variability of skeletal oxygen and carbon isotope signatures of cultured *Porites* corals: temperature-controlled experiments, *Geochim. Cosmochim. Acta*, 69, 4453–4462.
- Suzuki, A., Y. Yokoyama, H. Kan, K. Minoshima, H. Matsuzaki, N. Hamanaka, and H. Kawahata (2008), Identification of 1771 Meiwa Tsunami deposits using a combination of radiocarbon dating and oxygen isotope microprofiling of emerged massive *Porites* boulders, *Quat. Geochronol.*, 3, 226–234, doi:10.1016/j.quageo.2007.12.002.

- Takikawa, T., H. Ichikawa, K. Ichikawa, and S. Kawae (2005), Extraordinary subsurface mesoscale eddy detected in the southeast of Okinawa in February 2002, *Geophys. Res. Lett.*, *32*, L17602, doi:10.1029/2005GL023842.
- Tani, M. (2010) Meridional heat transport interannual variability of the North Pacific subtropical circulation, *Weather service bulletin*, *77*, S43-S58.
- Thoppil, P. G., E. J. Metzger, H. E. Hurlburt, O. M. Smedstad, and H. Ichikawa (2016), The current system east of the Ryukyu Islands as revealed by a global ocean reanalysis, *Prog. Oceanogr.*, *141*, 239–258.
- Tian, J., Q. Yang, X. Liang, L. Xie, D. Hu, F. Wang, and T. Qu (2006), Observation of Luzon Strait transport, *Geophys Res Lett*, *33*, L19607, doi:10.1029/2006GL026272.
- Toggweiler, J.R. (1983), A six zone regionalized model for bomb radiotracers in CO₂ in the upper kilometer of the Pacific Ocean. *PhD Dissertation Thesis, Columbia University, New York*.
- Toggweiler, J. R., K. Dixon, and W. S. Broecker (1991), The Peru upwelling and the ventilation of the South Pacific thermocline. *Journal of Geophysical Research: Oceans*, *96*(C11), 20467-20497.
- Tomita, T., and T. Yasunari (1996), Role of the northeast winter monsoon in the biennial oscillation of the ENSO/monsoon system, *J. Meteor. Soc. Japan*, *74*, 399–413.
- Toole, J. M., R. C. Millard, Z. Wang, and S. Pu (1990), Observations of the Pacific North Equatorial Current bifurcation at the Philippine coast. *J. Phys. Oceanogr.*, *20*, 307-318.
- Tottori, K., M. Nagao, N. Morimoto, M. Inoue, A. Iwase, T. Shibuno, Y. Fujioka, H. Ohba, H. Kan, and A. Suzuki (2004), Relationship between sediments and water turbidity in coral reefs around Ishigaki Island, Ryukyus, *Journal of the Japanese Coral Reef Society 2004*, 1–19, DOI: 10.3755/jcrs.2004.1.
- Tozuka, T., T. Kagimoto, Y. Masumoto, and T. Yamagata (2002), Simulated multiscale variations in the western tropical Pacific: The Mindanao Dome revisited, *J. Phys. Oceanogr.*, *32*, 1338–1359
- Ulm, S. (2002), Marine and Estuarine Reservoir Effects in Central Queensland, Australia: Determination of ΔR Values, *Geoarchaeology - An Int. J.*, *17*(4), 319–348, doi:10.1002/gea.10017.

- Ulm, S. (2006), Australian Marine Reservoir Effects : A Guide to ΔR Values, *Aust. Archaeology*, 63, 57–60
- Wang, Q., and D. Hu (2006), Bifurcation of the North Equatorial Current derived from altimetry in the Pacific Ocean, *J. Hydrodynam.*, 18(5), 620–626, doi:10.1016/S1001-6058(06)60144-3.
- Wang, J., D. Tang, and Y. Sui (2010), Winter phytoplankton bloom induced by subsurface upwelling and mixed layer entrainment southwest of Luzon Strait, *J. Mar. Syst.*, 83(3), 141–149.
- Wang, Y. F., and H. F. Xu (2001), Prediction of trace metal partitioning between minerals and aqueous solutions: A linear free energy correlation approach, *Geochim. Cosmochim. Acta*, 65, 1529– 1543.
- Wijffels, S., E. Firing, and J. Toole (1995), The mean structure and variability of the Mindanao Current at 8°N. *J. Geophys. Res.*, 100, 18421–18435.
- Wu, C-R. (2013), Interannual modulation of the Pacific Decadal Oscillation (PDO) on the low-latitude western North Pacific. *Progress in Oceanography*, 110, 49-58.
- Wu, C.-R., and T.-L. Chiang (2007), Mesoscale eddies in the northern South China Sea, *Deep Sea Res., Part II*, 54(14), 1575–1588.
- Wu, C. R., Y. L. Wang, Y. F. Lin, T. L. Chiang, and C. C. Wu (2016), Weakening of the Kuroshio Intrusion into the South China Sea under the Global Warming Hiatus, *IEEE J. Sel. Top. Appl. Earth Obs. Remote Sens.*, 9(11), 5064–5070, doi:10.1109/JSTARS.2016.2574941.
- Wyrtki, K. (1961), Physical Oceanography of the Southeast Asian Waters, *Scripps Inst. of Oceanogr., Univ. of Calif., La Jolla*.
- Vargas, G., S. Pantoja, J. A. Rutllant, C. B. Lange, and L. Ortlieb (2007), Enhancement of coastal upwelling and interdecadal ENSO-like variability in the Peru-Chile Current since late 19th century, *Geophys. Res. Lett.*, 34, L13607, doi:10.1029/2006GL028812.
- Yamane, M., Y. Yokoyama, Y. Miyairi, H. Suga, H. Matsuzaki, R. B. Dunbar, and N. Ohkouchi (2014), Compound-specific ^{14}C dating of IODP Expedition 318 core U1357A obtained off the Wilkes Land Coast, Antarctica, *Radiocarbon*, 56(3), 1009–1017.

- Yamamoto, H (1999), Coral Skeletal Growth Records-Ocean Climate Change Relationship, *JAMSTECR*, 39, 17-33
- Yamano, H., K. Hori, M. Yamauchi, O. Yamagawa, and A. Ohmura (2001), Highest-latitude coral reef at Iki Island, Japan, *Coral Reefs*, 20, 9–12.
- Yamazaki, A., T. Watanabe, U. Tsunogai, F. Iwase, and H. Yamano (2016), A 150-year variation of the Kuroshio transport inferred from coral nitrogen isotope signature, *Paleoceanography*, 31, 838–846, doi:10.1002/2015PA002880.
- Yang, Q., J. Tian, and W. Zhao (2010), Observation of Luzon Strait transport in summer 2007. *Deep Sea Res. Part I.*, 57, 670-676. doi:10.1016/j.dsr.2010.02.004.
- Yang, H., G. Lohmann, W. Wei, M. Dima, M. Ionita, and J. Liu (2016), Intensification and poleward shift of subtropical western boundary currents in a warming climate, *J. Geophys. Res. Ocean.*, 121(7), 4928–4945, doi:10.1002/2015JC011513.
- Yaremchuk, M., and T. Qu (2004), Seasonal Variability of the Large-Scale Currents near the Coast of the Philippines, *J. Phys. Oceanogr.*, 34, 844–855.
- Yoneda, M., Y. Shibata, A. Tanaka, T. Uehiro, M. Morita, M. Uchida, T. Kobayashi, C. Kobayashi, R. Suzuki, K. Miyamoto, B. Hancock, C. Dibden, and J. S. Edmonds (2004), AMS ^{14}C measurement and preparative techniques at NIES-TERRA, *Nucl. Instruments Methods Phys. Res. Sect. B Beam Interact. with Mater. Atoms*, 223–224, 116–123, doi:https://doi.org/10.1016/j.nimb.2004.04.026.
- Yoneda, M., H. Uno, Y. Shibata, R. Suzuki, Y. Kumamoto, K. Yoshida, T. Sasaki, A. Suzuki, and H. Kawahata (2007), Radiocarbon marine reservoir ages in the western Pacific estimated by pre-bomb molluscan shells, *Nucl. Instruments Methods Phys. Res. Sect. B Beam Interact. with Mater. Atoms*, 259(1), 432–437, doi:10.1016/j.nimb.2007.01.184.
- Yokoyama, Y., J. B. Anderson, M. Yamane, L. M. Simkins, Y. Miyairi, T. Yamazaki, M. Koizumi, H. Suga, K. Kusahara, L. Prothro, H. Hasumi, J. R. Southon, and N. Ohkouchi (2016), Widespread collapse of the Ross Ice Shelf during the late Holocene. *Proc. Natl. Acad. Sci.*, 113(9), 2354–2359.
- Yokoyama, Y., Y. Miyairi, H. Matsuzaki, and F. Tsunomori (2007), Relation between acid dissolution time in the vacuum test tube and time required for graphitization for AMS target preparation, *Nucl. Instruments Methods Phys.*

- Res. Sect. B Beam Interact. with Mater. Atoms*, 259(1), 330–334,
doi:10.1016/j.nimb.2007.01.176.
- Yokoyama, Y., M. Koizumi, H. Matsuzaki, Y. Miyairi, and N. Ohkouchi (2010),
Developing ultra small-scale radiocarbon sample measurement at the
University of Tokyo, *Radiocarbon*, 52(2), 310–318.
- Yokoyama, Y., A. Suzuki, F. Siringan, Y. Maeda, A. Abe-Ouchi, R. Ohgaito, H.
Kawahata, and H. Matsuzaki (2011), Mid-Holocene palaeoceanography of the
northern South China Sea using coupled fossil-modern coral and atmosphere-
ocean GCM model, *Geophys. Res. Lett.*, 38, L00F03,
doi:10.1029/2010GL044231.
- Yu, K., Q. Hua, J. Zhao, E. Hodge, D. Fink, and M. Barbetti (2010), Holocene marine
14 C reservoir age variability: Evidence from 230 Th-dated corals in the
South China Sea, *Paleoceanography*, 25(3), PA3205,
doi:10.1029/2009PA001831.
- Yuan, D. L., W. Q. Han, and D. X. Hu (2006), Surface Kuroshio path in the Luzon
Strait area derived from satellite remote sensing data, *J. Geophys. Res.*, 111,
C11007. <http://dx.doi.org/10.1029/2005JC003412>.
- Yuan, Y., Y.-H. Tseng, C. Yang, G. Liao, C. H. Chow, Z. Liu, X.-H. Zhu, and H. Chen
(2014), Variation in the Kuroshio intrusion: Modeling and interpretation of
observations collected around the Luzon Strait from July 2009 to March
2011, *J. Geophys. Res. Ocean.*, 119, 1–17, doi:10.1002/2013JC009776.
- Yuwaki, Y., M. Tsurudome, and K. Shimada (1971), On the amount of zooplankton
biomass and the upwelling process in the East of Taiwan, *Mem. Fac. Fish.
Kagoshima Univ.*, 20(1), 111–118.
- Zhang, X., B. Cornuelle, and D. Roemmich (2012), Sensitivity of Western boundary
transport at the Mean North Equatorial Current Bifurcation Latitude to wind
forcing, *J. Phys. Oceanogr.*, 42, 2056–2072, doi:10.1175/JPO-D-11-0229.1.
- Zhao, J., Y. Li, and F. Wang (2013), The role of mindanao dome in the variability of the
Pacific North equatorial current bifurcation, *J. Oceanogr.*, 69(3), 313–327,
doi:10.1007/s10872-013-0175-7.
- Zhang, Y., J. M. Wallace, and N. Iwasaka (1996) Is climate variability over the North
Pacific a linear response to ENSO?, *J. Climate*, 9, 1468–1478.

References

Zhang, Y., J. M. Wallace, and D. S. Battisti (1997), ENSO-like interdecadal variability: 1900–93., *J. Climate*, *10*, 1004–1020.

Appendix of Chapter 3

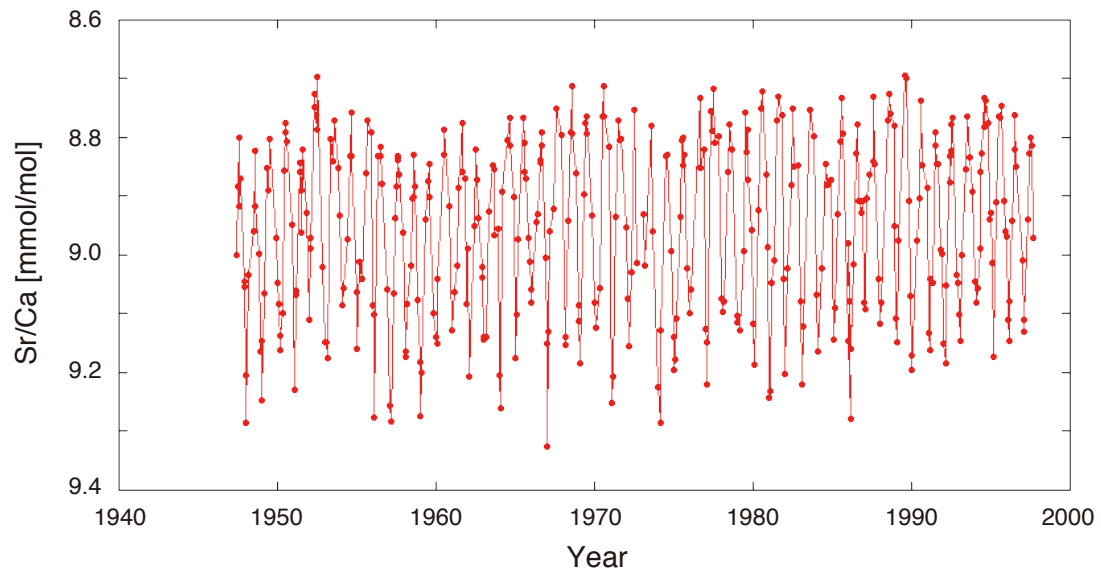


Figure A3.1 Sr/Ca ratio recorded in in the Ishigaki coral (IY02-02) From Hirabayashi et al. (2017a).

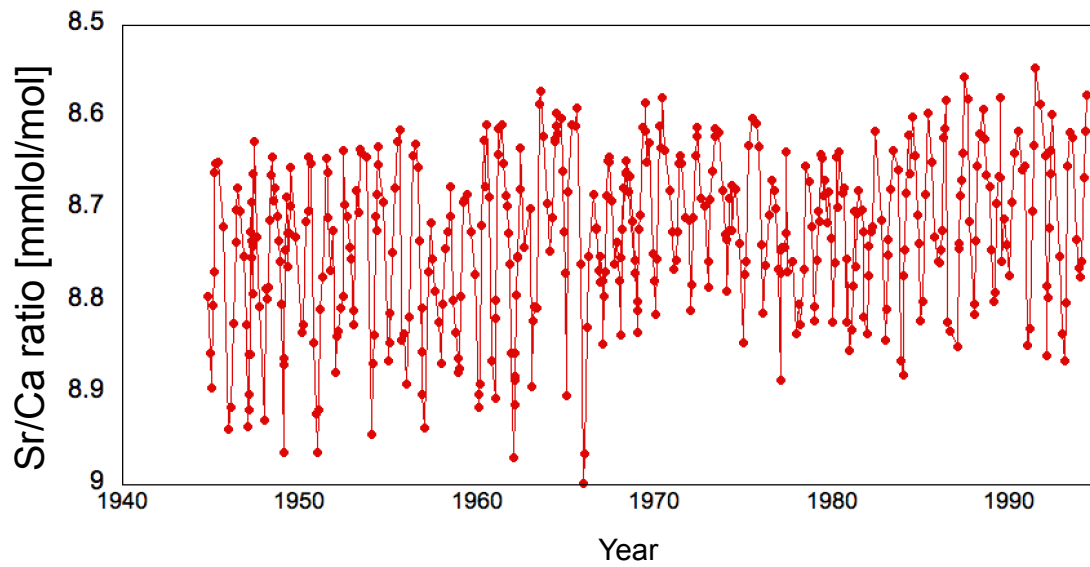


Figure A3.2 Sr/Ca ratio recorded in in the Currima coral (PCURIN03). From Hirabayashi et al. (2017b).

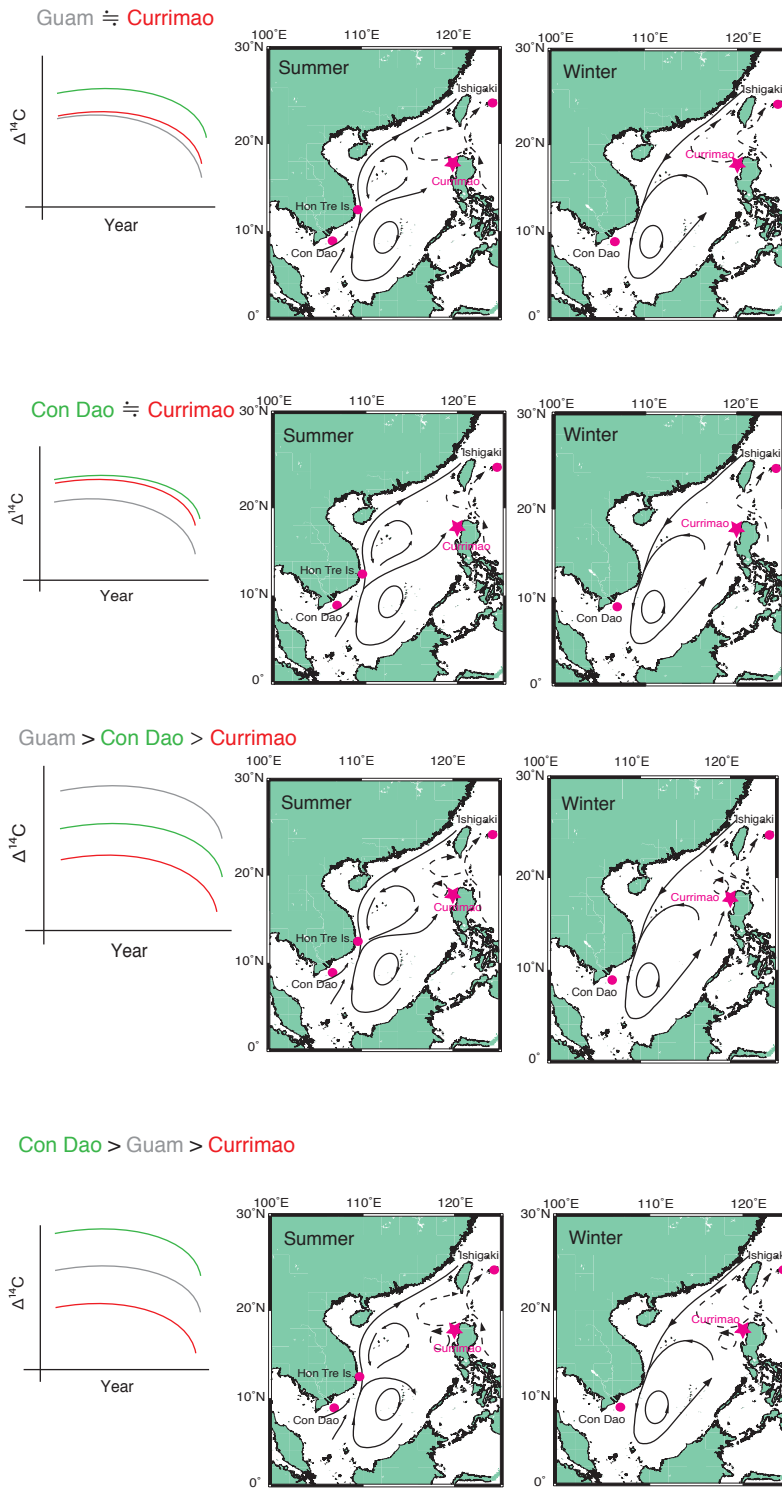


Figure A3.3 Schematic illustration of surface ocean circulation in the South China Sea. The main current (black solid lines) of the South China Sea is based on Wang and Li (2009). From Hirabayashi et al. (2017b).

Table A3.1

Radiocarbon data in the Ishigaki coral (IY02-02).

Lab. No	age	$\Delta^{14}\text{C}$ [‰]	err
YAUT-013635	1997.5	98.42	3.06
YAUT-013626	1997.1	97.43	3.29
YAUT-013639	1996.5	96.25	3.21
YAUT-013625	1996.2	103.32	3.46
YAUT-013637	1995.7	104.21	3.87
YAUT-013638	1995.6	97.48	3.71
YAUT-013636	1995.2	103.81	3.15
YAUT-013634	1994.7	108.28	4.06
YAUT-013624	1994.1	108.71	3.62
YAUT-013633	1993.5	103.88	4.09
YAUT-013623	1993.1	113.42	3.99
YAUT-013630	1992.5	112.11	4.80
YAUT-013612	1992.0	115.97	3.55
YAUT-013619	1991.5	122.49	4.18
YAUT-013613	1991.2	121.70	3.98
YAUT-013618	1990.3	123.92	3.41
YAUT-013617	1989.9	126.39	3.62
YAUT-013631	1989.6	128.94	4.33
YAUT-013632	1989.0	129.61	3.94
YAUT-013620	1988.7	126.49	3.54
YAUT-013605	1988.0	130.75	3.31
YAUT-019714	1987.9	143.13	6.97
YAUT-019704	1987.2	128.80	5.67
YAUT-013622	1986.6	131.25	3.61
YAUT-013610	1986.2	134.61	3.54
YAUT-013606	1985.6	134.29	3.55
YAUT-013609	1985.1	137.30	3.79
YAUT-013608	1984.6	133.58	3.94

YAUT-013611	1984.1	148.09	7.27
YAUT-013607	1983.6	147.55	3.11
YAUT-019707	1982.4	145.07	4.65
YAUT-016204	1981.7	142.27	4.99
YAUT-019715	1981.0	156.91	5.00
YAUT-016205	1980.6	144.58	4.53
YAUT-019733	1980.2	157.46	4.33
YAUT-017416	1979.4	144.90	13.15
YAUT-016206	1978.6	141.56	5.57
YAUT-017406	1977.1	152.03	9.19
YAUT-016210	1976.7	148.09	4.49
YAUT-016211	1976.1	147.03	6.57
YAUT-016212	1975.5	160.73	4.83
YAUT-016213	1975.1	155.03	4.40
YAUT-016214	1974.5	144.97	4.97
YAUT-017404	1973.6	140.23	14.90
YAUT-017409	1972.6	163.09	5.02
YAUT-017412	1971.5	151.02	5.65
YAUT-016218	1970.0	152.09	5.15
YAUT-016219	1969.5	158.59	5.16
YAUT-017408	1969.0	132.69	5.73
YAUT-016220	1968.6	125.45	5.12
YAUT-016221	1968.2	133.70	5.08
YAUT-016222	1967.6	128.91	5.10
YAUT-016225	1967.1	111.87	5.35
YAUT-016226	1966.7	108.19	4.49
YAUT-017428	1966.6	100.64	5.11
YAUT-016227	1966.0	99.34	5.58
YAUT-017413	1965.8	98.36	5.35
YAUT-016228	1965.5	93.33	5.62
YAUT-016229	1965.0	72.79	4.67
YAUT-016230	1964.7	62.50	4.48

YAUT-016234	1964.1	39.60	4.46
YAUT-016235	1963.6	26.56	4.36
YAUT-016236	1963.0	9.69	4.95
YAUT-016237	1962.5	-6.94	5.07
YAUT-016238	1962.1	-2.83	4.85
YAUT-016905	1961.7	-11.42	6.18
YAUT-019523	1961.3	-7.97	4.11
YAUT-016906	1961.2	2.55	8.28
YAUT-019509	1960.6	-16.23	4.32
YAUT-016907	1960.5	7.20	5.69
YAUT-019519	1960.5	-22.24	3.75
YAUT-019513	1960.3	-35.47	3.57
YAUT-016908	1960.1	-37.84	5.83
YAUT-016909	1959.6	-38.37	5.42
YAUT-016913	1959.0	-32.42	7.49
YAUT-016914	1958.6	-31.49	5.80
YAUT-016915	1958.1	-26.17	9.55
YAUT-019713	1958.1	-23.43	6.60
YAUT-019703	1957.7	-32.56	4.13
YAUT-019526	1957.6	-27.47	5.49
YAUT-017420	1957.1	-31.24	4.75
YAUT-019536	1956.5	-24.58	4.95
YAUT-019537	1956.3	-26.84	4.02
YAUT-017421	1956.1	-2.71	5.47
YAUT-019527	1956.0	8.94	4.41
YAUT-019722	1955.9	7.72	6.20
YAUT-016928	1955.7	49.49	5.94
YAUT-019524	1955.6	50.75	4.34
YAUT-017417	1955.0	-41.48	6.38
YAUT-016929	1954.7	-55.84	5.86
YAUT-017434	1954.1	-44.08	5.24
YAUT-017418	1953.6	-61.23	5.38

YAUT-016930	1953.2	-48.92	4.96
YAUT-017433	1953.0	-50.87	6.15
YAUT-019511	1952.6	-64.74	4.55
YAUT-017438	1952.0	-53.39	5.00
YAUT-017432	1951.2	-54.97	4.48
YAUT-017425	1951.1	-66.10	5.91
YAUT-016936	1950.5	-56.02	6.19
YAUT-017437	1950.2	-48.70	4.66
YAUT-019515	1949.9	-65.41	4.61
YAUT-017424	1949.5	-59.17	4.85
YAUT-019517	1949.2	-71.22	5.17
YAUT-019516	1948.8	-70.00	5.43
YAUT-016938	1948.6	-51.82	5.24
YAUT-019525	1948.0	-52.96	4.28
YAUT-016939	1947.7	-54.29	6.68
YAUT-017422	1947.6	-47.86	4.19
YAUT-019514	1947.4	-64.46	3.79

Table A3.2

Radiocarbon data in the Currimao coral (PCURIN03). For the samples which includes (s) in the Lab No., I conducted small-scale radiocarbon dating with the sample amount of 2-5 mg. For the samples of (*), I measured same samples twice and took an average of them. Data of the period from 1968 to 1995 were reported by Hirabayashi et al. (2017b).

Lab No.	Age	$\Delta^{14}\text{C}$	err
(s) YAUT-019723	1994.33	98.82	5.15
YAUT-023703	1994.00	96.20	3.48
YAUT-023706	1993.42	100.22	2.91
(s) YAUT-023505	1992.42	100.37	3.88
YAUT-021314	1992.08	99.31	3.16
(s) YAUT-019739	1991.42	107.20	3.43
YAUT-021315	1991.00	111.16	3.71
YAUT-021312	1990.50	105.64	4.30
YAUT-023704	1990.00	106.38	2.51
(s) YAUT-019706	1989.50	102.49	3.39
YAUT-023713	1989.08	108.14	3.76
YAUT-023709	1988.50	115.79	5.20
YAUT-023739	1988.00	106.78	2.40
(s) YAUT-019737	1987.42	118.57	2.88
YAUT-023737	1987.08	119.77	3.13
YAUT-023714	1986.42	126.72	5.35
YAUT-023716	1986.08	126.67	2.54
(s) YAUT-019732	1985.42	111.90	7.92
YAUT-023711	1985.00	121.96	5.58
YAUT-023736	1984.50	127.63	2.83
YAUT-023738	1984.00	136.03	2.70
(s) YAUT-019729	1983.42	137.06	3.85
YAUT-023712	1983.00	136.17	3.95

*	YAUT-023729	(s) YAUT-019734	1982.42	139.67	2.37
*	YAUT-023726	YAUT-023724	1982.00	144.32	2.28
*	(s) YAUT-019735	YAUT-023727	1981.50	145.64	2.90
*	(s) YAUT-023504	YAUT-023731	1981.00	139.48	3.15
*	YAUT-023725	(s) YAUT-019726	1980.42	153.03	2.76
*	YAUT-023407	YAUT-023404	1980.00	145.51	3.59
*	(s) YAUT-019728	(s) YAUT-023730	1979.42	143.02	2.45
	YAUT-023406		1979.00	134.99	6.14
	YAUT-023719		1978.50	152.46	3.34
	YAUT-023734		1978.00	144.38	5.00
	YAUT-021308		1977.42	152.93	3.57
*	YAUT-023733	YAUT-023337	1977.08	131.90	2.63
	YAUT-023723		1976.62	147.20	4.23
	YAUT-021304		1976.58	130.96	5.01
	YAUT-024017		1976.08	134.24	7.14
	(s) YAUT-019727		1975.50	162.30	4.42
	YAUT-023707		1975.00	141.10	4.27
	YAUT-023721		1974.50	157.43	2.82
*	YAUT-024018	YAUT-024023	1974.03	140.94	4.00
	YAUT-024025		1973.42	178.05	5.71
	YAUT-024027		1973.37	171.37	5.00
	(s) YAUT-019717		1973.00	148.04	3.29
	(s) YAUT-019725		1972.42	165.89	6.05
	YAUT-023717		1972.00	137.82	3.58
	YAUT-023339		1971.42	138.01	3.89
	(s) YAUT-019718		1971.08	137.17	3.71
	(s) YAUT-019712		1970.42	140.07	6.35
	YAUT-023405		1970.08	138.83	4.82
	(s) YAUT-019709		1969.50	144.77	6.29
	(s) YAUT-019719	YAUT-033309	1969.00	130.18	5.68
	YAUT-031104		1968.53	117.91	7.53
	(s) YAUT-019705	YAUT-032925	1968.42	128.30	7.76

Appendix of Chapter 3

YAUT-033337	1968.08	129.82	3.68
YAUT-031315	1967.46	143.81	5.24
YAUT-031133	1967.42	145.84	5.22
YAUT-033304	1967.08	112.31	3.36
YAUT-031103	1966.90	99.38	5.79
YAUT-032926	1966.58	119.04	3.29
YAUT-031132	1966.25	99.20	4.06
YAUT-033305	1966.00	106.21	2.89
YAUT-032928	1965.58	141.14	3.22
YAUT-031129	1965.53	139.12	4.99
YAUT-033303	1965.00	90.06	4.15
YAUT-031131	1964.94	80.29	6.43
YAUT-031102	1964.82	72.07	11.35
YAUT-031105	1964.70	114.91	4.89
YAUT-032929	1964.42	115.61	3.17
YAUT-033333	1964.08	94.50	3.78
YAUT-031126	1963.71	91.11	4.69
YAUT-032915	1963.58	97.52	3.71
YAUT-033306	1963.08	63.77	3.18
YAUT-031106	1962.67	75.90	6.78
YAUT-032931	1962.42	52.19	3.19
YAUT-031128	1962.26	18.84	6.13
YAUT-032924	1962.08	-4.91	3.26
YAUT-031139	1961.75	-3.30	3.82
YAUT-032918	1961.42	1.11	4.13
YAUT-033319	1961.36	2.29	3.33
YAUT-033338	1961.31	-4.58	3.58
YAUT-033336	1961.21	-2.81	4.12
YAUT-031109	1961.16	5.01	8.47
YAUT-032932	1961.10	-3.70	3.07
YAUT-032919	1961.00	-6.09	2.83
YAUT-033313	1960.88	-8.65	3.06

Appendix of Chapter 3

YAUT-031111	1960.83	-15.78	8.99
YAUT-033326	1960.79	-12.12	3.47
YAUT-033312	1960.58	-8.58	2.82
YAUT-033317	1960.54	-13.98	2.97
YAUT-032917	1960.50	-4.84	3.74
YAUT-033324	1960.44	-0.46	3.36
YAUT-032916	1960.18	-23.37	4.00
YAUT-031138	1960.15	-28.33	4.82
YAUT-032923	1960.08	-13.41	2.92
YAUT-032911	1959.42	-10.54	3.31
YAUT-031112	1959.19	-9.88	5.46
YAUT-032933	1959.17	-16.37	2.79
YAUT-033406	1959.03	-23.52	3.19
YAUT-032913	1959.00	-37.47	3.53
YAUT-033405	1958.96	-28.24	3.88
YAUT-031137	1958.50	-24.67	4.05
YAUT-031312	1958.46	-22.20	4.68
YAUT-032912	1958.00	-28.46	3.10
YAUT-033302	1957.51	-38.54	3.29
YAUT-033325	1957.46	-37.35	4.51
YAUT-031113	1957.42	-23.27	7.74
YAUT-033402	1957.36	-37.47	3.37
YAUT-033403	1957.31	-35.23	5.48
YAUT-033328	1957.26	-38.14	2.90
YAUT-032806	1957.00	-37.43	3.05
YAUT-031136	1956.80	-47.36	4.29
YAUT-031313	1956.77	-44.48	3.74
YAUT-032905	1956.50	-44.97	3.39
YAUT-032902	1956.00	-51.17	3.36
YAUT-031115	1955.83	-38.97	4.36
YAUT-032906	1955.67	-40.88	3.07
YAUT-032904	1955.63	-39.73	3.67

Appendix of Chapter 3

YAUT-032809	1955.16	-40.11	3.05
YAUT-033404	1955.12	-51.40	4.19
YAUT-033316	1955.08	-39.30	3.12
YAUT-031116	1955.04	-12.28	8.17
YAUT-032903	1955.00	-32.85	2.75
YAUT-033339	1954.90	-27.25	2.81
YAUT-032938	1954.81	-20.95	2.88
YAUT-033329	1954.71	-40.97	3.52
YAUT-033323	1954.61	-50.36	2.73
YAUT-033318	1954.51	-56.01	2.73
YAUT-032803	1954.42	-50.71	3.02
YAUT-031123	1954.36	-65.05	4.15
YAUT-031117	1954.18	-58.05	7.40
YAUT-032811	1954.08	-62.22	3.74
YAUT-031124	1953.50	-65.30	3.48
YAUT-031118	1953.14	-56.17	6.18
YAUT-032909	1953.00	-69.94	3.02
YAUT-031125	1952.87	-69.73	3.60
YAUT-031119	1952.51	-70.30	8.02
YAUT-033331	1952.42	-70.45	3.59
YAUT-032936	1952.00	-54.03	3.02
YAUT-033311	1951.50	-69.05	2.94
YAUT-033315	1951.00	-67.62	3.52
YAUT-032937	1950.50	-53.20	3.02
YAUT-033332	1950.08	-67.75	2.59
YAUT-032815	1949.50	-56.77	4.22
YAUT-032807	1949.08	-64.55	3.18
YAUT-032813	1948.42	-69.50	2.94
YAUT-032812	1948.00	-55.86	3.03
YAUT-032816	1947.42	-63.67	3.99
YAUT-032819	1947.08	-66.37	2.99
YAUT-032804	1946.50	-61.68	2.98

Appendix of Chapter 3

YAUT-032817	1946.00	-65.75	3.24
YAUT-032818	1945.42	-68.08	3.67
YAUT-032802	1945.00	-61.01	2.96

Appendix of Chapter 4

Local marine reservoir age variability during the mid-Holocene

Appendix of Chapter 4

本章については、5年以内に雑誌などで刊行予定のため、非公開。

References

- Cutler, K. B., S. C. Gray, G. S. Burr, R. L. Edwards, F. W. Taylor, G. Cabioch, J. W. Beck, H. Cheng, and J. Moore (2004), Radiocarbon Calibration and Comparison to 50 Kyr BP with Paired ^{14}C and ^{230}Th Dating of Corals from Vanuatu and Papua New Guinea, *Radiocarbon*, 46(3), 1127–1160, doi:DOI: 10.1017/S0033822200033063.
- Dykoski, C. A., R. L. Edwards, H. Cheng, D. Yuan, Y. Cai, M. Zhang, Y. Lin, J. Qing, Z. An, and J. Revenaugh (2005), A high-resolution, absolute-dated Holocene and deglacial Asian monsoon record from Dongge Cave, China, *Earth Planet. Sci. Lett.*, 233(1), 71–86, doi:https://doi.org/10.1016/j.epsl.2005.01.036.
- Edwards, R. L., J. W. Beck, G. S. Burr, D. J. Donahue, J. M. A. Chappell, A. L. Bloom, E. R. M. Druffel, and F. W. Taylor (1993), A Large Drop in Atmospheric $^{14}\text{C}/^{12}\text{C}$ and Reduced Melting in the Younger Dryas, Documented with ^{230}Th Ages of Corals, *Science*, 260(5110), 962–968.
- Esat, T. (1995), Charge collection thermal ion mass spectrometry of thorium, *International Journal of Mass Spectrometry and Ion Processes*, 148, 159–170.
- Fairbanks, R. G., R. A. Mortlock, T.-C. Chiu, L. Cao, A. Kaplan, T. P. Guilderson, T. W. Fairbanks, A. L. Bloom, P. M. Grootes, and M.-J. Nadeau (2005), Radiocarbon calibration curve spanning 0 to 50,000 years BP based on paired $^{230}\text{Th}/^{234}\text{U}/^{238}\text{U}$ and ^{14}C dates on pristine corals, *Quat. Sci. Rev.*, 24(16), 1781–1796, doi:https://doi.org/10.1016/j.quascirev.2005.04.007.
- Fontugne, M., M. Carré, I. Bentaleb, M. Julien, and D. Lavallée (2004), Radiocarbon reservoir age variations in the south Peruvian upwelling during the Holocene, *Radiocarbon*, 46(2), 531–537, doi:10.2458/azu_js_rc.46.4187.
- Hamanaka, N., H. Kan, Y. Nakashima, Y. Yokoyama, T. Okamoto, T. Ohashi, H. Adachi, H. Matsuzaki, and N. Hori (2015), Holocene reef-growth dynamics on Kodakara Island (29°N, 129°E) in the Northwest Pacific, *Geomorphology*, 243, 27–39, doi:10.1016/j.geomorph.2015.04.011.
- Hirabayashi, S., Y. Yokoyama, A. Suzuki, Y. Miyairi, and T. Aze (2017c), Short-term fluctuations in regional radiocarbon reservoir age recorded in coral skeletons

- from the Ryukyu Islands in the north-western Pacific, *Jouenal Quat. Sci.*, 32(1), 1–6, doi:10.1002/jqs.2923.
- Hua, Q., G. E. Webb, J. Zhao, L. D. Nothdurft, M. Lybolt, G. J. Price, and B. N. Opdyke (2015), Large variations in the Holocene marine radiocarbon reservoir effect reflect ocean circulation and climatic changes, *Earth Planet. Sci. Lett.*, 422, 33–44, doi:10.1016/j.epsl.2015.03.049.
- Huang, E., J. Tian, and S. Steinke (2011), Millennial-scale dynamics of the winter cold tongue in the southern South China Sea over the past 26ka and the East Asian winter monsoon, *Quat. Res.*, 75(1), 196–204, doi:https://doi.org/10.1016/j.yqres.2010.08.014.
- Kajita, H., A. Yamazaki, T. Watanabe, C. C. Wu, C. C. Shen, and T. Watanabe (2017), Holocene sea surface temperature variations recorded in corals from Kikai Island, Japan, *Geochem. J.*, 51(4), e9–e14, doi:10.2343/geochemj.2.0482.
- Konishi, K., A. Omura, and O. Nakamichi (1974) Radiometric coral ages and sea level records from the late Quaternary reef complexes of the Ryukyu Islands, *Proceedings of the Second International Coral Reef Symposium*, 2,565–613.
- Latorre, C., R. De Pol-Holz, C. Carter, and C. M. Santoro (2017), Using archaeological shell middens as a proxy for past local coastal upwelling in northern Chile, *Quat. Int.*, 427, 128–136, doi:10.1016/j.quaint.2015.11.079.
- Lewis, S. E., R. A. J. Wüst, J. M. Webster, G. A. Shields, W. Renema, J. M. Lough, and G. Jacobsen (2012), Development of an inshore fringing coral reef using textural, compositional and stratigraphic data from Magnetic Island, Great Barrier Reef, Australia, *Mar. Geol.*, 299–302, 18–32. doi:https://doi.org/10.1016/j.margeo.2012.01.003
- Lin, Y.-S., K.-Y. Wei, I.-T. Lin, P.-S. Yu, H.-W. Chiang, C.-Y. Chen, C.-C. Shen, H.-S. Mii, and Y.-G. Chen (2006), The Holocene Pulleniatina Minimum Event revisited: Geochemical and faunal evidence from the Okinawa Trough and upper reaches of the Kuroshio current, *Mar. Micropaleontol.*, 59(3), 153–170, doi:https://doi.org/10.1016/j.marmicro.2006.02.003.
- McGregor, H. V., M. K. Gagan, M. T. McCulloch, E. Hodge, and G. Mortimer (2008), Mid-Holocene variability in the marine ¹⁴C reservoir age for northern coastal Papua New Guinea, *Quat. Geochronol.*, 3(3), 213–225, doi:https://doi.org/10.1016/j.quageo.2007.11.002.

- Ortlieb, L., G. Vargas, and J. F. Saliège (2011), Marine radiocarbon reservoir effect along the northern Chile-southern Peru coast (14-24°S) throughout the Holocene, *Quat. Res.*, 75(1), 91–103, doi:10.1016/j.yqres.2010.07.018.
- Ota, Y., and A. Omura (1992), Contrasting styles and rates of tectonic uplift of coral reef terraces in the Ryukyu and Daito Islands, southwestern Japan, *Quat. Int.*, 15–16, 17–29, doi:https://doi.org/10.1016/1040-6182(92)90033-X.
- Paterne, M., L. K. Ayliffe, M. Arnold, G. Cabioch, N. Tisnérat-Laborde, C. Hatté, E. Douville, and E. Bard (2004), Paired ¹⁴C and ²³⁰Th/U Dating of Surface Corals from the Marquesas and Vanuatu (Sub-Equatorial Pacific) in the 3000 to 15,000 Cal Yr Interval, *Radiocarbon*, 46(2), 551–566, doi:DOI: 10.1017/S0033822200035608.
- Reimer, P., E. Bard, A. Bayliss, J. W. Beck, P. G. Blackwell, C. B. Ramsey, C. E. Buck, H. Cheng, R. L. Edwards, M. Friedrich, P. M. Grootes, T. P. Guilderson, H. Haflidason, I. Hajdas, C. Hatté, T. J. Heaton, D. L. Hoffmann, A. G. Hogg, K. A. Hughen, K. F. Kaiser, B. Kromer, S. W. Manning, M. Niu, R. W. Reimer, D. A. Richards, E. M. Scott, J. R. Southon, R. A. Staff, C. S. M. Turney, and J. van der Plicht (2013), IntCal13 and Marine13 Radiocarbon Age Calibration Curves 0–50,000 Years cal BP, *Radiocarbon*, 55(4), 1869–1887, doi:10.2458/azu_js_rc.55.16947.
- Seki, A., Y. Yokoyama, A. Suzuki, Y. Kawakubo, T. Okai, Y. Miyairi, H. Matsuzaki, N. Namizaki, and H. Kan (2012), Mid-Holocene sea-surface temperature reconstruction using fossil corals from Kume Island, Ryukyu, Japan, *Geochem. J.*, 46, e27–e32.
- Shen, C.-C., F. P. Siringan, K. Lin, C.-F. Dai, and S.-Y. Gong (2010), Sea-level rise and coral-reef development of Northwestern Luzon since 9.9ka, *Palaeogeogr. Palaeoclimatol. Palaeoecol.*, 292(3), 465–473.
- Sikes, E. L., C. R. Samson, T. P. Guilderson, and W. R. Howard (2000), Old radiocarbon ages in the southwest Pacific Ocean during the last glacial period and deglaciation, *Nature*, 405, 555–559, doi:10.1038/35014581.
- Stuiver, M., and T. F. Braziunas (1993), Modeling atmospheric ¹⁴C influences and ¹⁴C ages of marine samples to 10 000 B.C., *Radiocarbon*, 35, 137–191.
- Taylor, R.E., and R. Berger (1967), Radiocarbon content of marine shells from the Pacific coast of central and south America, *Science*, 158, 1180–1182.

- Toth, L. T., R. B. Aronson, H. Cheng, and R. L. Edwards (2015), Holocene variability in the intensity of wind-gap upwelling in the tropical eastern Pacific, *Paleoceanography*, 30(8), 1113–1131, doi:10.1002/2015PA002794.
- Ujiié, Y., H. Ujiié, A. Taira, T. Nakamura, and K. Oguri (2003), Spatial and temporal variability of surface water in the Kuroshio source region, Pacific Ocean, over the past 21,000 years: Evidence from planktonic foraminifera, *Mar. Micropaleontol.*, 49(4), 335–364, doi:10.1016/S0377-8398(03)00062-8.
- Ulm, S., F. Petchey, and A. Ross (2009), Marine reservoir corrections for Moreton Bay, Australia, *Archaeol. Oceania*, 44(3), 160–166.
- Xiang, R., Y. Sun, T. Li, D. W. Oppo, M. Chen, and F. Zheng (2007), Paleoenvironmental change in the middle Okinawa Trough since the last deglaciation: Evidence from the sedimentation rate and planktonic foraminiferal record, *Palaeogeogr. Palaeoclimatol. Palaeoecol.*, 243(3), 378–393, <https://doi.org/10.1016/j.palaeo.2006.08.016>.
- Yamaguchi, M., Y. Ota, A. Omura, and T. Nakamura (2004), Local Marine Reservoir Effects and Climate Changes Deduced from α -spectrometric $^{230}\text{Th}/^{234}\text{U}$ and AMS ^{14}C Dates of Holocene Fossil Corals Collected from Taiwan, *Quat. Res.*, 43(3), 181–188, doi:10.1017/CBO9781107415324.004.
- Yokoyama, Y., A. Suzuki, F. Siringan, Y. Maeda, A. Abe-Ouchi, R. Ohgaito, H. Kawahata, and H. Matsuzaki (2011), Mid-Holocene palaeoceanography of the northern South China Sea using coupled fossil-modern coral and atmosphere-ocean GCM model, *Geophys. Res. Lett.*, 38, L00F03, doi:10.1029/2010GL044231.
- Yoneda, M., H. Uno, Y. Shibata, R. Suzuki, Y. Kumamoto, K. Yoshida, T. Sasaki, A. Suzuki, and H. Kawahata (2007), Radiocarbon marine reservoir ages in the western Pacific estimated by pre-bomb molluscan shells, *Nucl. Instruments Methods Phys. Res. Sect. B Beam Interact. with Mater. Atoms*, 259(1), 432–437, doi:10.1016/j.nimb.2007.01.184.
- Yu, K., Q. Hua, J. Zhao, E. Hodge, D. Fink, and M. Barbetti (2010), Holocene marine ^{14}C reservoir age variability: Evidence from ^{230}Th -dated corals in the South China Sea, *Paleoceanography*, 25(3), PA3205, doi:10.1029/2009PA001831.

Yu, K., and T. Qu (2013), Imprint of the pacific decadal oscillation on the South China Sea throughflow variability, *Journal of Climate*, 26(24), 9797-9805.